

DOCTOR OF PHILOSOPHY

A Hammerstein-bilinear approach with application to heating ventilation and air conditioning systems

Zajic, Ivan

Award date:
2013

Awarding institution:
Coventry University

[Link to publication](#)

General rights

Copyright and moral rights for the publications made accessible in the public portal are retained by the authors and/or other copyright owners and it is a condition of accessing publications that users recognise and abide by the legal requirements associated with these rights.

- Users may download and print one copy of this thesis for personal non-commercial research or study
- This thesis cannot be reproduced or quoted extensively from without first obtaining permission from the copyright holder(s)
- You may not further distribute the material or use it for any profit-making activity or commercial gain
- You may freely distribute the URL identifying the publication in the public portal

Take down policy

If you believe that this document breaches copyright please contact us providing details, and we will remove access to the work immediately and investigate your claim.

**A Hammerstein-bilinear Approach with
Application to
Heating Ventilation and Air
Conditioning Systems**

Ivan Zajíc

BEng European Engineering
MSc Control Engineering

September 2013

A thesis submitted in partial fulfilment of the University's requirements
for the degree of Doctor of Philosophy.

Control Theory and Applications Centre
Coventry University

Abstract

This thesis considers the development of a Hammerstein-bilinear approach to nonlinear systems modelling, analysis and control system design, which builds on and extends the applicability of an existing bilinear approach. The underlying idea of the Hammerstein-bilinear approach is to use the Hammerstein-bilinear system models to capture various physical phenomena of interest and subsequently use these for model based control system designs with the premise being that of achieving enhanced control performance. The advantage of the Hammerstein-bilinear approach is that the well structured system models allow techniques that have been originally developed for linear systems to be extended and applied, while retaining moderate complexity of the corresponding system identification schemes and nonlinear model based control designs.

In recognition of the need to be able to identify the Hammerstein-bilinear models a unified suite of algorithms, being the extensions to the simplified refined instrumental variable method for parameter estimation of linear transfer function models, is proposed. These algorithms are able to operate in both the continuous-time and discrete-time domains to reflect the requirements of the intended purposes of the identified models with the emphasis being placed on straightforward applicability of the developed algorithms and recognising the need to be able to operate under realistic practical system identification scenarios. Moreover, the proposed algorithms are also applicable to parameter estimation of Hammerstein and bilinear models, which are special cases of the wider Hammerstein-bilinear model class.

The Hammerstein-bilinear approach has been applied to an industrial heating, ventilation and air conditioning (HVAC) system, which has also been the underlying application addressed in this thesis. A unique set of dynamic control design purpose oriented air temperature and humidity Hammerstein-bilinear models of an environmentally controlled clean room manufacturing zone has been identified. The greater insights afforded by the knowledge of the system nonlinearities then allow for enhanced control tuning of the associated commercial HVAC control system leading to an improved overall control performance.

Acknowledgements

I would like to thank and express my gratitude to Prof. Keith J. Burnham and Dr. Tomasz Larkowski for supervising me throughout this enjoyable research project and the overall PhD programme. Keith introduced me to this project, gave me real sense for control engineering and passionately supported me through my graduate career, while Tomasz provided me with system identification expertise, patient assistance and guidance.

I would like to give special thanks to my industrial advisor Mr. Dean Hill from Abbott Diabetes Care UK without whom this project would not have even started. Dean enthusiastically helped me with the research work on the site and through close collaboration and many discussions has helped to shape the presented research work. I would also like to thank Mr. Dave Terry and his team for providing invaluable expertise on HVAC systems. This research work has been fully funded by Abbott Diabetes Care UK as part of a continuous improvement programme. I am very grateful for this financial support.

Lastly, I would like to acknowledge and thank Dr. Joe C. Whitehouse and Dr. Peter J. Reeve for valuable discussions and for creating an enjoyable working atmosphere.

Contents

	Page
Abstract	ii
Acknowledgements	iii
Contents	iv
1 Introduction, motivation and outline of approach	1
1.1 Introduction	1
1.2 Outline of thesis	5
1.3 Contributions	7
2 Background to Hammerstein-bilinear models	9
2.1 Introduction	9
2.2 Definition of bilinear models	11
2.3 Special observation	15
2.3.1 Exploiting the observation in system identification	16
2.3.2 Demonstration	17
2.3.3 Numerical study	21
2.4 Discrete-time bilinear models	22
2.4.1 Exact discretisation	22
2.4.2 Approximate discretisation	24
2.4.3 Input-output representation	26
2.5 Definition of Hammerstein-bilinear models	28
2.5.1 Preliminary HVAC system considerations	28
2.5.2 Hammerstein model parameterization	30
2.6 Selected static and dynamic properties	31
2.7 Conclusions	37

3	Parameter estimation methods in continuous-time domain	39
3.1	Introduction	39
3.1.1	Dynamic bilinear models	41
3.1.2	Hammerstein-bilinear models	43
3.1.3	Problem formulation	44
3.2	Simplified refined instrumental variable method	46
3.2.1	SRIVC method configured for bilinear model estimation	53
3.3	Bilinear SRIVC (BSRIVC) method	55
3.3.1	Comments	61
3.4	Hammerstein-bilinear model estimation	62
3.4.1	Hammerstein-bilinear SRIVC (HBSRIVC) method	64
3.4.2	Constrained HBSRIVC method	71
3.4.3	Hammerstein SRIVC (HSRIVC) method	74
3.4.4	Constrained HSRIVC method	78
3.4.5	Comments	80
3.5	Numerical study	81
3.5.1	Case scenario I	84
3.5.2	Case scenario II	89
3.6	Conclusions	90
4	Parameter estimation methods in discrete-time domain	95
4.1	Introduction	95
4.1.1	Problem formulation	97
4.2	Simplified refined instrumental variable method	99
4.3	Hammerstein SRIV (HSRIV) method	102
4.3.1	Constrained HSRIV method	106
4.4	Over-parameterized HSRIV (HSRIV-OV) method	109
4.4.1	SRIV estimation of the over-parameterized model	109
4.4.2	Inferring unique parameter vector defining the HB model	112
4.5	Numerical study	114
4.5.1	Results	115
4.6	Conclusions	116
5	Modelling of heating ventilation and air conditioning system	121
5.1	Introduction	121
5.2	Plant details	122
5.2.1	Dehumidification unit	124
5.2.2	Air handling unit	128

5.2.3	Fresh air plant	131
5.2.4	Control and monitoring system	131
5.3	System identification setup	132
5.3.1	Manufacturing zone temperature model	134
5.3.2	Manufacturing zone humidity model	136
5.4	Zone temperature submodel	138
5.4.1	Data-based model	138
5.4.2	First principles considerations	142
5.5	Air handling unit temperature submodel	148
5.5.1	First principles analysis	149
5.5.2	Preliminary system identification	152
5.5.3	Final system identification	158
5.5.4	Adjustment of estimated parameters for a new operating point	161
5.6	Manufacturing zone humidity model	165
5.6.1	Trend model	166
5.6.2	Gas valve characteristic	169
5.6.3	Final system identification	171
5.6.4	Adjustment of estimated parameters for a new operating point	175
5.7	Conclusions	179
6	Control analysis and tuning of an industrial HVAC control sys- tem	181
6.1	Introduction	181
6.1.1	Control algorithm	183
6.1.2	Control requirements	186
6.2	Control analysis: Manufacturing zone temperature model	187
6.2.1	Steady-state characteristic	189
6.2.2	Process gain and time constants	192
6.2.3	Model order reduction	198
6.3	Control analysis: Manufacturing zone humidity model	200
6.4	Control tuning	203
6.4.1	Closed-loop system stability	206
6.5	Implementation results	208
6.5.1	Evaluation of implementation results	210
6.6	Gas consumption analysis	213

6.6.1 Observations	215
6.7 Conclusions	216
7 Conclusions & future research directions	218
7.1 Conclusions	218
7.1.1 Heating ventilation and air conditioning system application	221
7.2 Proposals for future work	223
References	224
Appendices	234
A Models of HVAC system components	235
A.1 Control valve ideal model	235
B Essential background to Psychrometrics	237
B.1 Dry-bulb temperature	238
B.2 Specific and relative humidity	238
B.3 Dew-point and frost-point temperatures	240
B.4 Conversion between relative humidity and dew-point temperature	241

Chapter 1

Introduction, motivation and outline of approach

1.1 Introduction

The work in this thesis has been motivated by the intended application to heating, ventilation and air conditioning (HVAC) systems with the view of improving the energy utilisation of these systems via enhanced control performance. The *bilinear approach* to modelling and control of nonlinear real-world systems, such as the considered HVAC system application, has been found to be practically realizable and of great benefit in the past (Burnham 1991, Goodhart 1991, Disdell 1995, Dunoyer 1996, Minihan 2001, Ziemian 2002, Martineau 2004, Ekman 2005, Larkowski 2009). This approach places an emphasis on use of bilinear model structures for nonlinear systems modelling, analysis and controller design. The bilinear system models represent an important class of nonlinear models that are defined to be linear in both state and control when considered independently, with the nonlinearity arising from coupled terms involving products of system state and control input (Mohler 1973). By formulating the model appropriately the bilinear coupled terms could also be represented by products of system output and input signals, i.e. the output is defined as a system state.

The advantage of the bilinear approach is that a well structured ‘nearly-linear’ system model allows techniques that have been originally developed for linear systems to be extended and applied. Adopting a bilinear model retains a well structured framework, which contains the well known notional concepts such as time constant and process gain. When adopting a bilinear approach these concepts become system input dependent quantities which can be appropriately

modelled. In contrast, whilst it is possible to obtain a complex nonlinear model of a nonlinear system, the resulting model may not necessarily lend itself for the purpose of system analysis and model based control design, e.g. when use is made of methods such as neural networks and/or fuzzy logic (Burnham, Zajic & Larkowski 2011).

Considering the underlying application to the HVAC systems addressed in this thesis, the most relevant dynamic nonlinear processes are the heat transfer process and the compartmental processes where both can be successfully modelled by bilinear model structures (Underwood & Yik 2004, Ekman 2005). Additionally the HVAC system components such as control valves, dampers, and static power characteristics of pumps and fans introduce static, memoryless nonlinearities, which can be classified as Hammerstein-type models (Eskinat, Johnson & Luyben 1991, Janczak 2005). The following relatively simple, yet rather typical, example 1.1 concerning a through-flow water heater shows how a static input nonlinearity in a cascaded connection with a bilinear dynamic subsystem naturally arises.

Example 1.1 The water heaters of similar functionality can be found for example in households as gas or electric showers. The water heater maintains the outlet water temperature, denoted $T_{wo}(t)$ [K], at the desired value by means of regulating the water mass flow rate, denoted $\dot{m}(t)$ [kg/s], through the heater as depicted in Figure 1.1a. In other words the water heater *regulates heat transfer through flow*. The greater the water mass flow rate the lesser the heat, denoted $q(t)$ [W], is exchanged between the water and the heat reservoir, so that the outlet water temperature approaches the inlet water temperature, denoted T_{wi} [K]. On the contrary, a high outlet water temperature can be achieved by maintaining a low water mass flow rate through the heater so that there is enough time for heat to be exchanged between the heat reservoir and the heated water. Note that time varying variables are denoted with the time variable (t) in rounded brackets, defined in seconds [s], while the variables and coefficients which are assumed to be constant in this example are denoted without (t).

The water mass flow rate is regulated by the flow control valve which is modelled by the following relationship

$$\dot{m}(t) = M_w \phi(u(t)), \tag{1.1}$$

where $u(t)$ denotes the valve stem fractional position in the range of $\langle 0, 1 \rangle$, where 0 corresponds to a fully closed valve and 1 to fully opened. M_w denotes the constant maximal water mass flow rate for a fully open valve, i.e. $u(t) = 1$, and

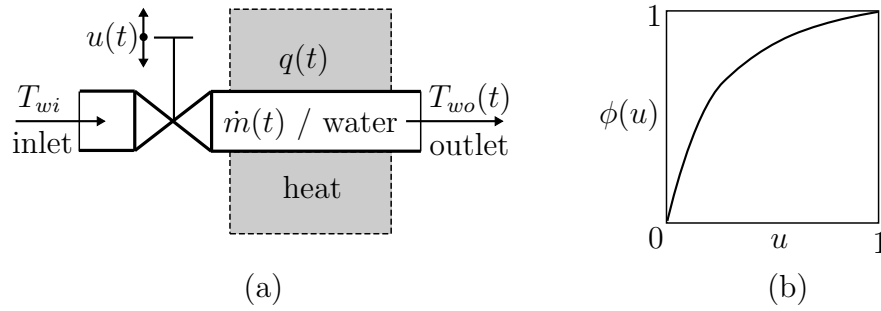


Figure 1.1: The subfigure (a) depicts the through-flow water heater, and the subfigure (b) shows the flow control valve static characteristic.

$\phi(\cdot)$ represents the valve static characteristic depicted in Figure 1.1b. Such a valve static characteristic would in practice correspond to a so called installed linear valve characteristic, see (Underwood 1999) and Appendix A.1.

A lumped parameter modelling approach is adopted to capture the underlying dynamics of the water heater. The water heater is assumed to behave as a perfectly mixed vessel, i.e. a single-compartmental model is created. In this model the outlet water temperature is the same as the mean temperature of the whole water content of the vessel (in this case a long metal pipe). Further, for clarity within this example, the heat exchange material (metal pipe) and water thermal capacities are lumped together and modelled as one combined effect. Based on these assumptions an energy balance equation for the water can thus be expressed

$$C \frac{dT_{wo}(t)}{dt} = \dot{m}(t)c_{pw} [T_{wi} - T_{wo}(t)] - q(t), \quad (1.2a)$$

$$q(t) = UA [T_{wo}(t) - T_q] \quad (1.2b)$$

where C [J/K] denotes the overall thermal capacity, c_{pw} [J/kgK] is the specific water thermal capacity, U [W/m^2K] denotes the overall heat transfer coefficient, A [m^2] denotes the overall effective heat exchange area, and T_q [K] denotes the constant temperature of the outer side of the metal pipe.

Defining and denoting the system output as $y(t) = T_{wo}(t)$ and the system input as the valve opening $u(t)$, the dynamic model of the water heater governed by (1.1) and (1.2) can be re-expressed in an input-output form as follows

$$\frac{dy(t)}{dt} = -\Theta_1 y(t) + \Theta_2 \phi(u(t)) + \Theta_3 y(t) \phi(u(t)) + \Theta_4 T_q \quad (1.3)$$

where the coefficients $\Theta_{1,\dots,4}$ are defined as $\Theta_1 = UA/C$, $\Theta_2 = M_w c_{pw} T_{wi}/C$,

$\Theta_4 = \Theta_1$, and $\Theta_3 = -M_w c_{pw}/C$. In (1.3) one can observe the bilinear product term between the system input and the output (system state), i.e. $\Theta_3 y(t)\phi(u(t))$, and the memoryless nonlinear transformation of the control input $\phi(u(t))$, which demonstrates that these types of nonlinearities namely, static input (or Hammerstein) and bilinear product terms, arise naturally in HVAC applications. ■

Motivated by the physical phenomena occurring in a general HVAC system, such as that described in the above example 1.1, there is a natural interest to introduce a Hammerstein-bilinear model structure. This model structure is then defined as a memoryless static input nonlinearity in a cascaded connection with a bilinear dynamic submodel. The Hammerstein-bilinear model structure can be viewed as a natural extension to the bilinear system model structures, which even further extends the modelling and approximation capabilities of the bilinear models while exploiting the concept of retaining a well structured nonlinear model. Indeed, it is against this background that the proposed extension to the now well established bilinear approach is proposed, namely that of a new *Hammerstein-bilinear approach* to modelling and control of real-world systems. Subsequently, in both approaches, i.e. bilinear and Hammerstein-bilinear, knowledge of the nonlinear models is essential, which further prompts the need to develop the corresponding model parameter estimation techniques.

It is desirable that such parameter estimation techniques are straightforwardly applicable and able to work sufficiently well under realistic practical system identification scenarios, e.g. limited amount of measured input-output data, input signal not persistently exciting, having limited *a priori* knowledge regarding the system dynamics and presence of coloured (non-white) measurement noise. Furthermore, such proposed parameter estimation techniques should be able to operate in both continuous-time and discrete-time domains to reflect the needs of a particular system identification scenario as well as the various intended purposes of the identified models. For example, the continuous-time models are suitable for the physical interpretability of parameter estimates while the discrete-time models are desirable for control system implementation and realisation in a digital computer environment. Based on these requirements, therefore, it is proposed to extend the simplified refined instrumental variable method (Young 1976, Young & Jakeman 1979, Jakeman & Young 1979, Young & Jakeman 1980, Young, Garnier & Gilson 2008) for linear transfer function model parameter estimation to encompass a bilinear and Hammerstein-bilinear model class both in the continuous-time and discrete-time domains.

1.2 Outline of thesis

The logical flow of the research work carried out within the thesis has a top-down structure, where the developments presented in one chapter directly depend on the developments carried out in the previous chapter (and chapters). The outline of the presented research work is given chapter by chapter in the order as they appear in this thesis.

Chapter 2 This chapter provides essential background to bilinear and Hammerstein system models both in continuous and discrete-time domains together with a corresponding literature review. A continuous-time single-input single-output bilinear model in an input-output form, used for system identification purposes, is presented. It is shown that under appropriately chosen parametric constraints this bilinear model can be interpreted as a two-input single-output linear in structure transfer function model so that the reviewed linear parameter estimation methods can be applied. Despite the fact that an exact discretisation of bilinear (nonlinear) continuous-time models is not necessarily structure preserving an approximate, yet related, discrete-time single-input single-output bilinear model in an input-output form is presented. A multi-input single-output linear in structure transfer function representation of this discrete-time bilinear model is also presented, which promotes the use of linear parameter estimation methods. Subsequently, the Hammerstein-bilinear model structure is introduced and the corresponding static and dynamic properties are highlighted, which leads to the notion of a Hammerstein-bilinear approach.

Chapter 3 In this chapter various extensions to the simplified refined instrumental variable method for linear transfer function model parameter estimation designed to encompass both bilinear and Hammerstein-bilinear model classes in the continuous-time domain are presented. A detailed literature review related to the estimation of linear, bilinear and Hammerstein models in the continuous-time domain is provided. A state variable filtering approach is followed to obtain the time derivatives of input-output signals required for parameter estimation purposes; two types of prefilters are proposed giving rise to two distinct groups of algorithms. The first group of algorithms makes use of the linear optimal prefilters, which promotes the use of linear estimation methods. The second and more general group of algorithms is based on the time-step quasi-linear interpretation of the bilinear

models and uses adaptive, input dependent, prefilters. In the conclusions of this chapter a list of the reviewed and derived extensions to the reviewed algorithms is presented in a concise tabulated form.

Chapter 4 In a similar manner to Chapter 3, the extensions to the simplified refined instrumental variable method are presented to encompass a bilinear and Hammerstein-bilinear model class in the discrete-time domain. Since, it is possible to interpret the discrete-time bilinear models in the multi-input single-output linear in structure form, only the linear prefilters are required. The designed discrete-time parameter estimation algorithms then complement the continuous-time counterpart algorithms proposed in Chapter 3.

Chapter 5 In this chapter the use of selected parameter estimation algorithms proposed in Chapters 3 and 4 is demonstrated on the modelling challenge of the industrial HVAC system located at Abbott Diabetes Care, Witney, UK. The practical aspects of system identification are shown, including model order selection, processing of raw measured data and adjustment of the estimated nonlinear model parameters for any given operating point. Furthermore, some of the advantages of using continuous-time models in gaining physical insight into the investigated system are demonstrated.

Chapter 6 The advantages of having a well structured nonlinear model are demonstrated on a control oriented system analysis and subsequent tuning of a commercial industrial control system. During this analysis the identified Hammerstein-bilinear models obtained in Chapter 5 are applied. Subsequently, real-time trials are carried out showing enhanced control performance of the investigated HVAC control system. Furthermore, an energy consumption analysis of the modelled HVAC system is carried out, where, again the knowledge of the nonlinearity of the system is beneficial, thus further reinforcing the need for the Hammerstein-bilinear models, and indeed the proposed Hammerstein-bilinear approach, which is considered to have wide applicability when dealing with practical nonlinear systems.

Chapter 7 Provides the main conclusions of the research and highlights areas for immediate work and potential areas for further fruitful research.

1.3 Contributions

The main research contributions of the author are summarised and listed in the order as they appear in this thesis.

- Building on an existing bilinear approach, and prompted by the HVAC system application, a new approach, termed the Hammerstein-bilinear approach to nonlinear system modelling, analysis and control systems design has been proposed.
- A special relation between two distinct continuous-time bilinear model structures has been revealed, where, under appropriately chosen parametric constraints, the two models yield identical output responses and share the same model parameters. While the first bilinear model can be interpreted, purely for parameter estimation purposes, as a two-input single-output linear in structure transfer function model, the second model cannot. This observation has been exploited in the development of linear based estimation algorithms, where by virtue of estimating the parameters of the transfer function model the parameters of the second bilinear model are also obtained.
- Building on the simplified refined instrumental variable method for parameter estimation of linear transfer function models a unified suite of algorithms for the identification of bilinear and Hammerstein-bilinear models in both the continuous-time domain and discrete-time domain have been proposed, and have been successfully applied to a HVAC system.
- A unique set of control oriented air temperature and humidity continuous-time Hammerstein-bilinear models of an environmentally controlled clean room manufacturing zone in Abbott Diabetes Care have been identified. Relevant practical aspects of system identification when using the proposed parameter estimation methods have been shown. Furthermore, the use of continuous-time models has allowed a physically meaningful insight into the system to be gained, which has led to the derivation of a manufacturing zone heat gain temperature model used for the purpose of control tuning.
- Adjustment of estimated model parameters for bilinear and Hammerstein-bilinear models for any given operating point has been demonstrated on the identified HVAC system models.

- Control oriented analysis of the HVAC system based on the set of identified Hammerstein-bilinear models has been conducted. Subsequent control tuning of the commercial HVAC control system has led to an enhanced control performance, creating scope for subsequent reduction in energy consumption.

Chapter 2

Background to Hammerstein-bilinear models

2.1 Introduction

The purpose of this chapter is to give an essential background to Hammerstein and bilinear system models and especially to the combination of these two model classes, i.e. the Hammerstein-bilinear (HB) model, which is used throughout this thesis. Bilinear systems and systems which can be approximated with sufficient accuracy by bilinear models naturally occur in man-made systems and in nature (Mohler 1973). Bilinear system models are characterised by input dependent dynamic behaviour and cannot exhibit neither input multiplicity nor output multiplicity in their steady-state. Since the physical phenomena are described by physical laws, the bilinear models were originally defined in a continuous-time (CT) state-space framework. The state of a bilinear system evolves not just according to the system input and current state, as it would be in the case of linear systems, but also according to a product between the system input and state. Bilinear models are therefore defined to be *linear* in both state and control when considered independently, with the *bilinearity* (or nonlinearity) arising from coupled terms involving products of the system state and control input. It is this close connection to linear systems, which makes the bilinear models particularly appealing and as such many techniques developed for linear systems can be extended and applied to the bilinear case (Burnham et al. 2011).

Much work has been done in the area of modelling and control for bilinear systems, with many real-world processes being more appropriately, and possibly more conveniently, described using bilinear models. From first principles consid-

erations, in a similar manner as shown in Example 1.1, many processes exhibit inherent bilinear dynamic behaviour in the continuous-time domain. These nonlinear processes may be found in areas such as engineering, ecology, medicine and socioeconomics, for comprehensive overviews, see, for example, (Mohler 1973, Bruni, DiPillo & Koch 1974, Mohler & Kolodziej 1980). In HVAC applications the most relevant nonlinear processes are heat transfer (Underwood & Yik 2004) and compartmental processes (Ekman 2005).

The Hammerstein models are characterised by a memoryless static nonlinear element in series with a linear dynamic submodel. While the model dynamics are entirely defined by the linear submodel the steady-state characteristic is determined by the product of a static element and the linear submodel steady-state gain. Hammerstein models can exhibit input multiplicity due to the static nonlinear element scaling the input, which is a desirable feature, but cannot exhibit the output multiplicity. For example, (Eskinat et al. 1991) modelled an experimental heat exchanger and also simulated a high-purity distillation column by both Hammerstein and linear dynamic models and compared their performances. The authors concluded that the results obtained are satisfactory and favour of the Hammerstein-type models. However, it is known that the underlying dynamic behaviour of these systems is input dependent, i.e. bilinear, as opposed to a purely linear dynamic behaviour. Consequently, this observation leads naturally to the idea of extending the Hammerstein model structure by replacing the linear dynamic submodel by a bilinear model structure. Indeed it is against this background that the proposal for the HB model structure is formed.

The HB model combines the advantages of its constituent submodels and can exhibit both, input dependent dynamic behaviour and increased flexibility of the steady-state characteristic including the input multiplicity. Furthermore, the model structure remains relatively simple, yet mathematically well structured, and can be favourably exploited by extensions to existing parameter estimation schemes and for the purpose of control system design. To the best of the author's knowledge, so far very little has been published in the study of such a nonlinear model structure and its control.

Some encouraging examples where the HB model have been successfully applied or have naturally appeared are: Thomson, Schooling & Soufian (1996) consider system identification of a pilot-scale parallel-tube heat exchanger in a black-box manner, i.e. physical laws are not used for preliminary model structure selection. Albeit the identification of a model structure is carried out entirely in a black-box manner the best (in the sense of minimal simulation error) final model

resembles the HB model structure. Motivated by underlying physical relations (Zajic, Larkowski, Hill & Burnham 2012) successfully used the HB model for system identification of an industrial air handling unit. Larkowski & Burnham (2011) adopted the HB model for identification of a simulated continuous stirred tank reactor. From first principles considerations the continuous stirred tank reactor does not have exactly a HB model structure, however due to the flexibility offered by the HB model, an excellent model fit has been achieved. The control of the zone temperature via a variable-air-volume (VAV) box unit is considered in (Huang 2011). Here the overall HVAC system model is based on first principles considerations and the final model used by the nonlinear model based predictive controller has a HB model structure.

2.2 Definition of bilinear models

A state-space representation of a continuous-time single-input single-output (SISO) deterministic bilinear model takes the form

$$\frac{d}{dt}\mathbf{x}(t) = \mathbf{A}\mathbf{x}(t) + \mathbf{b}u(t) + u(t)\mathbf{N}\mathbf{x}(t) \quad (2.1a)$$

$$y(t) = \mathbf{c}^T\mathbf{x}(t) \quad (2.1b)$$

where $\mathbf{x}(t) = [x_1(t), \dots, x_n(t)]^T$ denotes the $(n \times 1)$ state vector, $y(t)$ the (1×1) system output, $u(t)$ the (1×1) system input, \mathbf{A} the $(n \times n)$ system matrix, \mathbf{b} the $(n \times 1)$ input vector and \mathbf{c} is the $(n \times 1)$ output vector. Linear models coexist as a special subclass of bilinear models and can be obtained by setting the $(n \times n)$ matrix \mathbf{N} of bilinear coefficients to null.

In general, bilinear models can be found and formulated in different forms. The parameter estimation methods developed and applied in this thesis make use of an input-output model relation (external description) rather than the state-space model representation (internal description). Therefore, the input-output model representation must exist and be of a ‘convenient form’ which can be favourably exploited by the designed model parameter estimation algorithms. Bearing in mind the class of bilinear models appearing in HVAC applications and the corresponding parameter estimation algorithms, the phase variable canonical

form of the following matrices is used throughout this thesis

$$\mathbf{A} = \begin{bmatrix} 0 & 1 & \cdots & 0 \\ \vdots & & \ddots & \vdots \\ 0 & 0 & \cdots & 1 \\ -\alpha_n & -\alpha_{n-1} & \cdots & -\alpha_1 \end{bmatrix}, \quad \mathbf{N} = \begin{bmatrix} 0 & 0 & \cdots & 0 \\ \vdots & & & \vdots \\ 0 & 0 & \cdots & 0 \\ \eta_n & \eta_{n-1} & \cdots & \eta_1 \end{bmatrix} \quad (2.2)$$

$$\mathbf{c}^T = \begin{bmatrix} \beta_m & \cdots & \beta_0 & 0 \end{bmatrix}, \quad \mathbf{b}^T = \begin{bmatrix} 0 & \cdots & 0 & 1 \end{bmatrix}$$

in which $m < n$ and \mathbf{A} , \mathbf{N} , \mathbf{c}^T and \mathbf{b}^T comprise real valued coefficients $\alpha_1, \dots, \alpha_n$, β_0, \dots, β_m and η_1, \dots, η_n , respectively. The same class of state-space bilinear models has been successfully applied in the work of (Dunoyer 1996) focusing on control and identification of bilinear systems and also in the application to a high-temperature industrial furnace, see (Martineau, Burnham, Haas, Andrews & Heeley 2003) and references given therein. It is assumed that the system (2.1) is subject to zero initial conditions, i.e.

$$\mathbf{x}(0) = 0, \quad \frac{d}{dt}\mathbf{x}(0) = 0, \quad \dots, \quad \frac{d^n}{dt^n}\mathbf{x}(0) = 0 \quad (2.3)$$

By eliminating the states in (2.1), defined by matrices (2.2), the following input-output representation, i.e. differential equation, can be obtained

$$y^{(n)}(t) + \alpha_1 y^{(n-1)}(t) + \cdots + \alpha_n y^{(0)}(t) = \beta_0 u^{(m)}(t) + \cdots + \beta_m u^{(0)}(t) + \eta_1 y^{(n-1)}(t)u^{(0)}(t) + \cdots + \eta_n y^{(0)}(t)u^{(0)}(t) \quad (2.4)$$

where $x^{(p)}(t)$ denotes the p^{th} time-derivative of the continuous-time signal $x(t)$. A commonly used compact form of (2.4) is written as

$$\boxed{A(s)y(t) = B(s)u(t) + u(t) \sum_{i=1}^n \eta_i s^{n-i} y(t)} \quad (2.5)$$

with

$$A(s) = s^n + \alpha_1 s^{n-1} + \cdots + \alpha_n \quad (2.6a)$$

$$B(s) = \beta_0 s^m + \beta_1 s^{m-1} + \cdots + \beta_m \quad (2.6b)$$

where s denotes the differential operator defined as $s^p x(t) = \frac{d^p x(t)}{dt^p}$. Further, in the case where the product terms are present, as in the bilinear model (2.5), the operator s is defined such that it operates (acts) only on the signal(s) on its right

hand side, i.e. $u(t)s^p x(t) = u(t)\frac{d^p x(t)}{dt^p}$. Hereinafter, when referring to the term ‘continuous-time bilinear model’, the model structure (2.5) is implied. Note, that yet another continuous-time bilinear model structure is introduced later on in equation (2.16). Under appropriately chosen parametric constraints this bilinear model structure is a subset of the bilinear model structure introduced in (2.5), which is favourably exploited by some of the designed parameter estimation methods.

The following example demonstrates state elimination in the state-space model (2.2) towards obtaining its input-output realisation. This approach will be used in Chapter 5, where the water-to-air heat exchanger temperature model will be derived from physical laws.

Example 2.1 Consider a third order state-space continuous-time bilinear model defined by (2.2) and with $n = 3$ and $m = 2$. Rewrite this state-space canonical model into its equivalent input-output representation, which is entirely described by measured input-output variables $u(t)$ and $y(t)$, respectively.

The third order state-space model (2.2) can be rewritten from its compact matrix form into a set of equations, using the s operator, as follows

$$sx_1(t) = x_2(t) \tag{2.7a}$$

$$sx_2(t) = x_3(t) \tag{2.7b}$$

$$sx_3(t) = -[\alpha_3 - \eta_3 u(t)]x_1(t) - [\alpha_2 - \eta_2 u(t)]x_2(t) - [\alpha_1 - \eta_1 u(t)]x_3(t) + u(t) \tag{2.7c}$$

$$y(t) = \beta_2 x_1(t) + \beta_1 x_2(t) + \beta_0 x_3(t) \tag{2.7d}$$

Noting that $x_2(t) = sx_1(t)$ and $x_3(t) = s^2 x_1(t)$, it is possible to substitute for $x_2(t)$ and $x_3(t)$ in (2.7c) and in (2.7d) leading to

$$s^3 x_1(t) = -[\alpha_3 - \eta_3 u(t)]x_1(t) - [\alpha_2 - \eta_2 u(t)]sx_1(t) - [\alpha_1 - \eta_1 u(t)]s^2 x_1(t) + u(t) \tag{2.8a}$$

$$y(t) = \beta_2 x_1(t) + \beta_1 sx_1(t) + \beta_0 s^2 x_1(t) \tag{2.8b}$$

In order to eliminate the state x_1 in (2.8a), equation (2.8b) can be rearranged with respect to the state $x_1(t)$, i.e.

$$x_1(t) = \frac{y(t)}{\beta_0 s^2 + \beta_1 s + \beta_2} \tag{2.9}$$

and noting that the time derivatives of state $x_1(t)$, i.e. $sx_1(t)$, $s^2x_1(t)$ and $s^3x_1(t)$, are required, taking the time derivatives of (2.9) gives

$$sx_1(t) = \frac{sy(t)}{\beta_0s^2 + \beta_1s + \beta_2}, \quad s^2x_1(t) = \frac{s^2y(t)}{\beta_0s^2 + \beta_1s + \beta_2}, \quad s^3x_1(t) = \frac{s^3y(t)}{\beta_0s^2 + \beta_1s + \beta_2} \quad (2.10)$$

and substituting (2.9) and (2.10) into (2.8a) for the state $x_1(t)$ and its time derivatives leads to the desired input-output realisation

$$\begin{aligned} s^3y(t) = & -[\alpha_3 - \eta_3u(t)]y(t) - [\alpha_2 - \eta_2u(t)]sy(t) \\ & - [\alpha_1 - \eta_1u(t)]s^2y(t) + u(t)[\beta_0s^2 + \beta_1s + \beta_2] \end{aligned} \quad (2.11)$$

Equation (2.11) can be further expressed in a more compact form, as defined in (2.5), i.e.

$$[s^3 + \alpha_1s^2 + \alpha_2s + \alpha_3]y(t) = [\beta_0s^2 + \beta_1s + \beta_2]u(t) + u(t) \sum_{i=1}^3 \eta_i s^{3-i}y(t) \quad \blacksquare$$

A diagrammatic representation of the state-space model (2.1), defined by matrices (2.2), is provided in Figure 2.1. Being able to express the input-output bilinear model (2.5) in its state-space form provides a convenient way for the actual implementation of such a model in Matlab/Simulink software.

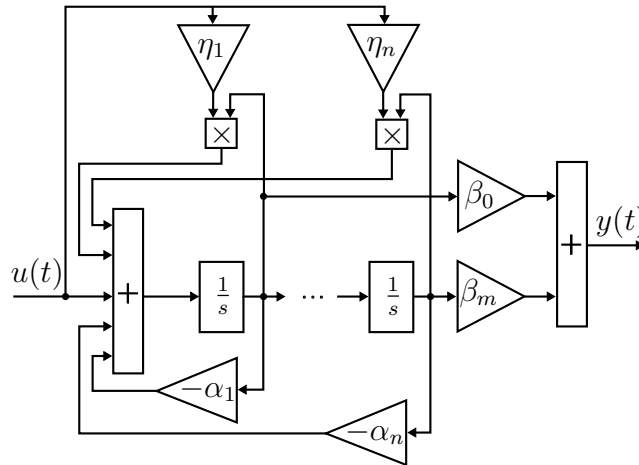


Figure 2.1: Block diagram representation of bilinear model structure.

Remark 2.1 It has often been found in practice that a minimal number ($n \leq 3$) of bilinear product terms can provide an adequate model for the purpose of simulation and especially for control. Examples of such systems are: high-temperature industrial furnace (Martineau et al. 2003), activated sludge process

(Ekman 2008) and industrial air handling unit (Zajic et al. 2012). ■

Remark 2.2 Because of the intended application to HVAC systems a particular subclass of state-space bilinear models has been selected, defined by state-space matrices (2.2), which yields unique input-output representation conveniently consisting only of products of system input and time derivatives of system output (2.5). However, this does not imply that all bilinear models in input-output form consist only from such input-output products. Rather, depending on the selection of system states, system output, and the definition of system matrices, the equivalent input-output model structure can be regarded as being generally nonlinear. For example the state-space model structure considered in (Brehe & Unbehauen 1998), which can be deduced from (2.2) by re-defining vectors \mathbf{b}^T and \mathbf{c}^T as

$$\begin{aligned} \mathbf{b}^T &= \begin{bmatrix} 0 & \beta_0 & \cdots & \beta_m \end{bmatrix} \\ \mathbf{c}^T &= \begin{bmatrix} 1 & 0 & \cdots & 0 \end{bmatrix} \end{aligned} \quad (2.13)$$

has the following input-output realisation

$$\begin{aligned} A(s)y(t) &= B(s)u(t) + u(t) \sum_{i=1}^n \eta_i s^{n-i} y(t) \\ &+ \sum_{j=2}^n \sum_{i=0}^{j-2} \alpha_j \beta_i s^{j-2-i} u(t) - u(t) \sum_{j=2}^n \sum_{i=0}^{j-2} \eta_j \beta_i s^{j-2-i} u(t) \end{aligned} \quad (2.14)$$

which is considerably more complex than the representation (2.5). This alternative representation is presented here just to show that there are numerous ways in which the bilinear models have been interpreted by different authors.

Comparing models (2.5) and (2.14) it is observed that additional products of input and input time derivatives are present. Additionally, it is observed that the input-output model parameters are not independent since parameter terms $\alpha_j \beta_i$ and $\eta_j \beta_i$ are present. Specifically, the original state-space model has $2n + m + 1$ parameters, while the input-output model (2.14) has $3n - 1 + \max(m + 1, n - 1)$ parameters, which is also noted in (Pearson & Kotta 2004). ■

2.3 Special observation

During the research on the first principles modelling of heat exchangers and the representation of the resulting bilinear models in input-output model form a spe-

cial relation between two bilinear model structures has been observed. Defining the polynomial $E(s)$ consisting of coefficients η_i , $i = 1, \dots, n$, which are part of bilinear model (2.5), such that

$$E(s) = \eta_1 s^{n-1} + \dots + \eta_n \quad (2.15)$$

Under the condition that the polynomial $E(s)$, defined in (2.15), and the polynomial $B(s)$, defined in (2.6b), have the same roots; the original bilinear model (2.5) has equivalent dynamic and static behaviour as the following bilinear model

$$A(s)y(t) = B(s)u(t) + \sum_{i=1}^n \eta_i s^{n-i} \{u(t)y(t)\} \quad (2.16)$$

The curly parentheses around the term $u(t)y(t)$ indicate that the differential operator acts on the product of signals $u(t)$ and $y(t)$. In the original bilinear model (2.5) the differential operator acts only on the output signal $y(t)$, while the input signal $u(t)$ is a multiplying factor, effectively ‘scaling’ the η_i parameters.

Additionally, if the first $n - 1$ parameters of polynomial $E(s)$ are not present, then the order of polynomial $B(s)$ is not restricted. In this special case, the only present bilinear term in the original bilinear model (2.5) is $u(t)\eta_n y(t)$, which is directly equivalent to the corresponding term $\eta_n u(t)y(t)$ of the model (2.16).

2.3.1 Exploiting the observation in system identification

Defining input signals $u_1(t) = u(t)$ and $u_2(t) = u(t)y(t)$, the newly presented SISO continuous-time bilinear model (2.16) can be formulated in the following two-input single-output (TISO) transfer function form

$$y(t) = \frac{B(s)}{A(s)}u_1(t) + \frac{E(s)}{A(s)}u_2(t) \quad (2.17)$$

Assuming the input-output signals $u_1(t)$, $u_2(t)$ and $y(t)$ are known, measured, the transfer function model (2.17) can be viewed as linear, which facilitates the use of existing and well established linear parameter estimation methods. Therefore, by virtue of estimating the parameters of the transfer function model (2.17), the parameters of the original bilinear model (2.5) are also estimated. The second input $u_2(t)$ consists of the measured, noisy, output $y(t)$. This in effect creates an *errors-in-variables* identification scenario, (Larkowski 2009), causing bias in the parameter estimates. The instrumental variable parameter estimation meth-

ods, presented in Chapter 3, are able to overcome this problem by replacing the measured output by an instrumental variable series.

The need for polynomial $B(s)$ to have the same roots as polynomial $E(s)$ is certainly restricting and case specific, however not so uncommon in the case of HVAC systems. Consider the motivational Example 1.1, where the simplified first principles model of through-flow water heater has been developed. Assigning the thermal capacities to both, water and metal pipe, denoted C_1 and C_2 , respectively, creates a model of two state equations

$$C_1 s T_{wo}(t) = \dot{m}(t) c_{pw} [T_{wi} - T_{wo}(t)] - UA [T_{wo}(t) - T_m(t)] \quad (2.18a)$$

$$C_2 s T_m(t) = UA [T_{wo}(t) - T_m(t)] - UA [T_m(t) - T_q] \quad (2.18b)$$

where $T_m(t)$ [K] is the mean temperature of the metal pipe and water mass flow rate is defined as $\dot{m}(t) = M_w u(t)$. To simplify the state equations the heat transfer coefficient U and the pipe's surface area A are assumed to be the same for the inner and outer walls of the pipe. Defining and denoting the system output as $y(t) = T_{wo}(t)$ and the system input as $u(t)$, the dynamic model of the water heater governed by (2.18) can be re-expressed in an input-output form as follows

$$s^2 y(t) = -\alpha_1 s y(t) - \alpha_2 y(t) + \beta_0 s u(t) + \beta_1 u(t) + \eta_1 u(t) s y(t) + \eta_2 u(t) y(t) + o \quad (2.19)$$

where the individual coefficients are: $\alpha_1 = (2UAC_1 + UAC_2)/(C_1C_2)$, $\alpha_2 = (2U^2A^2 - U^2A^2)/(C_1C_2)$, $\beta_0 = M_w c_{pw} T_{wi} C_2 / (C_1 C_2)$, $\beta_1 = M_w c_{pw} T_{wi} 2UA / (C_1 C_2)$, $\eta_1 = -M_w c_{pw} C_2 / (C_1 C_2)$, $\eta_2 = -M_w c_{pw} 2UA / (C_1 C_2)$, and the static offset is $o = U^2 A^2 T_q / (C_1 C_2)$. It is clear that in this case the roots of polynomials $B(s) = \beta_0 s + \beta_1$ and $E(s) = \eta_1 s + \eta_2$ are the same and the polynomial $B(s)$ is scaled by the negative value of inflow water temperature $-T_{wi}$.

2.3.2 Demonstration

The original bilinear model (2.5) is expressed in a compact polynomial form

$$A(s)y_1(t) = B(s)u(t) + u(t)E(s)y_1(t) \quad (2.20)$$

with the polynomials $A(s)$ and $B(s)$ being defined in (2.6) and the polynomial $E(s)$ defined in (2.15). In model (2.20) the polynomial $E(s)$ operates on the output signal $y_1(t)$ only and this filtering order should be retained. Note, for the purpose of the demonstration, that the output signal is denoted $y_1(t)$ instead of

$y(t)$. Similarly, for the second bilinear model the output signal is denoted $y_2(t)$ and (2.16) is also expressed in a compact polynomial form, hence

$$\bar{A}(s)y_2(t) = \bar{B}(s)u(t) + \bar{E}(s) \{u(t)y_2(t)\} \quad (2.21)$$

The polynomials $\bar{A}(s)$, $\bar{B}(s)$ and $\bar{E}(s)$ are defined to be equivalent to polynomials $A(s)$, $B(s)$ and $E(s)$, respectively, but may have restrictive parametric values.

The task is to establish under what conditions, for a given input signal $u(t)$, the output signals $y_1(t)$ and $y_2(t)$ of the two considered bilinear models (2.20) and (2.21), respectively, match. Specifically, assuming that the output signal $y_1(t)$ is known (measured) and is used as a part of the second input term of the second bilinear model (2.21), then the simulated output $y_2(t)$ of this model must be the same as $y_1(t)$. In other words, the second bilinear model (2.21) must be able to fit the measured output $y_1(t)$ from (2.20). This, in return, would allow the parameters of the first bilinear model (2.20) to be estimated by estimating the parameters of the second bilinear model (2.21).

The output of the first bilinear model (2.20) can be obtained (simulated) by interpreting the originally input-output model in a time-step quasi-linear transfer function form, hence

$$\begin{aligned} A(s)y_1(t) &= B(s)u(t) + u(t)E(s)y_1(t) \\ [A(s) - u(t)E(s)]y_1(t) &= B(s)u(t) \\ y_1(t) &= \frac{B(s)}{[A(s) - u(t)E(s)]}u(t) \end{aligned} \quad (2.22)$$

and defining the input dependent polynomial as

$$A(s, u(t)) = A(s) - u(t)E(s) \quad (2.23)$$

it follows that

$$y_1(t) = \frac{B(s)}{A(s, u(t))}u(t) \quad (2.24)$$

Note that the individual coefficients of polynomial $A(s, u(t))$ are then $\alpha_i(u(t)) = \alpha_i - \eta_i u(t)$ for $i = 1, \dots, n$. To enhance the readability of the equations the simpler notation is adopted, where the dependence on $u(t)$ is denoted as dependence on t , i.e. $A(s, u(t))$ becomes $A(s, t)$.

It is not possible to fully express the second bilinear model (2.21) in terms of its output, so that only the following transfer function form interpretation is

possible

$$y_2(t) = \frac{\bar{B}(s)}{\bar{A}(s)}u(t) + \frac{\bar{E}(s)}{\bar{A}(s)}\{u(t)y_2(t)\} \quad (2.25)$$

Premise: It will now to be shown, that if the parameters of the first and second bilinear models (2.20) and (2.21) are selected accordingly

$$\begin{aligned} \bar{A}(s) &= A(s) \\ \bar{B}(s) &= k\bar{E}(s) = kE(s) = B(s) \\ \bar{E}(s) &= E(s) \end{aligned} \quad (2.26)$$

then $y_1(t) = y_2(t)$ for a given input signal $u(t)$. The two models share the same parameters and the roots of the polynomials $E(s)$ and $B(s)$ are identical. The variable k denotes a real number valued gain (a scaling factor). Consequently, whilst the parametric values of polynomials $E(s)$ and $B(s)$ may differ, the roots will be the same. Equating output signals $y_1(t)$ and $y_2(t)$, implies substituting output $y_1(t)$ for the output $y_2(t)$ in (2.25), hence

$$\frac{B(s)}{A(s,t)}u(t) = \frac{\bar{B}(s)}{\bar{A}(s)}u(t) + \frac{\bar{E}(s)}{\bar{A}(s)}\left\{u(t)\frac{B(s)}{A(s,t)}u(t)\right\} \quad (2.27)$$

In order for the above equation to hold, the right hand side expression must reduce to the left hand side expression. Therefore, considering the premise and the relationship given in (2.26) and re-expressing (2.27) in terms of $A(s)$, $E(s)$ and $kE(s)$ only, gives

$$\frac{kE(s)}{A(s,t)}u(t) = \frac{kE(s)}{A(s)}u(t) + \frac{E(s)}{A(s)}\left\{u(t)\frac{kE(s)}{A(s,t)}u(t)\right\} \quad (2.28)$$

$$\frac{kE(s)}{A(s,t)}u(t) = \frac{E(s)}{A(s)}\left\{ku(t) + u(t)\frac{kE(s)}{A(s,t)}u(t)\right\} \quad (2.29)$$

Filtering the input signal $u(t)$ through an autoregressive process $1/A(s,t)$ and then through an inverse $A(s,t)$ of this process gives back the original signal $u(t)$. This can be written such that

$$u(t) = A(s,t)\frac{1}{A(s,t)}u(t) \quad (2.30)$$

Substituting (2.30) for the first appearing $u(t)$ on the right hand side of (2.29)

gives

$$\frac{kE(s)}{A(s,t)}u(t) = \frac{E(s)}{A(s)} \left\{ kA(s,t) \frac{1}{A(s,t)}u(t) + u(t) \frac{kE(s)}{A(s,t)}u(t) \right\} \quad (2.31)$$

and expanding the input dependent polynomial $A(s,t)$ according to (2.23) leads to

$$\frac{kE(s)}{A(s,t)}u(t) = \frac{E(s)}{A(s)} \left\{ k[A(s) - u(t)E(s)] \frac{1}{A(s,t)}u(t) + u(t) \frac{kE(s)}{A(s,t)}u(t) \right\} \quad (2.32)$$

The right hand side of (2.32) then simplifies as follows

$$\frac{kE(s)}{A(s,t)}u(t) = \frac{E(s)}{A(s)} \left\{ \left(k[A(s) - u(t)E(s)] + u(t)kE(s) \right) \frac{1}{A(s,t)}u(t) \right\} \quad (2.33)$$

$$\frac{kE(s)}{A(s,t)}u(t) = \frac{E(s)}{A(s)} \left\{ \left(kA(s) - ku(t)E(s) + u(t)kE(s) \right) \frac{1}{A(s,t)}u(t) \right\} \quad (2.34)$$

$$\frac{kE(s)}{A(s,t)}u(t) = \frac{E(s)}{A(s)} \left\{ kA(s) \frac{1}{A(s,t)}u(t) \right\} \quad (2.35)$$

$$= \frac{kE(s)}{A(s,t)}u(t) \quad (2.36)$$

as required. Equation (2.36) shows that for a given input signal $u(t)$, the two considered bilinear models generate the same outputs, subject to the selected parameter set, defined in (2.26).

To further highlight that the chosen second bilinear model (2.21) is able to emulate the first bilinear model (2.20), it is observed that these differ in the structure of their last nonlinear (bilinear) terms only. Therefore, one nonlinear term must be a subset of the other term, so that for the selected parameter set (2.26) the two models are identical, cf. (2.36). The nonlinear term of the second bilinear model (2.21), i.e.

$$\sum_{i=1}^n \eta_i s^{n-i} \{u(t)y(t)\} \quad (2.37)$$

is expanded using the differentiation product rule. The nonlinear terms associated with the individual parameters η_i , for $i = n, n-1, \dots, 1$, are then stacked in a Pascal triangle-like form. Hence for the case $n = 4$, and without loss of generality,

it may be deduced that

$$\begin{array}{rcl}
 & & \eta_n : \quad u(t)y(t) \\
 & & \eta_{n-1} : \quad u^{(1)}(t)y(t) \quad u(t)y^{(1)}(t) \\
 & & \eta_{n-2} : \quad u^{(2)}(t)y(t) \quad 2u^{(1)}(t)y^{(1)}(t) \quad u(t)y^{(2)}(t) \\
 \eta_{n-3} : & & u^{(3)}(t)y(t) \quad 3u^{(2)}(t)y^{(1)}(t) \quad 3u^{(1)}(t)y^{(2)}(t) \quad u(t)y^{(3)}(t) \\
 & & \vdots
 \end{array}$$

From which it is noted that the terms encircled by the dashed black line correspond exactly to the four bilinear terms of the first bilinear model (2.20), i.e

$$u(t) \sum_{i=n-3}^n \eta_i s^{n-i} y(t) \quad (2.38)$$

2.3.3 Numerical study

Under the parametric constraints stated in the premise and the relation (2.26), the outputs of the two considered bilinear models are simulated and compared. The first bilinear model is simulated according to

$$y_1(t) = \frac{B(s)}{A(s, t)} u(t) \quad (2.39)$$

with the input dependent polynomial $A(s, t)$ defined in (2.23). The second bilinear model is simulated according to

$$y_2(t) = \frac{B(s)}{A(s)} u(t) + \frac{E(s)}{A(s)} \{u(t)y_2(t)\} \quad (2.40)$$

Since $B(s) = kE(s)$, equation (2.40) further simplifies to

$$y_2(t) = \frac{E(s)}{A(s)} \{ku(t) + u(t)y_2(t)\} \quad (2.41)$$

which can be viewed as a nonlinear, internal feedback, dynamic model. In this model, the output signal is scaled (multiplied) by the input signal $u(t)$ in the internal feedback path.

The selected model orders are $n = 4$ and $m = 3$, and the chosen model

parameters are

$$A(s) = s^4 + 0.0445s^3 + 6.545 \times 10^{-4}s^2 + 3.485 \times 10^{-6}s + 3.9 \times 10^{-9} \quad (2.42)$$

$$B(s) = 9.75 \times 10^{-3}s^3 + 2.2425 \times 10^{-3}s^2 + 1.6575 \times 10^{-4}s + 3.9 \times 10^{-6} \quad (2.43)$$

$$E(s) = -9.75 \times 10^{-5}s^3 - 2.2425 \times 10^{-5}s^2 - 1.6575 \times 10^{-6}s - 3.9 \times 10^{-8} \quad (2.44)$$

The roots of $A(s)$ are -0.02 , -0.0015 , -0.013 and -0.01 . The roots of $B(s)$ and $E(s)$ are -0.1 , -0.08 and -0.05 . The scaling factor gain k , defined such that $B(s) = kE(s)$, is -100 . Both models, i.e. (2.39) and (2.41), are implemented in the Simulink (software version 2010b) programming environment. The variable-step size Dorman-Price `ode45` numerical solver is selected. When importing sampled input signals to Simulink a function block `from workspace` is used. This function block uses a standard linear Lagrangian interpolation of the signal inter-sample behaviour. The input signals are sampled at 1 [s].

The simulation results are presented in Figure 2.2 for two distinct inputs. The first input is a multi-level stair case signal and the second input is a sinusoidal signal, these are shown in the left and right lower plots of Figure 2.2, respectively. The discrepancy between the simulated outputs $y_1(t)$ and $y_2(t)$, defined as the difference $y_1(t) - y_2(t)$, is shown in the upper plots of Figure 2.2. The observed discrepancy is approximately 10^{-13} . The small, but yet not null, discrepancy is caused by the numerical accuracy limitations of the presented simulation results. Hence this discrepancy is virtually zero indicating that the two simulated output signals do in fact match, which is evident from the middle plots in Figure 2.2.

2.4 Discrete-time bilinear models

There are at least three different ways of obtaining and/or defining a discrete-time bilinear model, which are introduced hereafter. Also, whilst these models are related to each other via the common continuous-time model the different discretisation methods lead to models that are not equivalent.

2.4.1 Exact discretisation

The exact discretisation of continuous-time nonlinear state-space models, e.g. (2.1), is in principle possible although it generally does not lead to useful results in practice (Pearson 1999, p. 13). The common problem is the increase in the

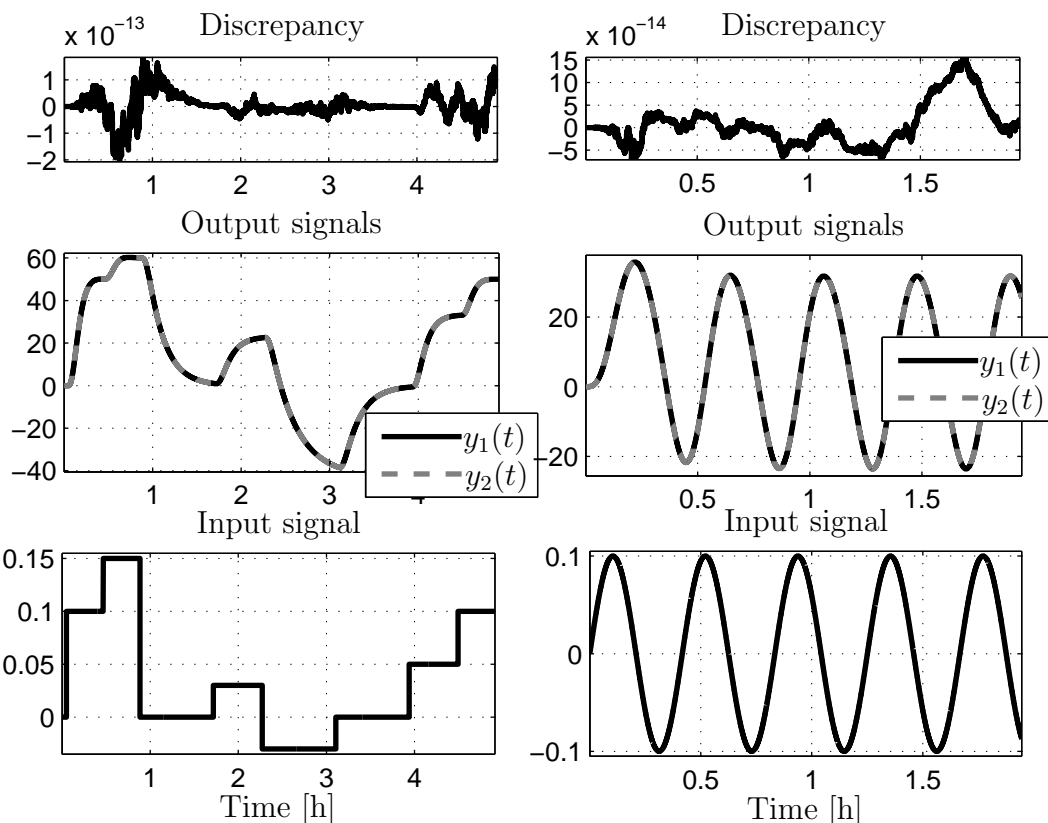


Figure 2.2: Simulation of two bilinear models, having the same constraint parameters (i.e. $B(s) = kE(s)$). Left part of the figure shows simulation results for multi-level stair case input signal, while the right part of the figure considers sinusoidal input signal.

discrete-time model complexity and that the exact discretisation is *not structure preserving* as it would be in the linear case. To illustrate this point, consider the continuous-time bilinear model (2.5) having first order linear dynamics, i.e. $n = 1$ and $m = 0$, hence

$$sy(t) = -\alpha y(t) + \beta u(t) + \eta u(t)y(t) \quad (2.45)$$

Assume uniformly sampled $u(t)$ and $y(t)$ signals at sampling instances $t_k = kh$, where h denotes the sampling interval and k is the integer valued discrete time index, and define the notation $x(k) = x(t_k)$. Now, consider the zero-order-hold assumption on the input signal, i.e. $u(t) = u(k-1)$ for $t_{k-1} \leq t < t_k$, which allows (2.45) to be re-expressed as

$$sy(t) = [-\alpha + \eta u(k-1)]y(t) + \beta u(k-1) \quad (2.46)$$

Given the initial condition $y(t) = y(k-1)$ at $t = t_{k-1}$ the expression (2.46) integrates to (Pearson 2003), i.e.

$$y(k) = \left[y(k-1) + \frac{\beta u(k-1)}{\eta u(k-1) - \alpha} \right] \exp[-(\alpha - \eta u(k-1))h] - \frac{\beta u(k-1)}{\eta u(k-1) - \alpha} \quad (2.47)$$

The following remark clarifies the use of nomenclature for sampled signals.

Remark 2.3 When dealing with purely discrete-time models the nomenclature for a general discrete-time signal is $x(k)$. However, when dealing with models and parameter estimation methods in the continuous-time domain the notation for a sampled general signal is $x(t_k)$. This distinction is preferred in order to emphasize that the original continuous-time signals $x(t)$ are sampled at discrete time instances $t_k = kh$. ■

In the work of (Dunoyer, Balmer, Burnham & James 1997) the structure preserving exact discretisation method for bilinear systems governed by the time-invariant continuous-time model (2.45) has been proposed. Although, the continuous-time model structure is preserved, the parameters of the resulting discrete-time bilinear model are input dependent quantities and the exact solution to the discretisation problem is implicit.

2.4.2 Approximate discretisation

A state-space representation of discrete-time SISO deterministic bilinear model takes the form

$$\mathbf{x}(k+1) = \mathbf{A}_d \mathbf{x}(k) + \mathbf{b}_d u(k) + u(k) \mathbf{N}_d \mathbf{x}(k) \quad (2.48a)$$

$$y(k) = \mathbf{c}_d^T \mathbf{x}(k) \quad (2.48b)$$

The model (2.48) can be obtained from the continuous-time state-space bilinear model (2.1) by adopting the Euler forward approximate difference discretisation method in which the time derivatives are simply replaced by differences, then $\mathbf{A}_d = \mathbf{I} + \mathbf{A}h$, $\mathbf{B}_d = \mathbf{B}h$, $\mathbf{N}_d = \mathbf{N}h$, $\mathbf{c}_d^T = \mathbf{c}^T$. \mathbf{I} is the identity matrix of the same dimension as \mathbf{A} .

It is important to note that albeit the model structure similarity of discrete- and continuous-time state-space models (2.1) and (2.48), respectively, the qualitative behaviour, accuracy and stability of the discrete-time model is sampling

interval dependent. This is, for example, noted by (Ekman 2005) who proposes a new approximate structure preserving discretisation method for bilinear models, which is somewhat less sampling interval dependent.

Again, in a similar manner as highlighted in the continuous-time case, the general discrete-time state-space model (2.48) does not exhibit convenient input-output realisation. This is shown in the following example, which can be found in (Pearson & Kotta 2004).

Example 2.2 Consider the discrete-time state-space model (2.48) with the following matrices

$$\mathbf{A}_d = \begin{bmatrix} 0 & 1 \\ a_1 & a_2 \end{bmatrix}, \quad \mathbf{N}_d = \begin{bmatrix} n_{11} & n_{12} \\ n_{21} & n_{22} \end{bmatrix}, \quad \mathbf{c}_d = \begin{bmatrix} 1 \\ 0 \end{bmatrix}, \quad \mathbf{b}_d = \begin{bmatrix} b_1 \\ b_2 \end{bmatrix} \quad (2.49)$$

having the state vector $\mathbf{x}(k) = [x_1(k) \ x_2(k)]^T$. The state-space model can then be re-expressed as a set of two difference equations, i.e.

$$x_1(k+1) = x_2(k) + b_1 u(k) + u(k)n_{11}x_1(k) + u(k)n_{12}x_2(k) \quad (2.50a)$$

$$x_2(k+1) = a_1 x_1(k) + a_2 x_2(k) + b_2 u(k) + u(k)n_{21}x_1(k) + u(k)n_{22}x_2(k) \quad (2.50b)$$

Noting that $x_1(k) = y(k)$ and $x_1(k+1) = y(k+1)$ equation (2.50a) can be expressed in terms of $x_2(k)$ such that

$$x_2(k) = \frac{y(k+1) - u(k)n_{11}y(k) - b_1 u(k)}{1 + n_{12}u(k)} \quad (2.51)$$

Now, substituting the expression (2.51) into the second equation (2.50b) for $x_2(k)$ leads to the input-output realisation

$$\begin{aligned} y(k) &= [1 + n_{12}u(k-1)] [a_1 y(k-2) + n_{21}y(k-2)u(k-2) + b_2 u(k-2)] \\ &\quad + n_{11}y(k-1)u(k-1) + b_1 u(k-1) + \left[\frac{1 + n_{12}u(k-1)}{1 + n_{12}u(k-2)} \right] \\ &\quad \times [a_2 + n_{22}u(k-2)] [y(k-1) - n_{11}y(k-2)u(k-2) - b_1 u(k-2)] \end{aligned} \quad (2.52)$$

The resulting input-output model representation is a rational nonlinear autoregressive moving average with exogenous input (NARMAX) model structure. ■

2.4.3 Input-output representation

Historically the term ‘bilinear model’ has been defined in the continuous-time state-space framework (Mohler 1973). It has been shown that exact discretisation is not structure preserving and that approximate discretisation is structure preserving; however, the equivalent input-output realisation is open to wide interpretation, see (2.52). Because of this generality some constraints on the model parameters need to be imposed, in a similar manner as in Section 2.2, where a phase variable canonical form of the continuous-time state-space model was considered.

In recognition of the above discretisation issues and the fact that many parameter estimation methods are based directly on input-output model representations the following discrete-time bilinear model is defined

$$A(z^{-1})y(k) = B(z^{-1})u(k) + \sum_{i=1}^n \sum_{j=1}^n c_{i,j}u(k-i)y(k-j) \quad (2.53)$$

with

$$\begin{aligned} A(z^{-1}) &= 1 + a_1z^{-1} + \dots + a_nz^{-n} \\ B(z^{-1}) &= b_1z^{-1} + \dots + b_mz^{-m} \end{aligned}$$

where z^{-1} denotes a backward shift operator defined as $z^{-1}x(k) = x(k-1)$ and $n \geq m$. This model structure is broadly adopted by a number of different authors, see (Pearson 1999, p. 95) and references given therein. Note that the term ‘bilinear model’ is now defined as being linear in both the *system output* and the control input when considered independently, and being bilinear when considered jointly. Although related, the discrete-time input-output bilinear model (2.53) is *not* necessarily equivalent to the discrete-time state-space bilinear model (2.48) in a minimal state-space sense, i.e. controllable and observable realisation. The state-space realisability of input-output bilinear models is analysed in (Baheti, Mohler & Spang 1980, Kotta, Nomn & Zinober 2003, Belikov, Kotta & Kotta 2010).

Since this thesis is primarily concerned with parameter estimation methods making use of the input-output model representation, and since the model (2.53) is flexible enough to approximate the nonlinear phenomena present in HVAC systems, the term ‘discrete-time bilinear model’ as defined by (2.53) is adopted hereandafter unless it is explicitly stated otherwise.

The discrete-time bilinear model (2.53) is further divided into the following distinct subclasses (Pearson 1999, p. 96), i.e.

1. Linear models $c_{i,j} = 0 \forall i, j$
2. Diagonal models $c_{i,j} = 0 \forall i \neq j$
3. Superdiagonal models $c_{i,j} = 0 \forall i > j$
4. Subdiagonal models $c_{i,j} = 0 \forall i < j$

For example the superdiagonal model subclass, when subject to a Gaussian white zero mean input sequence, is capable of localized burst-like (high in output amplitude) behaviour. Such time-series models have been used in the analysis of earthquakes and underground explosions (Pearson 1999). Note, that the subdiagonal and diagonal model subclass would be obtained if the continuous-time bilinear model (2.5) is discretised by the structure preserving Euler forward difference discretisation method.

Remark 2.4 For the purpose of system identification, it is noted that the SISO discrete-time bilinear model can be expressed in a form of multi-input single-output (MISO) linear in structure model. Such a formulation then enables the use of existing, well established, parameter estimation methods developed for linear systems. Since the input-output data are measured, the signal products $y(k-i)u(k-j)$ in (2.53) are known. This allows $n \times n$ additional inputs to be formed, such that

$$u_{i,j}(k) = u(k-i)y(k-j) \quad \text{for } i = 1, \dots, n, \text{ and } j = 1, \dots, n \quad (2.54)$$

Having defined the inputs (2.54), the MISO linear in structure model is then

$$A(z^{-1})y(k) = B(z^{-1})u(k) + \sum_{i=1}^n \sum_{j=1}^n c_{i,j} u_{i,j}(k) \quad (2.55)$$

which can be re-expressed in the following compact transfer function form

$$y(k) = \frac{B(z^{-1})}{A(z^{-1})}u(k) + \sum_{i=1}^n \sum_{j=1}^n \frac{c_{i,j}}{A(z^{-1})}u_{i,j}(k) \quad (2.56)$$

where some $c_{i,j}$ parameters are allowed to be zero. ■

2.5 Definition of Hammerstein-bilinear models

The Hammerstein models are characterised by a memoryless static nonlinear element in series with a linear dynamic submodel (Eskinat et al. 1991). The only nonlinearity is in the steady-state gain and the dynamics is not reference dependent. The notion of a Hammerstein model is extended in this thesis for the bilinear case such that the linear dynamic submodel is replaced by a bilinear model as indicated in Figure 2.3. The system input $u(t)$ is scaled by the nonlinear block $\phi(\cdot)$ and transformed into the intermediate variable $v(t) = \phi(u(t))$, which then effectively acts as the input for the bilinear subsystem (BS) dynamic block. The intermediate input signal $v(t)$ is usually either not available or is unmeasurable in practice. The overall Hammerstein-bilinear model combines the advantages of its constituent submodels and can exhibit both, input dependent dynamic behaviour and increased flexibility of the steady-state characteristic including input multiplicity.

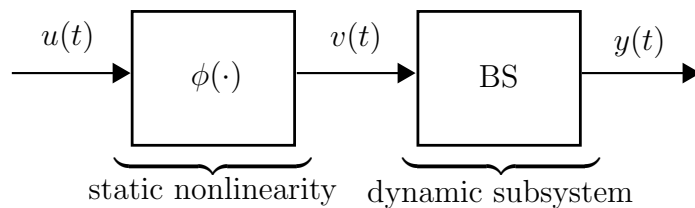


Figure 2.3: Block diagram representation of Hammerstein-bilinear model structure.

2.5.1 Preliminary HVAC system considerations

In the HVAC system application the common sources of the static nonlinearity are variable speed drives, control dampers, fan and pump static characteristic (performance curves) and control/modulating valves (Underwood 1999, Singhal & Salsbury 2007). The control valves are of particular interest here since these components are present in the HVAC system application considered in Chapter 5.

The static relationship between the valve stem position and the flow rate of controlled fluid at constant pressure drop across the valve is termed the *valve inherent characteristic*. The two most commonly encountered characteristics are: linear and equal percentage (Levenmore 2000), which are determined by the valve plug geometry. Whether the linear or equal percentage valve is used depends on

the HVAC application, i.e. the valve purpose. For example, in a central heating application, the valve is designed such that it linearises the relationship between the heat output of the radiator and the hot water flow rate in steady-state. In this way the radiator heat output is linearly proportional to control valve stem movement leading to an easier control problem situation.

The valve modulation causes pressure drops across the valve and also pressure changes in the whole controlled pipe circuit (pipe-work). When the valve is installed the relation between the valve stem position and the flow rate depends on the relation of the pressure drop across the valve to that of the rest of the pipe circuit. The link between the circuit and the valve size is quantitatively expressed by so called valve authority, denoted N_v , see (Levenmore 2000, p. 3-13). The valve inherent characteristic is then modified by the valve authority yielding the *valve installed characteristic*. The valve authority is defined in a range $(0, 1)$, when $N_v = 1$ the inherent and installed characteristics are the same. Figure 2.4 illustrates the shape of linear and equal percentage valve installed characteristics for cases $N_v = 1, 0.1$ and 0.01 . The ideal model of the control valve is provided in Appendix A.1.

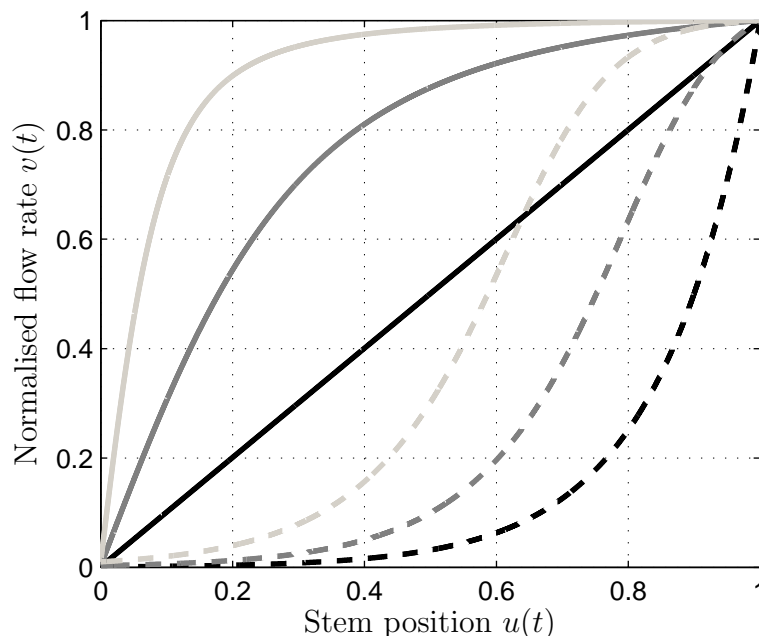


Figure 2.4: Linear (solid lines) and equal percentage (dashed lines) installed valve characteristics for valve authority $N_v = 1$ (black colour), $N_v = 0.1$ (dark grey colour) and $N_v = 0.01$ (light grey colour). The valve leakage (a let-by) is 0.1%.

2.5.2 Hammerstein model parameterization

Appropriate parameterization (approximation) of the static nonlinear function is required during the system identification exercise. Such parameterization should be of low dimension approximating the static nonlinearity well without overfitting (Young 2011, p. 335). There are, however, a number of decisions and compromises which must be made when selecting suitable parameterization.

In the case there is no *a priori* knowledge on the shape of the static nonlinearity it is most straightforward to use a polynomial function

$$v(t) = \phi(u(t)) = p_1u(t) + p_2u^2(t) + \dots + p_ru^r(t) \quad (2.57)$$

where r is the polynomial order and p_i , $i = 1, \dots, r$, are constant parameters. The advantages of using a polynomial function are simplicity, flexibility and also that the function (2.57) is linear in the parameters so that the ordinary linear least squares method can be used to estimate the p_i parameters. The disadvantage of using a polynomial function is that many parameters are required to be estimated. For example, the valve static characteristic is uniquely defined by the single parameter, valve authority N_v , but to model the valve characteristic with the polynomial function at least a third order polynomial is required. This leads to the risks of over parameterization, poorly defined parameter estimates and optimisation convergence issues. Also the information content of the measured input-output data must be sufficient enough throughout the whole intended model operation range otherwise misleading results can be obtained. Such input-output data might be difficult to obtain in practice, especially at the start and end points of the nonlinear functions. Naturally, the estimated polynomial function cannot be used outside the region of operation for which no data were provided during the estimation stage. Another disadvantage of using simple polynomials is the fact that such functions do not level off, i.e. for an input $u(t) = \pm\infty$ the polynomial function goes to $v(t) = \pm\infty$. However, the HVAC component static curves commonly do level off (saturate). Further discussion on parameterization of nonlinear functions can be found in (Beven, Leedal, Smith & Young 2012) together with other possible suitable parameterizations, e.g. sum of radial basis functions.

Some identification methods, such as the state dependent parameter (SDP) estimation method provided in (Young 2011), are able to estimate the shape of the static nonlinearity in a non-parametric manner. When the general shape of the static nonlinear function is known, then appropriate parameterization can

be selected. For example (Taylor, Shaban, Stables & Ako 2007) applied a SDP algorithm in the identification of an axial fan characteristic. The SDP algorithm clearly identified the S-shaped fan characteristic and the following logistic growth like relation has been selected for the final parameterization

$$v(t) = \phi(u(t)) = \frac{p_1}{1 + e^{-p_2(u(t)-p_3)^{1/p_4}}} \quad (2.58)$$

where p_i , $i = 1, \dots, 4$, are constant parameters to be estimated. Note that the function (2.58) is nonlinear with respect to the parameters p_i , so that some suitable optimisation routine together with the initial conditions must be selected in order to estimate the parameters p_i .

In the case where *a priori* knowledge on the shape and nature of the static nonlinearity is available, then such knowledge can be used directly. Such knowledge might be obtained from open loop experiments, engineering knowledge, first principles modelling assumptions or just direct experience. Based on the experience with HVAC systems (Singhal & Salsbury 2007) postulate that following exponential relation

$$v(t) = \phi(u(t)) = \frac{1 - e^{-pu(t)}}{1 - e^{-p}} \quad (2.59)$$

and a series connection of two of such exponential relations is in most cases sufficient. The single exponential relation (2.59) is capable of approximating the linear valve characteristic and a series of two of such relations is capable of approximating the S-shaped equal percentage characteristic, see Figure 2.4, and of course other HVAC components.

2.6 Selected static and dynamic properties

From the versatile application of bilinear models and from the fact that the general continuous-time bilinear models are recognised as being good approximators to a large class of nonlinear systems it can be anticipated that the HB models can exhibit an even richer versatility. As previously indicated, the research into the parameter estimation of these models is narrowed here towards the HVAC application by appropriately selecting the relevant model structures in both, continuous-time and discrete-time domains, i.e. models (2.5) and (2.53). Therefore, the discussion regarding the HB model structure properties is restricted to these particular models only. Furthermore, without loss of generality, only the continuous-time bilinear model is studied in the following discussion and analogous conclusions

could be made if the discrete-time bilinear model had been used instead. The discrete-time case is briefly discussed in (Larkowski & Burnham 2011).

For the sake of clarity the static (memoryless) input nonlinearity is parameterized by polynomial function of order r so that the investigated HB model structure is represented by

$$v(t) = \phi(u(t)) = p_1 u(t) + p_2 u^2(t) + \dots + p_r u^r(t) \quad (2.60a)$$

$$A(s)y(t) = B(s)v(t) + v(t) \sum_{i=1}^n \eta_i s^{n-i} y(t) \quad (2.60b)$$

Due to the close connection of bilinear models to linear models, it is possible to combine the bilinear product terms, in (2.60b), with the polynomial $A(s)$ leading to the linear in structure input dependent time varying differential equation, cf. (2.24), i.e.

$$A(s, t)y(t) = B(s)v(t) \quad (2.61)$$

where the input dependent time varying polynomial $A(s, t)$ is defined as

$$A(s, t) = \left[A(s) - v(t) \sum_{i=1}^n \eta_i s^{n-i} \right] \quad (2.62)$$

The individual coefficients of the polynomial $A(s, t)$ are $\alpha_i(t) = \alpha_i - \eta_i v(t)$ for $i = 1, \dots, n$. Subsequently, the linear time varying differential equation (2.61) can be expressed in the following time-step quasi-linear transfer function form, (Dunoyer 1996), i.e.

$$y(t) = \frac{B(s)}{A(s, t)} v(t) = \frac{\beta_0 s^m + \beta_1 s^{m-1} + \dots + \beta_m}{s^n + \alpha_1(t) s^{n-1} + \dots + \alpha_n(t)} v(t) \quad (2.63)$$

The notion of a transfer function, and the ability to express bilinear models in time-step quasi-linear transfer function form, is used as a basis in the subsequent Chapter 3 devoted to parameter estimation of Hammerstein-bilinear models. It should be noted, however, that expressing the continuous-time nonlinear models in transfer function form should be done with caution and as such should be used only as a stepping stone in the development of the identification approaches. To proceed some remarks on the use of the polynomial $A(s, t)$ are necessary.

Remark 2.5 Because of the time varying nature of the polynomial $A(s, t)$ the rules regarding the manipulation of linear polynomials are no longer valid. The sequence in which the signal $v(t)$ is filtered through the polynomials $B(s)$ and

$1/A(s, t)$ in (2.63) is crucial unlike in the linear case. For example, considering two linear polynomials $A(s)$ and $B(s)$ the following relation holds

$$\frac{1}{A(s)} (B(s)v(t)) = B(s) \left(\frac{1}{A(s)} v(t) \right) \quad (2.64)$$

where the parentheses indicate the filtering order. However, in the nonlinear case the sequence in which the signal $v(t)$ is filtered through $B(s)$ and $1/A(s, t)$, $m < n$ and $m > 0$, is important since these polynomials do not commute; hence in general

$$\frac{1}{A(s, t)} (B(s)v(t)) \neq B(s) \left(\frac{1}{A(s, t)} v(t) \right) \quad (2.65)$$

Note that for the special case $m = 0$ the polynomial $B(s)$ effectively reduces to a gain, i.e. $B(s) = \beta_0$, and the following holds

$$\frac{1}{A(s, t)} (\beta_0 v(t)) = \beta_0 \left(\frac{1}{A(s, t)} v(t) \right) \quad (2.66)$$

since scaling by gain is a memoryless operation.

Considering the implementation of the continuous-time state-space bilinear model provided in Figure 2.1, the correct implementation or use of the time varying transfer function (2.63) is

$$y(t) = B(s) \left(\frac{1}{A(s, t)} v(t) \right) \quad (2.67)$$

A similar observation has been made in (Ekman 2005, p. 89) regarding nonlinear filtering in the discrete-time domain. ■

The dynamic and steady-state behaviour of the HB model is dependent on both the bilinear submodel and the static nonlinearity. To visualise this point consider the time-step quasi-linear transfer function (2.63) interpretation of the bilinear submodel. It is noted, that for different input values the $\alpha_i(t)$ coefficients change leading to different equivalent linear models. Furthermore, since the input $u(t)$ is scaled by the static input nonlinearity $\phi(u(t))$, the input dependent dynamics of the bilinear submodel will also depend on the selection of $\phi(u(t))$. Whereas, the dynamic behaviour of the commonly used Hammerstein models is entirely determined by the dynamic linear submodel.

The overall steady-state characteristic of the HB model is defined by its constituent submodels, i.e. the static nonlinearity transforming the input signal and the bilinear dynamic submodel. With reference to the final value theorem, see

for example (Nise 2008), the steady-state characteristic of the overall HB model is given by

$$y_{ss} = \frac{\beta_m}{\alpha_n - \eta_n \phi(u_{ss})} \phi(u_{ss}) \quad (2.68)$$

where the subscript ss denotes the steady-state value. Knowing the steady-state characteristic allows two important expressions to be calculated, which are namely the steady-state gain, denoted SSG , and the process gain, denoted K . The steady-state gain is defined as the ratio of steady-state output to steady-state input, i.e.

$$SSG = \frac{\beta_m}{\alpha_n - \eta_n \phi(u_{ss})} \frac{\phi(u_{ss})}{u_{ss}} \quad (2.69)$$

where the SSG of the bilinear submodel is $\beta_m / (\alpha_n - \eta_n \phi(u_{ss}))$ and the SSG of the input static nonlinearity is given by $\phi(u_{ss}) / u_{ss}$. The SSG provides more detailed insight into the steady-state properties of the nonlinear system and can be used for the purpose of equipment sizing and the design of system components as well as during the control system design stage. The process gain is defined as the sensitivity of the system output (process variable) to changes in the system input (manipulated variable). Taking the derivative of steady-state characteristic (2.68) with respect to control input u_{ss} leads to

$$K = \frac{\beta_m}{\alpha_n - \eta_n \phi(u_{ss})} \frac{d\phi(u_{ss})}{du_{ss}} + \frac{\beta_m \eta_n \phi(u_{ss})}{(\alpha_n - \eta_n \phi(u_{ss}))^2} \frac{d\phi(u_{ss})}{du_{ss}} \quad (2.70)$$

and the derivative of the input static nonlinearity in this case is

$$\frac{d\phi(u_{ss})}{du_{ss}} = \sum_{k=1}^r k p_k u_{ss}^{k-1} \quad (2.71)$$

The concept of process gain is important in control system design in which the knowledge of the system sensitivity to the applied control signal is essential. Note, that the physical units of the SSG and K can be derived as the ratio of the units of the system output to the system input, respectively. However, the units of the SSG and K will not be stated here, since the units of the considered input-output signals will differ throughout this thesis. Although, the units of the SSG and K are not explicitly provided, by knowing the units of the input-output signals these can always be determined.

The steady-state characteristics (2.68) of the bilinear submodel (2.60b) for different cases of the bilinear term η_n are illustrated in Figure 2.5 for $\alpha_n = 1$ and $\beta_n = 5$. Clearly, if η_n is zero, equation (2.68) represents a linear model, hence

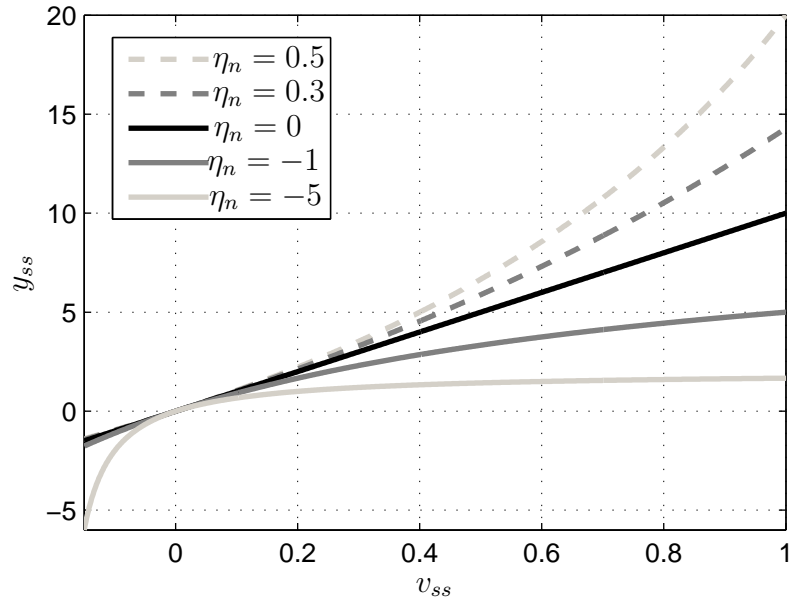


Figure 2.5: Steady-state characteristic of the bilinear submodel for a range of different values of parameter η_n .

linear models may be considered as a special subclass. A consequence of this close relationship between linear and bilinear models is that many techniques developed for linear models can be extended and applied to the bilinear case. Positive values of η_n result in a gain which increases as v_{ss} increases, typical of exothermic chemical processes. Conversely, negative η_n produces a gain, which decreases as v_{ss} increases, leading to eventual saturation, and is typical of many industrial systems. Should a system exhibit bilinear characteristic of the form illustrated in Figure 2.5, then it is pertinent to consider adopting a bilinear systems modelling and control approach.

It can be verified that the horizontal asymptote of the steady-state characteristic, obtained for $v_{ss} \rightarrow \pm\infty$, is given by $-\beta_m/\eta_n$, whilst the vertical asymptote, obtained for $y_{ss} \rightarrow \pm\infty$, is given by $(1 - \alpha_n)/\eta_n$.

The following example illustrates the input dependent steady-state and dynamic behaviour of an exemplary HB model.

Example 2.3 As pointed out in Remark 2.1 a minimal order of the dynamic bilinear submodel is often sufficient in practice. Therefore, consider the following

HB model with first order linear dynamics and a single bilinear term

$$v(t) = p_1 u(t) + p_2 u^2(t) + p_3 u^3(t) + p_4 u^4(t) \quad (2.72a)$$

$$(s + \alpha_1) y(t) = \beta_0 v(t) + \eta_1 v(t) s y(t) \quad (2.72b)$$

where $p_1 = 4.5544$, $p_2 = -17.4851$, $p_3 = 27.0102$, $p_4 = -13.0937$, $\alpha_1 = 0.001$, $\beta_0 = 0.01$ and $\eta_1 = -0.002$. The input static nonlinearity (2.72a) is depicted in the top left quadrant of Figure 2.6 by a solid black line, while the solid grey lines show the case where no static input nonlinearity is considered, i.e. $v(t) = u(t)$, and only the bilinear submodel remains. The steady-state characteristic (2.68) is shown in the top right quadrant of Figure 2.6 and the process gain (2.70) is provided in the left bottom quadrant of Figure 2.6. The dynamic behaviour of the HB model can be, in this case, conveniently expressed by a time constant of the process, denoted T [s]. The time constant is the time it takes for a process to reach approximately 63.2% of its final steady-state value when subject to a step change in the process input, see for example (Nise 2008), and is computed as

$$T = \frac{1}{\alpha_1(t)} = \frac{1}{\alpha_1 - \eta_1 v(t)} \quad (2.73)$$

The process time constant is given in the right bottom quadrant of the Figure 2.6.

In the above example with a negative bilinear parameter η_1 the saturation like behaviour can be observed in Figure 2.6, see top right quadrant. For increasing value of input signal u_{ss} the process gain decreases and eventually saturates. Due to the static input nonlinearity the process gain is not monotonically decreasing, but even increases at value of around $u_{ss} = 0.4$. This is in stark contrast to the behaviour of a purely bilinear model, where the process gain would monotonically decrease as indicated by the grey solid line. With an increasing magnitude of the input signal u_{ss} the time constant decreases and the process dynamics becomes faster. Similarly to the process gain, the value of the time constant is not decreasing monotonically and even increases at a value of around $u_{ss} = 0.4$. ■

Since the dynamics is affected by the input, the stability of Hammerstein-bilinear model is also input dependent. This property is clearly observed in the case of the exemplary model considered (2.72), where for stability it is required that the time varying equivalent ‘linear pole’ remains on the left hand side of the s-plane, i.e. $\alpha_1 - \eta_1 \phi(u(t)) < 0$. This condition implies that the magnitude of the input must be restrained to $\frac{\alpha_1}{\eta_1} < \phi(u(t))$. For the more general higher order

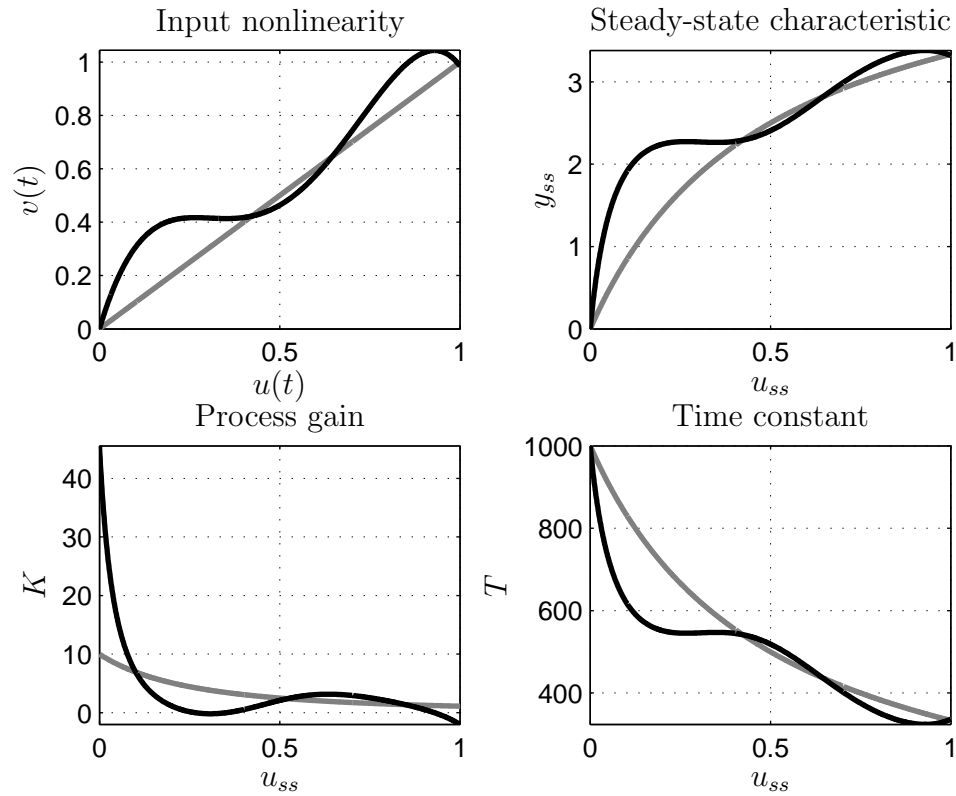


Figure 2.6: The input dependent steady-state and dynamic characteristics of the Hammerstein-bilinear model (solid black line) and purely bilinear model (grey solid line), i.e. $v(t) = u(t)$.

case (2.60) the real part of n time varying (complex) poles must be negative for stability. A detailed discussion on the stability of continuous-time and discrete-time bilinear models is provided in (Pearson 1999, Verdult 2002).

2.7 Conclusions

In this chapter the Hammerstein-bilinear model class has been introduced with relevant examples to HVAC systems. The Hammerstein-bilinear model class has been defined as a cascaded connection of the memoryless static nonlinear element scaling the input of the bilinear dynamic submodel. It has been shown, that the Hammerstein-bilinear model combines the advantages of its constituent submodels and can exhibit both, input dependent dynamic behaviour and increased flexibility of the steady-state characteristic including the input multiplicity. Furthermore, since the input to the bilinear submodel is scaled by the static nonlinear function, the input dependent dynamic behaviour of the bilinear submodel will

also depend on the shape of such static nonlinear function.

A novel observation regarding the relation between two types of continuous-time bilinear model structures has been made. It has been shown that two bilinear model structures are equivalent if the model parameters are constrained in a predefined way. While it is not possible to estimate the model parameters of the first bilinear model structure by existing and well established linear parameter estimation methods, this is, however, possible in the case of the second bilinear model structure due to its close relation to linear models. Therefore, by virtue of estimating the parameters of the second bilinear model structure, the parameters of the first bilinear model are also estimated. This observation, is then greatly exploited by some of the designed continuous-time parameter estimation methods in the subsequent Chapter 3.

Chapter 3

Parameter estimation methods in continuous-time domain

3.1 Introduction

The general system identification procedure, or rather a cycle, consists of stages such as experiment design, optimal system input design, model structure selection including noise model selection, suitable parameterization of static input nonlinearity, model order selection, estimation of effective pure time delay between input and output signals, and, of course, estimation of model parameters (coefficients). The choices regarding a criterion of fit between the measured data and the model and also an actual way of evaluating the resulting models must be also made. The system identification cycle is rather well understood in the case of linear time-invariant discrete-time (Ljung 1999) and continuous-time (Garnier & Wang 2008, Young 2011) dynamic models, but the same cannot be said in the case of nonlinear models. For example, the design of optimally exciting input signal or suitable parameterization of the static input nonlinearity might be a peculiar task in practice and can be solved based on expert knowledge and engineering insight rather than on analytical mathematical tools. This chapter is dedicated to the problem of parameter estimation of linear, bilinear and Hammerstein-bilinear model structures in the continuous-time domain only. Chapter 5, then considers the modelling challenge of the industrial HVAC system, where the complete system identification cycle is treated separately with respect to individual HVAC system components and subsystems.

There are several advantages of using continuous-time models for identification over the discrete-time counterparts and only the most relevant advantages to

subsequent HVAC system analysis are briefly mentioned, for a comprehensive overview see (Rao & Unbehauen 2006, Garnier & Wang 2008, Garnier & Young 2012). In many cases a first principles modelling approach is applicable or the physical phenomena governing the main system dynamics are known and help to suggest the ‘correct’ model structure. The linear and nonlinear continuous-time models then naturally arise from such physical considerations, hence the *a priori* physical knowledge is preserved and incorporated in such a CT model structure. Moreover, in contrast to linear models, the nonlinear (bilinear) models can be discretised only approximately, cf. Subsection 2.4.1. If the original nonlinear model structure is required to be preserved then system identification in the continuous-time domain becomes more of a necessity. In the case when the CT model structure is known, however, and the model parameters are not, then these might be estimated directly from the measured input-output signals, i.e. a grey-box modelling approach. Such parameter estimates are then physically meaningful and can provide further physical insight into the modelled (analysed) system, e.g. detection of fouling in heat exchangers (Jonsson, Lalot, Palsson & Desmet 2007). A very often stated advantage of parameter estimation in the CT domain, over estimation in the discrete-time (DT) domain, is the ability to handle stiff systems, i.e. systems which contain both slow and fast dynamics. An example of a stiff system could be a temperature model of a building comprising the building envelope (walls and insulation) and the air contained within this envelope (Zajic et al. 2012). The thermal capacity of the building envelope is an order of magnitude higher than the thermal capacity of the air. Therefore, it takes considerable more time for the building envelope to change temperature compared to the air leading to presence of two distinct dynamic modes, i.e. slow and fast mode, respectively.

Historically, two main approaches to parameter estimation in the CT domain were devised, which are namely the direct and the indirect approach. The indirect approach involves estimation of the DT model from measured sampled input-output signals first, followed by a transformation to the CT domain. This approach is, however, not necessarily suitable because the benefits of being able to handle stiff systems and structure preservation properties are lost. As the name implies, in the case of the direct approach the CT model is estimated directly, which is the approach taken in this thesis. One of the problems when attempting to directly estimate the CT model is the need for the time derivatives of the input-output signals, which are either not measured for practical reasons or even unobtainable. Various methods have been developed to reconstruct the time

derivatives or transfer the identification problem into a set of known algebraic equations. These methods differ in simplicity of implementation and computation, handling of initial conditions, accuracy, noise filtering properties, or whether the CT model is formulated in a state-space, transfer function (TF) or differential equation form. A survey of parameter estimation methods for linear CT models can be found in (Young 1981) and for linear and nonlinear CT models in (Rao & Unbehauen 2006). The following section briefly summarises popular and/or relevant parameter estimation methods suitable for the bilinear case.

3.1.1 **Dynamic bilinear models**

Karanam, Frick & Mohler (1978) approximate the input-output signals by a series of piecewise constant orthogonal Walls functions, reduce the identification problem to algebraic form and by adopting the integral equation approach to estimate the unknown CT model parameters. Similarly, Berhe & Unbehauen (1998) applied the Hartley modulating functions based method to replace the unknown time derivatives with the known derivatives of the modulating functions. A rather different approach has been devised in (Young, Foster & Lees 1993, Coca & Billings 1999), where the time derivatives are directly computed from the measured (noisy) input-output signals. The method uses a fixed interval smoothing Kalman filter based algorithm and a class of random walk models (Young 2011). The use of state variable filters (SVF) is a classical approach of obtaining time derivatives from measured input-output signals in linear model estimation theory. The input-output signals are filtered through a linear filter or a chain of linear filters so that the filtered time derivatives are generated and used for subsequent parameter estimation. However, in the case of nonlinear models the linear filter does not normally commute, cf. Remark 2.5. Therefore, Kohr (1963) proposed to use so called delayed state variables filters (ideal transport lag device) and Tsang & Billings (1994) further improved the implementation of the delayed SVF.

A computationally straightforward yet powerful and statistically efficient method for parameter estimation of linear DT transfer function models is the simplified refined instrumental variable (SRIV) method and the refined instrumental variable (RIV) method (Young 1976, Young & Jakeman 1979, Jakeman & Young 1979). The SRIV and RIV algorithms and their closely related counterparts for CT model identification (Young & Jakeman 1980, Young et al. 2008), abbreviated SRIVC and RIVC, respectively, create together an unified time domain approach to parameter estimation for linear models. One of the contribu-

tions of this chapter is the proposed extension of the SRIVC algorithm which is capable of estimation of higher order CT bilinear models directly from sampled input-output data, abbreviated BSRIVC. Additionally, based on the special observation, made in Section 2.3, regarding the possibility of expressing SISO CT bilinear model as a TISO CT linear model, the SRIVC algorithm is configured for such a case in Subsection 3.2.1. The *en bloc* solution (non-recursive, single iteration of a batch of data) to SRIVC and BSRIVC algorithms is presented, while its on-line recursive implementation is left for potential future work.

The reviewed and extended SRIVC algorithm is a direct parameter estimation method, which uses sampled (discrete), noisy, input-output signals and is based on the SVF approach. The purpose of the optimally selected SVF is twofold, first, to obtain the filtered unknown time derivatives, second, to noise prefilter the measured input-output signals. In the case of white, zero mean, additive measurement noise with Gaussian amplitude distribution the SRIVC algorithm yields asymptotically unbiased statistically efficient (minimum variance) parameter estimates. Another feature of the SRIVC algorithm is the use of instrumental variables (IV), which together with the optimal prefilters form the core of the algorithm. If it occurs that the noise model assumptions are violated, i.e. the additive noise is not white but coloured (a very real situation in practice), then the SRIVC algorithm is still able to provide consistent and asymptotically unbiased parameter estimates. The optimal CT prefilters are commonly implemented in a digital computer environment, therefore a discrete-time approximation is required. The inherent IV nature of the algorithm helps to attenuate the approximation errors caused by such a digital implementation of the CT optimal prefilters. Additionally, the SRIVC method is known for its rapid convergence properties, see (Liu, Wang & Zheng 2011, Young 2011).

The RIVC method is statistically optimal under the assumption of an autoregressive moving-average (ARMA) additive noise model and is suitable for identification of CT hybrid Box-Jenkins transfer function models (Young et al. 2008). This model is hybrid in the sense that the deterministic part of the model is estimated in the CT domain, while the noise model is estimated in DT domain. The optimal identification of linear and bilinear CT models under the assumption of coloured additive noise, i.e. use of the RIVC method as a core algorithm of the BSRIVC method, is left as an area of further work.

3.1.2 Hammerstein-bilinear models

The methods devoted to parameter estimation of Hammerstein models can be broadly classified into two categories, namely, iterative and noniterative methods, (Eskinat et al. 1991, Janczak 2005). Both methods were originally developed for parameter estimation in the DT domain.

In the case of the input static nonlinearity being parameterized by a linear-in-parameters polynomial-type function, as defined in (2.57), or in general by basis functions with *a priori* known structure, then a well known noniterative over-parameterization method, proposed by Hsia (1968), can be applied. The original SISO bilinear-in-parameters Hammerstein model is converted into a MISO linear-in-parameters auxiliary model, from which the individual parameters of the Hammerstein model are then inferred. In the work of Hsia (1968) the linear transfer function has no zeros, this assumption has been further relaxed in (Chang & Luus 1971). Subsequently, Hsia (1968) proposed a multi-stage noniterative method, which accounts for coloured output noise. Stoica & Söderström (1982) investigate the use of IV methods for identification of Hammerstein models, comment on the selection of persistently exciting input signals, and state the necessary consistency conditions. The input-output signals must be sufficiently informative to encompass the whole operating range. This is addressed in (Barker, Tan & Godfrey 2004), who proposed an optimisation procedure for the design of optimal multi-level input signals.

The need for estimation of Hammerstein models in the CT domain, under realistic noise conditions, has been recognised recently in (Laurian, Gilson, Garnier & Young 2008, Ni, Garnier & Gilson 2012). The authors proposed to use the SRIVC and the RIVC algorithms for the estimation of Hammerstein CT hybrid Box-Jenkins models within the context of the over-parameterization method. Unfortunately, because of the parameter estimates over-parameterization (parameter redundancy) it is not possible to infer the static and dynamic model parameters from the auxiliary model consistently, see e.g. (Young 2011, p. 336). The problem of recovering the individual submodel parameters is further discussed in Chapter 4, where the over-parameterization method is applied in the DT setting.

The iterative backfitting methods are able to overcome such parameter estimate inconsistency by solving for the static and dynamic part of the Hammerstein model separately (Eskinat et al. 1991). Improved accuracy of iterative methods, over noniterative (over-parameterization) methods, has been reported in the works of Gallman (1976) and Le, Markovsky, Freeman & Rogers (2010). The principle of the iterative (relaxation) algorithm, proposed by Narendra & Gall-

man (1966), is based on the following idea: First, suppose the parameters of the static nonlinear block are known, then it is possible to compute the intermediate input to the dynamic submodel and estimate its parameters. Second, knowing the dynamic submodel parameters, compute the refined static nonlinear block parameter estimates and repeat step one and two until convergence occurs. The limitations of such an iterative method are potential convergence problems. The algorithm convergence properties have been examined in (Liu & Bai 2007, Bai & Li 2010).

Two related methods for parameter estimation of CT Hammerstein-bilinear models are proposed and are based on the Narendra & Gallman (1966) iterative algorithm. Both methods postulate that a linear-in-parameters polynomial function of finite order is used to parameterize the static input nonlinear block. The identification algorithm, then exploits this property by separately solving two interconnected least squares problems. Such a method is computationally efficient and it is known in the literature as a bilinear parameterization method (Ljung 1999). The first method is based on the SRIVC algorithm configured for parameter estimation of TISO bilinear models and is abbreviated HSRIVC. The second method, abbreviated HBSRIVC, is based on a more general, earlier proposed, BSIVC algorithm. To date, no work on estimation of Hammerstein and Hammerstein-bilinear models in the CT domain setting, using iterative methods, as presented in this chapter, has been reported/found.

If the static input nonlinearity is characterized by a function, which is nonlinear with respect to its parameters, a closed form solution cannot be formulated and some sort of a constrained nonlinear optimisation routine must be employed. However, it is beyond the scope of the current research to investigate such nonlinear optimisation routines, since their application is case specific and each problem should be treated as such.

3.1.3 Problem formulation

It is assumed that the continuous-time Hammerstein-bilinear model is described by the following single-input single-output differential equation

$$A(s)x(t) = B(s)v(t - \tau) + v(t - \tau) \sum_{i=1}^n \eta_i s^{n-i} x(t) \quad (3.1)$$

where the constant coefficient polynomials $A(s)$ and $B(s)$ of orders n and m , respectively, are defined in (2.5) and repeated below

$$\begin{aligned} A(s) &= s^n + \alpha_1 s^{n-1} + \cdots + \alpha_n \\ B(s) &= \beta_0 s^m + \beta_1 s^{m-1} + \cdots + \beta_m, \quad m < n \end{aligned}$$

The differential equation (3.1) relates the delayed intermediate input $v(t - \tau)$ to the noise-free (unobserved) output $x(t)$; the quantity τ is a pure time (transportation) delay in time units and is assumed to be an integer valued multiple of the sampling time interval, i.e. $\tau = kh$ for $k = 0, 1, 2, \dots$. Note, that some η_i parameters can be set to zero. The model input $u(t)$ is related to intermediate input via a static (memoryless) nonlinear function $v(t) = \phi(u(t))$ characterised by p_i , $i = 1, \dots, r$, parameters. It is assumed that the static input nonlinearity is parameterized by a linear-in-parameters r^{th} order polynomial function, i.e.

$$v(t) = \phi(u(t)) = p_1 u(t) + p_2 u^2(t) + \cdots + p_r u^r(t) \quad (3.2)$$

Next, it is assumed that the input-output signals are uniformly sampled (measured), at sampling time interval h , and the sampled signals are denoted $u(t_k)$ and $y(t_k)$, where $t_k = kh$, cf. Remark 2.3 on nomenclature used. Further, it is assumed that the sampling time interval is sufficiently short to permit CT model identification from sampled input-output signals. The output observation (measurement) equation then takes the following form

$$y(t_k) = x(t_k) + \xi(t_k) \quad (3.3)$$

where $x(t_k)$ is the sampled noise-free output and $y(t_k)$ is the measured output corrupted by an additive measurement noise $\xi(t_k)$. The additive measurement noise is modelled as white, normally distributed, zero mean, uncorrelated sequence denoted $e(t_k)$, i.e. $\xi(t_k) = e(t_k) = \mathcal{N}(0, \sigma_e^2)$, which corresponds to the output error model structure (Ljung 1999). The selection of the additive measurement noise being white is not necessarily a valid assumption in practice, however provided that the identification algorithm is based on an instrumental variables method, then consistent results are still obtained.

The complete parameter estimation problem then consists of the estimation

of an unknown parameter vector, comprising a set of stacked vectors, defined as

$$\boldsymbol{\theta} = \begin{bmatrix} \boldsymbol{\theta}_l \\ \boldsymbol{\theta}_b \\ \boldsymbol{\theta}_n \end{bmatrix} \quad (3.4)$$

based on N uniformly sampled measurements of input-output signals, i.e. data set $Z^N = \{u(t_k), y(t_k)\}_{k=1}^N$. The parameter vector $\boldsymbol{\theta}$ contains parameters corresponding to the linear dynamic part, the bilinear part and the static input nonlinearity of the HB model, which are defined, respectively, as

$$\boldsymbol{\theta}_l = \begin{bmatrix} \alpha_1 & \cdots & \alpha_n & \beta_0 & \cdots & \beta_m \end{bmatrix}^T \quad (3.5a)$$

$$\boldsymbol{\theta}_b = \begin{bmatrix} \eta_1 & \cdots & \eta_m \end{bmatrix}^T \quad (3.5b)$$

$$\boldsymbol{\theta}_n = \begin{bmatrix} p_1 & \cdots & p_r \end{bmatrix}^T \quad (3.5c)$$

The identification problem further consists of model order determination, time delay estimation and selection of appropriate static input parameterization, which is assumed to be known *a priori*. For simplicity, therefore, and without loss of generality the time delay is set to null, i.e. $\tau = 0$, and is ignored in the following sections.

3.2 Simplified refined instrumental variable method

The reviewed iterative SRIVC method is designed for direct parameter estimation of linear time invariant CT models from sampled input-output signals. The CT linear model can be viewed as a subclass of a wider HB model class by setting the parameters associated with the bilinear terms to zero, i.e. $\eta_i = 0$, for $i = 1, \dots, m$, and choosing the static input nonlinearity to be linear with unity gain, i.e. $v(t) = u(t)$, so that the HB model (3.1) reduces to a linear differential equation, hence

$$x^{(n)}(t) + \alpha_1 x^{(n-1)}(t) + \cdots + \alpha_n x^{(0)}(t) = \beta_0 u^{(m)}(t) + \cdots + \beta_m u^{(0)}(t) \quad (3.6)$$

The output observation equation remains the same (3.3); rewriting the expression (3.6) in a compact transfer function form (assuming zero initial conditions) leads

to the overall linear CT TF model

$$x(t) = \frac{B(s)}{A(s)}u(t) \quad (3.7a)$$

$$y(t_k) = x(t_k) + e(t_k) \quad (3.7b)$$

The objective, now, is to estimate the parameter vector $\boldsymbol{\theta}_l$ (3.5a), based on the data set $Z^N = \{u(t_k), y(t_k)\}_{k=1}^N$, despite the unfavourable noise influence.

The first and the most common step towards the estimation of parameter vector $\boldsymbol{\theta}_l$ is to formulate a scalar cost function, denoted V , reflecting the difference between the measured and modelled data, and to minimise this cost function with respect to such an unknown parameter vector, i.e.

$$\hat{\boldsymbol{\theta}}_l = \arg \min_{\boldsymbol{\theta}_l} V(\boldsymbol{\theta}_l) \quad (3.8)$$

The estimate is denoted by a hat and the minimised cost function $V(\boldsymbol{\theta}_l)$ is defined as

$$V(\boldsymbol{\theta}_l) = \sum_{k=1}^N \varepsilon^2(t_k) \quad (3.9)$$

where N denotes the total number of samples, or observations, and $\varepsilon(t_k)$ is an error function at the k^{th} time instant. As pointed out in (Young 1981), it is the particular choice of the error function which distinguishes one estimation methodology from an other. In order to estimate the linear transfer function model (3.7), the straightforward choice of the error function is the difference between the measured and modelled output

$$\varepsilon(t_k) = y(t_k) - \frac{B(s)}{A(s)}u(t_k) \quad (3.10)$$

used by the output error methods (Young 1981). Alternatively, the equation error methods are based on the minimisation of the difference between the measured and one step ahead predicted output, i.e.

$$\varepsilon(t_k) = A(s)y(t_k) - B(s)u(t_k) \quad (3.11)$$

which facilitates the use of the least squares method. Noting the noise model formulation (3.7b) the equation error function (3.11) is then coloured by the

$A(s)$ polynomial such that

$$\varepsilon(t_k) = A(s)y(t_k) - B(s)u(t_k) = A(s)e(t_k) \quad (3.12)$$

It is apparent that such a choice for the error function would induce an asymptotic bias in the parameter estimates, because the equation error function is no longer white and the least squares algorithm performs unsatisfactorily in statistical terms in such a situation. Therefore, similarly to the prediction error method (PEM), the following prefilter is formulated

$$f(s) = \frac{1}{A(s)} \quad (3.13)$$

so that the error function (3.12) now takes the form

$$\varepsilon(t_k) = \frac{1}{A(s)} [A(s)y(t_k) - B(s)u(t_k)] = e(t_k) \quad (3.14)$$

Since, the polynomial operators commute in this linear case it is possible to prefilter signals $y(t_k)$ and $u(t_k)$ first, leading to the desired error function

$$\varepsilon(t_k) = A(s)y_f(t_k) - B(s)u_f(t_k) \quad (3.15)$$

where the subscript f denotes the filtering operation by filter (3.13), hence

$$y_f(t_k) = \frac{1}{A(s)}y(t_k), \quad u_f(t_k) = \frac{1}{A(s)}u(t_k) \quad (3.16)$$

Comparing, the error functions (3.10) and (3.15), it can be noted that these are equivalent. Assuming, that the linear prefilter (3.13) is known prior to the parameter estimation, the use of the error function (3.15) then permits for the direct estimation of the linear TF models by least squares based methods.

Implementation of prefilters (3.16), which are effectively CT linear differential equations, requires selection of a numerical integration method (a solver) with either, fixed, or variable integration step size (discretisation interval). The signal $u(t_k)$ (or $y(t_k)$) is uniformly sampled at sampling time interval h , which is often more coarse than the integration step size. Therefore, the filtering operation (3.16) assumes interpolation of the inter-sample behaviour of $u(t_k)$ (or $y(t_k)$) in some manner, in order to allow for numerical integration. In most cases a zero-order-hold or first-order-hold inter-sample behaviour assumption is sufficient. The filtering operation (3.16) also inherently provides the filtered time derivatives

as the inputs to the integrators in the prefilter, which is shown in Figure 3.1. Therefore, the function of the prefilter $1/A(s)$ is twofold, firstly to filter the noise on the measured signals and pre-whiten them, secondly, the filter acts as a state variable filter and reconstructs the filtered time derivatives from the measured noisy signals.

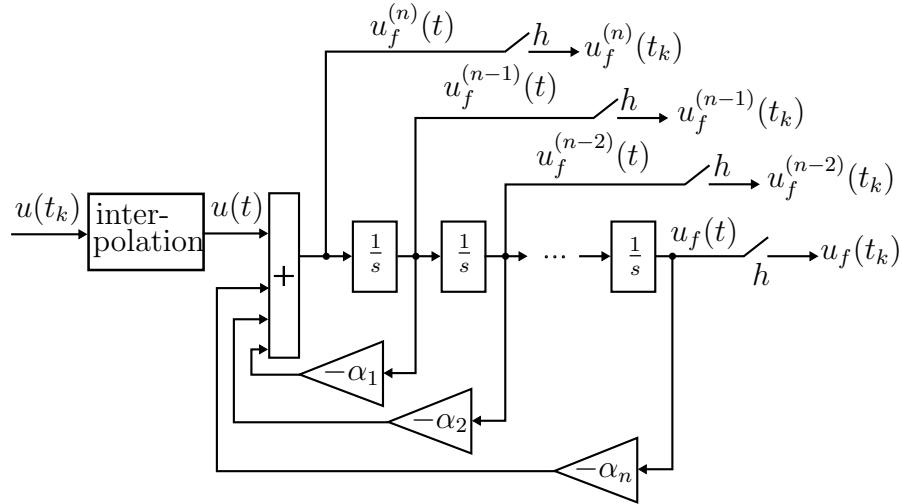


Figure 3.1: Diagrammatic representation of filtering operation $u_f(t_k) = u(t_k)/A(s)$.

In order to obtain the explicit solution for θ_l the equation error (3.15) is formulated in the following pseudo-linear regression form

$$\varepsilon(t_k) = y_f^{(n)}(t_k) - \varphi_f^T(t_k)\theta_l \quad (3.17)$$

$$\varepsilon(t_k) = y_f^{(n)}(t_k) - \hat{y}(\theta_l, t_k) \quad (3.18)$$

where $\hat{y}(\theta_l, t_k)$ denotes the one step ahead prediction of $y_f^{(n)}(t_k)$ and $\varepsilon(t_k)$ is the residual. The parameter vector θ_l is defined in (3.5a), and the regression vector is defined as

$$\varphi_f^T(t_k) = \left[-y_f^{(n-1)}(t_k) \quad \cdots \quad -y_f^{(0)}(t_k) \quad u_f^{(m)}(t_k) \quad \cdots \quad u_f^{(0)}(t_k) \right] \quad (3.19)$$

The IV least squares *en bloc* solution of the optimisation problem (3.8) is then (Young 2011), i.e.

$$\hat{\theta}_l = \left[\sum_{k=1}^N \hat{\varphi}_f(t_k)\varphi_f^T(t_k) \right]^{-1} \sum_{k=1}^N \hat{\varphi}_f^T(t_k)y_f^{(n)}(t_k) \quad (3.20)$$

where $\hat{\varphi}_f(t_k)$ is the prefiltered instrumental variable regression vector and in the

context of the SRIVC method is formulated as follows

$$\hat{\boldsymbol{\varphi}}_f^T(t_k) = \left[-\hat{x}_f^{(n-1)}(t_k) \quad \cdots \quad -\hat{x}_f^{(0)}(t_k) \quad u_f^{(m)}(t_k) \quad \cdots \quad u_f^{(0)}(t_k) \right] \quad (3.21)$$

The instrumental variable vector is a noise free (modelled) version of the regression vector $\boldsymbol{\varphi}_f^T(t_k)$, where the noise free output is generated from the auxiliary model

$$\hat{x}(t_k) = \frac{B(s, \hat{\boldsymbol{\theta}}_l)}{A(s, \hat{\boldsymbol{\theta}}_l)} u(t_k) \quad (3.22)$$

It is noted, that in order to generate (simulate) output $\hat{x}(t_k)$, which is subsequently used by the IV parameter estimator (3.20), the estimated parameter vector $\hat{\boldsymbol{\theta}}_l$ is required to be known first. Similarly, the regression vectors $\boldsymbol{\varphi}_f^T(t_k)$ and $\hat{\boldsymbol{\varphi}}_f^T(t_k)$ consist of filtered time derivatives of the signals $u(t_k)$, $y(t_k)$ and $\hat{x}(t_k)$, where the optimal prefilter (3.13) is not known *a priori* in most practical cases. Therefore, (Young 2011) and references given therein, proposed, the following SRIVC iterative (relaxation) algorithm to overcome this problem.

Algorithm 3.1 (SRIVC).

Stage 1 Initialisation: Compute an initial parameter vector estimate $\hat{\boldsymbol{\theta}}_l^j$, for $j = 0$, where j denotes the iteration number. The IV regression vector is initialised by choosing

$$\hat{\boldsymbol{\varphi}}_f^T(t_k) = \boldsymbol{\varphi}_f^T(t_k)$$

In order to generate filtered time derivatives, select the following state variable filter

$$f(s) = \frac{1}{A(s)} = \frac{1}{(s + \lambda)^n} \quad (3.23)$$

where λ is a single breakpoint frequency parameter and is selected to be larger or equal to the bandwidth of the system to be identified. The implementation of the filter is shown in Figure 3.1.

Stage 2 Iterative IV estimation

for $j = 1 : \text{convergence}$ (see (3.25))

- (1) Generate the instrumental variable series (modelled output) using the auxiliary model (3.22) based on the estimated parameter set

from the previous iteration step $\hat{\boldsymbol{\theta}}_l^{j-1}$, i.e.

$$\hat{x}(t_k) = \frac{B(s, \hat{\boldsymbol{\theta}}_l^{j-1})}{A(s, \hat{\boldsymbol{\theta}}_l^{j-1})} u(t_k)$$

- (2) Generate the filtered time derivatives of signals $y(t_k)$, $u(t_k)$ and $\hat{x}(t_k)$ using the filter $f(s, \hat{\boldsymbol{\theta}}_l^{j-1})$ defined in (3.13), hence

$$f(s, \hat{\boldsymbol{\theta}}_l^{j-1}) = \frac{1}{A(s, \hat{\boldsymbol{\theta}}_l^{j-1})}$$

where the filter is implemented as indicated in Figure 3.1.

- (3) Form the filtered regression vector $\boldsymbol{\varphi}_f^T(t_k)$ and the IV regression vector $\hat{\boldsymbol{\varphi}}_f^T(t_k)$ according to (3.19) and (3.21), respectively, and estimate the latest parameter vector using the *en bloc* IV least squares

$$\hat{\boldsymbol{\theta}}_l^j = \left[\sum_{k=1}^N \hat{\boldsymbol{\varphi}}_f(t_k) \boldsymbol{\varphi}_f^T(t_k) \right]^{-1} \sum_{k=1}^N \hat{\boldsymbol{\varphi}}_f^T(t_k) y_f^{(n)}(t_k)$$

end

Stage 3 Parametric error computation: Compute the estimated parametric error covariance matrix, denoted $\hat{\mathbf{P}}$, associated with the final parameter vector estimate

$$\hat{\mathbf{P}} = \hat{\sigma}_e^2 \left[\sum_{k=1}^N \hat{\boldsymbol{\varphi}}_f(t_k) \hat{\boldsymbol{\varphi}}_f^T(t_k) \right]^{-1} \quad (3.24)$$

where $\hat{\sigma}_e^2$ is the estimated noise variance defined in (3.26).

The Stage 1 of the SRIVC algorithm consists of computing an initial estimate of parameter vector $\hat{\boldsymbol{\theta}}_l^0$, which is then subsequently used in Stage 2. The relatively straightforward state variable filtering technique has been adopted for the purpose of time derivative generation, where the single breakpoint frequency parameter has to be selected based on some *a priori* knowledge. The need for the unknown instrumental variable series $\hat{x}(t_k)$ is avoided by setting $\hat{\boldsymbol{\varphi}}_f^T(t_k) = \boldsymbol{\varphi}_f^T(t_k)$, which leads to a standard least squares solution to optimisation problem (3.8). This particular choice of the state variable filter and IV regression vector may not

provide accurate parameter estimates, however this is not necessarily required at this initial stage. Another option is to identify the system in the discrete-time domain first and convert the resulting DT model into the CT domain, however the advantages of CT parameter estimation are lost; for further discussion see (Young 2011, p. 250) and references given therein.

The parameter vector is estimated in an iterative manner in Stage 2 until satisfactory convergence occurs. The convergence criterion is rather user specific than prescribed. The convergence criterion monitoring the maximum relative improvement of the parameter estimates used in (Liu et al. 2011) is also adopted here

$$\max_i \left| \frac{\hat{\theta}_l^{j+1}(i) - \hat{\theta}_l^j(i)}{\hat{\theta}_l^{j+1}(i)} \right| < \epsilon, \quad \text{for } i = 1, 2, \dots, p \quad (3.25)$$

The number of parameter estimates is denoted p and ϵ is a user specific small number close to zero. Note, that the maximum number of parameter estimates is $n + m + 1$, but some parameters can be set zero. Other choices of the convergence criterion are also possible, such as achieved cost or relative improvement of the difference between the simulated and measured system output.

The final Stage 3 is optional since not in all situations the estimated parametric errors are required to be known. The estimated parametric error covariance matrix $\hat{\mathbf{P}}$ is computed as defined in (3.24), where the estimated noise variance is required. In the case of the output error noise scenario (3.7b) and with reference to the equation error (3.17) expressed in the pseudo-linear regression form the noise variance can be estimated as follows

$$\hat{\sigma}_e^2 = \frac{1}{N - p} \sum_{k=1}^N \left[y_f^{(n)}(t_k) - \boldsymbol{\varphi}_f^T(t_k) \hat{\boldsymbol{\theta}}_l \right]^2 \quad (3.26)$$

where the difference $y_f^{(n)}(t_k) - \boldsymbol{\varphi}_f^T(t_k) \hat{\boldsymbol{\theta}}_l$ is a least squares residual and the final parameter vector estimate is used, i.e. $\hat{\boldsymbol{\theta}}_l = \hat{\boldsymbol{\theta}}_l^j$, $j = \text{end}$. The square root of the diagonal elements of $\hat{\mathbf{P}}$ are then approximately standard errors, denoted SE , associated with the individual estimated parameters, i.e.

$$SE_i = \sqrt{\hat{\mathbf{P}}_{i,i}}, \quad \text{for } i = 1, 2, \dots, p \quad (3.27)$$

3.2.1 SRIVC method configured for bilinear model estimation

The SRIVC algorithm 3.1 is applicable to the parameter estimation problem of a SISO CT bilinear model, which can be interpreted as a TISO CT linear in structure model, under the condition stated in Section 2.3, and repeated below for a white additive noise assumption

$$y(t_k) = \frac{B(s)}{A(s)}u_1(t_k) + \frac{E(s)}{A(s)}u_2(t_k) + e(t_k) \quad (3.28)$$

where the polynomial $E(s)$ is defined as

$$E(s) = \eta_1 s^{n-1} + \dots + \eta_n \quad (3.29)$$

allowing for some η parameters to be zero, so that the order of the polynomial $E(s)$ is the same as the order of the polynomial $B(s)$. The two input signals are formed as $u_1(t_k) = u(t_k)$ and $u_2(t_k) = u(t_k)y(t_k)$, respectively. This concept is illustrated in the following example.

Example 3.1 Consider a bilinear model having first order linear dynamics and one bilinear term, i.e.

$$(s + \alpha_1)x(t) = \beta_0 u(t) + \eta_1 u(t)x(t) \quad (3.30a)$$

$$y(t_k) = x(t_k) + e(t_k) \quad (3.30b)$$

The notation of the noise-free (unobserved) output $x(t)$ and the selection of a white, additive noise model is used in accordance with the problem formulation in Section 3.1.3. Rearranging (3.30a) in terms of the unobserved output $x(t)$, substituting the final expression for $x(t_k)$ in (3.30b) and assuming that the input $u(t_k)$ is uncorrelated with the noise $e(t_k)$, gives

$$(s + \alpha_1)y(t_k) = \beta_0 u(t_k) + \eta_1 u(t_k)y(t_k) + (s + \alpha_1)e(t_k) \quad (3.31)$$

Defining the new input $u_2(t_k) = u(t_k)y(t_k)$ and renaming the input $u(t_k)$ as $u_1(t_k)$, the original SISO bilinear model (3.31) is interpreted as time-invariant TISO linear in structure model, i.e.

$$(s + \alpha_1)y(t_k) = \beta_0 u_1(t_k) + \eta_1 u_2(t_k) + (s + \alpha_1)e(t_k) \quad (3.32)$$

which can be further written in a compact transfer function form as follows

$$y(t_k) = \frac{\beta_0}{s + \alpha_1} u_1(t_k) + \frac{\eta_1}{s + \alpha_1} u_2(t_k) + e(t_k) \quad (3.33)$$

It is thus demonstrated, that the first order linear TF model (3.33) resemble the general, higher order, model (3.28). ■

It is noted, that the second input $u_2(t_k)$, consisting of a product between input $u(t_k)$ and measured output $y(t_k)$, is noise contaminated due to the presence of measurement noise on the output. This in effect creates an *errors-in-variables* identification conceptual scenario, (Larkowski 2009), causing a bias in the parameter estimates. The use of optimal pre-filters helps to attenuate the influence of this input noise on the parameter estimates, see (Young 2011), so that the estimated model may suffice for practical purposes.

In general, it is desirable to avoid such parameter bias induced by measurement noise. In order to do so, the inherent IV feature of the SRIVC method can be extended for the bilinear case, by choosing the regression vector and the IV regression vector to be, respectively,

$$\varphi_f^T(t_k) = \begin{bmatrix} -y_f^{(n-1)}(t_k) & \cdots & -y_f^{(0)}(t_k) & u_{1,f}^{(m)}(t_k) & \cdots & u_{1,f}^{(0)}(t_k) \\ & & & u_{2,f}^{(n-1)}(t_k) & \cdots & u_{2,f}^{(0)}(t_k) \end{bmatrix} \quad (3.34a)$$

$$\hat{\varphi}_f^T(t_k) = \begin{bmatrix} -\hat{x}_f^{(n-1)}(t_k) & \cdots & -\hat{x}_f^{(0)}(t_k) & u_{1,f}^{(m)}(t_k) & \cdots & u_{1,f}^{(0)}(t_k) \\ & & & \hat{u}_{2,f}^{(n-1)}(t_k) & \cdots & \hat{u}_{2,f}^{(0)}(t_k) \end{bmatrix} \quad (3.34b)$$

where

$$\begin{aligned} u_{1,f}^{(i)}(t_k) &= u_f^{(i)}(t_k) && \text{for } i = 0, \dots, m \\ u_{2,f}^{(i)}(t_k) &= \{uy\}_f^{(i)}(t_k) && \text{for } i = 0, \dots, n-1 \\ \hat{u}_{2,f}^{(i)}(t_k) &= \{u\hat{x}\}_f^{(i)}(t_k) && \text{for } i = 0, \dots, n-1 \end{aligned} \quad (3.35)$$

The curly parentheses indicate that the inputs $u_2(t_k)$ and $\hat{u}_2(t_k)$ are formed first and then filtered. In the IV regression vector (3.34b) the measured output is replaced by the simulated output $\hat{x}(t_k)$, including the measured output within the second input. The corresponding estimated parameter set is then defined as

$$\theta_{lb} = \begin{bmatrix} \theta_l \\ \theta_b \end{bmatrix} \quad (3.36)$$

where parameter vector comprises the two sets $\boldsymbol{\theta}_l$ and $\boldsymbol{\theta}_b$ defined in (3.5a) and (3.5b), respectively, stacked in a partitioned vector.

The SRIVC algorithm configured for bilinear model estimation is then implemented in virtually same manner as the SRIVC algorithm 3.1 for linear model estimation, with the following main differences:

- The originally estimated parameter set $\boldsymbol{\theta}_l$ is replaced with $\boldsymbol{\theta}_{lb}$ defined in (3.36).
- In Stage 2, Step 1, the instrumental variable series is generated according to

$$\hat{x}(t_k) = \frac{B(s, \hat{\boldsymbol{\theta}}_{lb}^{j-1})}{A(s, \hat{\boldsymbol{\theta}}_{lb}^{j-1}, t_k)} u(t_k)$$

where $A(s, t_k)$ is defined in (2.62).

- In Stage 2, Step 3, the regression vector $\boldsymbol{\varphi}_f^T(t_k)$ and the IV regression vector are redefined according to (3.34a) and (3.34b), respectively.

3.3 Bilinear SRIVC (BSRIVC) method

In recognition of the need to estimate higher order bilinear models in the continuous-time domain the SRIVC method, which has been originally devised for parameter estimation of linear transfer function models, is extended to the bilinear case. The CT bilinear model can be viewed as a subclass of the wider HB model class by choosing the static input nonlinearity to be linear with unity gain, i.e. $v(t) = u(t)$, so that the HB model (3.1) reduces to a SISO bilinear differential equation

$$A(s)x(t) = B(s)u(t) + u(t) \sum_{i=1}^n \eta_i s^{n-i} x(t) \quad (3.37)$$

and the output observation equation, defined in (3.3), remains the same, hence

$$y(t_k) = x(t_k) + e(t_k) \quad (3.38)$$

The constant coefficient polynomials $A(s)$ and $B(s)$ of orders n and m , respectively, are defined in (2.5). The objective, now, is to estimate the parameter vector comprising the sets $\boldsymbol{\theta}_l$ (3.5a) and $\boldsymbol{\theta}_b$ (3.5b), based on the measured data set $Z^N = \{u(t_k), y(t_k)\}_{k=1}^N$.

Motivated by the TISO linear in structure approach in Subsection 3.2.1, and defining for convenience, and for ease of explanation, $u_1(t) = u(t)$ and $u_{1+i}(t) =$

$u(t)s^{n-i}x(t)$, an equivalent representation of (3.37) becomes

$$\begin{aligned} A(s)x(t) &= B(s)u_1(t) + \eta_i u_{i+1}(t) \\ x(t) &= \frac{B(s)}{A(s)}u_1(t) + \frac{\eta_i}{A(s)}u_{i+1}(t), \quad \text{for } i = 1, \dots, n \end{aligned} \quad (3.39)$$

which may be interpreted as linear in structure MISO representation. (Note, that this convenient notation, i.e. $u_1(t)$ and $u_{1+i}(t)$, will be re-interpreted in subsequent sections.) Based on the experience gained in developing the somewhat restricted TISO approach the aim here is to extend the methodology to develop/configure a SRIVC for the more general (i.e. unrestricted) bilinear case. However, the problem with such an approach is that the higher order time derivatives of the output signal, i.e. $s^{n-i}x(t)$, required to form the inputs $u_{i+1}(t)$, are unknown. It is not possible to generate such output derivatives using the linear prefilter $f(s)$ introduced in (3.13), since the signal $x(t)$ (or its measured counterpart $y(t)$) is an output of nonlinear model, hence the use of linear prefilter would be inadequate.

The proposal developed have to overcome this problem, namely that of obtaining the time derivatives of the nonlinear (bilinear) function, the bilinear model is represented in an alternative SISO time-step quasi-linear transfer function form, see (2.63), hence

$$x(t) = \frac{B(s)}{A(s, t)}u(t) \quad (3.40)$$

with the input dependent polynomial $A(s, t)$ defined as

$$\begin{aligned} A(s, t) &= A(s) - u(t) \sum_{i=1}^n \eta_i s^{n-i} \\ A(s, t) &= s^n + (\alpha_1 - \eta_1 u(t)) s^{n-1} + \dots + (\alpha_n - \eta_n u(t)) \\ A(s, t) &= s^n + \alpha_1(t) s^{n-1} + \dots + \alpha_n(t) \end{aligned} \quad (3.41)$$

where $\alpha_i(t) = \alpha_i - \eta_i u(t)$, for $i = 1, \dots, n$. Following the derivation of the SRIVC algorithm in the preceding Section 3.2 the nonlinear adaptive prefilter is then defined as

$$f(s, t) = \frac{1}{A(s, t)} \quad (3.42)$$

Note, that the prefilter $f(s, t)$ is no longer linear and its special formulation allows the time derivatives of the input-output signals of the bilinear model to be obtained.

Substituting the bilinear model represented in the time-step quasi-linear transfer function form (3.40) into the output observation equation (3.38) and invoking the Remark 2.5 on filtering order, leads to

$$y(t_k) = B(s) \left(\frac{1}{A(s, t_k)} u(t_k) \right) + e(t_k) \quad (3.43)$$

where the parenthesis indicate the filtering order. Noting the selection of the error function $\varepsilon(t_k)$ in (3.14) to be, in fact, the white noise sequence $e(t_k)$, the error function for the bilinear model estimation is derived as follows

$$\begin{aligned} y(t_k) &= B(s) \left(\frac{1}{A(s, t_k)} u(t_k) \right) + e(t_k) \\ e(t_k) &= y(t_k) - B(s) \left(\frac{1}{A(s, t_k)} u(t_k) \right) \\ \varepsilon(t_k) &= y(t_k) - B(s) \left(\frac{1}{A(s, t_k)} u(t_k) \right) \end{aligned} \quad (3.44)$$

In order to obtain the closed form least squares solution to the given parameter estimation problem, re-express the error function $\varepsilon(t_k)$ from its output error formulation into an equation error form, i.e. multiplying both sides of (3.44) by filter $f(s, t_k)$ gives

$$\begin{aligned} \frac{1}{A(s, t_k)} \varepsilon(t_k) &= \frac{1}{A(s, t_k)} \left[y(t_k) - B(s) \left(\frac{1}{A(s, t_k)} u(t_k) \right) \right] \\ \frac{1}{A(s, t_k)} \varepsilon(t_k) &= \frac{1}{A(s, t_k)} y(t_k) - \frac{1}{A(s, t_k)} B(s) \left(\frac{1}{A(s, t_k)} u(t_k) \right) \end{aligned} \quad (3.45)$$

and multiplying both sides of (3.45) by $A(s, t_k)$ leads to the final expression for the error function

$$\begin{aligned} A(s, t_k) \frac{1}{A(s, t_k)} \varepsilon(t_k) &= A(s, t_k) \frac{1}{A(s, t_k)} y(t_k) - A(s, t_k) \frac{1}{A(s, t_k)} B(s) \left(\frac{1}{A(s, t_k)} u(t_k) \right) \\ \varepsilon(t_k) &= A(s, t_k) \frac{1}{A(s, t_k)} y(t_k) - B(s) \left(\frac{1}{A(s, t_k)} u(t_k) \right) \\ \varepsilon(t_k) &= A(s, t_k) y_f(t_k) - B(s) u_f(t_k) \end{aligned} \quad (3.46)$$

where the subscript f denotes the filtering operation by the nonlinear adaptive filter (3.42), hence

$$y_f(t_k) = \frac{1}{A(s, t_k)} y(t_k), \quad u_f(t_k) = \frac{1}{A(s, t_k)} u(t_k) \quad (3.47)$$

cf. (3.16). For brevity, the subscript f denoting the filtering operation is used whether the filter is linear, i.e. $f(s)$, or nonlinear, i.e. $f(s, t_k)$. From this point onward, when the subscript f is used the nonlinear filtering operation is applied unless stated otherwise. Note, that the linear filter is a special case of the nonlinear filter when the parameters associated with the bilinear terms are set to null. The nonlinear filtering operation (3.47) is implemented as shown in Figure 3.2. Finally, it is also noted that although $1/A(s, t_k)$ does not commute with the polynomial $B(s)$ in this nonlinear case, cf. Remark 2.5, it has been possible to apply the nonlinear filtering operation (3.47) and express the error function in an equation error form.

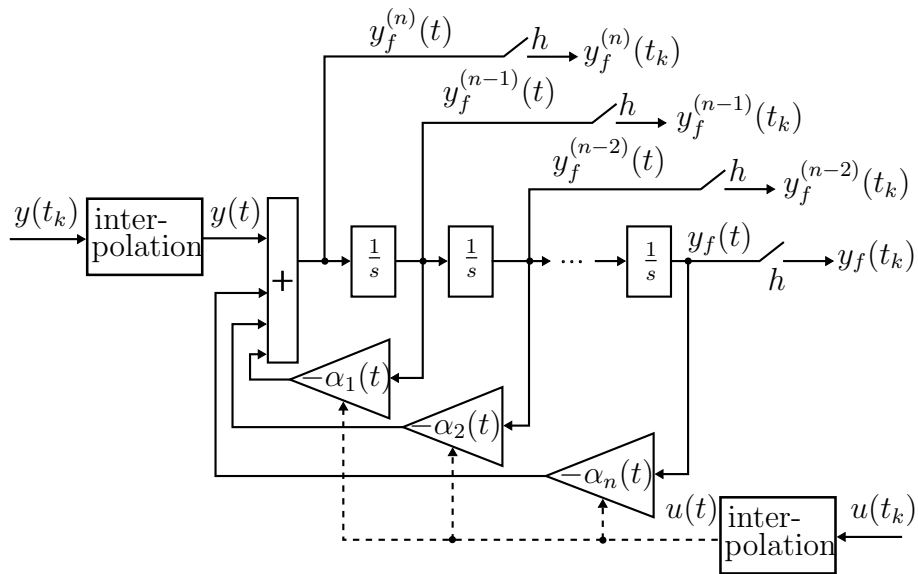


Figure 3.2: Diagrammatic representation of filtering operation $y_f(t_k) = y(t_k)/A(s, t_k)$. The input dependent parameters of polynomial $A(s, t_k)$ are scheduled according to $\alpha_i(t_k) = \alpha_i - \eta_i u(t_k)$, for $i = 1, \dots, n$.

The next step is to express the error function (3.46) in a pseudo-linear regression form so that an IV least squares solution can be obtained, hence equation (3.46) becomes

$$y_f^{(n)}(t_k) = - \sum_{i=1}^n \alpha_i(t_k) y_f^{(n-i)}(t_k) + \sum_{i=0}^m \beta_i u_f^{(m-i)}(t_k) + \varepsilon(t_k) \quad (3.48)$$

and expanding the input dependent parameters $\alpha_i(t_k)$, defined in (3.41) as $\alpha_i(t_k) =$

$\alpha_i - \eta_i u^{(0)}(t_k)$, leads to

$$y_f^{(n)}(t_k) = - \sum_{i=1}^n \alpha_i y_f^{(n-i)}(t_k) + \sum_{i=0}^m \beta_i u_f^{(m-i)}(t_k) + u^{(0)}(t_k) \sum_{i=i}^n \eta_i y_f^{(n-i)}(t_k) + \varepsilon(t_k) \quad (3.49)$$

The above expansion of the $\alpha_i(t_k)$ parameters is a necessary (important) step taken in order to allow for estimation of the η_i parameters, which would otherwise have been ‘hidden’ in the nonlinear prefilter. Note, that the input $u^{(0)}(t_k)$ in the third (bilinear) term is not filtered. Equation (3.49) can be expressed in a more compact vector form by utilising the parameter vector $\boldsymbol{\theta}_{lb}$, defined in (3.36), and regression vector $\boldsymbol{\varphi}_f^T(t_k)$, i.e.

$$\varepsilon(t_k) = y_f^{(n)}(t_k) - \boldsymbol{\varphi}_f^T(t_k) \boldsymbol{\theta}_{lb} \quad (3.50)$$

where the regression vector is defined as

$$\boldsymbol{\varphi}_f^T(t_k) = \begin{bmatrix} -y_f^{(n-1)}(t_k) & \cdots & -y_f^{(0)}(t_k) & u_f^{(m)}(t_k) & \cdots & u_f^{(0)}(t_k) \\ u^{(0)}(t_k) y_f^{(n-1)}(t_k) & \cdots & u^{(0)}(t_k) y_f^{(0)}(t_k) \end{bmatrix} \quad (3.51)$$

and re-introducing the earlier notation, see (3.39), define the inputs $u_1(t_k) = u(t_k)$ and $u_{1+i}(t_k) = u^{(0)}(t_k) y_f^{(n-i)}(t_k)$, for $i = 1, \dots, n$. The regression vector (3.51) can be further expressed in its final form, which resembles the desired MISO linear in structure model interpretation (3.39), i.e.

$$\boldsymbol{\varphi}_f^T(t_k) = \begin{bmatrix} -y_f^{(n-1)}(t_k) & \cdots & -y_f^{(0)}(t_k) & u_{1,f}^{(m)}(t_k) & \cdots & u_{1,f}^{(0)}(t_k) \\ u_2(t_k) & \cdots & u_{1+n}(t_k) \end{bmatrix} \quad (3.52)$$

Recall that the parameter vector $\boldsymbol{\theta}_{lb}$ (3.36) consisting of vectors $\boldsymbol{\theta}_l$ (3.5a) and $\boldsymbol{\theta}_b$ (3.5b) is given by

$$\boldsymbol{\theta}_{lb} = \begin{bmatrix} \boldsymbol{\theta}_l \\ \boldsymbol{\theta}_b \end{bmatrix} \quad (3.53)$$

The IV least squares solution is then similar to (3.20), that is

$$\hat{\boldsymbol{\theta}}_{lb} = \left[\sum_{k=1}^N \hat{\boldsymbol{\varphi}}_f(t_k) \boldsymbol{\varphi}_f^T(t_k) \right]^{-1} \sum_{k=1}^N \hat{\boldsymbol{\varphi}}_f^T(t_k) y_f^{(n)}(t_k) \quad (3.54)$$

where $\hat{\varphi}_f(t_k)$ is the IV regression vector and in the context of the proposed BSRIVC method is formulated as follows

$$\hat{\varphi}_f^T(t_k) = \begin{bmatrix} -\hat{x}_f^{(n-1)}(t_k) & \cdots & -\hat{x}_f^{(0)}(t_k) & u_{1,f}^{(m)}(t_k) & \cdots & u_{1,f}^{(0)}(t_k) \\ & & & \hat{u}_2(t_k) & \cdots & \hat{u}_{1+n}(t_k) \end{bmatrix} \quad (3.55)$$

where $\hat{u}_{1+i}(t_k) = u^{(0)}(t_k)\hat{x}_f^{(n-i)}(t_k)$, for $i = 1, \dots, n$. The IV regression vector is a noise free (modelled) version of the regression vector $\varphi_f^T(t_k)$, where the noise free output is generated from the following auxiliary bilinear model

$$\hat{x}(t_k) = \frac{B(s, \hat{\theta}_{lb})}{A(s, \hat{\theta}_{lb}, t_k)} u(t_k) \quad (3.56)$$

Similarly, as in the case of SRIVC algorithm 3.1, it is noted that in order to generate the instrumental variable series $\hat{x}(t_k)$ and apply the optimal adaptive prefilter (3.42) on signals $u(t_k)$, $y(t_k)$ and $\hat{x}(t_k)$, the estimated parameter vector $\hat{\theta}_{lb}$ is required to be known first. Following the basic SRIVC procedure, it is proposed, therefore, to use the following three stage BSRIVC iterative (relaxation) algorithm to overcome this initialisation problem.

Algorithm 3.2 (BSRIVC).

Stage 1 Initialisation: Compute an initial parameter vector estimate $\hat{\theta}_{lb}^j$, for $j = 0$, where j denotes the iteration number. The IV regression vector is initialised by choosing

$$\hat{\varphi}_f^T(t_k) = \varphi_f^T(t_k)$$

In order to generate filtered time derivatives, select the following (linear) state variable filter

$$f(s, t_k) = \frac{1}{A(s, t_k)} = \frac{1}{(s + \lambda)^n}$$

where λ is a single breakpoint frequency parameter and is selected to be larger or equal to the bandwidth of the system to be identified. The implementation of the filter is shown in Figure 3.2.

Stage 2 Iterative IV estimation

for $j = 1 : \text{convergence}$ (see (3.25) and replace $\hat{\theta}_l$ with $\hat{\theta}_{lb}$)

- (1) Generate the instrumental variable series (modelled output) using the auxiliary model (3.56) based on the estimated parameter vector from the previous iteration step $\hat{\boldsymbol{\theta}}_{lb}^{j-1}$, i.e.

$$\hat{x}(t_k) = \frac{B(s, \hat{\boldsymbol{\theta}}_{lb}^{j-1})}{A(s, \hat{\boldsymbol{\theta}}_{lb}^{j-1}, t_k)} u(t_k)$$

- (2) Generate the filtered time derivatives of signals $y(t_k)$, $u(t_k)$ and $\hat{x}(t_k)$ using the filter $f(s, \hat{\boldsymbol{\theta}}_{lb}^{j-1}, t_k)$ defined in (3.42), hence

$$f(s, \hat{\boldsymbol{\theta}}_{lb}^{j-1}, t_k) = \frac{1}{A(s, \hat{\boldsymbol{\theta}}_{lb}^{j-1}, t_k)}$$

where the filter is implemented as indicated in Figure 3.2.

- (3) Form the filtered regression vector $\boldsymbol{\varphi}_f^T(t_k)$ and the IV regression vector $\hat{\boldsymbol{\varphi}}_f^T(t_k)$ according to (3.52) and (3.55), respectively, and compute the latest parameter vector estimate using the *en bloc* IV least squares

$$\hat{\boldsymbol{\theta}}_{lb}^j = \left[\sum_{k=1}^N \hat{\boldsymbol{\varphi}}_f(t_k) \boldsymbol{\varphi}_f^T(t_k) \right]^{-1} \sum_{k=1}^N \hat{\boldsymbol{\varphi}}_f^T(t_k) y_f^{(n)}(t_k)$$

end

Stage 3 Parametric error computation: Compute the estimated parametric error covariance matrix, denoted $\hat{\mathbf{P}}$, associated with the final parameter vector estimate

$$\hat{\mathbf{P}} = \hat{\sigma}_e^2 \left[\sum_{k=1}^N \hat{\boldsymbol{\varphi}}_f(t_k) \hat{\boldsymbol{\varphi}}_f^T(t_k) \right]^{-1}$$

where $\hat{\sigma}_e^2$ is the estimated noise variance defined in (3.26) with $\hat{\boldsymbol{\theta}}_l = \hat{\boldsymbol{\theta}}_{lb}$ and $p = 2n + m + 1$.

3.3.1 Comments

In Stage 1 the initial estimate of the parameter vector $\hat{\boldsymbol{\theta}}_{lb}^0$ is computed and subsequently used in Stage 2. In order to generate the signal time derivatives the rela-

tively straightforward (linear) state variable filtering technique has been adopted similarly to the SRIVC algorithm 3.1. Therefore, it is assumed that the choice of the pre-filter $f(s, t_k) = 1/A(s, t_k) = 1/A(s)$, i.e. the η_i parameters are initially null, is appropriate despite the fact that the estimated model is bilinear and not linear. In other words, the identified system is assumed to be linear to start with. Such an initial choice of the prefilter may, however, cause convergence problems in Stage 2. While the convergence properties of the SRIVC algorithm are proven in (Liu et al. 2011), the same cannot be stated about the proposed BSRIVC algorithm despite the obvious similarities. The overall estimation problem is indeed nonlinear due to the presence of the input dependent prefilter $f(s, t_k)$ and as in any nonlinear optimisation problem the ‘appropriate’ choice of the initial conditions is important in achieving desired (global) solution.

If the initialisation described in previous paragraph does not yield convergence, it is proposed to estimate a reduced order, auxiliary, bilinear model first, having only a single bilinear term $\eta_n u(t_k)y(t_k)$. The remaining unmodelled bilinear terms are then treated as part of the noise model. To estimate this auxiliary model the SRIVC algorithm 3.1 configured for bilinear model estimation, i.e. the TISO approach, is applied. The application and initialisation of the SRIVC algorithm is more straightforward since the overall estimation problem is linear and less sensitive to the initial choice of the $A(s)$ polynomial used in the prefilter $f(s)$, see (Liu et al. 2011). Subsequently, this model is used to initialise the BSRIVC algorithm.

3.4 Hammerstein-bilinear model estimation

In this section the HBSRIVC and HSRIVC algorithms for parameter estimation of CT HB models are proposed. It is postulated that the static input nonlinearity can be approximated by a linear-in-parameters polynomial of finite order r . The identification algorithm exploits this property by separately solving two interconnected least squares problems in an iterative (backfitting) manner. For convenience, the equations governing the general CT HB model introduced in

(3.2), (3.1) and (3.3) are repeated below

$$v(t) = \phi(u(t)) = \sum_{i=1}^r p_i u^i(t) \quad (3.57a)$$

$$A(s)x(t) = B(s)v(t) + v(t) \sum_{i=1}^n \eta_i s^{n-i} x(t) \quad (3.57b)$$

$$y(t_k) = x(t_k) + e(t_k) \quad (3.57c)$$

The model parameters to be determined are contained in the vector $\boldsymbol{\theta}$ defined as

$$\boldsymbol{\theta} = \begin{bmatrix} \boldsymbol{\theta}_l \\ \boldsymbol{\theta}_b \\ \boldsymbol{\theta}_n \end{bmatrix} = \begin{bmatrix} \boldsymbol{\theta}_{lb} \\ \boldsymbol{\theta}_n \end{bmatrix} \quad (3.58)$$

with $\boldsymbol{\theta}_{lb} = [\boldsymbol{\theta}_l^T \boldsymbol{\theta}_b^T]^T$ and the individual parameter vectors are defined in (3.5). Note, that $\boldsymbol{\theta}$ is divided into two sub-vectors $\boldsymbol{\theta}_{lb}$ and $\boldsymbol{\theta}_n$, respectively, with parameters corresponding to the two component submodels. The overall identification task can be expressed as follows

$$\hat{\boldsymbol{\theta}} = \arg \min_{\boldsymbol{\theta}} V(\boldsymbol{\theta}) \quad (3.59)$$

The estimate is denoted by a hat and the minimised cost function $V(\boldsymbol{\theta})$ is defined as

$$V(\boldsymbol{\theta}) = \sum_{k=1}^N \varepsilon(t_k)^2 = \sum_{k=1}^N [y(t_k) - \hat{y}(\boldsymbol{\theta}, t_k)]^2 \quad (3.60)$$

where N denotes the total number of samples and $\hat{y}(\boldsymbol{\theta}, t_k)$ is the predicted output.

The bilinear parameterization method solves (3.59)-(3.60) in two steps by estimating a minimal number of parameters that defines the HB model. In Step 1, it is postulated that the estimate of the parameters describing the static nonlinear block, $\boldsymbol{\theta}_n$, is available. Thus, by knowing the static nonlinear block parameters it is then possible to compute the intermediate input $v(t)$ and then an estimate of the parameters corresponding to bilinear submodel, $\boldsymbol{\theta}_{lb}$, is sought. This is obtained by solving the following optimisation problem, i.e.

Step 1:

$$\hat{\boldsymbol{\theta}}_{lb}^j = \arg \min_{\boldsymbol{\theta}_{lb}} V_1(\boldsymbol{\theta}_{lb}, \boldsymbol{\theta}_n^{j-1}) \quad (3.61)$$

where

$$V_1(\boldsymbol{\theta}_{lb}, \boldsymbol{\theta}_n^{j-1}) = \sum_{k=1}^N [y(t_k) - \hat{y}(\boldsymbol{\theta}_{lb}, \boldsymbol{\theta}_n^{j-1}, t_k)]^2 \quad (3.62)$$

and j denotes the iteration index. Subsequently, in Step 2 the estimate of $\boldsymbol{\theta}_{lb}$ is set to the value calculated in Step 1 and the estimate of $\boldsymbol{\theta}_n$ is determined from Step 2:

$$\hat{\boldsymbol{\theta}}_n^j = \arg \min_{\boldsymbol{\theta}_n} V_2(\boldsymbol{\theta}_{lb}^j, \boldsymbol{\theta}_n) \quad (3.63)$$

where

$$V_2(\boldsymbol{\theta}_{lb}^j, \boldsymbol{\theta}_n) = \sum_{k=1}^N [y(t_k) - \hat{y}(\boldsymbol{\theta}_{lb}^j, \boldsymbol{\theta}_n, t_k)]^2 \quad (3.64)$$

Next, the iteration index increases, i.e. $j = j + 1$, and the entire scheme is re-iterated until convergence.

Because the optimisation problems in Steps 1 and 2 are both linear with respect to the optimised parameters the corresponding solutions can be obtained in a closed analytical form via a least squares based technique. To solve for the unknown parameter vector $\boldsymbol{\theta}_{lb}$ in Step 1 the BSRIVC algorithm 3.2 is applied. Alternatively, if the SISO bilinear submodel can be formulated as a linear TISO model, under the condition stated in Section 2.3, the SRIVC algorithm can be used instead, as described in Subsection 3.2.1. The actual implementation of the overall estimation scheme differs depending on whether the BSRIVC algorithm or SRIVC algorithm has been used in Step 1, resulting in two distinct, proposed, HBSRIVC and HSRIVC algorithms, respectively.

3.4.1 Hammerstein-bilinear SRIVC (HBSRIVC) method

Considering Step 2, to obtain the estimate of the parameter vector $\boldsymbol{\theta}_n$ the model output must be expressed in a pseudo-linear regression form. Therefore, to start with, use is made of the time varying interpretation of the HB structure, cf. (3.43), i.e.

$$y^{(n)}(t_k) = - \sum_{i=1}^n \alpha_i(t_k) y^{(n-i)}(t_k) + \sum_{i=0}^m \beta_i v^{(m-i)}(t_k) + e(k) \quad (3.65)$$

where $\alpha_i(t_k) = \alpha_i - \eta_i v^{(0)}(t_k)$, for $i = 1, \dots, n$. Because the input-output time derivatives are unknown in (3.65) the filtering operation is applied, cf. (3.48), leading to

$$y_f^{(n)}(t_k) = - \sum_{i=1}^n \alpha_i(t_k) y_f^{(n-i)}(t_k) + \sum_{i=0}^m \beta_i v_f^{(m-i)}(t_k) + \varepsilon(t_k) \quad (3.66)$$

Since the input to the bilinear submodel of the overall HB model is $v(t_k)$ the nonlinear prefilter is defined as

$$f(s, t) = \frac{1}{A(s, t)} \quad (3.67)$$

with the adaptive, intermediate input dependent, polynomial $A(s, t)$ given by

$$\begin{aligned} A(s, t) &= s^n + (\alpha_1 - \eta_1 v(t)) s^{n-1} + \dots + (\alpha_n - \eta_n v(t)) \\ A(s, t) &= s^n + \alpha_1(t) s^{n-1} + \dots + \alpha_n(t) \end{aligned}$$

Comparing the above defined prefilter (3.67) with the prefilter used for the parameter estimation of bilinear models (3.42) the difference is that the input to the bilinear submodel is $v(t_k)$ and not $u(t_k)$, otherwise the functionality of the prefilter remains unchanged. Furthermore, since the prefilter is scheduled by the intermediate input $v(t_k)$, which in turn depends on the shape of the static input nonlinearity, the prefilter performance thus depend not only on the estimate of α_i and η_i , for $i = 1, \dots, n$, but also on the estimate of p_i , for $i = 1, \dots, r$. The prefilter used for the parameter estimation of bilinear models (3.42) can be viewed as a special case of the prefilter (3.67) for $v(t_k) = u(t_k)$, therefore the same notation is adopted for both prefilters.

The following remark clarifies the filtering operation of the intermediate input signal $v(t_k)$ in (3.66).

Remark 3.1 Recalling the definition of the filter $f(s, t)$ in (3.67) and the definition of the static input nonlinearity (3.57a), the following holds

$$v_f(t) = \frac{1}{A(s, t)} v(t) = \frac{1}{A(s, t)} \sum_{l=1}^r p_l u^l(t) \quad (3.68)$$

and it is postulated in Remark 2.5 that the following is true

$$\frac{1}{A(s, t)} \sum_{l=1}^r p_l u^l(t) = \sum_{l=1}^r p_l \left\{ \frac{1}{A(s, t)} u^l(t) \right\} \quad (3.69)$$

In other words, it is possible to filter the individual components of $v(t)$, i.e. powers of input signal $u(t)$, separately as a MISO system, and the weighted sum of these filtered signals is equal to $v_f(t)$. Note, that for clarity in (3.70) the subscript l is used in (3.68) instead of subscript i as originally defined in (3.57a). The individual filtered time derivatives of the intermediate input signal in (3.66) are then obtained from

$$v_f^{(m-i)}(t) = \sum_{l=1}^r p_l \{u^l\}_f^{(m-i)}(t), \quad \text{for } i = 1, \dots, m \quad (3.70)$$

where the curly parenthesis indicate that the filtering operation is performed on the signals $u^l(t)$, for $l = 1, \dots, r$, i.e. the powers of signal $u(t)$. ■

Considering the above Remark 3.1 and substituting the polynomial expression (3.70) for $v_f(t_k)$ in (3.66) gives

$$y_f^{(n)}(t_k) = - \sum_{i=1}^n \alpha_i(t_k) y_f^{(n-i)}(t_k) + \sum_{i=0}^m \beta_i \sum_{l=1}^r p_l \{u^l\}_f^{(m-i)}(t_k) + \varepsilon(t_k) \quad (3.71)$$

which, due to the separability of the MISO structure, can be also expressed as

$$y_f^{(n)}(t_k) = - \sum_{i=1}^n \alpha_i(t_k) y_f^{(n-i)}(t_k) + \sum_{i=1}^r p_i \sum_{l=0}^m \beta_l \{u^i\}_f^{(m-l)}(t_k) + \varepsilon(t_k) \quad (3.72)$$

Rearranging the above expression (3.72) into pseudo-linear regression form leads to

$$\begin{aligned} \varepsilon(t_k) &= y_f^{(n)}(t_k) + \sum_{i=1}^n \alpha_i(t_k) y_f^{(n-i)}(t_k) - \boldsymbol{\varphi}_f^T(t_k) \boldsymbol{\theta}_n \\ \varepsilon(t_k) &= \bar{y}_f(t_k) - \boldsymbol{\varphi}_f^T(t_k) \boldsymbol{\theta}_n \end{aligned} \quad (3.73)$$

where

$$\bar{y}_f(t_k) = y_f^{(n)}(t_k) + \sum_{i=1}^n \alpha_i(t_k) y_f^{(n-i)}(t_k) \quad (3.74)$$

$$\boldsymbol{\varphi}_f^T(t_k) = \left[w_1(t_k) \quad \dots \quad w_r(t_k) \right] \quad (3.75)$$

$$w_i(t_k) = \sum_{l=0}^m \beta_l \{u^i\}_f^{(m-l)}(t_k), \quad \text{for } i = 1, \dots, r \quad (3.76)$$

Subsequently, the least squares *en bloc* solution to the optimisation problem (3.63)

is

$$\hat{\boldsymbol{\theta}}_n = \left[\sum_{k=1}^N \boldsymbol{\varphi}_f(t_k) \boldsymbol{\varphi}_f^T(t_k) \right]^{-1} \sum_{k=1}^N \boldsymbol{\varphi}_f^T(t_k) \bar{y}_f(t_k) \quad (3.77)$$

The newly formulated signals $w_i(t_k)$, $i = 1, \dots, r$, within the regression vector (3.75), are not affected by measurement noise. Therefore, there is no need for use of the instrumental variable method, which leads to the standard least squares solution (3.77) of the optimisation problem (3.63). Note, the presence of intermediate input dependent parameters $\alpha_i(t_k)$ in (3.74), which are given by

$$\alpha_i(t_k) = \alpha_i - \eta_i v^{(0)}(t_k) = \alpha_i - \eta_i \sum_{l=1}^r p_l \{u^l\}^{(0)}(t_k), \quad \text{for } i = 1, \dots, n \quad (3.78)$$

where the dependence of parameters $\alpha_i(t_k)$ on currently estimated parameter set $\hat{\boldsymbol{\theta}}_n$ is clearly evident. In the context of the HBSRIVC algorithm this dependency does not impose any problems since the parameter set $\hat{\boldsymbol{\theta}}_n$ is estimated in an iterative manner so that the most recent estimate is always used, i.e. $\alpha_i(\hat{\boldsymbol{\theta}}_{lb}^j, \hat{\boldsymbol{\theta}}_n^{j-1}, t_k)$.

Having established the core content of the bilinear parameterization method comprising of Steps 1 and 2 the full HBSRIVC iterative algorithm takes the following form:

Algorithm 3.3 (HBSRIVC).

Stage 1 Initialisation: Compute an initial parameter vector estimate $\hat{\boldsymbol{\theta}}_{lb}^j$, for $j = 0$, where j denotes the iteration index. Choose the static input nonlinearity to be linear with unity gain $v(t) = u(t)$, hence setting $\hat{\boldsymbol{\theta}}_n^0 = [1 \ 0 \ \dots \ 0]^T$. The IV regression vector (3.55) is initialised by choosing

$$\hat{\boldsymbol{\varphi}}_f^T(t_k) = \boldsymbol{\varphi}_f^T(t_k)$$

In order to generate filtered time derivatives, select the following (linear) state variable filter

$$f(s, t_k) = \frac{1}{A(s, t_k)} = \frac{1}{(s + \lambda)^n}$$

where λ is a single breakpoint frequency parameter and is selected to be larger or equal to the bandwidth of the system to be identified. The implementation of the filter is shown in Figure 3.2.

Stage 2 Iterative estimation

for $j = 1$: convergence (see (3.80))

(Step 1.a) Knowing the latest estimate of the static input nonlinearity compute the intermediate input to the dynamic submodel

$$v(t_k) = \phi(\hat{\boldsymbol{\theta}}_n^{j-1}, u(t_k)) = \sum_{i=1}^r \hat{\boldsymbol{\theta}}_n^{j-1}(i) u^i(t_k)$$

(Step 1.b) Generate the instrumental variable series using the estimated parameter set from the previous iteration step

$$\hat{x}(t_k) = \frac{B(s, \hat{\boldsymbol{\theta}}_{lb}^{j-1})}{A(s, \hat{\boldsymbol{\theta}}_{lb}^{j-1}, \hat{\boldsymbol{\theta}}_n^{j-1}, t_k)} v(t_k)$$

(Step 1.c) Generate the filtered time derivatives of signals $y(t_k)$, $v(t_k)$ and $\hat{x}(t_k)$ using the filter $f(s, t_k)$ defined in (3.67), i.e.

$$f(s, \hat{\boldsymbol{\theta}}_{lb}^{j-1}, \hat{\boldsymbol{\theta}}_n^{j-1}, t_k) = \frac{1}{A(s, \hat{\boldsymbol{\theta}}_{lb}^{j-1}, \hat{\boldsymbol{\theta}}_n^{j-1}, t_k)}$$

where the filter is implemented as indicated in Figure 3.2 with the scheduling signal being the intermediate input $v(t_k)$ and not $u(t_k)$.

(Step 1.d) Form the filtered regression vector $\boldsymbol{\varphi}_f^T(t_k)$ and the IV regression vector $\hat{\boldsymbol{\varphi}}_f^T(t_k)$ according to (3.52) and (3.55), respectively, in which the input $u(t_k)$ is replaced with the input $v(t_k)$. Compute the latest parameter vector estimate using the *en bloc* IV least squares

$$\hat{\boldsymbol{\theta}}_{lb}^j = \left[\sum_{k=1}^N \hat{\boldsymbol{\varphi}}_f(t_k) \boldsymbol{\varphi}_f^T(t_k) \right]^{-1} \sum_{k=1}^N \hat{\boldsymbol{\varphi}}_f^T(t_k) y_f^{(n)}(t_k)$$

(Step 2.a) Generate the filtered time derivatives of signals $y(t_k)$ and $u^i(t_k)$, for $i = 1, \dots, r$, using the filter $f(s, t_k)$ defined in (3.67), i.e.

$$f(s, \hat{\boldsymbol{\theta}}_{lb}^j, \hat{\boldsymbol{\theta}}_n^{j-1}, t_k) = \frac{1}{A(s, \hat{\boldsymbol{\theta}}_{lb}^j, \hat{\boldsymbol{\theta}}_n^{j-1}, t_k)}$$

(Step 2.b) Form the filtered regression vector $\boldsymbol{\varphi}_f^T(t_k)$ according to (3.75) and form the output $\bar{y}_f(t_k)$ defined in (3.74). Obtain the

latest least squares estimate of the parameter vector $\hat{\boldsymbol{\theta}}_n$

$$\hat{\boldsymbol{\theta}}_n^j = \left[\sum_{k=1}^N \boldsymbol{\varphi}_f(t_k) \boldsymbol{\varphi}_f^T(t_k) \right]^{-1} \sum_{k=1}^N \boldsymbol{\varphi}_f^T(t_k) \bar{y}_f(t_k)$$

end

Stage 3 Parametric error computation: Compute the estimated parametric error covariance matrices denoted $\hat{\mathbf{P}}_{lb}$ and $\hat{\mathbf{P}}_n$ associated with the final parameter vector estimates $\hat{\boldsymbol{\theta}}_{lb}$ and $\hat{\boldsymbol{\theta}}_n$, respectively, hence

$$\hat{\mathbf{P}}_{lb} = \hat{\sigma}_e^2 \left[\sum_{k=1}^N \hat{\boldsymbol{\varphi}}_f(t_k) \hat{\boldsymbol{\varphi}}_f^T(t_k) \right]^{-1} \quad (3.79a)$$

$$\hat{\mathbf{P}}_n = \hat{\sigma}_e^2 \left[\sum_{k=1}^N \boldsymbol{\varphi}_f(t_k) \boldsymbol{\varphi}_f^T(t_k) \right]^{-1} \quad (3.79b)$$

where the appropriate regression vectors $\hat{\boldsymbol{\varphi}}_f(t_k)$ and $\boldsymbol{\varphi}_f(t_k)$ are used as defined in Steps 1 and 2. The estimated noise variances $\hat{\sigma}_e^2$ and $\hat{\sigma}_e^2$ are defined in (3.82a) and (3.82b), respectively.

In Stage 1 the initial estimate of the parameter vector $\hat{\boldsymbol{\theta}}_{lb}^0$ is computed and subsequently used in Stage 2. The parameter set defining the static input non-linearity is initialised with $\hat{\boldsymbol{\theta}}_n^0 = [1 \ 0 \ \dots \ 0]^T$, hence assuming the static input nonlinearity to be linear with unity gain, i.e. $v(t) = u(t)$. In other words, the estimated model is assumed to be purely bilinear to start with. If a more detailed *a priori* knowledge is available this can be used to further refine the initial ‘guess’ of the static input nonlinear function. Note, that the technical documentation of the modelled HVAC system components commonly contains expected static characteristics, hence these can be used in Stage 1.

Similar to the SRIVC and BSRIVC methods the selected convergence criterion adopted is to monitor the maximum relative change of the parameter estimates

$$\max_i \left| \frac{\hat{\boldsymbol{\theta}}^{j+1}(i) - \hat{\boldsymbol{\theta}}^j(i)}{\hat{\boldsymbol{\theta}}^{j+1}(i)} \right| < \epsilon, \quad \text{for } i = 1, 2, \dots, p \quad (3.80)$$

where the parameter vector $\hat{\boldsymbol{\theta}} = \left[\hat{\boldsymbol{\theta}}_{lb}^T \ \hat{\boldsymbol{\theta}}_n^T \right]^T$ is defined in (3.58) and the number of

estimated parameters is $p = 2n + m + r + 1$. Other convergence criterion, which has been found useful in practice, is to monitor the value of the integral of absolute error (or its relative change) between measured and modelled (simulated) system output defined as

$$IAE_j = \frac{1}{N} \sum_{k=1}^N |y(t_k) - \hat{x}(\hat{\boldsymbol{\theta}}^j, t_k)| \quad (3.81)$$

and to choose the estimated parameter vector $\hat{\boldsymbol{\theta}}^j$ corresponding to the minimal value of the computed IAE_j , for $j = 1, \dots, \text{end}$. In the case where the model is intended for simulation purposes the IAE convergence criterion is an appropriate choice, since it reflects ability of the model to simulate measured system output.

Considering the selection of the cost function (3.60), it can be seen that the IAE criterion is not explicitly minimised, when estimating parameter vector $\hat{\boldsymbol{\theta}}$. Based on the experience of the author, it has been noticed, that in some cases the minimal value of IAE criterion can be reached before the maximum relative change of parameter estimates reaches predefined threshold value ϵ . Additionally, when conducting data acquisition experiments on an actual HVAC system, in some instances, the negative effect of slowly acting load disturbances is unavoidable, causing trends in measured data, e.g. due to changes in outdoor air temperature which may cause such trends. It is not necessarily feasible to remove such slow trends from the measured data prior to the parameter estimation exercise, especially in the case of the estimated model being nonlinear. The HBSRIVC algorithm then tends to explain such slow trends by overfitting the estimated static input nonlinearity to the measured data. The IAE convergence criterion has been found to be useful, and perhaps more appropriate, in these instances and returns more realistic static input nonlinearity estimates.

One of the advantages of the developed iterative backfitting HBSRIVC method is the separate estimation of parameter sets $\hat{\boldsymbol{\theta}}_{lb}$ and $\hat{\boldsymbol{\theta}}_n$, this allows for subsequent computation of the standard errors associated with the individual estimated parameter sets. In the case of noniterative over-parameterization methods it is not possible to compute standard errors associated with the $\hat{\boldsymbol{\theta}}_n$ parameter vector and other tools, such as Monte Carlo simulation studies, must be used to recover such standard error estimates, see (Young 2011).

In the final, optional, Stage 3 of the HBSRIVC algorithm the parametric error covariance matrices $\hat{\mathbf{P}}_{lb}$ and $\hat{\mathbf{P}}_n$ are estimated, which can be subsequently used to compute the standard errors associated with the individual estimated parameter sets $\hat{\boldsymbol{\theta}}_{lb}$ and $\hat{\boldsymbol{\theta}}_n$. To compute the covariance matrices $\hat{\mathbf{P}}_{lb}$ and $\hat{\mathbf{P}}_n$, defined in (3.79a) and (3.79b), respectively, the corresponding noise variance estimates must

be computed first, i.e.

$$\hat{\sigma}_e^2 = \frac{1}{N - p_1} \sum_{k=1}^N \left[y_f^{(n)}(t_k) - \boldsymbol{\varphi}_f^T(t_k) \hat{\boldsymbol{\theta}}_{lb} \right]^2 \quad (3.82a)$$

$$\hat{\sigma}_{\bar{e}}^2 = \frac{1}{N - p_2} \sum_{k=1}^N \left[\bar{y}_f(t_k) - \boldsymbol{\varphi}_f^T(t_k) \hat{\boldsymbol{\theta}}_n \right]^2 \quad (3.82b)$$

where the appropriate regression vectors $\boldsymbol{\varphi}_f(t_k)$ are used as defined in Steps 1 and 2 when computing noise variances $\hat{\sigma}_e^2$ and $\hat{\sigma}_{\bar{e}}^2$, respectively. The variable $p_1 = 2n + m + 1$ denotes the number of parameters associated with vector $\hat{\boldsymbol{\theta}}_{lb}$, and $p_2 = r$ is the number of parameters associated with vector $\hat{\boldsymbol{\theta}}_n$. The square roots of the diagonal elements of $\hat{\mathbf{P}}_{lb}$ and $\hat{\mathbf{P}}_n$ are then approximately standard errors associated with the individual estimated parameters, hence

$$SE_i^{lb} = \sqrt{\hat{\mathbf{P}}_{i,i}^{lb}}, \quad \text{for } i = 1, 2, \dots, p_1 \quad (3.83a)$$

$$SE_i^n = \sqrt{\hat{\mathbf{P}}_{i,i}^n}, \quad \text{for } i = 1, 2, \dots, p_2 \quad (3.83b)$$

3.4.2 Constrained HBSRIVC method

The overall steady-state characteristic of the HB model is determined by its constituent submodels, i.e. the static nonlinearity scaling the input signal and the bilinear dynamic submodel. Having the measured input-output data, it is not possible to uniquely distinguish between the contributions of the individual submodels to the overall steady-state characteristic due to the redundancy in the parameters of the static input function. This is shown in the following example.

Example 3.2 Two distinct HB models are considered, which have the same overall steady-state characteristic. The first HB model has first order linear dynamics, a single bilinear term and the static input nonlinearity is parameterized by a linear-in-parameters r^{th} order polynomial function

$$v(t) = \tilde{p}_1 u(t) + \tilde{p}_2 u^2(t) + \dots + \tilde{p}_r u^r(t) \quad (3.84a)$$

$$x^{(1)}(t) = -\alpha_1 x(t) + \beta_0 v(t) + \eta_1 v(t) x^{(1)}(t) \quad (3.84b)$$

where $\tilde{p}_i = p_0 p_i$, for $i = 1, \dots, r$, are polynomial function parameters and p_0 acts

as a scaling gain. The second HB model is defined as

$$v(t) = p_1 u(t) + p_2 u^2(t) + \dots + p_r u^r(t) \quad (3.85a)$$

$$x^{(1)}(t) = -\alpha_1 x(t) + \tilde{\beta}_0 v(t) + \tilde{\eta}_1 v(t) x^{(1)}(t) \quad (3.85b)$$

where $\tilde{\beta}_0 = \beta_0 b_0$ and $\tilde{\eta}_1 = \eta_1 b_0$. Comparing models (3.84) and (3.85) it is clearly evident that the two models perform the same, however the constituent submodel parameters differ. ■

In order to overcome the redundancy in the parameters of the static input function a constrained solution must be sought. A widely adopted approach is to normalise the leading coefficient p_1 in (3.57a) to unity, see e.g. (Eskinat et al. 1991, Laurian et al. 2008). Alternatively, the static input function can be constrained such that $v(t) = u(t)$ for $u(t) = 1$. The static input function, defined in (3.57a), is repeated below for convenience

$$v(t) = p_1 u(t) + p_2 u^2(t) + \dots + p_r u^r(t) \quad (3.86)$$

To satisfy the constraint $v(t) = u(t) = 1$, i.e. substituting number one for $v(t)$ and $u(t)$ in (3.86), leads to

$$1 = p_1 + p_2 + \dots + p_r \quad (3.87)$$

subsequently a decision to constrain parameter p_1 , such that

$$p_1 = 1 - \sum_{i=2}^r p_i \quad (3.88)$$

implies that only parameters p_i , for $i = 2, \dots, r$, need to be estimated. The constrained parameter p_1 is then computed according to (3.88). Substituting (3.88) in the original polynomial function (3.86) gives the final expression for the constrained static nonlinear function

$$v(t) = u(t) + \sum_{i=2}^r p_i [-u(t) + u^i(t)] \quad (3.89)$$

It is convenient to normalise the input signal in the range $\langle 0, 1 \rangle$, where 1 corresponds to a maximal value of input signal $u(t)$. Such normalisation is a common practice in HVAC systems literature, (Underwood 1999), and is also adopted here. In fact it was this normalisation which prompted the idea to constrain the

coefficients as in (3.87), hence $u(t) \in \langle 0, 1 \rangle$. Note, that there is a redundancy in what parameters can be selected and constrained. For example, the parameter p_2 could be chosen instead of parameter p_1 . This leads to different solutions of the constrained estimation problem, and, in practice, to different parameter vector estimates.

Considering Step 2 of the bilinear parameterization method (3.63), in order to obtain the constrained estimate of parameter vector $\boldsymbol{\theta}_n$ the polynomial expression (3.89) is substituted for $v_f(t_k)$ in (3.66)

$$\begin{aligned} y_f^{(n)}(t_k) = & - \sum_{i=1}^n \alpha_i(t_k) y_f^{(n-i)}(t_k) + \sum_{i=0}^m \beta_i u_f^{(m-i)}(t_k) \\ & + \sum_{i=0}^m \beta_i \sum_{l=2}^r p_l \{ -u + u^l \}_f^{(m-i)}(t_k) + \varepsilon(t_k) \end{aligned} \quad (3.90)$$

and rearranging with respect to the p_l parameters gives

$$\begin{aligned} y_f^{(n)}(t_k) = & - \sum_{i=1}^n \alpha_i(t_k) y_f^{(n-i)}(t_k) + \sum_{i=0}^m \beta_i u_f^{(m-i)}(t_k) \\ & + \sum_{i=2}^r p_i \left[- \sum_{l=0}^m \beta_l u_f^{(m-l)}(t_k) + \sum_{l=0}^m \beta_l \{ u^i \}_f^{(m-l)}(t_k) \right] + \varepsilon(t_k) \end{aligned} \quad (3.91)$$

In order to obtain the least squares solution provided in (3.77) the above expression (3.91) is formulated in pseudo-linear regression form

$$\begin{aligned} \varepsilon(t_k) = & y_f^{(n)}(t_k) + \sum_{i=1}^n \alpha_i(t_k) y_f^{(n-i)}(t_k) - \sum_{i=0}^m \beta_i u_f^{(m-i)}(t_k) - \boldsymbol{\varphi}_f^T(t_k) \boldsymbol{\theta}_n \\ \varepsilon(t_k) = & \bar{y}_f(t_k) - \boldsymbol{\varphi}_f^T(t_k) \boldsymbol{\theta}_n \end{aligned} \quad (3.92)$$

where

$$\boldsymbol{\theta}_n = \left[p_2 \quad \cdots \quad p_r \right]^T \quad (3.93)$$

$$\bar{y}_f(t_k) = y_f^{(n)}(t_k) + \sum_{i=1}^n \alpha_i(t_k) y_f^{(n-i)}(t_k) - \sum_{i=0}^m \beta_i u_f^{(m-i)}(t_k) \quad (3.94)$$

$$\boldsymbol{\varphi}_f^T(t_k) = \left[w_2(t_k) \quad \cdots \quad w_r(t_k) \right] \quad (3.95)$$

$$w_i(t_k) = - \sum_{l=0}^m \beta_l u_f^{(m-l)}(t_k) + \sum_{l=0}^m \beta_l \{ u^i \}_f^{(m-l)}(t_k), \quad \text{for } i = 2, \dots, r$$

Note, that only $r - 1$ polynomial function parameters need to be estimated now.

The HBSRIVC algorithm in its constrained form is then implemented in virtually the same manner as the unconstrained HBSRIVC algorithm 3.3 with the following differences:

- In Stage 1 the static input nonlinear function is defined in (3.89) and initialised with $\hat{\boldsymbol{\theta}}_n^0 = [0 \ 0 \ \dots \ 0]^T$.
- Stage 2 in Step (1.a) the intermediate input to the dynamic submodel is computed according to

$$v(t_k) = \phi(\hat{\boldsymbol{\theta}}_n^{j-1}, u(t_k)) = u(t_k) + \sum_{i=2}^r \hat{\boldsymbol{\theta}}_n^{j-1}(i) [-u(t_k) + u^i(t_k)]$$

- Stage 2 in Step (2.b) the filtered regression vector $\boldsymbol{\varphi}_f^T(t_k)$ is defined in (3.95), the output $\bar{y}_f(t_k)$ is defined in (3.94), and the parameter vector $\boldsymbol{\theta}_n$ is redefined according to (3.93).

3.4.3 Hammerstein SRIVC (HSRIVC) method

In the SISO bilinear dynamic model, provided in (3.57b) and repeated below, i.e.

$$A(s)x(t) = B(s)v(t) + v(t) \sum_{i=1}^n \eta_i s^{n-i} x(t) \quad (3.96)$$

the output signal $x(t)$ is unknown and needs to be measured, hence substituting (3.96) for $x(t_k)$ in the output measurement equation (3.57c), and assuming that the noise is uncorrelated with the intermediate input $v(t_k)$, yields

$$A(s)y(t_k) = B(s)v(t_k) + v(t_k) \sum_{i=1}^n \eta_i s^{n-i} y(t_k) + A(s)e(t_k) \quad (3.97)$$

Interpreting the bilinear model (3.97) as a TISO linear dynamic model gives

$$A(s)y(t_k) = B(s)v(t_k) + \sum_{i=1}^n \eta_i \{vy\}^{(n-i)}(t_k) + A(s)e(t_k) \quad (3.98)$$

where the differential operator s is replaced by rounded parenthesis, i.e. $x^{(p)}(t)$ denotes the p^{th} time-derivative of signal $x(t)$, and the curly parenthesis indicate that the differential operator acts on the product of $v(t_k)$ and $y(t_k)$ signals. Noting, the definition of the error function $\varepsilon(t_k)$ in (3.14) and applying the linear

prefilter $f(s)$, defined in (3.13), the above expression may be reexpressed by

$$A(s)y_f(t_k) = B(s)v_f(t_k) + \sum_{i=1}^n \eta_i \{vy\}_f^{(n-i)}(t_k) + \varepsilon(t_k) \quad (3.99)$$

Using summation notation for the $A(s)$ and $B(s)$ polynomials and rearranging leads to

$$\begin{aligned} y_f^{(n)}(t_k) = & - \sum_{i=1}^n \alpha_i y_f^{(n-i)}(t_k) + \sum_{i=0}^m \beta_i v_f^{(m-i)}(t_k) \\ & + \sum_{i=1}^n \eta_i \{vy\}_f^{(n-i)}(t_k) + \varepsilon(t_k) \end{aligned} \quad (3.100)$$

Considering Step 2 of the bilinear parameterization method (3.63), in order to obtain the estimate of the parameter vector $\boldsymbol{\theta}_n$, with reference to Remark 3.1 on filtering operation of the intermediate input, the polynomial function (3.57a) is substituted for $v(t_k)$ in (3.100), hence

$$\begin{aligned} y_f^{(n)}(t_k) = & - \sum_{i=1}^n \alpha_i y_f^{(n-i)}(t_k) + \sum_{i=0}^m \beta_i \sum_{l=1}^r p_l \{u^l\}_f^{(m-i)}(t_k) \\ & + \sum_{i=1}^n \eta_i \sum_{l=1}^r p_l \{u^l y\}_f^{(n-i)}(t_k) + \varepsilon(t_k) \end{aligned} \quad (3.101)$$

Rearranging with respect to the p_l parameters, and changing the subscript l for i , gives

$$\begin{aligned} y_f^{(n)}(t_k) = & \sum_{i=1}^r p_i \left[\sum_{l=0}^m \beta_l \{u^i\}_f^{(m-l)}(t_k) + \sum_{l=1}^n \eta_l \{u^i y\}_f^{(n-l)}(t_k) \right] \\ & - \sum_{i=1}^n \alpha_i y_f^{(n-i)}(t_k) + \varepsilon(t_k) \end{aligned} \quad (3.102)$$

In order to obtain the least squares solution to the optimisation problem stated in (3.63) the above expression (3.102) is formulated in the pseudo-linear regression form

$$\begin{aligned} \varepsilon(t_k) = & y_f^{(n)}(t_k) + \sum_{i=1}^n \alpha_i y_f^{(n-i)}(t_k) - \boldsymbol{\varphi}_f^T(t_k) \boldsymbol{\theta}_n \\ \varepsilon(t_k) = & \bar{y}_f(t_k) - \boldsymbol{\varphi}_f^T(t_k) \boldsymbol{\theta}_n \end{aligned} \quad (3.103)$$

where

$$\bar{y}_f(t_k) = y_f^{(n)}(t_k) + \sum_{i=1}^n \alpha_i y_f^{(n-i)}(t_k) \quad (3.104)$$

$$\varphi_f^T(t_k) = \begin{bmatrix} w_1(t_k) & \cdots & w_r(t_k) \end{bmatrix} \quad (3.105)$$

$$w_i(t_k) = \sum_{l=0}^m \beta_l \{u^i\}_f^{(m-l)}(t_k) + \sum_{l=1}^n \eta_l \{u^i y\}_f^{(n-l)}(t_k), \quad \text{for } i = 1, \dots, r \quad (3.106)$$

and the parameter vector θ_n is defined in (3.5c). The main difference between the error function (3.73) of the HBSRIVC algorithm and the error function (3.103) of the HSRIVC algorithm is the presence of the measured, noise corrupted, output signal $y(t_k)$ in the regression vector (3.106), cf. (3.76). This would inevitably induce bias in parameter estimates. Therefore, the IV least squares solution to the optimisation problem (3.63) is formulated, hence

$$\hat{\theta}_n = \left[\sum_{k=1}^N \hat{\varphi}_f(t_k) \varphi_f^T(t_k) \right]^{-1} \sum_{k=1}^N \hat{\varphi}_f^T(t_k) \bar{y}_f(t_k) \quad (3.107)$$

In accordance with the SRIVC method, the filtered instrumental variable regression vector $\hat{\varphi}_f(t_k)$ is defined as

$$\hat{\varphi}_f(t_k) = \begin{bmatrix} \hat{w}_1(t_k) & \cdots & \hat{w}_r(t_k) \end{bmatrix} \quad (3.108)$$

$$\hat{w}_i(t_k) = \sum_{l=0}^m \beta_l \{u^i\}_f^{(m-l)}(t_k) + \sum_{l=1}^n \eta_l \{u^i \hat{x}\}_f^{(n-l)}(t_k), \quad \text{for } i = 1, \dots, r$$

where $\hat{x}(t_k)$ denotes the noise free simulated output.

Having established the core content of the bilinear parameterization method comprising of Steps 1 and 2 the full HSRIVC iterative algorithm takes the following form:

Algorithm 3.4 (HSRIVC).

Stage 1 Initialisation: Compute an initial parameter vector estimate $\hat{\theta}_{lb}^j$, for $j = 0$, where j denotes the iteration index. Choose the static input function (3.57a) to be linear with unity gain $v(t) = u(t)$, hence setting $\hat{\theta}_n^0 = [1 \ 0 \ \cdots \ 0]^T$. The IV regression vector (3.34) is initialised by

$$\hat{\varphi}_f^T(t_k) = \varphi_f^T(t_k)$$

In order to generate filtered time derivatives, select the following state variable filter

$$f(s) = \frac{1}{A(s)} = \frac{1}{(s + \lambda)^n}$$

where λ is a single breakpoint frequency parameter and is selected to be larger or equal to the bandwidth of the system to be identified. The implementation of the filter is shown in Figure 3.1.

Stage 2 Iterative estimation

for $j = 1$: convergence (see (3.80))

(Step 1.a) Knowing the latest estimate of the static input nonlinearity compute the intermediate input to the dynamic submodel

$$v(t_k) = \phi(\hat{\theta}_n^{j-1}, u(t_k)) = \sum_{i=1}^r \hat{\theta}_n^{j-1}(i) u^i(t_k)$$

(Step 1.b) Generate the instrumental variable series using the estimated parameter set from the previous iteration step

$$\hat{x}(t_k) = \frac{B(s, \hat{\theta}_{lb}^{j-1})}{A(s, \hat{\theta}_{lb}^{j-1}, \hat{\theta}_n^{j-1}, t_k)} v(t_k)$$

(Step 1.c) Generate the filtered time derivatives of signals $y(t_k)$, $\hat{x}(t_k)$. Additionally, generate derivatives of input signals $u_1(t_k)$, $u_2(t_k)$ and $\hat{u}_2(t_k)$, defined in (3.35), in which the input signal $u(t_k)$ is replaced with the intermediate input $v(t_k)$. Use filter $f(s)$ defined in (3.13), i.e.

$$f(s, \hat{\theta}_{lb}^{j-1}) = \frac{1}{A(s, \hat{\theta}_{lb}^{j-1})}$$

where the filter is implemented as indicated in Figure 3.1.

(Step 1.d) Form the filtered regression vector $\varphi_f^T(t_k)$ and the IV regression vector $\hat{\varphi}_f^T(t_k)$ according to (3.34). Compute the latest parameter vector estimate using

$$\hat{\theta}_{lb}^j = \left[\sum_{k=1}^N \hat{\varphi}_f(t_k) \varphi_f^T(t_k) \right]^{-1} \sum_{k=1}^N \hat{\varphi}_f^T(t_k) y_f^{(n)}(t_k)$$

(Step 2.a) Generate the filtered time derivatives of signals $y(t_k)$, $u^i(t_k)$, $\{u^i y\}(t_k)$, $\{u^i \hat{x}\}(t_k)$, for $i = 1, \dots, r$, using updated filter $f(s)$, i.e.

$$f(s, \hat{\theta}_{lb}^j) = \frac{1}{A(s, \hat{\theta}_{lb}^j)}$$

(Step 2.b) Form the filtered regression vectors $\varphi_f^T(t_k)$ and $\hat{\varphi}_f^T(t_k)$ according to (3.105) and (3.108), respectively. Form the output $\bar{y}_f(t_k)$ defined in (3.104). Obtain the latest least squares estimate

$$\hat{\theta}_n^j = \left[\sum_{k=1}^N \hat{\varphi}_f(t_k) \varphi_f^T(t_k) \right]^{-1} \sum_{k=1}^N \hat{\varphi}_f(t_k) \bar{y}_f(t_k)$$

end

Stage 3 Parametric error computation: Compute the estimated parametric error covariance matrices denoted $\hat{\mathbf{P}}_{lb}$ and $\hat{\mathbf{P}}_n$ associated with the final parameter vector estimates $\hat{\theta}_{lb}$ and $\hat{\theta}_n$, respectively, hence

$$\hat{\mathbf{P}}_{lb} = \hat{\sigma}_e^2 \left[\sum_{k=1}^N \hat{\varphi}_f(t_k) \hat{\varphi}_f^T(t_k) \right]^{-1}$$

$$\hat{\mathbf{P}}_n = \hat{\sigma}_e^2 \left[\sum_{k=1}^N \varphi_f(t_k) \varphi_f^T(t_k) \right]^{-1}$$

where the appropriate regression vectors $\hat{\varphi}_f(t_k)$ and $\varphi_f(t_k)$ are used as defined in Steps 1 and 2. The estimated noise variances $\hat{\sigma}_e^2$ and $\hat{\sigma}_e^2$ are defined in (3.82a) and (3.82b), respectively.

3.4.4 Constrained HSRIVC method

Following the same reasoning for imposing constraints on parameters of the static input function (3.57a), stated at the beginning of Subsection 3.4.2, the con-

strained polynomial expression (3.89) is substituted for $v(t_k)$ in (3.100), i.e.

$$\begin{aligned}
 y_f^{(n)}(t_k) = & - \sum_{i=1}^n \alpha_i y_f^{(n-i)}(t_k) + \sum_{i=0}^m \beta_i u_f^{(m-i)}(t_k) + \sum_{i=1}^n \eta_i \{uy\}_f^{(n-i)}(t_k) \\
 & + \sum_{i=0}^m \beta_i \sum_{l=2}^r p_l \{ -u + u^l \}_f^{(m-i)}(t_k) \\
 & + \sum_{i=1}^n \eta_i \sum_{l=2}^r p_l \{ -uy + u^l y \}_f^{(n-i)}(t_k) + \varepsilon(t_k)
 \end{aligned} \tag{3.109}$$

and rearranging with respect to the p_l parameters gives

$$\begin{aligned}
 y_f^{(n)}(t_k) = & - \sum_{i=1}^n \alpha_i y_f^{(n-i)}(t_k) + \sum_{i=0}^m \beta_i \{u\}_f^{(m-i)}(t_k) + \sum_{i=1}^n \eta_i \{uy\}_f^{(n-i)}(t_k) \\
 & + \sum_{i=2}^r p_i \left[- \sum_{l=0}^m \beta_l \{u\}_f^{(m-l)}(t_k) - \sum_{l=1}^n \eta_l \{uy\}_f^{(n-l)}(t_k) \right. \\
 & \left. + \sum_{l=0}^m \beta_l \{u^i\}_f^{(m-l)}(t_k) + \sum_{l=1}^n \eta_l \{u^i y\}_f^{(n-l)}(t_k) \right] + \varepsilon(t_k)
 \end{aligned} \tag{3.110}$$

In order to obtain the least squares solution the above expression (3.102) is then re-written in pseudo-linear regression form, hence

$$\varepsilon(t_k) = \bar{y}_f(t_k) - \boldsymbol{\varphi}_f^T(t_k) \boldsymbol{\theta}_n \tag{3.111}$$

where

$$\boldsymbol{\theta}_n = \left[p_2 \quad \cdots \quad p_r \right]^T \tag{3.112}$$

$$\begin{aligned}
 \bar{y}_f(t_k) = & y_f^{(n)}(t_k) + \sum_{i=1}^n \alpha_i y_f^{(n-i)}(t_k) \\
 & - \sum_{i=0}^m \beta_i \{u\}_f^{(m-i)}(t_k) - \sum_{i=1}^n \eta_i \{uy\}_f^{(n-i)}(t_k)
 \end{aligned} \tag{3.113}$$

$$\boldsymbol{\varphi}_f^T(t_k) = \left[w_2(t_k) \quad \cdots \quad w_r(t_k) \right] \tag{3.114}$$

$$\begin{aligned}
 w_i(t_k) = & - \sum_{l=0}^m \beta_l \{u\}_f^{(m-l)}(t_k) - \sum_{l=1}^n \eta_l \{uy\}_f^{(n-l)}(t_k) \\
 & + \sum_{l=0}^m \beta_l \{u^i\}_f^{(m-l)}(t_k) + \sum_{l=1}^n \eta_l \{u^i y\}_f^{(n-l)}(t_k), \quad \text{for } i = 2, \dots, r
 \end{aligned}$$

Note, that only $r - 1$ polynomial function parameters need to be estimated. Accordingly with HSRIVC algorithm 3.4, the filtered instrumental variable regression vector also needs to be defined, i.e.

$$\begin{aligned} \hat{\boldsymbol{\varphi}}_f(t_k) &= \begin{bmatrix} \hat{w}_2(t_k) & \cdots & \hat{w}_r(t_k) \end{bmatrix} & (3.115) \\ \hat{w}_i(t_k) &= - \sum_{l=0}^m \beta_l \{u\}_f^{(m-l)}(t_k) - \sum_{l=1}^n \eta_l \{u\hat{x}\}_f^{(n-l)}(t_k) \\ &\quad + \sum_{l=0}^m \beta_l \{u^i\}_f^{(m-l)}(t_k) + \sum_{l=1}^n \eta_l \{u^i\hat{x}\}_f^{(n-l)}(t_k), \quad \text{for } i = 2, \dots, r \end{aligned}$$

where the noise contaminated output $y(t_k)$ is replaced with the simulated output $\hat{x}(t_k)$.

The constrained HSRIVC algorithm is then implemented in virtually the same way as the unconstrained HSRIVC algorithm 3.4 with the following differences:

- In Stage 1 the static input nonlinear function is defined in (3.89) and initialised with $\hat{\boldsymbol{\theta}}_n^0 = [0 \ 0 \ \cdots \ 0]^T$.
- Stage 2, Step (1.a), the intermediate input to the dynamic submodel is computed according to

$$v(t_k) = \phi(\hat{\boldsymbol{\theta}}_n^{j-1}, u(t_k)) = u(t_k) + \sum_{i=2}^r \hat{\boldsymbol{\theta}}_n^{j-1}(i) [-u(t_k) + u^i(t_k)]$$

- Stage 2, Step (2.b), the filtered regression vector $\boldsymbol{\varphi}_f^T(t_k)$ is newly defined in (3.114), IV regression vector in (3.115), the output $\bar{y}_f(t_k)$ is defined in (3.113), and the parameter vector $\boldsymbol{\theta}_n$ is redefined according to (3.112).

3.4.5 Comments

The HBSRIVC algorithm has been created for parameter estimation of Hammerstein-bilinear models, however by setting parameters associated with the bilinear terms to zero, i.e. $\eta_i = 0$, for $i = 1, \dots, n$, and/or not considering the static input non-linearity, i.e. $v(t) = u(t)$, the HBSRIVC algorithm encompass the estimation of Hammerstein, bilinear, and linear models as special cases. For example, considering the case $v(t) = u(t)$, then the HBSRIVC algorithm reduces to the BSRIVC algorithm, and by further considering all η_i , for $i = 1, \dots, n$, to be zero, then the BSRIVC reduces to the SRIVC algorithm.

The HSRIVC algorithm can be viewed as being a complementary algorithm to the HBSRIVC algorithm. The main difference consists of the use of linear prefilters instead of adaptive, input dependent, prefilters used by the HBSRIVC algorithm. This creates a linear parameter estimation method, which is more straightforward to initialise. In Subsection 3.3.1, it has been suggested to use the SRIVC algorithm to help to initialise the full BSRIVC algorithm. Similarly, the HSRIVC algorithm can be used to obtain an approximate estimate of the static input function, subsequently this estimate can be used to initialise the HBSRIVC algorithm.

3.5 Numerical study

This section considers a Monte Carlo simulation (MCS) analysis that aims to empirically demonstrate the performance of the SRIVC, BSRIVC, HSRIVC and HBSRIVC algorithms. The bilinear and Hammerstein-bilinear models considered are chosen such that their behaviour (static and dynamic) is comparable to that observed on a real HVAC system. Therefore, based on this numerical study one can gain an insight into the expected performance of the proposed parameter estimation methods in practice. Additionally, the aim of this simulation study (and this Chapter as a whole) is not to benchmark algorithms such as well established SRIVC method with the proposed BSRIVC method. The SRIVC algorithm is used as a reference point to gain an insight about the corresponding performance of the proposed BSRIVC method, which is specifically designed for the estimation of higher order bilinear systems.

Two case scenarios are considered. In both cases the static input nonlinearity is parameterized by a third order constrained polynomial, defined in (3.89), i.e.

$$v(t) = u(t) + \sum_{i=2}^3 p_i [-u(t) + u^i(t)], \quad \text{for } u(t) \in \langle 0, 1 \rangle \quad (3.116)$$

where the parameter p_1 , of the equivalent unconstrained polynomial function (3.88), is computed from

$$p_1 = 1 - \sum_{i=2}^3 p_i \quad (3.117)$$

The corresponding parameter set is

$$\boldsymbol{\theta}_n = \begin{bmatrix} p_2 & p_3 \end{bmatrix}^T = \begin{bmatrix} -4.4 & 2 \end{bmatrix}^T \quad (3.118)$$

and the static function is displayed in the right-lower plot of Figure 3.3. In this plot, the polynomial function, black solid line, is compared to a linear case, grey solid line, i.e. $v(t) = u(t)$.

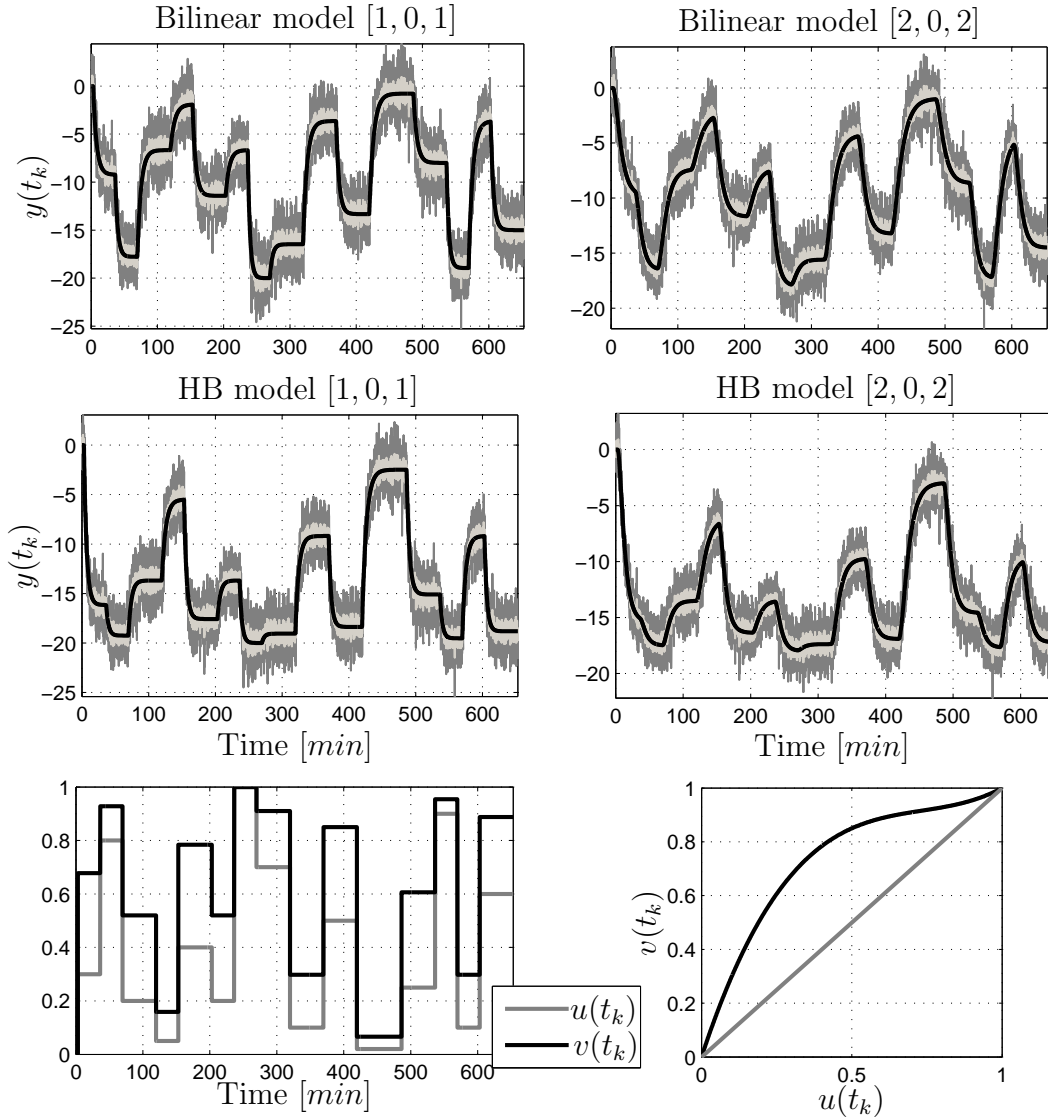


Figure 3.3: Upper-left and upper-right plots show simulated output $y(t_k)$ of bilinear models having orders $[n, m, n] = [1, 0, 1]$ and $[n, m, n] = [2, 0, 2]$, respectively. Middle-left and middle-right plots show simulated output $y(t_k)$ of HB model having orders $[n, m, n] = [1, 0, 1]$ and $[n, m, n] = [2, 0, 2]$, respectively. In each case, the solid black line represents noise free simulated output, solid light grey line is noisy output for NSR = 10 [%], solid dark grey line represents noisy output for NSR = 30 [%]. Seed value is 22 for each case. Lower-left plot shows input signal $u(t_k)$ and intermediate input $v(t_k)$, while lower right plot displays static function $v(t_k) = \phi(u(t_k))$, solid black line, and linear case $v(t_k) = u(t_k)$, solid grey line.

The system input is a multi-level stair-case signal with arbitrary chosen step amplitude and step time duration shown in the left-lower plot of Figure 3.3. The number of simulated data points is $N = 7836$, sampled at $h = 5$ [s], i.e. the overall simulation time is approximately 11 [h], which corresponds to a low sample size situation. Although, such an input is  necessarily strongly persistently exciting according to the definition provided in (Stoica & Söderström 1982) for Hammerstein systems, this input signal is considered to be practically realisable and applicable on an actual HVAC system. The Monte Carlo analysis is based on $M=100$ realizations where, for each realization, the noise $\xi(t_k) = e(t_k)$ is randomly generated using the Matlab (software version 2010b) function `randn` for seed values ranging from 1 to 100. The generated noise sequence is normalized such that the resulting noise-to-signal ratio (NSR) is fixed at 10 [%] and 30 [%], hence two noise scenarios are considered. The NSR is based on standard deviations, in percentage, and is defined as follows

$$\text{NSR} = 100 \times \frac{\text{SD}_e}{\text{SD}_x} \quad (3.119)$$

with the noise signal (SD_e) and noise free simulated output (SD_x) standard deviations given by, respectively,

$$\text{SD}_e = \sqrt{\frac{1}{N} \sum_{k=1}^N (e(t_k) - \bar{e}(t_k))^2} \quad \text{and} \quad \text{SD}_x = \sqrt{\frac{1}{N} \sum_{k=1}^N (x(t_k) - \bar{x}(t_k))^2} \quad (3.120)$$

where the bar over a variable denotes the mean value, i.e. mean value of signal $x(t_k)$ is $\bar{x}(t_k) = (1/N) \sum_{k=1}^N x(t_k)$.

The convergence criterion monitoring the maximum relative change of parameter estimate, defined in (3.80) for a general parameter vector $\hat{\theta}$, for all parameter estimation algorithms considered, is selected to be $\epsilon = 1 \times 10^{-7}$. The general prefilter $f(s, t)$, defined in (3.67), is implemented in Simulink (software version 2010b) programming environment. All estimated systems adopted in subsequent subsections, Case scenario 1 and Case scenario 2, are also implemented in Simulink. The variable-step size Dormand-Price `ode45` numerical solver is selected. When importing sampled input-output signals to Simulink a function block `from workspace` is used. This function block uses, by a default, a linear Lagrangian interpolation of the signal inter-sample behaviour.

Several model fit criteria are evaluated and are common to both Case scenarios. An integral of absolute error between measured and simulated system

output, defined as

$$IAE = \frac{1}{N} \sum_{k=1}^N |y(t_k) - \hat{x}(\hat{\boldsymbol{\theta}}, t_k)| \quad (3.121)$$

is computed for each noise realization and overall mean values are tabulated. The mean value of estimated noise variance $\hat{\sigma}_e^2$ is evaluated for each Monte Carlo simulation analysis and is compared to the true variance of the applied noise $e(t_k)$. The noise variance estimate is computed according to (3.82a), where a suitable regression vector must be selected based on a considered Case scenario. To be able to comment on the accuracy of estimated parameter sets for the two noise scenarios, the following norm is evaluated for each noise realization

$$AC(\hat{\boldsymbol{\theta}}) = \sqrt{\sum_{i=1}^p (\boldsymbol{\theta}(i) - \hat{\boldsymbol{\theta}}(i))^2} \quad (3.122)$$

where p is the number of parameters within the currently evaluated vector $\hat{\boldsymbol{\theta}}$.

3.5.1 Case scenario I

The HB system is assumed to take the following form

$$sx(t) = -\alpha_1 x(t) + \beta_0 v(t) + \eta_1 v(t)x(t) \quad (3.123a)$$

$$y(t_k) = x(t_k) + e(t_k) \quad (3.123b)$$

with the true parameter vectors

$$\boldsymbol{\theta}_l = \begin{bmatrix} \alpha_1 & \beta_0 \end{bmatrix}^T = \begin{bmatrix} 0.0025 & -0.1 \end{bmatrix}^T \quad (3.124a)$$

$$\boldsymbol{\theta}_b = \begin{bmatrix} \eta_1 \end{bmatrix}^T = \begin{bmatrix} -0.0025 \end{bmatrix}^T \quad (3.124b)$$

and the static function nonlinearity is as defined in (3.117). Since the bilinear submodel (3.123) can be interpreted as a TISO linear in structure model during the estimation stage, the SRIVC and HSRIVC algorithms are applicable. In order to gradually gain an insight into the proposed estimation methods, two distinct cases are considered. Firstly, only the bilinear submodel (3.123), with $v(t_k) = u(t_k)$, is used to represent the system, so that the SRIVC and BSRIVC algorithms are applied only. Secondly, the full HB system, governed by (3.117) and (3.123), is estimated by the HSRIVC and HBSRIVC algorithms. The corresponding input-output data for these two cases are plotted in the left part of Figure 3.3.

The input dependent steady-state gain SSG , according to definition (2.69), varies in the range $SSG \in \langle -40, -20 \rangle$ for corresponding values of input signal $u(t) \in \langle 0, 1 \rangle$. The negative value of steady-state gain may, for example, indicate a cooling HVAC system application, where the SSG relates to maximal cooling capacity of the system. The time constant T , defined in (2.73), varies in the range $T \in \langle 400, 200 \rangle$ [s] for input values $u(t) \in \langle 0, 1 \rangle$. The negative sign of η_1 parameter indicates saturation type steady-state characteristic of the dynamic submodel. The static input nonlinearity is also of a saturation type. Therefore, it is believed that the combination of these two submodels creates a difficult system identification scenario, where the estimation method must be able to distinguish between the contributions of the individual submodels to the overall steady-state characteristic.

The prefilters of the SRIVC, BSRIVC, HSRIVC and HBSRIVC algorithms are initialised with the same single breakpoint frequency parameter equal to $\lambda = 0.005$. Additionally, in the case of the BSRIVC and HBSRIVC algorithms, the parameters associated with the bilinear terms are initialised with zero, i.e. $\eta_1 = 0$. The static input nonlinearity is assumed to be linear $v(t) = u(t)$, hence setting $\hat{\theta}_n^0 = [0 \ 0]^T$. Note, that the SRIVC and HSRIVC algorithms, by their design, consider the dynamic part of the system to be linear (interpretable as linear), while the other two algorithms consider the system to have bilinear dynamics. By the current choice of the initial parameters, the adaptive prefilters of the BSRIVC and HBSRIVC algorithms are set for the linear case, even though the true system has bilinear dynamics. Therefore, albeit virtually the same initial setting of all examined algorithms, the BSRIVC and HBSRIVC algorithms, are from this point of view disadvantaged.

The Monte Carlo simulation analysis results are summarised in Tables 3.1 and 3.2. Since two distinct systems have been estimated, i.e. bilinear system and HB system, only the appropriate algorithms should be compared with each other directly, which are the SRIVC together with BSRIVC, and the HSRIVC together with HBSRIVC.

Table 3.1 presents the single run and MCS results for the considered algorithms. Small standard deviations (SD) of estimated parameters, computed from the MCS analysis, are reported. In all cases the standard errors (SE) on the parameter estimates are reasonably matched to the SD values. Although, the SRIVC and BSRIVC algorithms perform virtually the same, the HSRIVC outperforms the HBSRIVC algorithm by a margin. The HBSRIVC algorithm has higher SD values, as compared to HSRIVC. Additionally, the HBSRIVC algo-

Table 3.1: Monte Carlo simulation (MCS) results for simulation example in Case scenario I. SR denotes the single run results for seed value 22, SE denotes the standard error on the estimates, SD denotes the standard deviation of the MCS estimates.

Parameter		α_1	β_0	η_1	p_2	p_3
True values		2.5×10^{-3}	-0.1	-2.5×10^{-3}	-4.4	2
NSR=10 [%]						
SRIVC	$\hat{\theta}$	2.4827×10^{-3}	-0.09938	-2.4861×10^{-3}	-	-
(SR)	SE	0.7904×10^{-5}	0.3092×10^{-3}	1.1186×10^{-5}	-	-
SRIVC	mean	2.4931×10^{-3}	-0.09972	-2.4934×10^{-3}	-	-
(MCS)	SD	1.1893×10^{-5}	0.4356×10^{-3}	1.5076×10^{-5}	-	-
BSRIVC	$\hat{\theta}$	2.4907×10^{-3}	-0.09986	-2.5032×10^{-3}	-	-
(SR)	SE	1.2049×10^{-5}	0.5017×10^{-3}	1.7037×10^{-5}	-	-
BSRIVC	mean	2.5002×10^{-3}	-0.10006	-2.5033×10^{-3}	-	-
(MCS)	SD	1.0965×10^{-5}	0.4976×10^{-3}	2.1423×10^{-5}	-	-
HSRIVC	$\hat{\theta}$	2.4906×10^{-3}	-0.09870	-2.4436×10^{-3}	-4.4413	2.0220
(SR)	SE	0.7691×10^{-5}	0.2971×10^{-3}	1.0327×10^{-5}	0.01247	0.00877
HSRIVC	mean	2.4944×10^{-3}	-0.09949	-2.4804×10^{-3}	-4.4129	2.0071
(MCS)	SD	1.2367×10^{-5}	0.6854×10^{-3}	3.4224×10^{-5}	0.05047	0.03286
HBSRIVC	$\hat{\theta}$	2.4927×10^{-3}	-0.10003	-2.5101×10^{-3}	-4.3784	1.9846
(SR)	SE	1.2097×10^{-5}	0.4947×10^{-3}	1.5593×10^{-5}	0.01175	0.00825
HBSRIVC	mean	2.5000×10^{-3}	-0.10018	-2.5101×10^{-3}	-4.3899	1.9933
(MCS)	SD	1.1993×10^{-5}	1.4334×10^{-3}	8.1139×10^{-5}	0.09628	0.06041
NSR=30 [%]						
SRIVC	$\hat{\theta}$	2.4608×10^{-3}	-0.09871	-2.4731×10^{-3}	-	-
(SR)	SE	2.3406×10^{-5}	0.9174×10^{-3}	3.3267×10^{-5}	-	-
SRIVC	mean	2.4916×10^{-3}	-0.09970	-2.4948×10^{-3}	-	-
(MCS)	SD	3.5585×10^{-5}	1.3049×10^{-3}	4.5205×10^{-5}	-	-
BSRIVC	$\hat{\theta}$	2.4907×10^{-3}	-0.09986	-2.5032×10^{-3}	-	-
(SR)	SE	1.2049×10^{-5}	0.5017×10^{-3}	1.7037×10^{-5}	-	-
BSRIVC	mean	2.501×10^{-3}	-0.10019	-2.5107×10^{-3}	-	-
(MCS)	SD	3.2824×10^{-5}	1.4924×10^{-3}	6.4342×10^{-5}	-	-
HSRIVC	$\hat{\theta}$	2.4849×10^{-3}	-0.09706	-2.3653×10^{-3}	-4.5062	2.0557
(SR)	SE	2.2994×10^{-5}	0.8760×10^{-3}	3.0447×10^{-5}	0.03760	0.02644
HSRIVC	mean	2.4958×10^{-3}	-0.09939	-2.4741×10^{-3}	-4.4212	2.0110
(MCS)	SD	3.6986×10^{-5}	2.0547×10^{-3}	10.2690×10^{-5}	0.15107	0.09841
HBSRIVC	$\hat{\theta}$	2.4782×10^{-3}	-0.10016	-2.5346×10^{-3}	-4.3305	1.9508
(SR)	SE	3.6064×10^{-5}	1.4827×10^{-3}	4.6877×10^{-5}	0.03522	0.02472
HBSRIVC	mean	2.4968×10^{-3}	-0.10130	-2.5728×10^{-3}	-4.3265	1.9541
(MCS)	SD	3.5828×10^{-5}	4.8691×10^{-3}	27.4970×10^{-5}	0.31491	0.19633

rithm failed to converge in four cases for a high noise scenario only. However, with

Table 3.2: Monte Carlo simulation results for simulation example in Case scenario I. The true noise variances σ_e^2 of the bilinear system for $NSR = 10$ [%] and $NSR = 30$ [%] are 0.3260 and 2.9344, respectively. The true noise variances σ_e^2 of the HB system for $NSR = 10$ [%] and $NSR = 30$ [%] are 0.2816 and 2.5348, respectively.

		IAE	$\hat{\sigma}_e^2$	$AC(\hat{\theta}_{lb})$	$AC(\hat{\theta}_n)$	Iter
NSR=10 [%]						
SRIVC	mean	0.4558	0.3264	4.1403×10^{-4}	-	4.6667
	SD	1.4240×10^{-3}	0.3990×10^{-3}	3.1323×10^{-4}	-	0.4880
BSRIVC	mean	0.4558	0.3261	4.0809×10^{-4}	-	13.400
	SD	1.4199×10^{-3}	0.1065×10^{-3}	2.8839×10^{-4}	-	0.5071
HSRIVC	mean	0.4236	0.2821	7.0198×10^{-4}	4.8883×10^{-2}	345.40
	SD	1.3278×10^{-3}	0.4851×10^{-3}	4.8227×10^{-4}	3.7849×10^{-2}	4.6105
HBSRIVC	mean	0.4237	0.2818	11.408×10^{-4}	9.0695×10^{-2}	304.67
	SD	1.3331×10^{-3}	0.3230×10^{-3}	8.8322×10^{-4}	6.8972×10^{-2}	16.504
NSR=30 [%]						
SRIVC	mean	1.3674	2.9370	1.0750×10^{-3}	-	4.8667
	SD	4.2764×10^{-3}	3.6153×10^{-3}	0.7925×10^{-3}	-	0.5164
BSRIVC	mean	1.3675	2.9346	1.2277×10^{-3}	-	13.200
	SD	4.2594×10^{-3}	0.9665×10^{-3}	0.8636×10^{-3}	-	0.8619
HSRIVC	mean	1.2708	2.5385	1.7706×10^{-3}	0.1454	349.80
	SD	3.9947×10^{-3}	4.2762×10^{-3}	1.2025×10^{-3}	0.1083	14.872
HBSRIVC	mean	1.2713	2.5362	3.6892×10^{-3}	0.2837	352.00
	SD	4.0733×10^{-3}	4.2646×10^{-3}	3.4259×10^{-3}	0.2529	119.67

a different, more accurate initialisation convergence could have been achieved.

Table 3.2 compares the mean and associated SD values of IAE , $\hat{\sigma}_e^2$, $AC(\hat{\theta}_{lb})$, and $AC(\hat{\theta}_n)$ performance criteria together with an average number of required iterations. All parameter estimation algorithms perform virtually the same in terms of the IAE criterion. The BSRIVC and HBSRIVC algorithms consistently provides noise variance estimates, which are closer to the true noise variances (stated in the Table caption). The SRIVC and HSRIVC algorithms achieve, in general, smaller values of the AC criterion. The exception is the BSRIVC algorithm in comparison with the SRIVC algorithm under the low noise conditions. The SRIVC algorithm, as compared to BSRIVC, requires a lower average number of iterations in achieving the prescribed convergence criterion. However, it should be stressed, that the computational efficiency in terms of number of iterations required or the time duration of the estimation procedure is not the focus of the current research. The HSRIVC and HBSRIVC algorithms need a similar average number of iterations to converge, however, the HSRIVC algorithms has

considerably lower SD values.

In Figure 3.4 the true (grey solid line) static function and system output is compared with the corresponding MCS estimates (black solid lines). The results are displayed for HSRIVC and HBSRIVC algorithms, under the high noise scenario, only. In the case of a low noise scenario the individual plots would be virtually identical. Similarly, the results for the SRIVC and BSRIVC algorithms are not distinguishable for any noise scenario, when plotted against each other, hence are not displayed. It is observed in Figure 3.4, that the static function estimates are less accurate when the HBSRIVC algorithm is used.

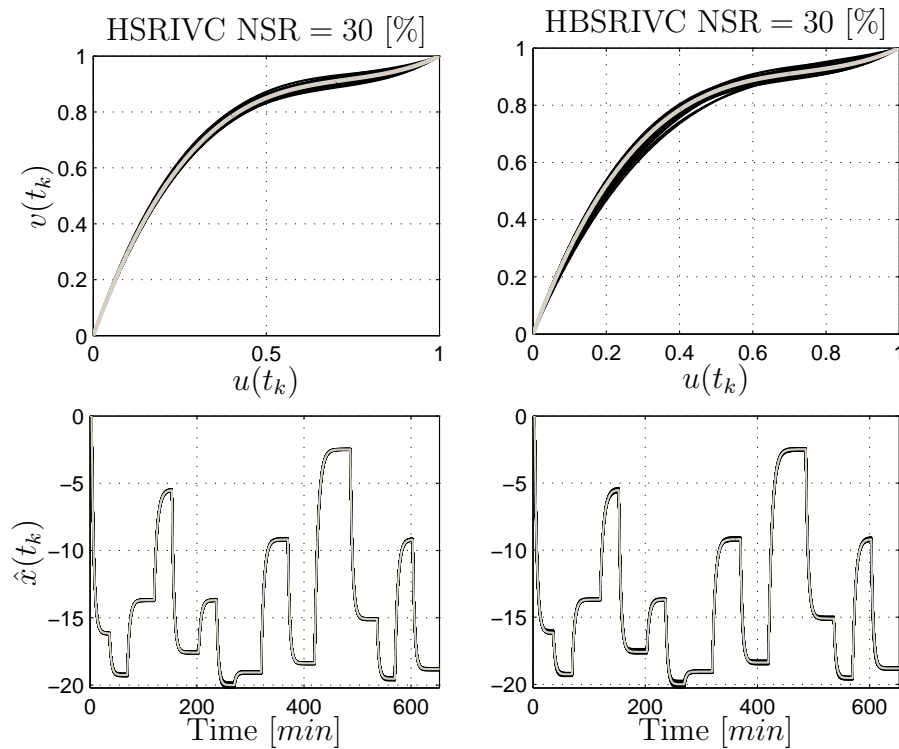


Figure 3.4: Monte Carlo simulation results for Case scenario I. Comparison of true (grey solid lines) and estimated (black solid lines) static functions and the system outputs. High noise scenario is considered only. Upper-left and lower-left plots show results for HSRIVC algorithm, while upper-right and lower-right plots show results for HBSRIVC algorithm.

3.5.2 Case scenario II

The HB system is assumed to take the following form

$$s^2x(t) = -\alpha_1sx(t) - \alpha_2x(t) + \beta_0v(t) + \eta_1v(t)sx(t) + \eta_2v(t)x(t) \quad (3.125a)$$

$$y(t_k) = x(t_k) + e(t_k) \quad (3.125b)$$

with the true parameter vectors

$$\boldsymbol{\theta}_l = \begin{bmatrix} \alpha_1 & \alpha_2 & \beta_0 \end{bmatrix}^T = \begin{bmatrix} 0.0045 & 0.0000045 & -0.000225 \end{bmatrix}^T \quad (3.126a)$$

$$\boldsymbol{\theta}_b = \begin{bmatrix} \eta_1 & \eta_2 \end{bmatrix}^T = \begin{bmatrix} -0.003 & -0.000008 \end{bmatrix}^T \quad (3.126b)$$

and the static function nonlinearity is as defined in (3.117). The considered system has second order linear dynamics, single input term and two bilinear terms, and as such cannot be interpreted as a TISO linear for the purpose of parameter estimation. Therefore, the SRIVC and HSRIVC algorithms are not applicable. Similarly to Case scenario I, in order to gain gradual insight into the performance of the proposed estimation methods, two cases are considered. Firstly, only the bilinear submodel (3.125), with $v(t_k) = u(t_k)$, is selected to represent the system. Secondly, the full HB system, governed by (3.117) and (3.125), is estimated. The corresponding input-output data for these two cases are plotted in the right part of Figure 3.3.

Since the dynamic submodel (3.125) is of order $n = 2$, then two, input dependent, time constants are present, which are $T_1 \in \langle 666.67, 400 \rangle$ [s] and $T_2 \in \langle 333.33, 200 \rangle$ [s] for input values $u(t) \in \langle 0, 1 \rangle$. The steady-state gain varies in a range $SSG \in \langle -50, -18 \rangle$ for corresponding values of input signal $u(t) \in \langle 0, 1 \rangle$. The system is not considered to be stiff, because the system time constants do not considerably differ in magnitude. However, it is believed that the saturation type steady-state characteristic of the dynamic submodel together with the saturation-like shaped static input function still creates a challenging system identification scenario.

The prefilters of the BSRIVC and HBSRIVC algorithms are initialised with the same single breakpoint frequency parameter equal to $\lambda = 0.01$ and the parameters associated with the bilinear terms are initialised with zero, i.e. $\eta_i = 0$, for $i = 1, 2$. The static input function is initialised with $\hat{\boldsymbol{\theta}}_n^0 = [-2.5 \ 1]^T$. This choice of the initial static function estimate is considered to be mild, yet helps to induce the convergence.

Table 3.3 presents the single run and MCS results for the two considered algorithms. In case of the BSRIVC algorithm small standard deviations of MCS estimates are reported. For the high noise scenario, the HBSRIVC algorithm yields somewhat larger standard deviations of MCS parameter estimates. In both cases, the standard errors on parameter estimates are rather optimistic, especially in the case of the HBSRIVC algorithm. Both algorithms successfully converged for all simulation runs. Table 3.4 compares the selected performance criteria together with an average number of required iterations. Both algorithms consistently provide noise variance estimates which are low in magnitude and close to the true noise variances (stated in the Table caption). The *IAE* values for a high noise scenario are almost exactly three times larger than the *IAE* values for the low noise scenario, in which the noise is also three times lower in terms of *NSR*. It is also noted, that the noise level does not seem to influence the required number of iterations considerably.

In Figure 3.5 the true (grey solid line) static function and system output is compared with the corresponding MCS estimates (black solid lines). The comparison is made for HBSRIVC algorithm only, for the low and high noise scenario. As expected, it is observed that the static function estimates are less accurate for the high noise scenario.

3.6 Conclusions

In this chapter, new parameter estimation methods for the identification of bilinear systems and Hammerstein-bilinear systems in continuous-time domain are proposed. The well established SRIVC algorithm for parameter estimation of linear continuous-time transfer function models, has been extended to the bilinear case. The proposed BSRIVC algorithm is designed to be capable for the estimation of higher order bilinear models directly from sampled input-output data, where the bilinear model is interpreted in time-step quasi-linear transfer function form. Exploiting the iterative nature of the BSRIVC algorithm, and postulating that the static input function is parameterized by a linear-in-parameters polynomial function of finite order, the HBSRIVC algorithm is developed for the estimation of Hammerstein-bilinear systems. This generalised estimation algorithm then automatically includes the BSRIVC and SRIVC algorithms as special cases. The proposed parameter estimation methods differ from the existing, reviewed methods, in their simplicity of implementation, usage and the noise scenarios under which the consistent parameter estimates are still obtained.

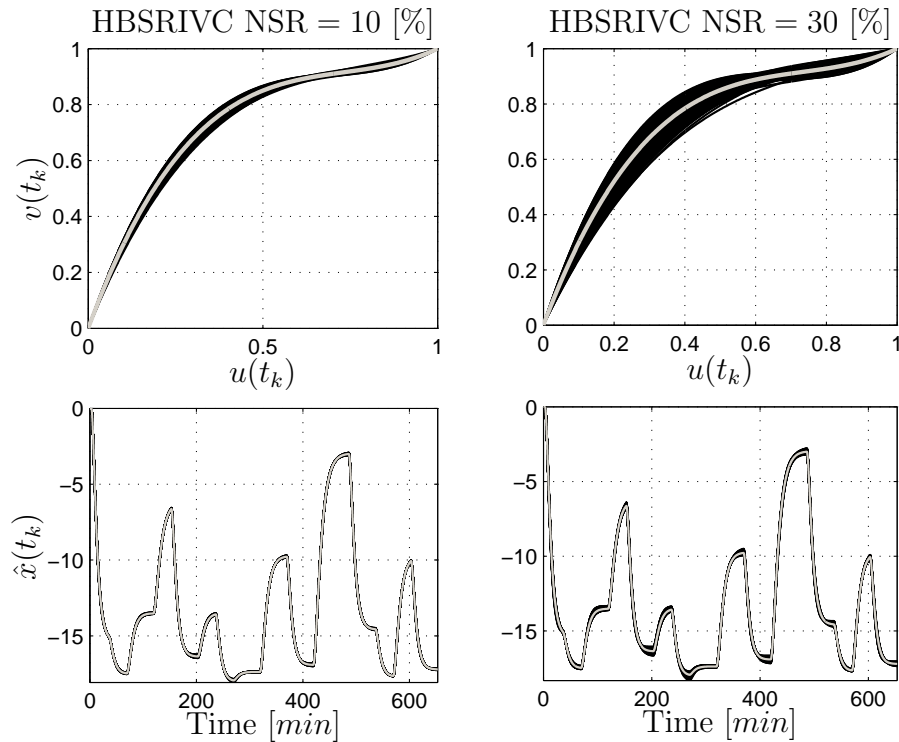


Figure 3.5: Monte Carlo simulation results for Case scenario II. Comparison of true (grey solid lines) and estimated (black solid lines) static functions and the system outputs. Low and high noise scenario are considered.

It has been noted, in Section 2.3, that under certain restricted conditions, the considered continuous-time single-input single-output bilinear model can be interpreted as a two-input single-output linear (in structure) transfer function model. Based on this observation, the SRIVC algorithm is configured for such an identification scenario and, similar to the HBSRIVC algorithm; the iterative backfitting HSRIVC algorithm is proposed for estimation of the Hammerstein(-bilinear) systems. Although, not an intended result, the iterative HSRIVC algorithm can be applied to the estimation problem of Hammerstein systems. Here, the currently predominant methods, which use SRIVC and further refined RIVC algorithms, are based on a two stage noniterative over-parameterization method. It is believed, that the currently proposed iterative methods, if convergence occurs, are capable of providing more accurate parameter estimates. This is demonstrated in the subsequent chapter, where a Hammerstein(-bilinear) model is estimated, in a discrete-time setting, using both the iterative and the noniterative methods.

The SRIVC and HSRIVC parameter estimation methods can be viewed as

being a complementary to the BSRIVC and HBSRIVC algorithms and can be used during the initialisation stages of these latter algorithms, respectively. The main difference consists in the use of linear prefilters instead of adaptive, input dependent, prefilters. This requires a linear parameter estimation methods, which are more straightforward to be initialised and applied.

In general, the reviewed and designed parameter estimation methods can be classified into two distinct groups based on the type of prefilters used. The SRIVC and HSRIVC algorithms use linear prefilters, while the BSRIVC and HBSRIVC algorithms use adaptive, input dependent, prefilters instead. Table 3.5 presents a comprehensive overview of the reviewed and designed extensions proposed in this chapter.

The *en bloc* solution, i.e. non-recursive or single iteration of a batch of data, to the SRIVC, BSRIVC, HSRIVC and HBSRIVC algorithms is presented, while its recursive implementation is left for potential future work. The recursive formulation offers additional insight into the modelled system in an off-line setting and, of course, can also be applied in on-line estimation applications. The RIVC parameter estimation method is statistically optimal under the assumption of an auto-regressive moving-average (ARMA) additive noise model and is suitable for the identification of hybrid Box-Jenkins transfer function models. The optimal identification of CT bilinear and CT Hammerstein-bilinear models under the assumption of coloured additive noise, i.e. use of the RIVC algorithm as a core algorithm instead of SRIVC algorithm, is also left for potential future work.

Similarly to the SRIVC algorithm, the proposed HBSRIVC and HSRIVC parameter estimation methods can both be potentially implemented in a discrete-time setting, i.e. use of discrete-time prefilters. However, due to the differences between continuous-time and discrete-time bilinear models, as stated in Chapter 2, there is no case for the HBSRIVC algorithm to be implemented in discrete-time setting. In particular, the selected CT bilinear model structure can be viewed as a subset of the considered DT bilinear model structure. The discrete-time bilinear model can be fully interpreted as multi-input single-output linear (in structure) transfer function model, which promotes the use of linear prefilters and linear estimation methods. Therefore, only the SRIVC and HSRIVC algorithms are implemented in a discrete-time setting in the subsequent chapter.

Table 3.3: Monte Carlo simulation results for Case scenario II. SR denotes the single run results for seed value 22, SE denotes the standard error on estimates, SD denotes the standard deviation of MCS estimates.

Parameter		α_1	α_2	β_0	η_1	η_2	p_2	p_3
True values		4.5×10^{-3}	4.5×10^{-6}	-2.25×10^{-4}	-3×10^{-3}	-8×10^{-6}	-4.4	2
NSR=10 [%]								
BSRIVC (SR)	$\hat{\theta}$	4.4327×10^{-3}	4.4167×10^{-6}	-2.2345×10^{-4}	-2.8268×10^{-3}	-8.0751×10^{-6}	-	-
	SE	2.6486×10^{-5}	1.9971×10^{-8}	1.0066×10^{-6}	4.6604×10^{-5}	3.991×10^{-8}	-	-
BSRIVC (MCS)	mean	4.4952×10^{-3}	4.4981×10^{-6}	-2.2527×10^{-4}	-3.0036×10^{-3}	-8.0243×10^{-6}	-	-
	SD	5.9259×10^{-5}	6.7605×10^{-8}	2.8351×10^{-6}	17.857×10^{-5}	14.564×10^{-8}	-	-
HBSRIVC (SR)	$\hat{\theta}$	4.3879×10^{-3}	4.3732×10^{-6}	-2.2622×10^{-4}	-3.0471×10^{-3}	-8.2239×10^{-6}	-4.1814	1.8608
	SE	2.7892×10^{-5}	1.8474×10^{-8}	0.9268×10^{-6}	4.1528×10^{-5}	3.5953×10^{-8}	0.01075	0.00765
HBSRIVC (MCS)	mean	4.4851×10^{-3}	4.485×10^{-6}	-2.2570×10^{-4}	-3.0192×10^{-3}	-8.0582×10^{-6}	-4.3613	1.9765
	SD	18.501×10^{-5}	16.947×10^{-8}	5.2049×10^{-6}	22.739×10^{-5}	44.548×10^{-8}	0.29819	0.17945
NSR=30 [%]								
BSRIVC (SR)	$\hat{\theta}$	4.3007×10^{-3}	4.2489×10^{-6}	-2.2013×10^{-4}	-2.4514×10^{-3}	-8.2164×10^{-6}	-	-
	SE	7.4669×10^{-5}	5.4980×10^{-8}	2.8219×10^{-6}	13.057×10^{-5}	11.547×10^{-8}	-	-
BSRIVC (MCS)	mean	4.4880×10^{-3}	4.4966×10^{-6}	-2.2594×10^{-4}	-3.0062×10^{-3}	-8.0798×10^{-6}	-	-
	SD	17.714×10^{-5}	20.322×10^{-8}	8.6336×10^{-6}	54.198×10^{-5}	43.683×10^{-8}	-	-
HBSRIVC (SR)	$\hat{\theta}$	4.1979×10^{-3}	4.1313×10^{-6}	-2.2829×10^{-4}	-3.0474×10^{-3}	-8.6394×10^{-6}	-3.7484	1.5856
	SE	7.5915×10^{-5}	4.8746×10^{-8}	2.5864×10^{-6}	11.608×10^{-5}	10.439×10^{-8}	0.03145	0.02247
HBSRIVC (MCS)	mean	4.5059×10^{-3}	4.4783×10^{-6}	-2.2785×10^{-4}	-2.9823×10^{-3}	-8.1917×10^{-6}	-4.2798	1.9296
	SD	52.294×10^{-5}	47.998×10^{-8}	14.183×10^{-6}	60.656×10^{-5}	119.59×10^{-8}	0.79332	0.47510

Table 3.4: Monte Carlo simulation results for simulation example in Case scenario II. The true noise variances σ_e^2 of the bilinear system for $NSR = 10$ [%] and $NSR = 30$ [%] are 0.2218 and 1.9960, respectively. The true noise variances σ_e^2 of the HB system for $NSR = 10$ [%] and $NSR = 30$ [%] are 0.1823 and 1.6408, respectively.

		IAE	$\hat{\sigma}_e^2$	$AC(\hat{\theta}_{lb})$	$AC(\hat{\theta}_n)$	Iter
NSR=10 [%]						
BSRIVC	mean	0.3768	0.2229	1.5732×10^{-4}	-	70.067
	SD	1.5913×10^{-3}	1.3914×10^{-3}	1.0219×10^{-4}	-	3.8816
HBSRIVC	mean	0.3414	0.1830	2.4569×10^{-4}	0.2734	449.80
	SD	1.4711×10^{-3}	1.0372×10^{-3}	1.5996×10^{-4}	0.2183	78.281
NSR=30 [%]						
BSRIVC	mean	1.1305	2.0062	4.7799×10^{-4}	-	73.933
	SD	4.7999×10^{-3}	12.625×10^{-3}	3.0756×10^{-4}	-	12.068
HBSRIVC	mean	1.0241	1.6465	6.6735×10^{-4}	0.7548	508.87
	SD	4.2126×10^{-3}	8.2448×10^{-3}	4.3828×10^{-4}	0.5470	51.810

Table 3.5: Summary of reviewed and designed algorithms for model parameter estimation in the continuous-time domain.

Linear optimal prefilters	
SRIVC	<ul style="list-style-type: none"> • Parameter estimation of linear TF models; algorithm is provided in Algorithm 3.1. • Parameter estimation of bilinear models formulated in a TISO linear in structure TF form, see Subsection 3.2.1.
HSRIVC	<ul style="list-style-type: none"> • Parameter estimation of Hammerstein models, where the dynamic submodel is a bilinear model interpreted in a TISO linear in structure TF form provided in Algorithm 3.4. • The HSRIVC algorithm with constrained static input nonlinear function is provided in Subsection 3.4.4.
Adaptive, input dependent, prefilters	
BSRIVC	<ul style="list-style-type: none"> • Parameter estimation of bilinear models interpreted in a time-step quasi-linear TF form; for implementation see Algorithm 3.2. • Includes SRIVC algorithm for linear TF model estimation as a special case.
HBSRIVC	<ul style="list-style-type: none"> • Parameter estimation of HB models; for implementation see Algorithm 3.3 • The HBSRIVC algorithm with constrained static input nonlinear function is provided in Subsection 3.4.2 • Includes SRIVC and BSRIVC algorithms as special cases.

Chapter 4

Parameter estimation methods in discrete-time domain

4.1 Introduction

The continuous-time parameter estimation methods introduced in Chapter 3 are formulated here in the discrete-time setting. The reviewed and extended simplified refined instrumental variable method is a unified time domain approach to parameter estimation for linear transfer function models. Since, the proposed HSRIVC and HBSRIVC algorithms, and their corresponding special cases SRIVC and BSRIVC algorithms, respectively, are based on this instrumental variable method, they are also directly applicable to the discrete-time case.

The general BSRIVC and HBSRIVC parameter estimation methods for CT bilinear and CT Hammerstein-bilinear models, respectively, are, however, not formulated here in their discrete-time setting. These methods target a specific class of CT bilinear models, introduced in (2.5), which can be viewed as a subclass of the currently considered DT bilinear model structure, see Subsection 2.4.3. The considered class of DT bilinear models can be fully interpreted in MISO linear in structure transfer function form, see Remark 2.4. Therefore, only the SRIVC and HSRIVC algorithms are implemented in the discrete-time setting. Both, the SRIVC and HSRIVC algorithms, have been proposed for parameter estimation of CT SISO bilinear models interpreted as TISO linear in structure transfer function models; the presented extension to the multi-input DT case does not impose any further problems. The discrete-time counterparts of the SRIVC and HSRIVC algorithms are abbreviated to SRIV and HSRIV, respectively.

While there was a need to use iterative schemes when estimating CT bilinear

models, this is not the case in the DT domain. This need has arisen from the interpretation of CT bilinear models in a time-step quasi-linear transfer function form during the filtering operation, i.e. use of the BSRIVC algorithm. The subsequent iterations were needed for the reconstruction of the unknown filtered bilinear input terms. Therefore, in order to estimate the parameters of the nonlinear static input function, being part of the CT Hammerstein-bilinear model structure, the iterative solution has also been adopted, i.e. use of the HBSRIVC algorithm. However, the situation is different in discrete-time domain, where the considered DT bilinear model can be directly interpreted as MISO linear in structure form. Firstly, this facilitates the use of linear parameter estimation methods, i.e. use of the SRIV algorithm. Secondly, there is no need to use an iterative solution when estimating the nonlinear static input function, hence a noniterative, over-parameterization, method, based on method proposed by (Hsia 1968), can be applied.

Although, the over-parameterization method can be applied when estimating the static part of the DT Hammerstein-bilinear model, the use of an iterative solution is still the preferred option, because of improved parameter estimation accuracy, i.e. the use of the designed HSRIV algorithm is preferred. The estimated Hammerstein-bilinear model is used for the purpose of control analysis and design, where an accurate estimate of both static and dynamic submodels is required. When using the over-parameterization method an auxiliary, over-parameterized, model is estimated first, from which the individual parameters of the Hammerstein-bilinear model are inferred. It has been reported in the works of (Gallman 1976) and (Le, Markovsky, Freeman & Rogers 2010), who considered the estimation problem of Hammerstein models only, that such inferred parameters are less efficient in terms of parameter accuracy. This is mainly caused by the parameter redundancy of the estimated auxiliary model, where such a problem cannot be fully overcome.

In order to demonstrate the performance of the proposed HSRIV algorithm, in terms of parameter estimation accuracy, a numerical study is presented in Section 4.5. In this study the HSRIV algorithm is compared with the noniterative, over-parameterized, version of the HSRIV algorithm, abbreviated HSRIV-OV. Although, the HSRIV-OV estimation method is presented here just for benchmark purposes, the parameter estimates obtained can be used to initialise the iterative HSRIV algorithm. In other words, the initial estimates obtained by the HSRIV-OV algorithm can be subsequently refined and used by the iterative HSRIV algorithm.

4.1.1 Problem formulation

The parameter estimation problem in the DT domain is formulated in a similar manner to the parameter estimation problem in the CT domain, which is presented in Subsection 3.1.3. The input to the discrete-time Hammerstein-bilinear (HB) model relates to the intermediate input via a static, memoryless, nonlinear function characterised by p_i , $i = 1, \dots, r$, parameters. It is assumed, that the static input nonlinearity is parameterized by the following linear-in-parameters r^{th} order polynomial function

$$v(k) = \phi(u(k)) = p_1 u(k) + p_2 u^2(k) + \dots + p_r u^r(k) \quad (4.1)$$

The dynamic part of the HB model is defined by the following single-input single-output difference equation

$$A(z^{-1})x(k) = B(z^{-1})v(k - \tau) + \sum_{i=1}^n \sum_{j=1}^n c_{i,j} v(k - i - \tau) x(k - j) \quad (4.2)$$

where the constant coefficient polynomials $A(z^{-1})$ and $B(z^{-1})$ of orders $n \geq m$, respectively, are defined in (2.53) and repeated below

$$\begin{aligned} A(z^{-1}) &= 1 + a_1 z^{-1} + \dots + a_n z^{-n} \\ B(z^{-1}) &= b_1 z^{-1} + \dots + b_m z^{-m} \end{aligned}$$

The difference equation (4.2) relates the delayed intermediate input $v(k - \tau)$ to the noise-free (unobserved) output $x(k)$. The constant τ denotes a pure time transportation delay in time units, and is assumed to be an integer valued number related to the sampling time interval, i.e. $\tau = kh$, for $k = 0, 1, 2, \dots, N$. Note, that some of the $c_{i,j}$ parameters associated with the nonlinear terms can be set to zero.

Next, it is assumed that the measured input-output data are uniformly sampled, at sampling time interval h . The sampled signals are denoted $u(k)$ and $y(k)$, cf. Remark 2.3 on nomenclature used. The output observation equation takes the following form

$$y(k) = x(k) + \xi(k) \quad (4.3)$$

where the measured output $y(k)$ is corrupted by an additive measurement noise $\xi(k)$. The additive measurement noise is modelled as white, normally distributed, zero mean, sequence denoted $e(k)$, i.e. $\xi(k) = e(k) = \mathcal{N}(0, \sigma_e^2)$.

The model order determination, including time delay estimation, is not considered hereinafter. Collecting relations (4.1), (4.2) and (4.3), which define the HB model and formulating the dynamic bilinear submodel (4.2) in the linear in structure MISO TF form, cf. Remark 2.4, gives

$$v(k) = \sum_{i=1}^r p_i u^i(k) \quad (4.4a)$$

$$x(k) = \frac{B(z^{-1})}{A(z^{-1})} v(k) + \sum_{i=1}^n \sum_{j=1}^n \frac{c_{i,j}}{A(z^{-1})} v_{i,j}(k) \quad (4.4b)$$

$$y(k) = x(k) + e(k) \quad (4.4c)$$

where the additional inputs are defined as

$$v_{i,j}(k) = v(k-i)x(k-j) \quad \text{for } i = 1, \dots, n, \text{ and } j = 1, \dots, n \quad (4.5)$$

The complete parameter estimation problem then consist of estimating the unknown parameter vector comprising the parameter sets for the linear, bilinear and static nonlinear parts

$$\boldsymbol{\theta} = \left[\boldsymbol{\theta}_l^T \quad \boldsymbol{\theta}_b^T \quad \boldsymbol{\theta}_n^T \right]^T \quad (4.6)$$

based on N uniformly sampled measured input-output data $Z^N = \{u(k), y(k)\}_{k=1}^N$. The parameter vectors defining linear dynamic part, bilinear part and static input nonlinearity, denoted $\boldsymbol{\theta}_l$, $\boldsymbol{\theta}_b$ and $\boldsymbol{\theta}_n$, respectively, are defined as

$$\boldsymbol{\theta}_l = \left[a_1 \quad \dots \quad a_n \quad b_1 \quad \dots \quad b_m \right]^T \quad (4.7a)$$

$$\boldsymbol{\theta}_b = \left[c_{1,1} \quad \dots \quad c_{n,1} \quad c_{n,2} \quad \dots \quad c_{n,n} \right]^T \quad (4.7b)$$

$$\boldsymbol{\theta}_n = \left[p_1 \quad \dots \quad p_r \right]^T \quad (4.7c)$$

Additionally, the parameter vector consisting only of parameters related to the dynamic part of the HB model is defined, i.e.

$$\boldsymbol{\theta}_{lb} = \left[\boldsymbol{\theta}_l^T \quad \boldsymbol{\theta}_b^T \right]^T \quad (4.8)$$

4.2 Simplified refined instrumental variable method

The SRIV algorithm is formulated for the case of parameter estimation of the dynamic part of the HB model (4.4). Therefore, the static input nonlinearity is assumed to be linear, i.e. (4.4a) reduces to $v(t) = u(t)$. In the present situation, the suitable error function $\varepsilon(k)$ for estimating the parameter set $\boldsymbol{\theta}_{lb}$ is defined as follows

$$\varepsilon(k) = \frac{1}{A(z^{-1})} \left[A(z^{-1})y(k) - B(z^{-1})u(k) - \sum_{i=1}^n \sum_{j=1}^n c_{i,j} u_{i,j}(k) \right] \quad (4.9)$$

which is in accordance with the equivalently defined error function in the CT setting (cf. (3.14)). The additional inputs are defined as $u_{i,j}(k) = u(k-i)y(k-j)$, for $i = 1, \dots, n$, and $j = 1, \dots, n$, where for realisability the unobserved output $x(k)$ in (4.5) is replaced with the measured output $y(t)$ under the assumption of input $u(k)$ being uncorrelated with the noise $e(k)$. It is noted, that the polynomial operators commute in this linear case, hence defining the linear prefilter

$$f(z^{-1}) = \frac{1}{A(z^{-1})} \quad (4.10)$$

the error function can be written as

$$\varepsilon(k) = A(z^{-1})y_f(k) - B(z^{-1})u_f(k) - \sum_{i=1}^n \sum_{j=1}^n c_{i,j} \{u_{i,j}\}_f(k) \quad (4.11)$$

The subscript f in (4.11) denotes that the input-output signals y , u and $u_{i,j}$ are prefiltered by $f(z^{-1})$, such that

$$y_f(k) = \frac{1}{A(z^{-1})}y(k), \quad u_f(k) = \frac{1}{A(z^{-1})}u(k), \quad \{u_{i,j}\}_f(k) = \frac{1}{A(z^{-1})}u_{i,j}(k) \quad (4.12)$$

The curly parentheses then indicate that the input signals $u_{i,j}$ are filtered by the prefilter $f(z^{-1})$.

In order to obtain the explicit solution for $\boldsymbol{\theta}_{lb}$ the minimised error function (4.11) is formulated in the pseudo-linear regression form

$$\varepsilon(k) = y_f(k) - \boldsymbol{\varphi}_f^T(k)\boldsymbol{\theta}_{lb} \quad (4.13)$$

where the regression vector is defined as

$$\boldsymbol{\varphi}_f^T(k) = \begin{bmatrix} -y_f(k-1) & \cdots & -y_f(k-n) & u_f(k-1) & \cdots & u_f(k-m) \\ \{u_{1,1}\}_f(k) & \cdots & \{u_{n,1}\}_f(k) & \{u_{n,2}\}_f(k) & \cdots & \{u_{n,n}\}_f(k) \end{bmatrix} \quad (4.14)$$

The IV least squares *en bloc* solution is then

$$\hat{\boldsymbol{\theta}}_{lb} = \left[\sum_{k=1}^N \hat{\boldsymbol{\varphi}}_f(k) \boldsymbol{\varphi}_f^T(k) \right]^{-1} \sum_{k=1}^N \hat{\boldsymbol{\varphi}}_f^T(k) y_f(k) \quad (4.15)$$

where $\hat{\boldsymbol{\varphi}}_f(k)$ denotes the instrumental variable regression vector, which is formulated as follows

$$\hat{\boldsymbol{\varphi}}_f^T(k) = \begin{bmatrix} -\hat{x}_f(k-1) & \cdots & -\hat{x}_f(k-n) & u_f(k-1) & \cdots & u_f(k-m) \\ \{\hat{u}_{1,1}\}_f(k) & \cdots & \{\hat{u}_{n,1}\}_f(k) & \{\hat{u}_{n,2}\}_f(k) & \cdots & \{\hat{u}_{n,n}\}_f(k) \end{bmatrix} \quad (4.16)$$

The simulated noise free output $\hat{x}(k)$ is selected as an instrumental variable series in (4.16), so that the IV additional inputs are then defined as

$$\hat{u}_{i,j}(k) = u(k-i)\hat{x}(k-j) \quad \text{for } i = 1, \dots, n, \text{ and } j = 1, \dots, n \quad (4.17)$$

where $\hat{x}(k)$ is the output of the following auxiliary model

$$\hat{x}(k) = \frac{1}{A(z^{-1}, \hat{\boldsymbol{\theta}}_l)} \left[B(z^{-1}, \hat{\boldsymbol{\theta}}_l) u(k) + \sum_{i=1}^n \sum_{j=1}^n c_{i,j}(\hat{\boldsymbol{\theta}}_b) u(k-i)\hat{x}(k-j) \right] \quad (4.18)$$

The notation $c_{i,j}(\hat{\boldsymbol{\theta}}_b)$ indicates that the estimated parameters $c_{i,j}$ are used, which are part of the estimated parameter vector $\hat{\boldsymbol{\theta}}_b$.

Similarly to the SRIVC algorithm 3.1, the SRIV algorithm is implemented as follows

Algorithm 4.1 (SRIV).

Stage 1 Initialisation: Compute an initial parameter vector estimate $\hat{\boldsymbol{\theta}}_{lb}^g$, for $g = 0$, where g denotes the iteration number. In (4.15), the filtered

regression and IV regression vectors are chosen as

$$\begin{aligned}\varphi_f^T(k) &= \varphi^T(k) \\ \hat{\varphi}_f^T(k) &= \varphi^T(k)\end{aligned}$$

where the filtered input-output signals are replaced by the directly measured, unfiltered, signals. Therefore, the SRIV algorithm is initiated by a simple least squares estimate of autoregressive with exogenous input (ARX) model.

Stage 2 Iterative IV estimation

for $g = 1$: convergence (see (4.20))

- (1) Generate the instrumental variable series (modelled output) using the auxiliary model (4.18) based on the estimated parameter set from the previous iteration step $\hat{\theta}_{lb}^{g-1}$, i.e.

$$\begin{aligned}\hat{x}(k) = \frac{1}{A(z^{-1}, \hat{\theta}_l^{g-1})} & \left[B(z^{-1}, \hat{\theta}_l^{g-1})u(k) \right. \\ & \left. + \sum_{i=1}^n \sum_{j=1}^n c_{i,j}(\hat{\theta}_b^{g-1})u(k-i)\hat{x}(k-j) \right]\end{aligned}$$

- (2) Prefilter signals $y(k)$, $u(k)$, $u_{i,j}(k)$, $\hat{x}(k)$ and $\hat{u}_{i,j}(k)$ by the filter

$$f(z^{-1}, \hat{\theta}_l^{g-1}) = \frac{1}{A(z^{-1}, \hat{\theta}_l^{g-1})}$$

- (3) Form the filtered regression vector $\varphi_f^T(k)$ and the IV regression vector $\hat{\varphi}_f^T(k)$ according to (4.14) and (4.16), respectively, and compute the latest parameter vector estimate using

$$\hat{\theta}_{lb}^g = \left[\sum_{k=1}^N \hat{\varphi}_f(k) \varphi_f^T(k) \right]^{-1} \sum_{k=1}^N \hat{\varphi}_f^T(k) y_f(k)$$

end

Stage 3 Parametric error computation: Compute the estimated parametric error covariance matrix associated with the final parameter vec-

tor estimate

$$\hat{\mathbf{P}} = \hat{\sigma}_e^2 \left[\sum_{k=1}^N \hat{\boldsymbol{\varphi}}_f(k) \hat{\boldsymbol{\varphi}}_f^T(k) \right]^{-1} \quad (4.19)$$

where $\hat{\sigma}_e^2$ denotes the estimated noise variance defined in (4.21).

Equivalently to the SRIVC algorithm 3.1, the convergence criterion monitoring the maximum relative change of parameter estimates is also used, i.e.

$$\max_i \left| \frac{\hat{\boldsymbol{\theta}}_{lb}^{g+1}(i) - \hat{\boldsymbol{\theta}}_{lb}^g(i)}{\hat{\boldsymbol{\theta}}_{lb}^{g+1}(i)} \right| < \epsilon, \quad \text{for } i = 1, 2, \dots, p \quad (4.20)$$

The number of parameter estimates is denoted p and ϵ is a user specific threshold limit. The rounded parentheses after vector $\hat{\boldsymbol{\theta}}_{lb}$ denote the vector index. Note, that the maximum number of parameter estimates is $n + m + (n \times n)$, but some parameters can be set zero. The noise variance estimate, required in (4.19), is computed by

$$\hat{\sigma}_e^2 = \frac{1}{N - p} \sum_{k=1}^N \left[y_f(k) - \boldsymbol{\varphi}_f^T(k) \hat{\boldsymbol{\theta}}_{lb} \right]^2 \quad (4.21)$$

where the final parameter vector estimate is used, i.e. $\hat{\boldsymbol{\theta}}_{lb} = \hat{\boldsymbol{\theta}}_{lb}^g$, for $g = \text{end}$.

4.3 Hammerstein SRIV (HSRIV) method

Equivalently to the HSRIVC algorithm 3.4, the HSRIV parameter estimation method is a two step, iterative, algorithm. In Step 1, it is postulated that the estimate of the parameters defining the static nonlinear block, $\boldsymbol{\theta}_n$, is already available. Thus, by knowing $\boldsymbol{\theta}_n$ it is then possible to compute the intermediate input $v(k)$ and, subsequently, the parameters corresponding to the bilinear submodel, $\boldsymbol{\theta}_{lb}$, are estimated. The estimate of $\boldsymbol{\theta}_{lb}$ is obtained by the SRIV algorithm 4.1, where the input $u(k)$ is replaced with $v(k)$.

Considering Step 2, the estimate of $\boldsymbol{\theta}_{lb}$ is available from the previous step. Subsequently, in order to estimate the parameter set $\boldsymbol{\theta}_n$, the HB model (4.4) must be rearranged with respect to this unknown parameter set and the new corresponding equation error $\varepsilon(k)$ must be formed. Substituting the polynomial function (4.4a) for $v(k)$ in bilinear model (4.4b) and then substituting the resulting expression for $x(k)$ in the measurement equation (4.4c), assuming that the

input $u(k)$ is uncorrelated with the noise $e(k)$, gives

$$y(k) = \frac{B(z^{-1})}{A(z^{-1})} \sum_{l=1}^r p_l u^l(k) + \sum_{i=1}^n \sum_{j=1}^n \frac{c_{i,j}}{A(z^{-1})} \sum_{l=1}^r p_l u^l(k-i) y(k-j) + e(k) \quad (4.22)$$

Rearranging (4.22) with respect to θ_n , which consists of the parameters p_l , $l = 1, \dots, r$, leads to

$$y(k) = \sum_{l=1}^r p_l \left[\frac{B(z^{-1})}{A(z^{-1})} u^l(k) + \sum_{i=1}^n \sum_{j=1}^n \frac{c_{i,j}}{A(z^{-1})} u^l(k-i) y(k-j) \right] + e(k) \quad (4.23)$$

Under the chosen noise scenario, a suitable error function is then formulated as

$$\varepsilon(k) = \frac{1}{A(z^{-1})} \left[A(z^{-1}) y(k) - \sum_{l=1}^r p_l \left[B(z^{-1}) u^l(k) + \sum_{i=1}^n \sum_{j=1}^n c_{i,j} u^l(k-i) y(k-j) \right] \right] \quad (4.24)$$

Noting the definition of prefilter $f(z^{-1})$ given in (4.10), the term $1/A(z^{-1})$ can be taken inside the brackets so that the error function can be expressed as

$$\varepsilon(k) = A(z^{-1}) y_f(k) - \sum_{l=1}^r p_l \left[B(z^{-1}) \{u^l\}_f(k) + \sum_{i=1}^n \sum_{j=1}^n c_{i,j} \{u^l(k-i) y(k-j)\}_f \right] \quad (4.25)$$

The curly parentheses in (4.25) indicate which signal or a product of signals is filtered, hence the powers of signal $u(k)$ are filtered and also the products of time shifted powers of signal $u(k)$ and time shifted signal $y(k)$ are filtered.

In order to obtain the least squares solution to the given estimation problem, the above expression (4.25) is formulated in the pseudo-linear regression form

$$\varepsilon(k) = \bar{y}_f(k) - \varphi_f^T(k) \theta_n \quad (4.26)$$

where

$$\bar{y}_f(k) = A(z^{-1})y_f(k) \quad (4.27)$$

$$\varphi_f^T(t_k) = \begin{bmatrix} w_1(k) & \cdots & w_r(k) \end{bmatrix} \quad (4.28)$$

$$w_l(k) = B(z^{-1})\{u^l\}_f(k) + \sum_{i=1}^n \sum_{j=1}^n c_{i,j} \{u^l(k-i)y(k-j)\}_f$$

for $l = 1, \dots, r$. The IV least squares solution is then

$$\hat{\theta}_n = \left[\sum_{k=1}^N \hat{\varphi}_f(k) \varphi_f^T(k) \right]^{-1} \sum_{k=1}^N \hat{\varphi}_f^T(k) \bar{y}_f(k) \quad (4.29)$$

In accordance with the SRIV algorithm, the instrumental variable regression vector $\hat{\varphi}_f(k)$ is defined as

$$\hat{\varphi}_f^T(t_k) = \begin{bmatrix} \hat{w}_1(k) & \cdots & \hat{w}_r(k) \end{bmatrix} \quad (4.30)$$

$$\hat{w}_l(k) = B(z^{-1})\{u^l\}_f(k) + \sum_{i=1}^n \sum_{j=1}^n c_{i,j} \{u^l(k-i)\hat{x}(k-j)\}_f$$

for $l = 1, \dots, r$, with the noise free simulated output $\hat{x}(k)$ selected as an instrumental variable. The simulated output is computed according to (4.18), where the input $u(k)$ is replaced with the intermediate input $v(k)$.

Discrete-time implementation of the HSRIVC algorithm 3.4, based on the DT HB model governed by (4.4), is summarised as follows

Algorithm 4.2 (HSRIV).

Stage 1 Initialisation: Compute an initial parameter vector estimate $\hat{\theta}_{lb}^g$, for $g = 0$, where g denotes the iteration number. The static input function is initialised with $\hat{\theta}_n^0 = [1 \ 0 \ \cdots \ 0]^T$, i.e. $v(k) = u(k)$. In (4.29), the filtered regression and IV regression vectors are chosen as

$$\varphi_f^T(k) = \varphi^T(k)$$

$$\hat{\varphi}_f^T(k) = \varphi^T(k)$$

where the filtered input-output signals are replaced by the directly measured, unfiltered, signals.

Stage 2 Iterative estimation

for $g = 1$: convergence

(Step 1.a) Compute the intermediate input to the dynamic submodel

$$v(k) = \sum_{i=1}^r \hat{\theta}_n^{g-1}(i) u^i(k)$$

(Step 1.b) Generate the instrumental variable series

$$\hat{x}(k) = \frac{1}{A(z^{-1}, \hat{\theta}_l^{g-1})} \left[B(z^{-1}, \hat{\theta}_l^{g-1}) v(k) + \sum_{i=1}^n \sum_{j=1}^n c_{i,j}(\hat{\theta}_b^{g-1}) v(k-i) \hat{x}(k-j) \right]$$

(Step 1.c) Prefilter signals $y(k)$, $v(k)$, $v_{i,j}(k)$, $\hat{x}(k)$ and $\hat{v}_{i,j}(k)$ by the filter

$$f(z^{-1}, \hat{\theta}_l^{g-1}) = \frac{1}{A(z^{-1}, \hat{\theta}_l^{g-1})}$$

where $v_{i,j}(k) = v(k-i)y(k-j)$ and $\hat{v}_{i,j}(k) = v(k-i)\hat{x}(k-j)$, for $i = 1, \dots, n$ and $j = 1, \dots, n$.

(Step 1.d) Form the regression vectors $\varphi_f^T(k)$ and $\hat{\varphi}_f^T(k)$, defined in (4.14) and (4.16), respectively, where all the inputs $u(k)$ are replaced with $v(k)$. Compute the latest parameter vector estimate using

$$\hat{\theta}_{lb}^g = \left[\sum_{k=1}^N \hat{\varphi}_f(k) \varphi_f^T(k) \right]^{-1} \sum_{k=1}^N \hat{\varphi}_f^T(k) y_f(k)$$

(Step 2.a) Prefilter signals contained in w_l and $\hat{w}_l(k)$, for $l = 1, \dots, r$, as defined in (4.28) and (4.30), respectively, using the updated filter, i.e.

$$f(z^{-1}, \hat{\theta}_l^g) = \frac{1}{A(z^{-1}, \hat{\theta}_l^g)}$$

(Step 2.b) Form the regression vectors $\varphi_f^T(k)$ and $\hat{\varphi}_f^T(k)$ according to (4.28) and (4.30), respectively. Form the output $\bar{y}_f(k)$ defined in

(4.27). Obtain the latest least squares estimate

$$\hat{\boldsymbol{\theta}}_n^g = \left[\sum_{k=1}^N \hat{\boldsymbol{\varphi}}_f(k) \boldsymbol{\varphi}_f^T(k) \right]^{-1} \sum_{k=1}^N \hat{\boldsymbol{\varphi}}_f(k) \bar{y}_f(k)$$

end

Stage 3 Parametric error computation: Compute the estimated parametric error covariance matrices denoted $\hat{\mathbf{P}}_{lb}$ and $\hat{\mathbf{P}}_n$ associated with the final parameter vector estimates $\hat{\boldsymbol{\theta}}_{lb}$ and $\hat{\boldsymbol{\theta}}_n$, respectively, hence

$$\hat{\mathbf{P}}_{lb} = \hat{\sigma}_e^2 \left[\sum_{k=1}^N \hat{\boldsymbol{\varphi}}_f(k) \hat{\boldsymbol{\varphi}}_f^T(k) \right]^{-1} \quad (4.32a)$$

$$\hat{\mathbf{P}}_n = \hat{\sigma}_e^2 \left[\sum_{k=1}^N \boldsymbol{\varphi}_f(k) \boldsymbol{\varphi}_f^T(k) \right]^{-1} \quad (4.32b)$$

where the appropriate regression vectors $\hat{\boldsymbol{\varphi}}_f(k)$ and $\boldsymbol{\varphi}_f(k)$ are used as defined in Steps 1 and 2.

Equivalently to the HSRIVC algorithm 3.4, the convergence criterion might be selected to monitor the maximum relative change of parameter estimates, see (3.80), or to monitor the value of the integral of absolute error (3.81). The estimate of the noise variances $\hat{\sigma}_e^2$ and $\hat{\sigma}_e^2$, defined in (4.32), is computed according to (4.21), where the input signal $u(k)$ is replaced with $v(k)$ and the output signal $y(k)$ is replaced with $\bar{y}(k)$, respectively.

4.3.1 Constrained HSRIV method

The constrained static nonlinear input function is derived in (3.89) and repeated below

$$v(k) = u(k) + \sum_{i=2}^r p_i [-u(k) + u^i(k)] \quad (4.33)$$

The function (4.33) is defined for the input signal $u(k)$ in a range $u(k) \in \langle 0, 1 \rangle$ and the parameter p_1 of the original, unconstrained, polynomial (4.4a) is then computed according to

$$p_1 = 1 - \sum_{i=2}^r p_i \quad (4.34)$$

Note, that the output $v(k)$ of the constrained polynomial (4.33), for a given input $u(k)$ and parameter set $p_i, i = 2, \dots, r$, would be the same as the output of the original polynomial function (4.4a), when the parameter p_1 is computed according to (4.34).

The constrained polynomial expression (4.33) is substituted for $v(k)$ in the bilinear model (4.4b), so that the expression (4.22) then takes the following form

$$\begin{aligned}
 y(k) = & \frac{B(z^{-1})}{A(z^{-1})} \left(u(k) + \sum_{l=2}^r p_l [-u(k) + u^l(k)] \right) + e(k) \\
 & + \sum_{i=1}^n \sum_{j=1}^n \frac{c_{i,j}}{A(z^{-1})} \left(u(k-i) + \sum_{l=2}^r p_l [-u(k-i) + u^l(k-i)] \right) y(k-j)
 \end{aligned} \tag{4.35}$$

Expressing (4.35) with respect to parameters $p_l, l = 2, \dots, r$, leads to

$$\begin{aligned}
 y(k) = & \frac{B(z^{-1})}{A(z^{-1})} u(k) + \sum_{i=1}^n \sum_{j=1}^n \frac{c_{i,j}}{A(z^{-1})} u(k-i) y(k-j) \\
 & + \sum_{l=2}^r p_l \left[-\frac{B(z^{-1})}{A(z^{-1})} u(k) - \sum_{i=1}^n \sum_{j=1}^n \frac{c_{i,j}}{A(z^{-1})} u(k-i) y(k-j) \right. \\
 & \left. + \frac{B(z^{-1})}{A(z^{-1})} u^l(k) + \sum_{i=1}^n \sum_{j=1}^n \frac{c_{i,j}}{A(z^{-1})} u^l(k-i) y(k-j) \right] + e(k)
 \end{aligned} \tag{4.36}$$

Similarly to the error function (4.25) of the unconstrained HSRIV algorithm, a suitable error function for the constrained HSRIV algorithm, consisting of pre-filtered signals, is formulated as

$$\begin{aligned}
 \varepsilon(k) = & A(z^{-1})y_f(k) - B(z^{-1})u_f(k) - \sum_{i=1}^n \sum_{j=1}^n c_{i,j} \{u(k-i)y(k-j)\}_f \\
 & - \sum_{l=2}^r p_l \left[-B(z^{-1})u_f(k) - \sum_{i=1}^n \sum_{j=1}^n c_{i,j} \{u(k-i)y(k-j)\}_f \right. \\
 & \left. + B(z^{-1})\{u^l\}_f(k) + \sum_{i=1}^n \sum_{j=1}^n c_{i,j} \{u^l(k-i)y(k-j)\}_f \right]
 \end{aligned} \tag{4.37}$$

The above expression (4.37) is then re-written in the pseudo-linear regression form

$$\varepsilon(k) = \bar{y}_f(k) - \boldsymbol{\varphi}_f^T(k) \boldsymbol{\theta}_n \tag{4.38}$$

where

$$\boldsymbol{\theta}_n = \begin{bmatrix} p_2 & \cdots & p_r \end{bmatrix}^T \quad (4.39)$$

$$\begin{aligned} \bar{y}_f(k) &= A(z^{-1})y_f(k) - B(z^{-1})u_f(k) \\ &\quad - \sum_{i=1}^n \sum_{j=1}^n c_{i,j} \{u(k-i)y(k-j)\}_f \end{aligned} \quad (4.40)$$

$$\boldsymbol{\varphi}_f^T(k) = \begin{bmatrix} w_2(k) & \cdots & w_r(k) \end{bmatrix} \quad (4.41)$$

$$\begin{aligned} w_l(k) &= -B(z^{-1})u_f(k) - \sum_{i=1}^n \sum_{j=1}^n c_{i,j} \{u(k-i)y(k-j)\}_f \\ &\quad + B(z^{-1})\{u^l\}_f(k) + \sum_{i=1}^n \sum_{j=1}^n c_{i,j} \{u^l(k-i)y(k-j)\}_f \end{aligned}$$

for $l = 2, \dots, r$. Due to the use of the constrained polynomial (4.33) only $r - 1$ parameters need to be estimated. The instrumental variable regression vector also needs to be defined, hence

$$\hat{\boldsymbol{\varphi}}_f(k) = \begin{bmatrix} \hat{w}_2(k) & \cdots & \hat{w}_r(k) \end{bmatrix} \quad (4.42)$$

$$\begin{aligned} \hat{w}_l(k) &= -B(z^{-1})u_f(k) - \sum_{i=1}^n \sum_{j=1}^n c_{i,j} \{u(k-i)\hat{x}(k-j)\}_f \\ &\quad + B(z^{-1})\{u^l\}_f(k) + \sum_{i=1}^n \sum_{j=1}^n c_{i,j} \{u^l(k-i)\hat{x}(k-j)\}_f \end{aligned}$$

for $l = 2, \dots, r$ and $\hat{x}(k)$ being the instrumental variables. The overall number of parameters to be estimated is $n + m + (n \times n) + (r - 1)$.

The constrained HSRIV algorithm 4.2 is then implemented with the following differences:

- In Stage 1 the constrained static input nonlinear function is as defined in (4.33) and is initialised with $\hat{\boldsymbol{\theta}}_n^0 = [0 \ 0 \ \cdots \ 0]^T$.
- Stage 2, Step (1.a), the intermediate input to the dynamic submodel is computed according to

$$v(k) = u(k) + \sum_{i=2}^r \hat{\boldsymbol{\theta}}_n^{g-1}(i) [-u(k) + u^i(k)]$$

- Stage 2, Step (2.b), the regression vector $\boldsymbol{\varphi}_f^T(k)$ is newly defined in (4.41),

the IV regression vector is defined in (4.42), the output $\bar{y}_f(k)$ is defined in (4.40), and the parameter vector θ_n is redefined according to (4.39).

4.4 Over-parameterized HSRIV (HSRIV-OV) method

In the first step of the proposed HSRIV-OV parameter estimation method, an over-parameterized auxiliary dynamic model is estimated by the SRIV algorithm 4.1. Subsequently, the unique parameter sets defining the static and dynamic submodels are inferred in the next estimation step. Since, it is not possible to uniquely distinguish between the contributions of the individual submodels to the overall steady-state gain from measured input-output data, see Example 3.2, the steady-state gain of the static function is chosen to be constrained.

4.4.1 SRIV estimation of the over-parameterized model

The over-parameterized model is obtained such that the constrained polynomial function (4.33) is substituted for $v(k)$ in the bilinear model (4.4b) and then the resulting expression is substituted for $x(k)$ in the measurement equation (4.4c), cf. (4.35), which leads to

$$y(k) = \frac{B(z^{-1})}{A(z^{-1})} \left(u(k) + \sum_{l=2}^r p_l [-u(k) + u^l(k)] \right) + e(k) \\ + \sum_{i=1}^n \sum_{j=1}^n \frac{c_{i,j}}{A(z^{-1})} \left(u(k-i) + \sum_{l=2}^r p_l [-u(k-i) + u^l(k-i)] \right) y(k-j) \quad (4.43)$$

The new input signal is introduced for the index $l = 2, \dots, r$, i.e.

$$\bar{u}_l(k) = -u(k) + u^l(k) \quad (4.44)$$

and also the following parameters are introduced

$$\bar{b}_{i,l} = p_l b_i \quad \text{for } i = 1, \dots, m \quad (4.45a)$$

$$\bar{c}_{i,j,l} = p_l c_{i,j} \quad \text{for } i = 1, \dots, n, \text{ and } j = 1, \dots, n \quad (4.45b)$$

Additionally, the over-parameterized constant coefficient polynomial $B(z^{-1})$ is defined

$$\bar{B}_l(z^{-1}) = p_l B(z^{-1}) = \bar{b}_{1,l} z^{-1} + \dots + \bar{b}_{m,l} z^{-m} \quad (4.46)$$

for $l = 2, \dots, r$. Using the newly defined input $\bar{u}_l(k)$, the bilinear coefficients $\bar{c}_{i,j,l}$ and the polynomial $\bar{B}_l(z^{-1})$ the model (4.43) is re-expressed as

$$\begin{aligned}
 y(k) = & \frac{B(z^{-1})}{A(z^{-1})}u(k) + \sum_{i=1}^n \sum_{j=1}^n \frac{c_{i,j}}{A(z^{-1})}u(k-i)y(k-j) \\
 & + \sum_{l=2}^r \frac{\bar{B}_l(z^{-1})}{A(z^{-1})}\bar{u}_l(k) + \sum_{l=2}^r \sum_{i=1}^n \sum_{j=1}^n \frac{\bar{c}_{i,j,l}}{A(z^{-1})}\bar{u}_l(k-i)y(k-j) + e(k)
 \end{aligned} \tag{4.47}$$

The over-parameterized model (4.47) has $n + r \times (m + n \times n)$ parameters, which is $(r - 1)(m + n \times n - 1)$ parameters more than the HB model (4.35) estimated by the constrained iterative HSRIV algorithm. This difference in the number of parameters is important even for moderate values of r and can affect the accuracy of the estimates, see (Le, Markovsky, Freeman & Rogers 2011).

The error function (4.9) for the over-parameterized model (4.47) takes the following form

$$\begin{aligned}
 \varepsilon(k) = & \frac{1}{A(z^{-1})} \left[A(z^{-1})y(k) - B(z^{-1})u(k) - \sum_{i=1}^n \sum_{j=1}^n c_{i,j}u(k-i)y(k-j) \right. \\
 & \left. - \sum_{l=2}^r \bar{B}_l(z^{-1})\bar{u}_l(k) - \sum_{l=2}^r \sum_{i=1}^n \sum_{j=1}^n \bar{c}_{i,j,l}\bar{u}_l(k-i)y(k-j) \right]
 \end{aligned} \tag{4.48}$$

Subsequently, the prefilter $1/A(z^{-1})$ is taken inside the brackets so that the error function can be expressed in an equation error form, hence

$$\begin{aligned}
 \varepsilon(k) = & A(z^{-1})y_f(k) - B(z^{-1})u_f(k) - \sum_{i=1}^n \sum_{j=1}^n c_{i,j}\{u(k-i)y(k-j)\}_f \\
 & - \sum_{l=2}^r \bar{B}_l(z^{-1})\{\bar{u}_l\}_f(k) - \sum_{l=2}^r \sum_{i=1}^n \sum_{j=1}^n \bar{c}_{i,j,l}\{\bar{u}_l(k-i)y(k-j)\}_f
 \end{aligned} \tag{4.49}$$

The equation error (4.49) can be further expressed in the pseudo-linear regression form, i.e.

$$\varepsilon(k) = y_f(k) - \boldsymbol{\varphi}_{of}^T(k)\boldsymbol{\theta}_o \tag{4.50}$$

where $\boldsymbol{\theta}_o$ is the vector of the parameters in the over-parameterized model (4.47) defined as

$$\boldsymbol{\theta}_o = \left[\boldsymbol{\theta}_{lb}^T \quad p_2\bar{\boldsymbol{\theta}}^T \quad \dots \quad p_r\bar{\boldsymbol{\theta}}^T \right]^T \tag{4.51}$$

In (4.51) the parameter vector $\boldsymbol{\theta}_{lb}^T$ is provided in (4.8) and the new parameter

vector $\bar{\theta}$ is formed such that

$$\bar{\theta} = \left[b_1 \quad \cdots \quad b_m \quad c_{1,1} \quad \cdots \quad c_{n,1} \quad c_{n,2} \quad \cdots \quad c_{n,n} \right]^T \quad (4.52)$$

From (4.51) it is evident that the number of estimated parameters increases with the increasing order r of the constrained polynomial function (4.33). The regression vector for the over-parameterized model, denoted $\varphi_{of}^T(k)$, is defined as follows

$$\varphi_{of}^T(k) = \left[\varphi_f^T(k) \quad \bar{\varphi}_2^T(k) \quad \cdots \quad \bar{\varphi}_r^T(k) \right]^T \quad (4.53)$$

where the regression vector $\varphi_f^T(k)$ has been already defined for the case of the SRIV estimation of the bilinear submodel only, and is provided in (4.14). The new regression vectors $\bar{\varphi}_l^T(k)$, $l = 2, \dots, r$, are defined as

$$\begin{aligned} \bar{\varphi}_l^T(k) = & \left[\{ \bar{u}_l \}_f(k-1) \quad \cdots \quad \{ \bar{u}_l \}_f(k-m) \right. \\ & \{ \bar{u}_l(k-1)y(k-1) \}_f \quad \cdots \quad \{ \bar{u}_l(k-n)y(k-1) \}_f \\ & \left. \{ \bar{u}_l(k-n)y(k-2) \}_f \quad \cdots \quad \{ \bar{u}_l(k-n)y(k-n) \}_f \right] \end{aligned} \quad (4.54)$$

where the input $\bar{u}_l(k)$ is introduced in (4.44). The SRIV algorithm 4.1 uses the simulated output $\hat{x}(k)$ as an instrumental variable, hence the corresponding instrumental variable regression vector for the considered HSRIV-OV algorithm is defined as follows

$$\hat{\varphi}_{of}^T(k) = \left[\hat{\varphi}_f^T(k) \quad \hat{\bar{\varphi}}_2^T(k) \quad \cdots \quad \hat{\bar{\varphi}}_r^T(k) \right]^T \quad (4.55)$$

where $\hat{\varphi}_f^T(k)$ is defined in (4.16) and

$$\begin{aligned} \hat{\bar{\varphi}}_l^T(k) = & \left[\{ \bar{u}_l \}_f(k-1) \quad \cdots \quad \{ \bar{u}_l \}_f(k-m) \right. \\ & \{ \bar{u}_l(k-1)\hat{x}(k-1) \}_f \quad \cdots \quad \{ \bar{u}_l(k-n)\hat{x}(k-1) \}_f \\ & \left. \{ \bar{u}_l(k-n)\hat{x}(k-2) \}_f \quad \cdots \quad \{ \bar{u}_l(k-n)\hat{x}(k-n) \}_f \right] \end{aligned} \quad (4.56)$$

for $l = 2, \dots, r$. The instrumental variable \hat{x} is then the output of the auxiliary model

$$\begin{aligned} \hat{x}(k) = & \frac{B(z^{-1}, \hat{\theta}_o)}{A(z^{-1}, \hat{\theta}_o)} u(k) + \sum_{i=1}^n \sum_{j=1}^n \frac{c_{i,j}(\hat{\theta}_o)}{A(z^{-1}, \hat{\theta}_o)} u(k-i) \hat{x}(k-j) \\ & + \sum_{l=2}^r \frac{\bar{B}_l(z^{-1}, \hat{\theta}_o)}{A(z^{-1}, \hat{\theta}_o)} \bar{u}_l(k) + \sum_{l=2}^r \sum_{i=1}^n \sum_{j=1}^n \frac{\bar{c}_{i,j,l}(\hat{\theta}_o)}{A(z^{-1}, \hat{\theta}_o)} \bar{u}_l(k-i) \hat{x}(k-j) \end{aligned} \quad (4.57)$$

Finally, the over-parameterized model (4.47) is estimated by the SRIV algorithm 4.1. Since, the presented SRIV algorithm has been introduced for the estimation of the bilinear dynamic submodel only, the estimated parameter vector, regression vectors and the auxiliary model used for the instrumental variable generation need to be redefined as follows: The estimated parameter vector $\boldsymbol{\theta}_o$ has been defined in (4.51) and the corresponding regression vectors are defined in (4.53) and in (4.55), respectively. The instrumental variable is generated from the auxiliary model introduced in (4.57).

4.4.2 Inferring unique parameter vector defining the HB model

Once the parameter vector $\boldsymbol{\theta}_o$ has been estimated the parameter vectors $\boldsymbol{\theta}_n$ and $\boldsymbol{\theta}_{lb}$, which correspond to the static and dynamic submodels of the overall HB model (4.4), respectively, need to be inferred. Due to the particular choice of the constrained polynomial function (4.33), the estimated parameter vector $\boldsymbol{\theta}_o$ has a special structure (4.51), such that the first part of this vector is the sought $\boldsymbol{\theta}_{lb}$. Therefore, by virtue of estimating the parameter vector $\boldsymbol{\theta}_o$ the estimate of $\boldsymbol{\theta}_{lb}$ is also obtained.

Subsequently, in order to infer the parameter vector $\boldsymbol{\theta}_n$, which consists of parameters p_l , $l = 2, \dots, r$, it is noted that the known (estimated) parameter set $\boldsymbol{\theta}_{lb}$, which is defined in (4.8) and repeated below

$$\boldsymbol{\theta}_{lb} = \begin{bmatrix} \boldsymbol{\theta}_l^T & \boldsymbol{\theta}_b^T \end{bmatrix}^T \quad (4.58)$$

can be also expressed as

$$\boldsymbol{\theta}_{lb} = \begin{bmatrix} a_1 & \dots & a_n & \bar{\boldsymbol{\theta}}^T \end{bmatrix}^T \quad (4.59)$$

where $\bar{\boldsymbol{\theta}}$, introduced in (4.52), is part of the estimated $\boldsymbol{\theta}_o$.

Therefore, the estimate of $\bar{\boldsymbol{\theta}}$, denoted $\hat{\bar{\boldsymbol{\theta}}}$, is known from the estimated vector $\boldsymbol{\theta}_{lb}$, cf. (4.59). Defining new parameter vector

$$\bar{\boldsymbol{\vartheta}}_l = p_l \bar{\boldsymbol{\theta}} \quad (4.60)$$

for $l = 2, \dots, r$, the parameter vector $\boldsymbol{\theta}_o$, defined in (4.51), can be expressed as

$$\boldsymbol{\theta}_o = \begin{bmatrix} \boldsymbol{\theta}_{lb}^T & \bar{\boldsymbol{\vartheta}}_2^T & \dots & \bar{\boldsymbol{\vartheta}}_r^T \end{bmatrix}^T \quad (4.61)$$

Considering the new definition of $\boldsymbol{\theta}_o$ provided in (4.61) and having the estimate of $\bar{\boldsymbol{\theta}}$ the individual estimated static parameters are computed as follows

$$\hat{\boldsymbol{p}}_l = \hat{\boldsymbol{v}}_l \left(\text{diag } \hat{\boldsymbol{\theta}} \right)^{-1} \quad \text{for } l = 2, \dots, r \quad (4.62)$$

where the hat denotes an estimated value and \boldsymbol{p}_l denotes $1 \times (m + nn)$ vector composing of p_l parameters only, i.e.

$$\boldsymbol{p}_l = \left[p_l \quad \cdots \quad p_l \right] \quad (4.63)$$

Equation (4.62) then indicates that every parameter p_l , $l = 2, \dots, r$, is estimated as many times as is the dimension of the vector $\bar{\boldsymbol{\theta}}$, which is $m + (n \times n)$ times.

Clearly, the estimated individual p_l parameters, being part of the vector \boldsymbol{p}_l , are not the same, because of the measurement noise influence and/or the influence of the unmodelled system dynamics. To solve for this parameter redundancy problem a simple approach is to take an average value, see e.g. (Eskinat et al. 1991, Ni et al. 2012). The average estimate of parameters p_l , for $l = 2, \dots, r$, is

$$\bar{\hat{p}}_l = \frac{1}{m + nn} \sum_i^{m+nn} \hat{\boldsymbol{p}}_l(i) \quad (4.64)$$

where the bar above the estimate \hat{p}_l denotes an average value.

Taking an average value of estimated vector \boldsymbol{p}_l means that some estimated p_l , $l = 2, \dots, r$, parameters are better (in terms of model parameter accuracy) than the others. The more reliable approach, reported in (Chang & Luus 1971), is to select only such p_l parameters from the vector \boldsymbol{p}_l , for $l = 2, \dots, r$, which minimise a predefined cost function. *This approach is also adopted in this work* and the cost is defined as an error between the measured and modelled output in a least squares sense, i.e.

$$U = \frac{1}{N} \sum_{k=1}^N \left[y(k) - \hat{x}(\hat{\boldsymbol{\theta}}_{lb}, \hat{\boldsymbol{\theta}}_n, k) \right]^2 \quad (4.65)$$

where N denotes the overall number of data samples and $\hat{x}(\hat{\boldsymbol{\theta}}_{lb}, \hat{\boldsymbol{\theta}}_n, k)$ denotes the simulated output based on the estimated parameter vector $\hat{\boldsymbol{\theta}}_{lb}$ and the currently evaluated $\hat{\boldsymbol{\theta}}_n$.

For completeness, there are at least two other approaches for inferring the estimates of $\boldsymbol{\theta}_{lb}$ and $\boldsymbol{\theta}_n$ reported in the literature. The first approach infers the individual p_l parameters by means of a least squares algorithm, see (Hsia

1976). Instead of taking an average value as suggested in (4.64), the least squares estimate is computed instead. The second approach, reported in (Bai 1998), uses singular value decomposition to separate the two parameter sets from the over-parameterized estimate of θ_o .

4.5 Numerical study

In this MCS simulation analysis the iterative constrained backfitting HSRIV algorithm, stated in Subsection 4.3.1, is compared with the noniterative HSRIV-OV algorithm stated in Section 4.4. The HSRIV-OV algorithm effectively comprises two distinct parts (stages). In the first part, denoted for clarity HSRIV-OV1, the over-parameterized auxiliary model is estimated as described in Subsection 4.4.1. Subsequently, in the second part, denoted for clarity HSRIV-OV2, the static and dynamic components of the overall HB model are recovered from this estimated auxiliary model as described in Subsection 4.4.2. In order to gain a more detailed insight into the performance of the two stage HSRIV-OV algorithm, the performance criteria for the estimated over-parameterized model, i.e. the algorithm HSRIV-OV1 used in the first stage, and the performance criteria for the recovered HB model, i.e. the algorithm HSRIV-OV2 used in the second stage, are evaluated and presented separately.

The CT HB system adopted in the Case scenario I of the MCS analysis presented in Subsection 3.5.1, governed by (3.116) and (3.123), is discretised and used here. Therefore, it is possible to directly compare the performance of the continuous-time HSRIVC (SRIVC) and discrete-time HSRIV (SRIV) algorithms. This also allows the indirect comparison of the HSRIVC and HSRIV-OV algorithms. The structure preserving Euler forward discretisation method is applied such that the discrete-time parameters of the bilinear submodel are $a_1 = \alpha_1 h - 1$, $b_1 = \beta_0 h$ and $c_{1,1} = \eta_1 h$. The resulting DT HB system having a constrained static input nonlinearity is

$$v(k) = u(k) + \sum_{i=2}^3 p_i [-u(k) + u^i(k)] \quad (4.66a)$$

$$x(k) = \frac{b_1 z^{-1}}{1 + a_1 z^{-1}} v(k) + \frac{c_{1,1}}{1 + a_1 z^{-1}} v(k-1)x(k-1) \quad (4.66b)$$

$$y(k) = x(k) + e(k) \quad (4.66c)$$

where the corresponding parameter sets, adopting a sampling interval $h = 5$ [s],

are

$$\boldsymbol{\theta}_n = \begin{bmatrix} p_2 & p_3 \end{bmatrix}^T = \begin{bmatrix} -4.4 & 2 \end{bmatrix}^T \quad (4.67a)$$

$$\boldsymbol{\theta}_{lb} = \begin{bmatrix} a_1 & b_1 & c_{1,1} \end{bmatrix}^T = \begin{bmatrix} -0.9875 & -0.5 & -0.0125 \end{bmatrix}^T \quad (4.67b)$$

Considering the HSRIV-OV algorithm, due to the increasing dimensionality of the estimation problem with the increasing order of the system, the higher order CT system presented in the Case scenario II, Subsection 3.5.2, is not used in this numerical study.

The design of the presented MCS simulation study is equivalent to that used for the continuous-time parameter estimation methods with $M = 100$ realisations, cf. Section 3.5. This also includes the selection of the same model fit and parameter accuracy criteria. The input-output signals and the static input non-linearity are shown in Figure 3.3. Two noise scenarios are considered, namely low and high, respectively. The NSR for the low noise scenario is fixed at 10 [%], which is anticipated to be present on an actual HVAC systems. The NSR for the high noise case scenario is 30 [%], which corresponds to a rather severe noise contamination. When initialising the iterative HSRIV algorithm the static input nonlinearity is assumed to be linear, i.e. $v(t) = u(t)$, hence setting $\hat{\boldsymbol{\theta}}_n^0 = [0 \ 0]^T$. Both the HSRIV and HSRIV-OV algorithms are initialised with a least squares estimate of an auxiliary ARX model. The results for SRIV estimation of the dynamic bilinear submodel only, i.e. $v(t) = u(t)$ in (4.66), are also provided.

4.5.1 Results

Table 4.1 presents the single run and MCS estimation results for the considered algorithms. The single run estimates are obtained for the noise seed value 22. In the case of SRIV and HSRIV algorithms, the SD (standard deviations) and SE (standard errors) values are reasonably matched. In both cases, the estimated standard errors are approximately two orders of magnitude smaller than the estimated parameters. Comparing the SD and SE values of the HSRIV-OV and HSRIV algorithms, it is noted that these are always higher in the case of the HSRIV-OV algorithm. This indicates a lower estimation accuracy for the HSRIV-OV algorithm.

A more comprehensive set of numerical results are provided in Table 4.2, where the mean and associated SD values of IAE , $\hat{\sigma}_e^2$, $AC(\hat{\boldsymbol{\theta}}_{lb})$, and $AC(\hat{\boldsymbol{\theta}}_n)$ performance criteria are given. The SRIV, HSRIV and HSRIV-OV1 algorithms consis-

tently provide noise variance estimates, which are close to the true noise variances (stated in the caption of Table 4.2). The IAE and $\hat{\sigma}_e^2$ model fit criteria for the HB model obtained by the HSRIV algorithm and for the over-parameterized model obtained by the HSRIV-OV1 algorithm are virtually the same. However, the HB model inferred from the over-parameterized model, obtained by the HSRIV-OV2 algorithm, performs poorly in terms of the $AC(\hat{\theta}_{lb})$ and $AC(\hat{\theta}_n)$ criteria. Comparing the HB models obtained by the HSRIV and HSRIV-OV2 algorithms, it is evident that the inferred parameter estimates are approximately three times less accurate. This indicates that the over-parameterized HB model, estimated in the first stage of the HSRIV-OV algorithm, i.e. HSRIV-OV1, is suitable for simulation purposes. However, the inferred HB model, obtained in the second stage of the HSRIV-OV algorithm, i.e. HSRIV-OV2, is neither suitable for simulation purposes nor for control design.

In Figures 4.1 and 4.2 the true (grey solid line) static function and system output are compared with the corresponding MCS estimates (black solid lines) for low and high noise scenarios, respectively. The results are displayed for the HSRIVC and HSRIVC-OV algorithms only. It is observed that the HSRIV algorithm is able to obtain accurate and consistent static function estimates, including the simulated outputs. Considering the HSRIV-OV algorithm, the static function estimates are widely spread around the true static function. This indicates a poor performance and inability to recover the static and dynamic components from the over-parameterized HB model consistently.

4.6 Conclusions

In this chapter, the discrete-time SRIV and HSRIV parameter estimation methods for bilinear and Hammerstein-bilinear model parameter estimation, respectively, have been introduced. In a similar manner to the fact that the bilinear model structure is a subset of a wider Hammerstein-bilinear model class, the SRIV algorithm can be viewed as a special case (or subset) of the more general HSRIV algorithm. Additionally, an over-parameterized, noniterative, counterpart to the iterative HSRIV algorithm, abbreviated HSRIV-OV, has also been proposed.

A Monte Carlo simulation analysis has shown that a better model fit can be obtained by the iterative HSRIV algorithm as compared to the HSRIV-OV algorithm. It is postulated, that the statistical efficiency of the HSRIV-OV algorithm is impaired by the fact that the over-parameterized model is estimated instead of the appropriately (i.e. minimum number of parameters) parameterized model.

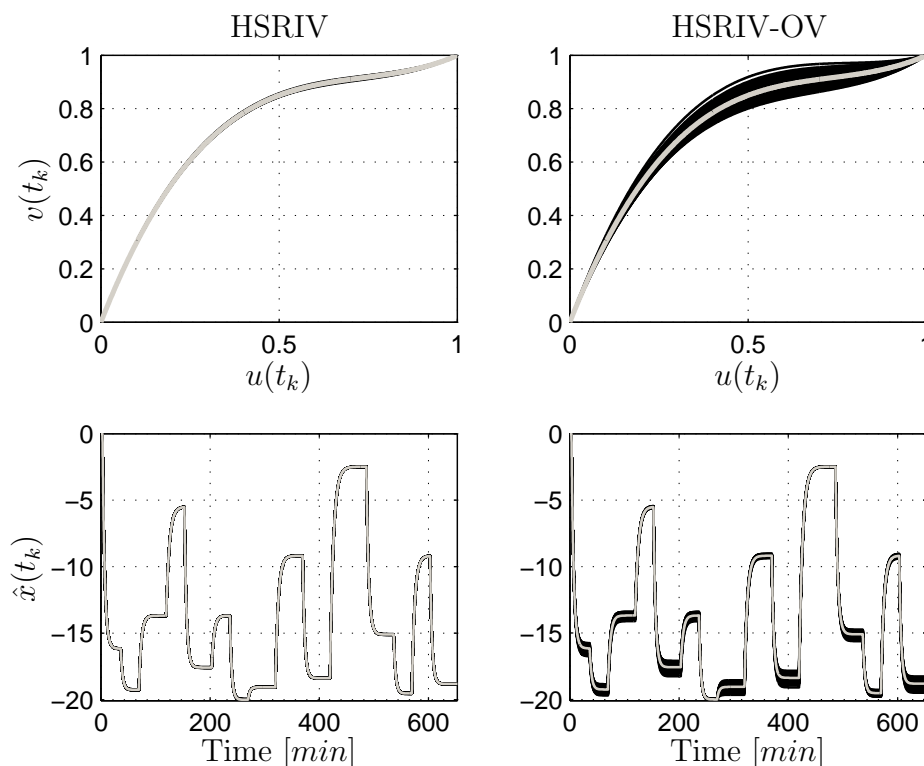


Figure 4.1: Monte Carlo simulation results for low noise scenario $NVR = 10$ [%]. The estimated HB models obtained by the HSRIV (left-hand side plots) and HSRIV-OV (right-hand side plots) algorithms are compared. The true static functions and system outputs (grey solid lines) are plotted against the estimated responses (black solid lines).

The HSRIV algorithm has been able to obtain consistent and accurate estimates of the individual static and dynamic submodels. This makes the HSRIV algorithm a suitable choice when estimating the DT Hammerstein-bilinear models for control analysis and design purposes. For example, some control methods are based on an inverse function of the estimated static input nonlinearity, so that the control performance then depends on an accurate estimate of such an input function.

The iterative HSRIV algorithm requires an initial estimate of the static input nonlinearity, which can be based on *a priori* technical knowledge. The accuracy of this initial estimate may then influence the convergence and overall performance of the algorithm. In the case of the HSRIV-OV algorithm, no *a priori* knowledge regarding the static input function estimate is required. The HSRIV-OV algorithm can be initialised in a straightforward manner based on a relatively simple least square estimate of an over-parameterized ARX model. Therefore, it is pro-

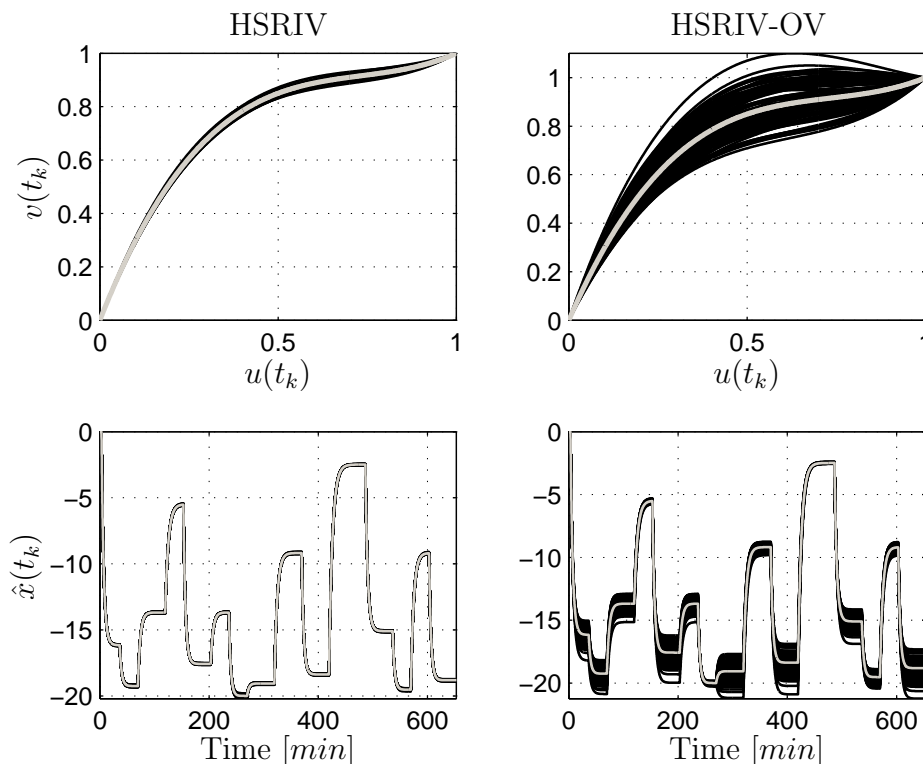


Figure 4.2: Monte Carlo simulation results for high noise scenario $NVR = 30$ [%]. The estimated HB models obtained by the HSRIV (left-hand side plots) and HSRIV-OV (right-hand side plots) algorithms are compared. The true static functions and system outputs (grey solid lines) are plotted against the estimated responses (black solid lines).

posed that the HSRIV-OV algorithm is used to obtain an initial parameter vector estimate, which can be subsequently refined by the HSRIV algorithm. Moreover, the presented discrete-time HSRIV and HSRIV-OV parameter estimation methods require, in general, less *a priori* knowledge during the initialisation stage than their CT counterparts. Therefore, when possible, the presented DT parameter estimation methods can be used to initialise the CT methods introduced in Chapter 3.

Table 4.1: Monte Carlo simulation (MCS) results. SR denotes a single run results for seed value 22, SE denotes the estimated standard error, SD denotes the standard deviation of MCS estimates.

Parameter		α_1	β_0	η_1	p_2	p_3
True values		-98.75×10^{-2}	-0.5	-12.5×10^{-3}	-4.4	2
SNR=10 [%]						
SRIV	$\hat{\theta}$	-98.7557×10^{-2}	-0.4983	-12.466×10^{-3}	-	-
(SR)	SE	3.9840×10^{-5}	1.5595×10^{-3}	5.6220×10^{-5}	-	-
SRIV	mean	-98.7504×10^{-2}	-0.4999	-12.503×10^{-3}	-	-
(MCS)	SD	5.9494×10^{-5}	2.1786×10^{-3}	7.5480×10^{-5}	-	-
HSRIV	$\hat{\theta}$	-98.7516×10^{-2}	-0.4956	-12.293×10^{-3}	-4.4336	2.0175
(SR)	SE	3.8794×10^{-5}	1.5021×10^{-3}	5.2046×10^{-5}	1.2453×10^{-2}	0.8762×10^{-2}
HSRIV	mean	-98.7496×10^{-2}	-0.4997	-12.481×10^{-3}	-4.4047	2.0023
(MCS)	SD	6.1938×10^{-5}	3.4496×10^{-3}	17.251×10^{-5}	5.0663×10^{-2}	3.2987×10^{-2}
HSRIV-OV	$\hat{\theta}$	-98.7620×10^{-2}	-0.4869	-11.385×10^{-3}	-4.2578	1.8343
(SR)	SE	6.9052×10^{-5}	2.6506×10^{-3}	8.9113×10^{-5}	-	-
HSRIV-OV	mean	-98.7500×10^{-2}	-0.4995	-12.475×10^{-3}	-4.4003	1.9961
(MCS)	SD	8.1579×10^{-5}	13.249×10^{-3}	67.621×10^{-5}	16.743×10^{-2}	11.215×10^{-2}
SNR=30 [%]						
SRIV	$\hat{\theta}$	-98.7668×10^{-2}	-0.4948	-12.400×10^{-3}	-	-
(SR)	SE	1.1797×10^{-4}	4.6268×10^{-3}	1.6718×10^{-4}	-	-
SRIV	mean	-98.7512×10^{-2}	-0.4999	-12.510×10^{-3}	-	-
(MCS)	SD	1.7803×10^{-4}	6.5264×10^{-3}	2.2634×10^{-4}	-	-
HSRIV	$\hat{\theta}$	-98.7547×10^{-2}	-0.4872	-11.894×10^{-3}	-4.4996	2.0519
(SR)	SE	1.1594×10^{-4}	4.4269×10^{-3}	1.5336×10^{-4}	3.7557×10^{-2}	2.6407×10^{-2}
HSRIV	mean	-98.7489×10^{-2}	-0.4991	-12.450×10^{-3}	-4.4131	2.0062
(MCS)	SD	1.8525×10^{-4}	10.342×10^{-3}	5.1761×10^{-4}	15.164×10^{-2}	9.8783×10^{-2}
HSRIV-OV	$\hat{\theta}$	-98.7852×10^{-2}	-0.4632	-9.126×10^{-3}	-3.9500	1.4883
(SR)	SE	1.9658×10^{-4}	7.3385×10^{-3}	2.2928×10^{-4}	-	-
HSRIV-OV	mean	-98.7497×10^{-2}	-0.4997	-12.485×10^{-3}	-4.4069	1.9878
(MCS)	SD	2.4624×10^{-4}	39.318×10^{-3}	20.069×10^{-4}	51.238×10^{-2}	34.095×10^{-2}

Table 4.2: Comprehensive Monte Carlo simulation results. The true noise variances σ_e^2 for the bilinear system for $NSR = 10$ [%] and $NSR = 30$ [%] are 0.3265 and 2.9384, respectively. The true noise variances σ_e^2 for the HB system for $NSR = 10$ [%] and $NSR = 30$ [%] are 0.2820 and 2.5378, respectively.

		IAE	$\hat{\sigma}_e^2$	$AC(\hat{\theta}_{lb})$	$AC(\hat{\theta}_n)$	Iter
SNR=10 [%]						
SRIV	mean	0.4561	0.3267	1.7644×10^{-3}	-	4.1333
	SD	0.1427×10^{-2}	0.4071×10^{-3}	1.2706×10^{-3}	-	0.3519
HSRIV	mean	0.4238	0.2824	2.8813×10^{-3}	4.8805×10^{-2}	348.93
	SD	0.1334×10^{-2}	0.4845×10^{-3}	1.9119×10^{-3}	3.5737×10^{-2}	4.6975
HSRIV-OV1	mean	0.4238	0.2824	-	-	5.5333
	SD	0.1340×10^{-2}	0.4978×10^{-3}	-	-	0.7432
HSRIV-OV2	mean	0.4431	0.3617	10.552×10^{-3}	16.619×10^{-2}	5.5333
	SD	2.2817×10^{-2}	94.080×10^{-3}	7.9864×10^{-3}	11.281×10^{-2}	0.7432
SNR=30 [%]						
SRIV	mean	1.3684	2.9408	5.2866×10^{-3}	-	5.6000
	SD	0.4281×10^{-2}	3.6859×10^{-3}	3.8030×10^{-3}	-	0.5071
HSRIV	mean	1.2715	2.5413	8.6225×10^{-3}	14.602×10^{-2}	352.07
	SD	0.4003×10^{-2}	4.2844×10^{-3}	5.7366×10^{-3}	10.690×10^{-2}	12.591
HSRIV-OV1	mean	1.2714	2.5412	-	-	7.8000
	SD	0.4019×10^{-2}	4.4348×10^{-3}	-	-	1.6125
HSRIV-OV2	mean	1.3312	3.2601	31.444×10^{-3}	50.208×10^{-2}	7.8000
	SD	7.7113×10^{-2}	0.8761	23.482×10^{-3}	35.262×10^{-2}	1.6125

Chapter 5

Modelling of heating ventilation and air conditioning system

5.1 Introduction

The goal of this chapter is to develop dynamic control design purpose oriented air temperature and humidity models of an environmentally controlled clean room manufacturing zone in Abbott Diabetes Care, UK. These models, which are Hammerstein-bilinear in structure, are subsequently used for control analysis and tuning of the corresponding HVAC control system. The aim is two-fold in terms of improved set-point tracking and reduced energy consumption.

The currently utilised control algorithm is a standard linear proportional-integral (PI) controller, which is tuned at one operating point based on a locally linearised model, see (Åström & Hägglund 2006). The common approach is to select a least stable point of operation for the control tuning purposes, so that the overall stability of the system is guaranteed over the whole operational range, see (Underwood 1990). However, due to the complexity, nonlinear characteristics and non-stationary operational conditions of the HVAC system the selection of such a critical operating point (control tuning) is a non-trivial task in practice (Underwood 1999). Therefore, the developed models should be flexible enough to replicate the main dynamic and static nonlinear characteristics of the considered HVAC system over the whole feasible operational range. Subsequently, such models would then allow for enhanced control analysis, which would result in a better informed selection of the critical point of operation and corresponding linearised model.

The system identification challenge lies in the fact that the investigated HVAC

system is already installed and fully integrated within the manufacturing plant (factory). In other words, the HVAC system is not installed on a testbed facility, which would allow comprehensive system identification experiments to be conducted in a controlled laboratory environment. This greatly limits the scope and type of possible experimentation, which can be conducted. Therefore, the research methodology and the resulting models have to comply with this limitation.

The chapter is structured as follows: The functionality of the investigated HVAC system and relevant technical details are provided in Section 5.2. In the following Section 5.3 the experimental setup is explained and the system inputs and outputs are selected. The overall control oriented temperature model of the manufacturing zone comprises two interconnected submodels, which are the zone temperature submodel and the air handling unit temperature submodel, provided in Sections 5.4 and 5.5, respectively. A unique control oriented humidity model of the environmentally controlled manufacturing zone is then provided in Section 5.6. Additionally, Sections 5.4, 5.5 and 5.6 commence with a literature review, which relates the developed models to the existing published models. The conclusions and final remarks are given in Section 5.7 and an essential background to psychrometrics is provided in Appendix B.

5.2 Plant details

The air conditioning system composes of four main components: namely, fresh air plant (FAP), chilled water (CHW) plant, low temperature hot water (LTHW) plant and the heating ventilation and air conditioning (HVAC) system. Consider the schematic diagram of the overall air conditioning system given in Figure 5.1. Firstly, the outdoor air progresses through the FAP, where the temperature of the air is constantly regulated between (5, 10) [°C]. Then, the pre-conditioned air enters the mixing box and is mixed with the return air from the controlled zone, i.e. manufacturing area. The mixing ratio of fresh air to return air is approximately 3:17. Subsequently, the air mixture progresses through the HVAC system, where the desired values of the air temperature and humidity (measured in terms of dew-point temperature) are achieved.

A more detailed description of the HVAC system is given in Figure 5.2. Considering Figure 5.2 and continuing from the stage, where the mixture of supply air and return air enters the HVAC system, it is then progressed through the dehumidification unit (DU). The dehumidification unit is Munster MX 5000 type,

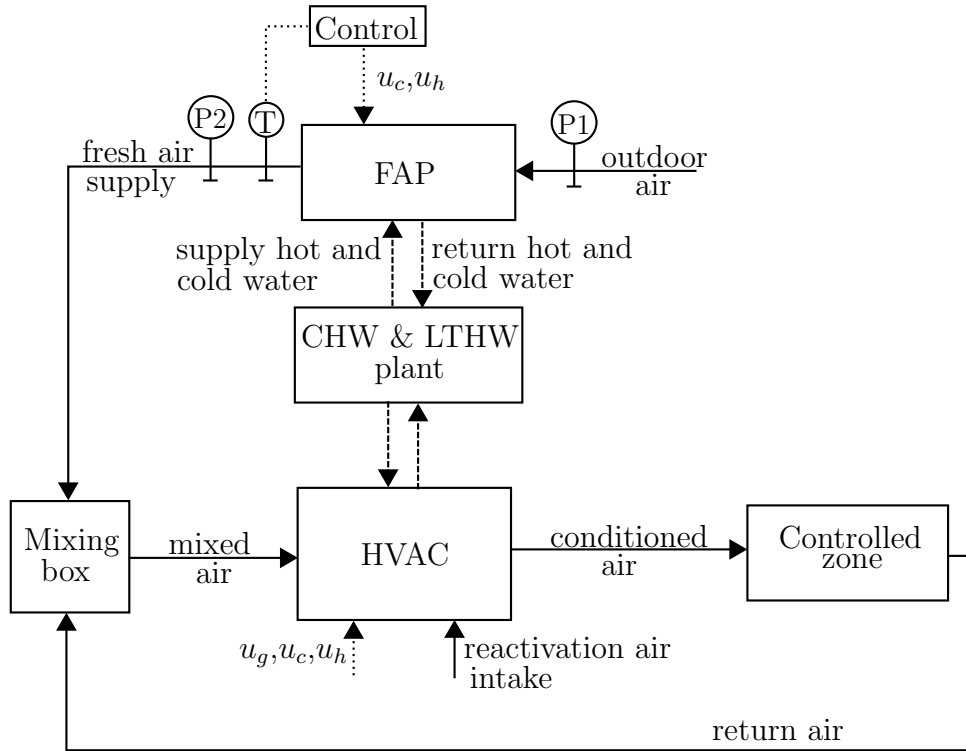


Figure 5.1: Schematic diagram of the overall air conditioning system.

where the type number refers to the air volumetric flow in $[m^3h^{-1}]$ for which the unit is designed. A portion of the return air (approximately 34%) is by-passed directly to the air handling unit (AHU) and is not treated by the DU. For the personnel comfort the designed air flow to the controlled zone is $2 [m^3s^{-1}]$, i.e. $7200 [m^3h^{-1}]$. The corresponding DU for this volumetric flow would be Munster MX 7200. However, such DU would be oversized for the current application and would constantly deliver too low humidity levels. Therefore, approximately 34% of the return air is led directly through the bypass to the AHU allowing for the use of an undersized DU, in this case Munster MX 5000. The volumetric flow in the bypass is controlled by dampers, whose position, in the setup considered, is fixed.

After dehumidification the processed air enters the AHU Wolf KG 160, where the air is heated or cooled depending on the operating requirements. The conditioned air is then driven by the extract fan into the controlled area. The controlled zone is a clean room production area, where, in order to avoid the environmental contamination by dust and other air pollutants, a higher air pressure than that atmospheric is maintained. This is achieved by having lower air outflow of $1.8 [m^3s^{-1}]$ from the controlled zone than the air inflow $2 [m^3s^{-1}]$, hence part of the

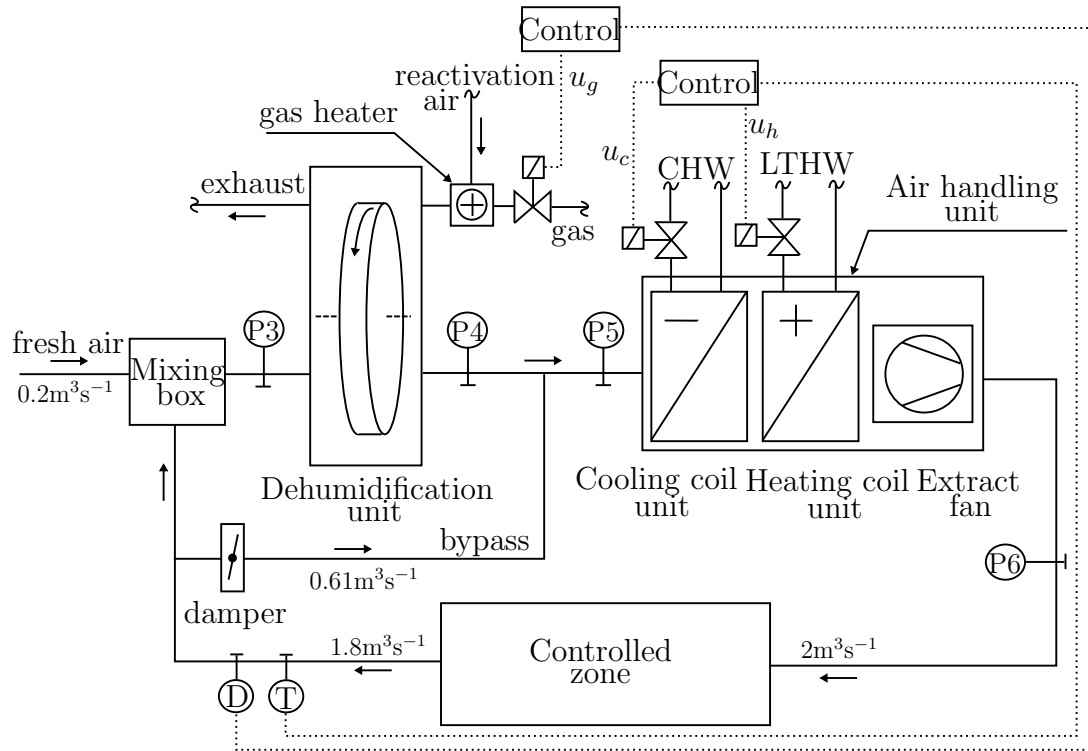


Figure 5.2: Block diagram of the modelled HVAC system.

air ventilates through gaps around doors and windows.

In the return duct a permanent dew-point temperature and temperature transmitter Vaisala DMT 348, measuring the state of the return air, is installed. The dew-point temperature measurement range is $(-70, 80)$ $^{\circ}\text{C}$ with ± 2 $^{\circ}\text{C}$ accuracy or better. The temperature range is $(0, 80)$ $^{\circ}\text{C}$ with accuracy of ± 0.2 $^{\circ}\text{C}$. This transmitter is used for the purpose of control, where the installation of the transmitter in the return duct permits the control system to compensate for any load disturbances within the controlled zone. Additionally, a set of probing sensors $P_{1,\dots,6}$ is installed for gaining technical insight into the investigated system and for identification purposes. The probing sensors are Vaisala HMD 40/50 Y relative humidity and temperature transmitters for HVAC applications. The measurement range for which the relative humidity reading accuracy is specified is $(10, 90)$ [%] with ± 3 [%] accuracy. The temperature range is $(-10, 60)$ $^{\circ}\text{C}$ with accuracy of ± 0.3 $^{\circ}\text{C}$.

5.2.1 Dehumidification unit

The main component of the DU is a large desiccant rotor, which is made of narrow air flutes formed in a honeycomb like structure. The air flutes are coated with

a moisture absorbent desiccant material, in this case, silica gel. The desiccant rotor itself is of homogenous symmetric structure and continuously rotates with a constant angular velocity of approximately 1/10 [rpm]. There are two separate counterflow streams of so called reactivation (regeneration) and process air, which simultaneously flow through the upper and lower part of the desiccant rotor, respectively. These two air streams are separated by a hard barrier and cannot mix with each other. This barrier then divides the rotor into corresponding reactivation (90°) and dehumidification (270°) sectors.

The functionality of the DU is described as follows. The process air, being the dehumidified air, is driven through the dehumidification sector. The silica gel absorbs the moisture from the process air and, because the desiccant rotor is hot, the process air is additionally warmed as well. The dry air is then delivered to the outlet and is supplied to the AHU unit for further treatment. Simultaneously, the outdoor air is heated by a gas driven reactivation heater and the resulting (hot) reactivation air is driven through the reactivation sector. This air then evaporates the moist from the silica gel and wet reactivation air is subsequently vented into an exhaust duct and back to the atmosphere. This process continuously repeats as the desiccant rotor rotates at constant speed.

The maximum power of the reactivation heater is 53.1 [kW] and with fully open gas supply valve the heater is able to increase the temperature of the supplied outdoor air by 95 [°C]. The power of the gas heater, hence the humidity of the outflow process air, is controlled by the central control system, where a dedicated PI controller is utilised. The controller drives an electronic actuator mounted to the gas valve, by applying the control action, denoted u_g . The gas valve itself has a lower safety limit of 24 [%] (low fire), hence it is never switched off due to the safety issues at the ignition stage.

Steady-state characteristic

Due to the coupled heat and mass transfer processes occurring within the desiccant rotor the dynamic and steady-state behaviour of the DU is inherently complex and nonlinear (Ge, Li, Wang & Dai 2008). Overall, there are four external inputs, these being the dry-bulb temperatures and the specific humidities of the process and reactivation air measured at the inlet, denoted $T_{p,in}$, $X_{p,in}$, $T_{r,in}$ and $X_{r,in}$, respectively. There are also four corresponding outputs, which are dry-bulb temperatures and specific humidities of the process and reactivation air at the outlet, denoted $T_{p,out}$, $X_{p,out}$, $T_{r,out}$ and $X_{r,out}$, respectively.

In order to gain an insight into the influence of the four inputs on the humidity

and temperature of the process air, it is desirable to obtain and plot a steady-state characteristic of the DU. However, it is not possible to measure such steady-state characteristics on the investigated HVAC system, because the inputs ($T_{r,in}$, $X_{r,in}$) are not measured (safety and technical reasons) and also these inputs are not constant and are greatly influenced by the outdoor weather conditions. Therefore, the static empirical model presented in (Beccali, Butera, Guanella & Adhikari 2003) is used instead. This model may not necessarily simulate the behaviour of the investigated HVAC unit, however it is deemed to be sufficient for gaining and insight into the basic functionality of the desiccant rotors. The model is valid for the following input ranges $T_{p,in} \in (20, 34)$ [$^{\circ}C$], $X_{p,in} \in (8, 15)$ [g/kg], $T_{r,in} \in (40, 80)$ [$^{\circ}C$] and $X_{r,in} \in (10, 16)$ [g/kg]. In Figure 5.3 the static characteristics between inputs ($T_{p,in}$, $X_{p,in}$) and outputs ($T_{p,out}$, $X_{p,out}$) are shown. The nominal values at which the characteristics are plotted are $T_{r,in} = 80$ [$^{\circ}C$] and $X_{r,in} = 12$ [g/kg]. Figure 5.4 shows the static characteristics between inputs ($T_{r,in}$, $X_{r,in}$) and outputs ($T_{p,out}$, $X_{p,out}$), for the nominal values of the second two inputs $T_{p,in} = 20$ [$^{\circ}C$], $X_{p,in} = 8$ [g/kg],

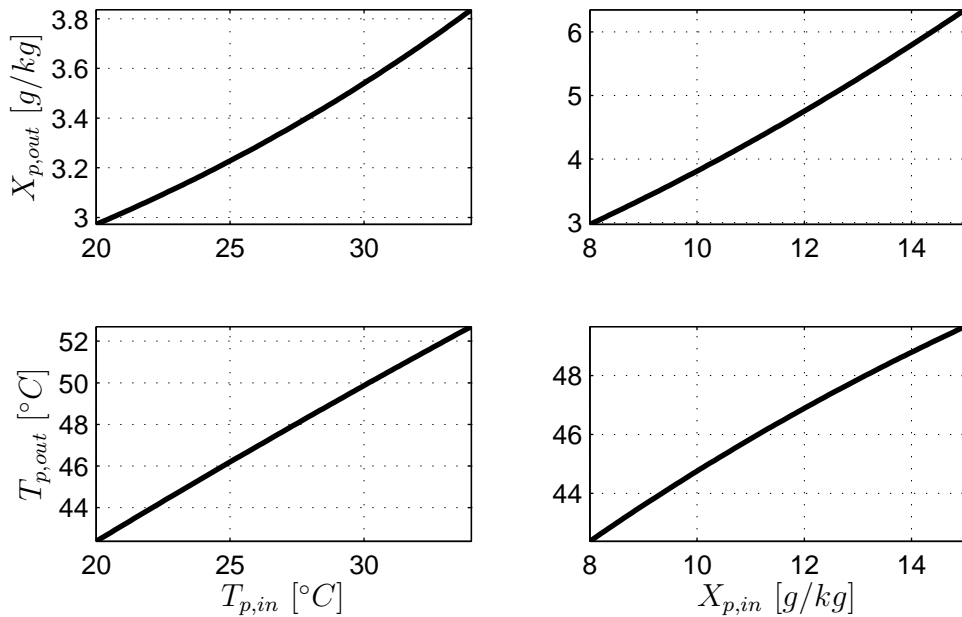


Figure 5.3: The steady-state characteristics of the DU at nominal values $T_{r,in} = 80$ [$^{\circ}C$] and $X_{r,in} = 12$ [g/kg].

Figure 5.3 shows that for increasing $X_{p,in}$ the value of $X_{p,out}$ also increases, as expected. Interestingly, the temperature $T_{p,out}$ significantly increases with increasing $X_{p,in}$. It is observed, in Figure 5.4, that the $X_{p,out}$ is inversely propor-

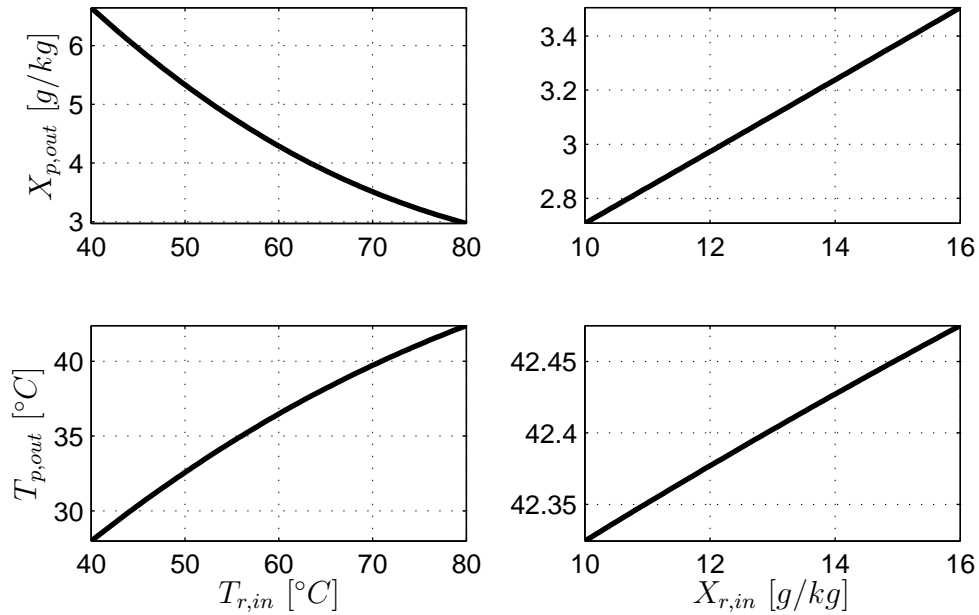


Figure 5.4: The steady-state characteristics of the DU at nominal values $T_{p,in} = 20$ [°C], $X_{p,in} = 8$ [g/kg].

tional to the reactivation air temperature $T_{r,in}$. This is an expected and desirable relationship upon which the DU is designed. Additionally, for an increasing value of $T_{r,in}$ the temperature $T_{p,out}$ also increases, which is, in general, an unwanted effect. In order to compensate for this temperature increase the AHU is commonly engaged in cooling model.

Special observation

A special observation, originating in the work of (Danne 2008), has been made regarding the oscillatory pattern in the measurement of the dew-point temperature. The dew-point temperature is measured by a sensor D, mounted in the return duct, for two constant gas valve spindle positions of $u_g = 30$ [%] and $u_g = 100$ [%], respectively. During this experiment the cooling and heating coils of the AHU have been switched off and only the extract fan has been left switched on, so that the air recirculates. The left-hand and right-hand side plots of Figure 5.5 show the measured dew-point temperature oscillatory pattern for the two gas valve positions. It can be observed that for a medium humidity level (left plot) the amplitude of the approximately sinusoidal signal has an average value of 0.13 [°C] with a time period of 5.85 [min]. For high humidity levels (right plot), the amplitude increases to an average value of 0.52 [°C] with a time period of

6.57 [min]. A similar observation has been made when measuring the dry-bulb temperature of the return air.

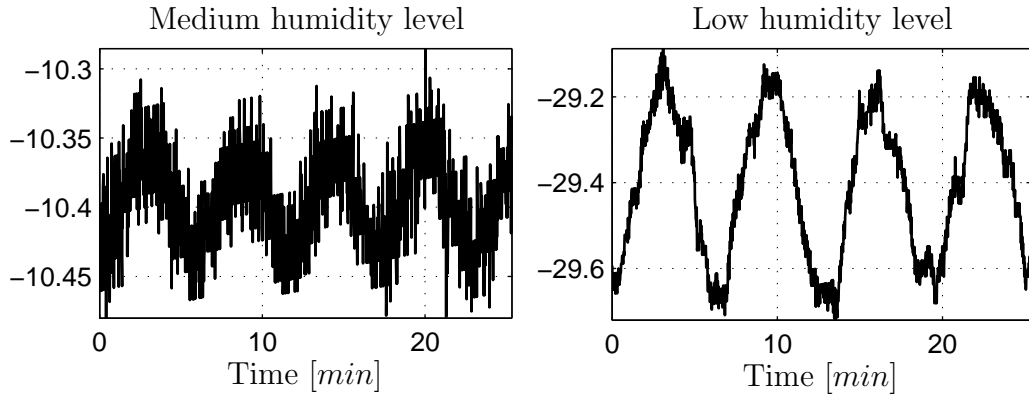


Figure 5.5: The left-hand and right-hand side plots show the measured dew-point temperature oscillatory pattern, in $^{\circ}C$, for constant gas valve positions of $u_g = 30$ [%] and $u_g = 100$ [%], respectively. The cooling and heating coils of the AHU are turned off.

No conclusive evidence of the cause of this oscillatory pattern has been found. The only active element of the investigated HVAC system has been the DU. Since both the dew-point temperature (directly related to the specific humidity) and the dry-bulb temperatures of the air are affected, it is assumed that the DU is the direct or indirect cause of the measured sustained oscillations. The possible, yet not proven, cause might be the closed loop nature of the air conditioning system itself. It can be seen from Figure 5.2, that the air recirculates, where the DU is an active nonlinear element in this loop. Therefore, the observed oscillations might be attributed to a limit-cycle phenomenon of such a nonlinear closed loop HVAC system setup.

It should be noted, that the oscillatory pattern observed in the measurement of dew-point and dry-bulb temperatures may unfavourably affect the parameter estimates of the designed models. This phenomenon is of a nonstationary character and is also not present (or rather detectable by the used sensors) at all times.

5.2.2 Air handling unit

The AHU, being the Wolf KG 160 type, comprises the cooling coil unit (CCU), the heating coil unit (HCU) and the main centrifugal fan. Depending on the demanded zone temperature set-point the processed air is sensibly (no moist

condensation) cooled or heated to achieve this demand. Both the CCU and HCU are water-to-air heat exchangers having cooling and heating capacities 45.3 [kW] and 6 [kW], respectively. The CCU is supplied with chilled water at designed supply temperature of 4.5 [°C] from the chilled water plant, denoted CHW in Figure 5.1. The HCU is supplied with low temperature hot water (LTHW) at 82 [°C] from the LTHW plant. The centrifugal fan is driven by an electric motor having 7.5 [kW] power. In order to prevent the electric motor from overheating, the motor is installed within the AHU such that the processed air cools down the motor.

During normal operational conditions the DU provides enough heat to compensate for any heat losses of the building, consequently the HCU is disabled by the control system for most of the time. Since the HCU is disabled under normal operating conditions, it is not further considered in the subsequent modelling stage, see Section 5.3 for more details. The CCU cooling capacity is alternated by means of the flow of chilled water. This is controlled by the cooling valve, which is modulated by a dedicated PI controller with the corresponding control action u_c . The cooling valve is a Siemens two-port seat valve VVF 45.65 DN 50/40. The valve has a linear characteristic for the range $\langle 0, 30 \rangle$ [%] of stem position and equal percentage characteristic in the range of $\langle 30, 100 \rangle$ [%], see Appendix A.1 for more details on the terminology used.

Special observation

A special observation has been made regarding the heat gains and losses of the AHU. In order to examine any potential heat gains and losses of the investigated AHU, an experiment has been conducted. During this experiment, both the CCU and HCU have been disabled, while the main centrifugal fan has been left switched on. The temperature of the inflow air to the AHU, denoted T_{ai} [°C], has been measured by sensor P_5 , which is located just before the AHU, see Figure 5.2. The outflow air temperature, denoted T_{ao} [°C], has been measured by sensor P_6 , which is located just after the AHU. The whole HVAC system has been switched to manual control mode and left at rest overnight to achieve steady-state. The gas valve position has been set to $u_g = 26$ [%] and the cooling valve has been completely closed $u_c = 0$ [%].

Figure 5.6 shows the measured T_{ai} and T_{ao} temperatures together with the corresponding gas valve position u_g . Firstly, it can be noted that T_{ai} and T_{ao} are steadily rising for the time period when $u_g = 26$ [%]. This is due to the influence of increasing outdoor temperature, which, through the reactivation air intake of

the DU, influences T_{ai} . During this time period, the outflow temperature is higher than the inflow temperature, i.e. $T_{ai} < T_{ao}$, by approximately $1.62\text{ }[^\circ\text{C}]$. This temperature rise is caused by the $7.5\text{ }[kW]$ electric fan motor located at the far end of the AHU. A portion of the electric motor's power is converted into heat, which is conducted and convected into the passing air.

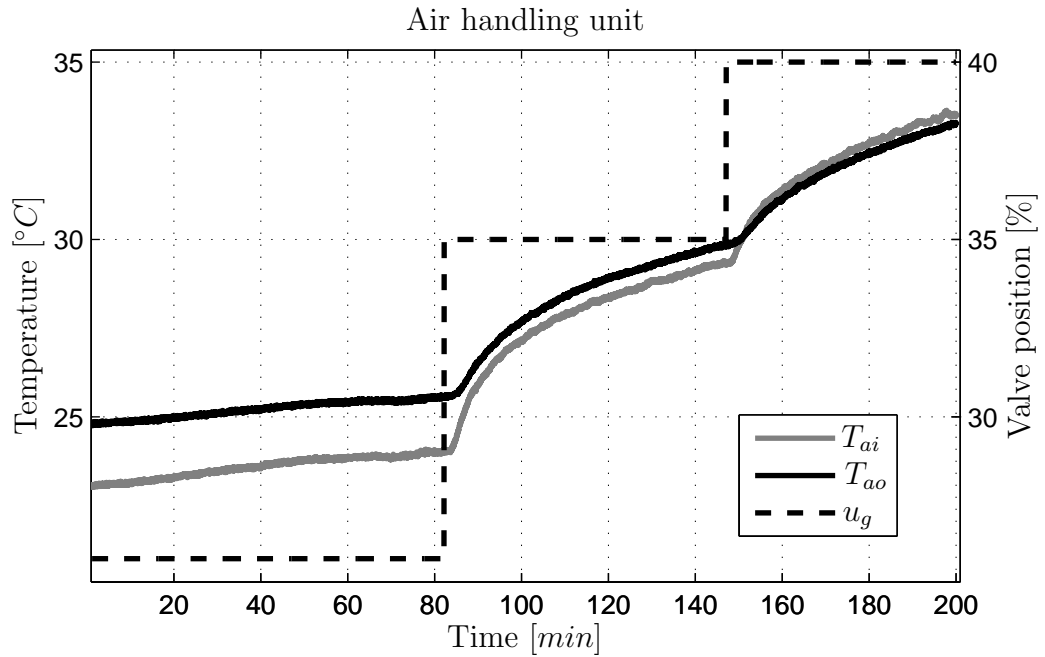


Figure 5.6: The inflow and outflow air temperatures of the AHU, denoted T_{ai} and T_{ao} , respectively, plotted against the gas valve position u_g . The CCU and HCU are disabled and only the main fan is in operation.

Subsequently, the gas valve has been opened to $u_g = 35\text{ }[\%]$ and then further to $u_g = 40\text{ }[\%]$. It is observed, in Figure 5.6, that with the gas valve being more opened the T_{ai} temperature rises and, consequently, also the temperature T_{ao} . For the inflow air temperature $30.1\text{ }[^\circ\text{C}]$, the inflow and outflow air temperatures are approximately equal, i.e. $T_{ai} = T_{ao} = 30.1\text{ }[^\circ\text{C}]$. Note, that this temperature has been measured when T_{ai} undergoes a dynamic change due to the change of gas valve position, hence this is not the steady-state value. After this point the outflow temperature is always lower, i.e. $T_{ai} > T_{ao}$.

It is concluded, that at the observed temperature of $30.1\text{ }[^\circ\text{C}]$ the constant heat gain from the electric motor is equal to the heat loss from the AHU. The heat loss from the AHU depends on the difference between the temperature of the processed air and the ambient air temperature. Therefore, when this temperature difference is large enough the heat losses are greater than the heat gain and, as a

consequence of that, $T_{ai} > T_{ao}$.

5.2.3 Fresh air plant

The main purpose of the FAP is to cool and pre-dehumidify the outdoor air. The FAP is effectively an AHU, which composes of a CCU, an electric heating plate and centrifugal fan. The dehumidification is performed by cooling down the air below its dew-point temperature, i.e. sensible and latent cooling occurs. Therefore, the actual temperature of the cooling element has to be lower than the dew-point temperature of the outdoor air. The CCU is supplied with chilled water at the designed supply temperature of 4.5 [°C] from the CHW, which is a sufficiently low temperature for a latent cooling application.

The FAP under consideration maintains the supply air temperature in the range of (5, 10) [°C]. In the case when the outdoor air is above 10 [°C] the CCU is switched on and the air is cooled down. The lower limit of 5 [°C] is due to the frost protection issues, since in the winter season dampers and other mechanical parts might freeze due to the low outdoor air temperature. To heat up the outdoor air the electric heating plate is used.

5.2.4 Control and monitoring system

The manufacturing requirements in ADC UK are such that the environmental conditions within the manufacturing zone are: the air dry-bulb temperature must lie within the range 21 ± 4 [°C] and the air relative humidity must be lower than 20 [%]. The corresponding dew-point temperature is -2.8 ± 3.3 [°C], which has been computed using relation B.12. The temperature and the relative humidity of the air within the manufacturing zone are constantly monitored by a building management system. This system uses a set of sensors which are independent of the control system and are not reviewed here.

The air conditioning system is controlled by a dedicated distributed control system, where each of the controllers utilises a PI algorithm together with an additional control logic, such as anti-windup logic and valve positioning logic. The feedback signal for the temperature control loop is the measured return air dry-bulb temperature. The temperature sensor is denoted T in Figure 5.2. The manufacturing zone temperature set-point is 21.5 [°C] with a dead band ± 0.5 [°C]. Depending on the measured temperature of the return air, the control logic decides whether to engage in cooling or heating mode, i.e. whether to use the CCU or HCU. The control set-point, denoted r , is thus $r = 22$ [°C] when the AHU

is in the cooling mode and $r = 21$ [°C] when the AHU is in the heating mode. In the case where the measured return air temperature is within the interval of $(21, 22)$ [°C], i.e. within the control dead band, no control action is taken.

The humidity control loop uses a dew-point temperature sensor, rather than a relative humidity sensor, to measure the return air humidity. This is due to the fact that the air dew-point temperature corresponds to the air water content directly and does not depend on the air dry-bulb temperature, hence it neglects the influence of the temperature control loop on the control of the DU. The control dew-point temperature set-point is $r = -10$ [°C]. Note that since the DU heats up the conditioned air, a cross-coupling between the DU and AHU temperature control loop exists.

5.3 System identification setup

The scope and type of possible experimentation is limited because the HVAC system is already installed on the manufacturing site. The main limits are summarised as follows: Not all external inputs acting on the system can be freely manipulated, e.g. external weather conditions would be a typical example. Not all inputs can be measured, in many cases this would mean to interfere with the air conditioning unit in an irreversible manner, e.g. drilling probing holes. The conditioned air recirculates, so that part of the return air is recovered and reused. However, this implies that the system itself operates in a natural closed loop setup, where some of the considered inputs are partially, or fully, caused by the system outputs. The HVAC system (unit) under consideration is a part of a complex network of alike HVAC units, which actively regulate the environmental conditions within adjacent active manufacturing zones. The individual HVAC units are interconnected via gas, chilled and hot water supply pipe networks. Inevitably, due to the normal operation of the adjoining HVAC units the pressure in such pipe networks fluctuates, which disturbs the performance of the investigated HVAC unit, i.e. the units interact.

The aim of this system identification study is to obtain control oriented air temperature and humidity models, which replicate the behaviour of the system over the whole operational range. Based on *a priori* knowledge, it is known that the system behaves in a nonlinear manner (Hammerstein-bilinear model characteristics) throughout its operational range. Therefore, the manipulated system inputs should excite the system over the whole range of operation under consideration. Consequently, the time duration of the measurement experiments

should be of sufficient length to allow the system to exhibit its main dynamic behaviour, so that the acquired input-output data are sufficiently informative. However, the long time duration of the data acquisition experiments allows for slow varying load disturbances to act on the system, which introduces offsets and trends into the measured data. The time duration of the conducted data acquisition experiments is in order of hours, during this time the outdoor weather conditions may significantly change and influence the collected data. Therefore, the designed models and corresponding input selection should reflect this. In order to minimise the influence of fast varying load disturbances, no personnel nor active machinery were present during the data acquisition procedure in the manufacturing zone.

Prior to every data acquisition experiment the system is allowed to settle, so that the system is then excited from its initial steady-state conditions. In order for the system to settle, the HVAC control system is disabled; in manual mode of operation the gas, cooling and heating valves are set at fixed positions. The measured steady-state values (baseline values) are subtracted from the signals, hence any constant offsets are removed and do not need to be estimated. Since the measured signals are affected by measurement noise a sample mean of the first 10 samples is taken as the baseline of the measured signal being considered. This is an important consideration due to the type of parameter estimation methods used. The applied estimation methods, introduced in the foregone Chapters 3 and 4, uses optimal prefilters. Since the baselines are subtracted from the measured input-output signals, these start approximately at a zero value. Subsequently, the optimal prefilters can be initialised with zero, which simplifies the use of the adopted parameter estimation methods. The measured input-output signals are sampled at $h = 1$ [s], which is the highest available sampling interval of the instrumentation device.

For each obtained model two model performance criteria are evaluated, namely, the integral of absolute error, denoted IAE [$^{\circ}C$], and the coefficient of determination, denoted R_T^2 [%]. The integral of absolute error is defined in (3.121) and for convenience repeated below

$$IAE = \frac{1}{N} \sum_{k=1}^N |e(t_k)| \quad (5.1)$$

where N is the number of data samples and the time index notation (t_k) emphasizes that the original continuous-time signal is sampled at discrete time instances, i.e. $t_k = kh$. The error, denoted $e(t_k)$, between the measured output, denoted

$y(t_k)$, and simulated model output, denoted $\hat{x}(t_k)$, is defined as

$$e(t_k) = y(t_k) - \hat{x}(t_k) \quad (5.2)$$

The *IAE* criterion then provides an average simulation error in the units of the evaluated output signal (in this case [$^{\circ}C$]). The coefficient of determination is defined as

$$R_T^2 = 100 \left(1 - \frac{\sigma_e^2}{\sigma_y^2} \right) \quad (5.3)$$

where the variances σ_e^2 and σ_y^2 are computed as follows

$$\sigma_e^2 = \frac{1}{N} \sum_{k=1}^N [e(t_k) - \bar{e}(t_k)]^2 \quad (5.4)$$

$$\sigma_y^2 = \frac{1}{N} \sum_{k=1}^N [y(t_k) - \bar{y}(t_k)]^2 \quad (5.5)$$

The bar above the variables in (5.4) and (5.5) denotes a sample mean. The R_T^2 criterion then provides a measure of how much of the measured output variance is explained (or captured) by the simulated output variance. In the case where the variances of measured and simulated output matches, i.e. the signals are the same, the R_T^2 criterion is 100 [%].

In the following two subsections the inputs and outputs of the designed manufacturing zone temperature and humidity models are selected. This selection, then defines the basic structure of the two considered models. Additionally, in both cases, it is assumed that the sensor and actuator dynamics are lumped within the dominant dynamics of the main modelled HVAC system components.

5.3.1 Manufacturing zone temperature model

The desired model is intended for control analysis and design, therefore the model output is the regulated temperature of the return air measured by sensor T, which is located in the main return duct, see Figure 5.2. The return air temperature (or room temperature) is denoted T_{ar} [$^{\circ}C$], see Figure 5.7.

The temperature control loop regulates cooling or heating valve positions of the AHU such that the demanded zone temperature set-point is achieved. During the normal mode of operation the DU provides enough heat, therefore the HCU of the AHU is disabled for most of the time and is active only during cold start up. To simplify identification and modelling of the AHU, only the

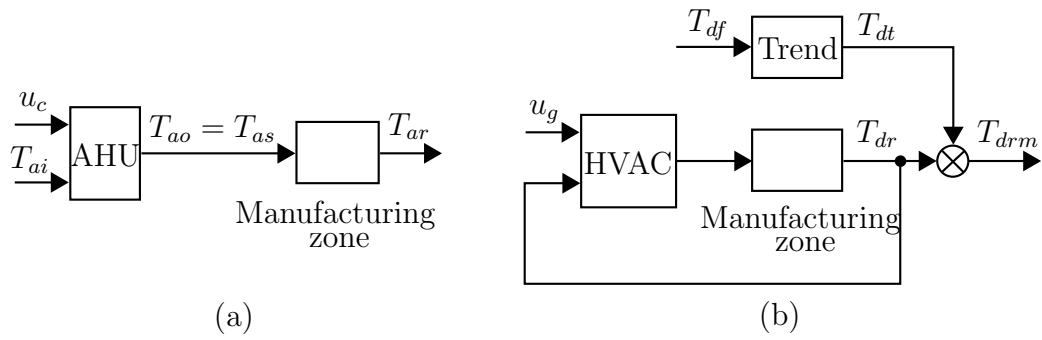


Figure 5.7: Schematic diagram showing the inputs and outputs of the manufacturing zone temperature model, provided in subfigure (a), and the manufacturing zone humidity model, provided in subfigure (b).

cooling coil has been considered in the experimental setup. The corresponding control (manipulated) input to the manufacturing zone temperature model is thus the cooling valve position signal u_c . In the case, when the AHU is designed and sized appropriately, the influence of the cooling coil and the heating coil on the temperature of passing air is equivalent, however having opposite effects. Therefore, it is anticipated that the identified manufacturing zone temperature model (including only CCU) can be also utilised in the model based tuning of the PI controller corresponding to the heating coil.

For the purposes of system identification and simulation the cooling valve position signal is normalised in the range $\langle 0, 1 \rangle$, where 0 corresponds to closed and 1 to fully opened valve. For the ease of reading, when referring to a particular valve position in the main text, this is expressed rather as a percentage of valve opening, i.e. $u_c = \langle 0, 1 \rangle \times 100$ [%] in ‘engineering units’. The same normalisation also applies to the gas valve position u_g used in the following Subsection 5.3.2.

The second selected input is the inflow air temperature to the AHU, denoted T_{ai} [$^{\circ}C$]. The temperature T_{ai} is measured by the sensor P_5 , see Figure 5.2. The inflow air temperature effectively acts as a load disturbance and changes the operating point of the AHU. The temperature T_{ai} is mainly affected by the operation of the DU and outdoor weather conditions.

The overall manufacturing zone temperature model composes of two subsystems, these being the AHU and the zone itself, and these have been identified separately. The cooling valve position and the temperature of the inflow air to the AHU are selected to be the inputs for the AHU submodel; the outflow air temperature, denoted T_{ao} [$^{\circ}C$], is the output of the AHU submodel. The outflow air of the AHU is also the supply air to the manufacturing zone. Therefore, the supply air temperature, denoted T_{as} [$^{\circ}C$], is used as the input to the zone tem-

perature submodel, where $T_{ao} = T_{as}$. The return air temperature, T_{ar} , is then the output of the zone temperature submodel as well as the output of the overall manufacturing zone temperature model. The air temperatures T_{ao} and T_{as} are measured by sensor P_6 , see Figure 5.2 for the location of the sensor.

In order to excite the system the cooling valve position has been adjusted by applying a stair case signal having a random normally distributed duration of steps between 9 and 30 [min]. Also the second input to the system, being the inflow air temperature, has been systematically adjusted. The only possible way of adjusting the inflow air temperature to the AHU, on the installed HVAC unit, is to modulate the gas valve of the DU.

Note that due to the experimental setup the inflow air temperature, T_{ai} , is partially correlated with the outflow air temperature, T_{ao} , of the AHU. Also the manufacturing zone supply air temperature, T_{as} , is correlated with the return air temperature, T_{ar} . This is caused by the air recirculation, i.e. an inherent closed loop nature of the HVAC system. Further, the inputs T_{ai} and T_{as} are both measured and contaminated by measurement noise, which leads to an errors-in-variables identification scenario.

5.3.2 Manufacturing zone humidity model

A schematic diagram showing the selected input and output signals of the manufacturing zone humidity model is provided in Figure 5.7. The model output is the regulated dew-point temperature of the return air measured by sensor D, which is located in the main return duct, see Figure 5.2. The measured return air dew-point temperature is denoted T_{drm} [$^{\circ}C$]. The manipulated input to the model is the gas valve position u_g .

The fresh air dew-point temperature, denoted T_{df} [$^{\circ}C$], influences significantly the measured humidity levels within the manufacturing zone through the fresh air intake of the HVAC system. Additionally, the dew-point temperature of the fresh air is closely related to the dew-point temperature of the outdoor air, which is used by the DU as reactivation air. Therefore a relatively simple linear trend model is identified. The input to this model is the dew-point temperature, T_{df} , measured by sensor P_2 , see Figure 5.1; the model output is the introduced trend, denoted T_{dt} [$^{\circ}C$]. Having the measured fresh air dew-point temperature, T_{df} , the resulting trend is computed and subsequently subtracted from the measured zone dew-point temperature, T_{drm} , giving the detrended zone dew-point temperature measurement, denoted T_{dr} , i.e. $T_{dr} = T_{drm} - T_{dt}$. The detrended T_{dr} is then used

for system identification purposes.

The system has been allowed to settle prior to the identification experiment with the gas valve being at low fire, $u_g = 24$ [%], and the cooling valve partially open at $u_c = 10$ [%] ($u_g = 0$). The system identification experiment is designed such that the gas valve position is gradually increased (a stair case signal) and then gradually closed. Consequently, the dew-point temperature, T_{dr} , gradually decreases, as the gas valve opens, and then returns, i.e. increases as the gas valve closes. Due to the operation of the DU, the zone dry-bulb temperature, T_{ar} , is also altered such that it increases and then returns, i.e. decreases during the experiment.

The efficiency of the DU, i.e. the amount of air moisture removed from the processed air at a given gas valve position, depends on the dry-bulb temperature of process and reactivation air entering the DU. The temperature of the reactivation air directly depends on the outdoor air temperature, which may vary during the data acquisition experiment. The influence of the outdoor air temperature on the humidity level within the manufacturing zone is ignored, because this influence is not considered to be significant and is not practically identifiable. The process air entering the DU is a mixture of fresh air and return air and its temperature is determined by the respective temperatures of these. The fresh air temperature is regulated by the FAP to be in the range of (5, 10) [°C]. The temperature of return air, T_{ar} , has been significantly affected as stated in the previous paragraph. Since the temperature change of T_{ar} is a direct cause of the DU operation, the identified humidity model inherently accounts for this temperature dependency (which is not desirable).

Note that the temperature control loop normally regulates the temperature T_{ar} to be at the demanded constant set-point. Consequently the temperature of the process air entering the DU is also approximately constant despite the operation of the DU. However, during the conducted data acquisition experiment the T_{ar} had risen approximately from 20 to 27 [°C] and the identified humidity model has accounted for this effect. Therefore, in order to mitigate this temperature rise (any further) and to avoid overheating of the manufacturing zone the cooling valve is opened at constant fixed position of $u_c = 10$ [%]. It would have been desirable to keep the temperature T_{ar} constant during the experiment so that the identified humidity model would more closely correspond to normal operation of the DU (under closed loop control). However, this would have meant to actively regulate this temperature by modulating the cooling valve position, which would inevitably introduce dynamic disturbances into the measurement of T_{drm} . The

resulting zone humidity model is, therefore, a compromise between a fully temperature dependent humidity model and a model which is practically realisable and identifiable.

5.4 Zone temperature submodel

Having the measured input and output data, being the supply and return air temperatures $T_{as}(t_k)$ and $T_{ar}(t_k)$, respectively, a continuous-time second order linear model is identified in a black-box manner, i.e. making use of the measured data only. The resulting model has the same structure as the models found in (Price, Young, Berckmans, Janssens & Taylor 1999) and (Youssef, Yen, Özcan & Berckmans 2011), where the temperature models of an experimental chamber have been identified using a data-based mechanistic (DBM) modelling approach. Subsequently, a lumped parameter first principles modelling approach is adopted in which the manufacturing zone is assumed to behave as perfectly mixed vessel. The resulting first principles model has the same model structure as that obtained based on measured data only. This confirms the ‘appropriateness’ of the selected model structure for the data-based identified model and allows a meaningful interpretation in physical terms. The identified zone temperature submodel and the conducted analysis were originally presented in (Zajic et al. 2012).

The subsequent analysis of the identified model, based on physical laws, additionally allows a heat load disturbance model to be obtained. The input to this model is a heat gain within the zone, denoted $q(t_k)$ [W], and the output is the temperature rise due to this heat gain. Such a model is then utilised for control system tuning purposes, where the knowledge of such a model is advantageous. Note that time varying variables are denoted with the time index (t_k) in rounded brackets, while the variables and coefficients which are assumed to be constant in the subsequent sections are denoted without (t_k).

5.4.1 Data-based model

Two separate data sets have been acquired 19th July and 20th July 2011, respectively, where the first data set is exclusively used for the purpose of parameter estimation and the second data set is used for subsequent model validation. In order to minimise the influence of errors-in-variables on estimated model parameters, the measured input signal $T_{as}(t_k)$ is noise prefiltered. A zero-phase second order Butterworth filter is designed with a cut-off frequency of 5^{-2} [Hz], see

(Ifeachor & Jervis 1993), selected mainly based on visual inspection. The sampling interval for the continuous-time manufacturing zone submodel estimation is selected to be $h = 1$ [s].

The simplified refined instrumental variable method for continuous-time system identification is used, see SRIVC algorithm 3.1. This method is particularly suitable for the considered application, as the system input is measured and the adaptive prefiltering helps to additionally attenuate the influence of errors-in-variables on the estimated parameters. Due to the use of prefilters within the SRIVC method and the presence of a constant offset in the measured output, the baselines are subtracted from measured input and output signals. The baselines are selected to be a mean value of the first ten samples, i.e. $\bar{T}_{as} = (1/10) \sum_{k=1}^{10} T_{as}(t_k) = 25.1460$ [$^{\circ}C$] and $\bar{T}_{ar} = (1/10) \sum_{k=1}^{10} T_{ar}(t_k) = 22.5690$ [$^{\circ}C$].

In order to determine the model order and presence of any pure time (transportation) delay the function `rivcid` in the Captain Toolbox for Matlab, (Taylor, Pedregal, Young & Tych 2007), has been applied. This function uses the SRIVC method to estimate a preselected set of CT linear TF models having different model orders. The model order is then determined based on the computed Young information criterion (*YIC*) for each estimated model, see (Young 2011). This heuristically defined model fit criterion places emphasis on low order models representing the system and is defined as follows

$$YIC = \ln \frac{\sigma_e^2}{\sigma_y^2} + \ln \left[\frac{1}{p} \sum_{i=1}^p \frac{\hat{\mathbf{P}}(i, i)}{\hat{\boldsymbol{\theta}}^2(i)} \right] \quad (5.6)$$

where the parameter p denotes the number of estimated parameters, estimated error covariance matrix $\hat{\mathbf{P}}$ is provided in (3.24), and the variances σ_e^2 and σ_y^2 are defined in (5.4) and (5.5), respectively. The first term of the *YIC* in (5.6) provides a measure of the ‘goodness’ of fit (cf. with R_T^2 defined in (5.3)). This logarithmic measure becomes lower as the variance of the residuals σ_e^2 decreases. The second term then gives a measure of how well the estimated model parameters are defined in terms of the normalised estimated parameter error variances. The second term is designed to indicate any potential over-parameterization and increases in value as the estimated total sum of parameter error variances increases. In general, the lower (the more negative) the value of *YIC* criterion the more suitable the model is. However other criteria such as R_T^2 should be also considered in the final model order selection, see (Young 2011) for a further discussion.

The final selected model, having $YIC = -17.6$, is a second order model with

a single zero in the numerator, i.e. $n = 2$ and $m = 1$. The estimated pure time delay is null. It is assumed that any pure time delay has been effectively captured by the dominant dynamics of the model. For this selected model, the SRIVC, as described in algorithm 3.1, has been applied with the following settings: The convergence criterion monitoring the maximum relative change of parameter estimate, defined in (3.25), is selected to be $\epsilon = 1 \times 10^{-10}$. The prefilter of the SRIVC algorithm is initialised with the single breakpoint frequency parameter equal to $\lambda = 0.01$. The final estimated model takes the form

$$T_{ar}(t_k) = \frac{\beta_0 s + \beta_1}{s^2 + \alpha_1 s + \alpha_2} T_{as}(t_k) + e(t_k) \quad (5.7)$$

where the estimated model parameters are

$$\alpha_1 = 53.3769 \times 10^{-4} \ (0.9352 \times 10^{-5}) \quad (5.8a)$$

$$\alpha_2 = 15.8771 \times 10^{-7} \ (0.6221 \times 10^{-8}) \quad (5.8b)$$

$$\beta_0 = 23.2968 \times 10^{-4} \ (0.3300 \times 10^{-5}) \quad (5.8c)$$

$$\beta_1 = 10.3538 \times 10^{-7} \ (0.4018 \times 10^{-8}) \quad (5.8d)$$

with the corresponding standard errors provided in the parentheses¹. The estimated standard errors are relatively small, compared to the value of estimated parameters, indicating good accuracy of the obtained parameter estimates.

The estimated model has two real poles with corresponding time constants $T_1 = 199.144$ [s] and $T_2 = 3162.73$ [s]. The steady-state gain is found to be $SSG = 0.6521$. Subsequently, the simulation results with $R_T^2 = 99.744$ [%] and $IAE = 0.103$ [°C] are presented in Figure 5.8 for the estimation data set, where the simulated system output is denoted by $\hat{x}(t_k)$. The performance criteria have also been evaluated for the validation data set and these are $R_T^2 = 99.688$ [%] and $IAE = 0.107$ [°C] and the simulation results are presented in Figure 5.9. At time step 560 [min] an outlier can be seen in the simulation error subplot in Figure 5.9. This outlier has been caused by a measurement error and has been kept in the measured data set, because this data set is used only for the validation and not for estimation purposes. The evaluated performance criteria for the validation and estimation data sets indicate an acceptable predictive performance of the estimated zone temperature submodel.

The simulation error (being also the model residuals), plotted in the lower

¹Note that for consistency in the estimates 4 decimal places accuracy is adopted. However, from an engineering viewpoint in any final implementation 3 significant figures would be normally adequate.

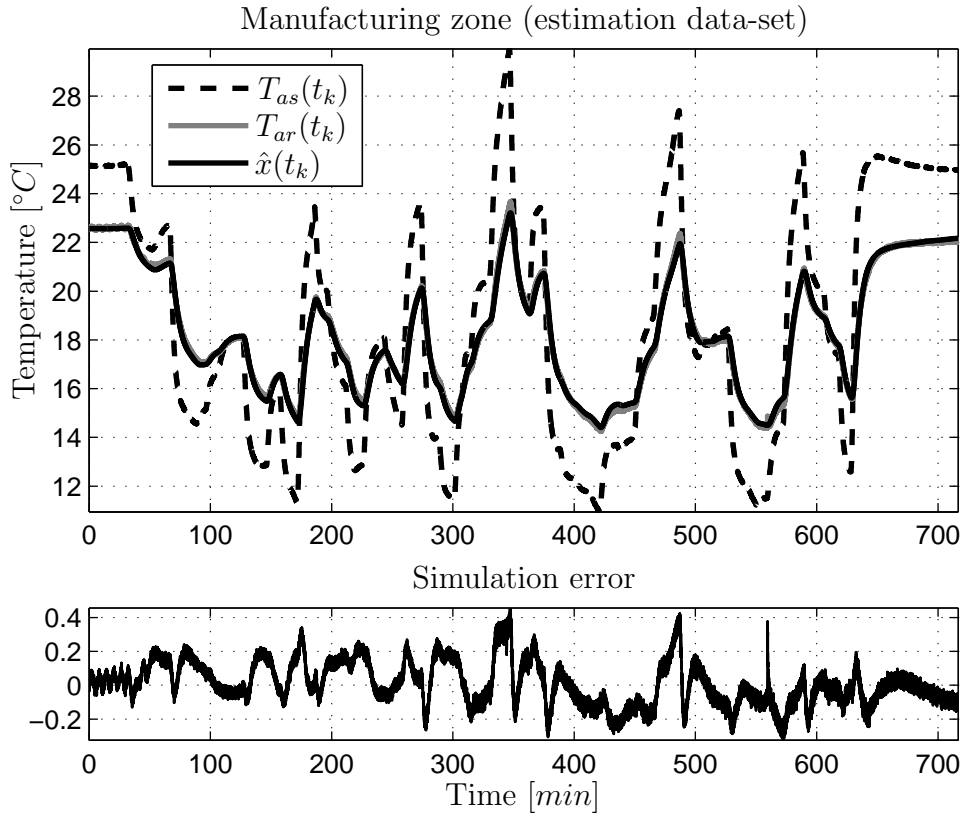


Figure 5.8: Measured manufacturing zone supply air temperature T_{as} (black dashed line) and zone return air temperature T_{ar} (grey solid line) are shown together with the simulated zone return air temperature (black solid line). Estimation data set is used.

part of Figure 5.8, is not a zero mean white noise signal. However, the SRIVC method assumes white additive noise disturbing the output, so the result indicates that the noise model assumptions were in fact not correct. Additionally, the sharp spikes can be observed when the input signal changes, which indicates that the estimated error $e(t_k)$ is partially correlated with the input signal T_{as} . This, further, indicates that the deterministic part of the model could not capture all of the deterministic processes caused by the system input. It is assumed, that the main cause of such correlation is the inherent closed loop setup of the investigated HVAC system, where the output T_{ar} recirculates and subsequently largely influences the input T_{as} . It is anticipated that this may have also affected the accuracy of the parameter estimates and that the reported SE are probably too optimistic. However, the calculated R_T^2 and IAE model fit measures are considered to be satisfactory. Therefore the model obtained is considered to be applicable for the intended control analysis and tuning purposes.

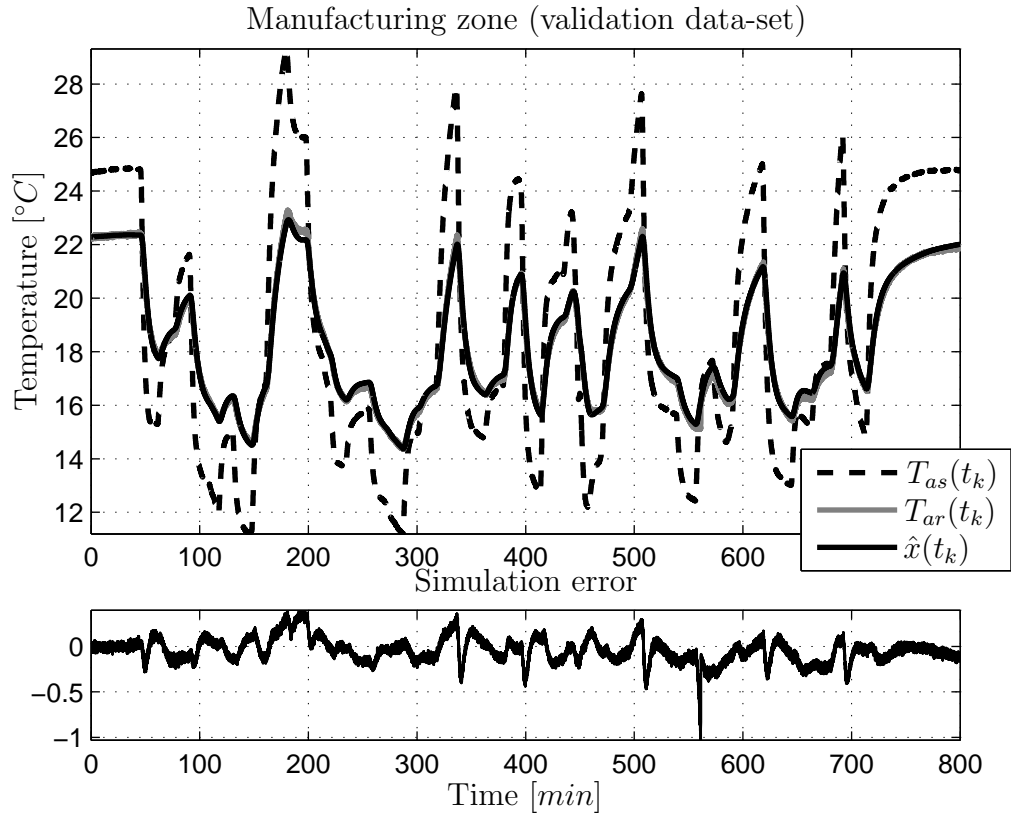


Figure 5.9: Measured manufacturing zone supply air temperature T_{as} (black dashed line) and zone return air temperature T_{ar} (grey solid line) are shown together with the simulated zone return air temperature (black solid line). Validation data set is used.

5.4.2 First principles considerations

A lumped parameter modelling approach has been adopted in which the manufacturing zone is assumed to behave as a perfectly mixed vessel. In this case the zone air temperature is homogenous in an entire zone volume and equal to the return air temperature T_{ar} . Consequently, the energy balance equations for the air within the zone and adjacent walls, are, respectively, given by

$$C_1 \frac{dT_{ar}(t)}{dt} = m_a c_a [T_{as}(t) - T_{ar}(t)] - U_1 A [T_{ar}(t) - T_w(t)] + q(t) \quad (5.9a)$$

$$C_2 \frac{dT_w(t)}{dt} = U_1 A [T_{ar}(t) - T_w(t)] - U_2 A [T_w(t) - T_a(t)] \quad (5.9b)$$

where C_1 [$J/^\circ C$] is the thermal air capacity, C_2 [$J/^\circ C$] thermal wall capacity, c_a [$J/kg^\circ C$] is the air specific heat capacity, m_a [kg/s] is the air mass-flow rate, U_1 and U_2 [$J/m^2^\circ C$] are the heat transfer coefficients on the inner and outer walls,

respectively, A [m^2] is the effective surface area of the walls, $T_w(t)$ [$^{\circ}C$] is the mean wall temperature, $T_a(t)$ [$^{\circ}C$] is the effective ambient temperature and $q(t)$ [W] is the heat load disturbance within the zone. The time index (t) is chosen, emphasising that the signals are not measured but generated by physical based models.

Using the differential operator s , defined as $s^p x(t) = \frac{d^p x(t)}{dt^p}$, allows the two differential equations of (5.9) to be conveniently exposed as

$$\left[s + \frac{m_a c_a}{C_1} + \frac{U_1 A}{C_1} \right] T_{ar}(t) = \frac{m_a c_a}{C_1} T_{as}(t) + \frac{U_1 A}{C_1} T_w(t) + \frac{1}{C_1} q(t) \quad (5.10a)$$

$$\left[s + \frac{U_1 A}{C_2} + \frac{U_2 A}{C_2} \right] T_w(t) = \frac{U_1 A}{C_2} T_{ar}(t) + \frac{U_2 A}{C_2} T_a(t) \quad (5.10b)$$

Introducing constant coefficients

$$a_1 = \frac{m_a c_a}{C_1} + \frac{U_1 A}{C_1} \quad (5.11a)$$

$$a_2 = \frac{U_1 A}{C_2} + \frac{U_2 A}{C_2} \quad (5.11b)$$

$$b_1 = \frac{m_a c_a}{C_1} \quad (5.11c)$$

$$b_2 = \frac{U_1^2 A^2}{C_2 m_a c_a} \quad (5.11d)$$

and combining the set of differential equations (5.10) such that the second equation (5.10b) is substituted for temperature $T_w(t)$ into the first equation (5.10a) the following transfer function is obtained

$$T_{ar}(t) = \frac{b_1}{s + a_1} \left\{ T_{as}(t) + \frac{b_2}{s + a_2} T_{ar}(t) + \frac{\frac{U_2}{U_1} b_2}{s + a_2} T_a(t) + \frac{1}{m_a c_a} q(t) \right\} \quad (5.12)$$

The combined transfer function (5.12) effectively represents a feedback connection of two first order dynamic processes, which has been also noted in (Price et al. 1999). A block diagram representation of the combined transfer function (5.12) is provided in Figure 5.10.

The transfer function (5.12) can be interpreted, in conjunction with the block diagram provided in Figure 5.10, as follows: The temperature of supply air $T_{as}(t)$ directly influences the zone air temperature $T_{ar}(t)$ through the first order dynamic process (forward path TF) having a time constant of

$$T_{f1} = \frac{1}{a_1} = \frac{C_1}{m_a c_a + U_1 A} \quad (5.13)$$

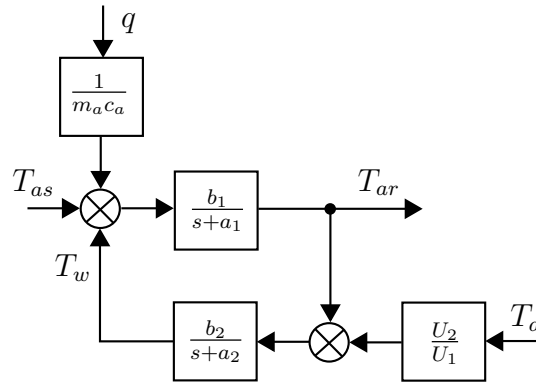


Figure 5.10: Feedback decomposition of the first principles model representing the zone temperature submodel dynamics.

Simultaneously, the air temperature, $T_{ar}(t)$, influences the wall temperature, $T_w(t)$, through the heat transfer process (feedback path TF), which also has first order dynamics with a corresponding time constant of

$$T_{f2} = \frac{1}{a_2} = \frac{C_2}{U_1 A + U_2 A} \quad (5.14)$$

The time constants T_{f1} and T_{f2} of the two dynamic modes are proportional to the thermal capacity of air C_1 and wall C_2 , respectively. Since, it can be assumed that $C_2 > C_1$, due to the wall material thermal properties, then also $T_{f2} > T_{f1}$. Subsequently, this slow heat transfer process influences the zone air temperature via the feedback path. Finally, it can be noted that the heat gain, $q(t)$, and ambient temperature, $T_a(t)$, are directly related to the temperatures, T_{as} and T_{ar} , via gains $1/(m_a c_a)$ and U_2/U_1 , respectively.

Expanding and rearranging the transfer function (5.12) with respect to T_{ar} gives the complete second order dynamic model representing the zone air temperature, i.e.

$$T_{ar}(t) = \frac{b_1 s + b_1 a_2}{s^2 + (a_1 + a_2)s + (a_1 a_2 - b_1 b_2)} \left\{ T_{as}(t) + \frac{1}{m_a c_a} q(t) \right\} + \frac{U_2 b_1 b_2}{U_1 [s^2 + (a_1 + a_2)s + (a_1 a_2 - b_1 b_2)]} T_a(t) \quad (5.15)$$

During the data collection experiment no heat gains were acting on the system, i.e. $q(t) = 0$. Furthermore, the ambient temperature $T_a(t)$ has not been measured. However, it is expected that it can be considered as being constant over the duration of the system identification experiment, i.e. $T_a(t) \simeq T_a$. Consequently,

T_a effectively introduces a constant offset in the measurements. The constant offset has been eliminated by subtracting the bases of measured signals in steady-state prior to parameter estimation. Subsequently, the transfer function (5.15) is expressed as

$$T_{ar}(t) = \frac{b_1s + b_1a_2}{s^2 + (a_1 + a_2)s + (a_1a_2 - b_1b_2)}T_{as}(t) + o \quad (5.16)$$

where the offset o is defined as

$$o = \frac{U_2b_1b_2}{U_1(a_1a_2 - b_1b_2)}T_a \quad (5.17)$$

Comparing the data-based identified model structure (5.7) and that obtained by physical considerations (5.16), it can be observed that these two are in fact the same, which validates the prior, data-based, selection of the second order model structure with a single zero.

Inferring available information from data-based model

The identified model is intended for the purpose of control tuning, where the current controller operates as a regulator only. In other words, the controller is required to follow a given, fixed, set-point while rejecting any load disturbances acting on the system. In order to tune the controller for the load disturbance rejection application, it is advantageous to obtain a load disturbance model itself. Comparing the data-based identified model (5.7) and that obtained via physical considerations (5.16), the following holds

$$\frac{\beta_0s + \beta_1}{s^2 + \alpha_1s + \alpha_2} \stackrel{!}{=} \frac{b_1s + b_1a_2}{s^2 + (a_1 + a_2)s + (a_1a_2 - b_1b_2)} \quad (5.18)$$

where the parameters α_1 , α_2 , β_0 and β_1 are known from the parameter estimation stage. Denoting the temperature rise of the air within the manufacturing zone caused by the heat gain $q(t)$ as $T_q(t)$ [$^{\circ}C$] and considering the relation (5.18) and the first principles model (5.15), the heat load disturbance model is inferred as

$$T_q(t) = \frac{\beta_0s + \beta_1}{s^2 + \alpha_1s + \alpha_2} \frac{1}{m_a c_a} q(t) \quad (5.19)$$

Since the manufacturing zone submodel is identified in the continuous-time domain, the model parameters have real physical meaning. Therefore, it is possible to multiply the parameters of the identified model by $1/(m_a c_a)$, hence obtaining

the heat load model. From technical sheets of the AHU the designed air mass-flow rate is $m_a = 2.4082 [kg/s]$ and $c_a = 1005 [J/^\circ Ckg]$. The computed mass-flow rate is a product between the rated volumetric flow, being $2 [m^3/s]$, and the density of air, being $1.2041 [kg/m^3]$.

The constant effective ambient temperature T_a can also be calculated. First, note that the sum of steady-state gains of the first and the second transfer function in (5.15), denoted SSG_1 and SSG_2 , respectively, is equal to unity, i.e.

$$SSG_1 = \frac{b_1 a_2}{a_1 a_2 - b_1 b_2} = \frac{\beta_1}{\alpha_2} \quad (5.20a)$$

$$SSG_2 = \frac{U_2 b_1 b_2}{U_1 (a_1 a_2 - b_1 b_2)} \quad (5.20b)$$

$$1 = SSG_1 + SSG_2 \quad (5.20c)$$

This is a consequence of energy conservation within the system. The SSG_1 provided in (5.20a) is known, since the ratio β_1/α_2 is known (estimated). Therefore, from (5.20c) the SSG_2 is calculated

$$SSG_2 = 1 - SSG_1 \quad (5.21)$$

In steady-state the following holds

$$\bar{T}_{ar} = SSG_1 \bar{T}_{as} + SSG_2 T_a \quad (5.22)$$

where the baselines \bar{T}_{ar} and \bar{T}_{as} are measured. Additionally, the offset o in (5.17) is equal to

$$o = SSG_2 T_a \quad (5.23)$$

hence the constant offset can be computed from (5.22) and (5.23) as

$$o = \bar{T}_{ar} - SSG_1 \bar{T}_{as} \quad (5.24)$$

Knowing the constant offset term from (5.24) and considering the definition of the offset term given in (5.23), the effective ambient temperature is computed as follows

$$T_a = \frac{\bar{T}_{ar} - SSG_1 \bar{T}_{as}}{1 - SSG_1} = \frac{22.5690 - 0.6521 \times 25.1460}{1 - 0.6521} = 17.7381 [^\circ C] \quad (5.25)$$

The estimated ambient temperature of $T_a = 17.74 [^\circ C]$ may seem to be underestimated at first, as a value around $21 [^\circ C]$ would rather be expected with respect

to the air temperatures of corresponding adjacent manufacturing zones. However, the relatively simple model used does also include the zone's floor, which has a lower temperature, possibly partially explaining the slightly low value of the estimated T_a .

The estimated second order TF model (5.7) can be decomposed into a feedback connection introduced in (5.12) using the equality of parameters in (5.18). This then provides even further insight into the physical properties of the system. The parameters a_1 , a_2 , b_1 and b_2 of the feedback TF form, defined in (5.11), can be calculated as follows

$$b_1 = \beta_0 = 23.2968 \times 10^{-4} \quad (5.26a)$$

$$a_2 = \frac{\beta_1}{b_1} = 44.4431 \times 10^{-5} \quad (5.26b)$$

$$a_1 = \alpha_1 - a_2 = 48.9326 \times 10^{-4} \quad (5.26c)$$

$$b_2 = \frac{a_1 a_2 - \alpha_2}{b_1} = 25.1968 \times 10^{-5} \quad (5.26d)$$

Knowing the parameters of the two first order processes the time constants, defined in (5.13) and in (5.14), can be computed together with the corresponding steady-state gains, denoted SSG_{f1} and SSG_{f2} , respectively, hence

$$T_{f1} = \frac{1}{a_1} = 204.363 \text{ [s]} \quad (5.27a)$$

$$T_{f2} = \frac{1}{a_2} = 2250.07 \text{ [s]} \quad (5.27b)$$

$$SSG_{f1} = \frac{b_1}{a_1} = 0.4761 \quad (5.27c)$$

$$SSG_{f2} = \frac{b_2}{a_2} = 0.5669 \quad (5.27d)$$

It is apparent that the fast process, having time constant T_{f1} , accounts for the direct influence of the controlled supply air, while the heat transfer process between the air and walls has slow dynamics and dominates the zone temperature over a long time horizon. The relatively large gain SSG_{f2} would indicate rather large heat losses, however, note, that approximately $0.2 \text{ [m}^3/\text{s]}$ of the air ventilates from the zone so that a higher air pressure than the atmospheric one is maintained (clean room production area).

Having computed the parameters of the two first order processes, given in (5.26), and based on the technical insight, the constants $m_a = 2.4082 \text{ [kg/s]}$ and $c_a = 1005 \text{ [J/}^\circ\text{Ckg]}$ are also known; it is then possible to compute the thermal

capacities C_1 and C_2 and parameter products U_1A and U_2A . From the definition of parameter b_1 in (5.11c), the thermal air capacity is computed as follows

$$C_1 = \frac{m_a c_a}{b_1} = 1.0389 \times 10^6 \left[\frac{J}{^\circ C} \right] \quad (5.28)$$

and knowing C_1 the product U_1A is then computed from (5.11a), i.e.

$$U_1A = (a_1 - b_1)C_1 = 2.6632 \times 10^3 \left[\frac{J}{^\circ C} \right] \quad (5.29)$$

Having computed U_1A it is then possible to calculate the thermal capacity C_2 from (5.11d), hence

$$C_2 = \frac{(U_1A)^2}{b_2 m_a c_a} = 1.1631 \times 10^7 \left[\frac{J}{^\circ C} \right] \quad (5.30)$$

Subsequently, knowing U_1A and C_2 , the product U_2A is computed from (5.11b), that is

$$U_2A = C_2 \left(a_2 - \frac{U_1A}{C_2} \right) = 2.5059 \times 10^3 \left[\frac{J}{^\circ C} \right] \quad (5.31)$$

It is interesting to note, that the ratio U_2/U_1 , used in the feedback interpretation of the TF (5.12), is also known, because U_1A and U_2A have been calculated, so that $(U_2A)/(U_1A) = U_2/U_1$. It is not possible to estimate the parameters U_1 and A separately, however the area A might be known from the technical documentation. Finally, considering the definition of the thermal capacity of the air $C_1 = V\rho c_a$, where V [m^3] denotes the zone volume and ρ [kg/m^3] denotes the density, and assuming $V = 10 \times 10 \times 3 = 300$ [m^3] and $\rho = 1.2041$ [kg/m^3], then the approximate value of C_1 would be 3.6304×10^5 [$J/^\circ C$]. This is almost three times less than the estimated value of 1.0389×10^6 [$J/^\circ C$]. It is assumed, that this overestimation may have been caused by several factors, e.g. biased parameter estimates and/or that the model does not take into account that 0.2 [m^3/s] of air ventilates out of the zone.

5.5 Air handling unit temperature submodel

In this section, a continuous-time Hammerstein-bilinear model representing the AHU is obtained. The considered system inputs are the inflow air temperature $T_{ai}(t_k)$ and the cooling valve stem fractional position $u_c(t_k)$, the system output is then the temperature of the outflow air $T_{ao}(t_k)$. In order to simplify the nota-

tion, the subscript c of the variable denoting the cooling valve position is omitted in this section, i.e. $u_c(t_k) \rightarrow u(t_k)$. The scope of possible experimentation is limited, because the AHU is already installed on the site, i.e. the measured input-output data may not be sufficiently informative for parameter estimation purposes. Therefore, with the knowledge of the first principles analysis a candidate nonlinear model structure is determined first and the model parameters are estimated based on the measured input-output data. Naturally, not all nonlinear regression terms suggested by such analysis are needed. Therefore, some of the regression terms of the originally determined nonlinear model structure are discarded, which results in a simplified and well structured Hammerstein-bilinear model. This model predicts the outflow air temperature with sufficient accuracy for the current application.

The main active component of the AHU is the cooling coil unit composing of the finned cold-water-to-air heat exchanger. The heat exchangers are nonlinear components and the modelling challenges of these have been addressed by many authors. In the work of Thomson, Schooling & Soufian (1996) the modelling of a pilot-scale parallel-tube heat exchanger carried out in a black-box manner has been considered. Although, the authors does not refer to the identified model as being of a HB form, the model obtained does indeed resemble the HB model structure proposed in this thesis. A grey-box modelling approach to the identification of heat exchangers has been adopted in (Underwood & Crawford 1991, Underwood 2000, Ghiaus, Chicinas & Inard 2007). This approach has resulted in accurate yet rather complex models, which are not considered to be suitable for the current application. Furthermore, some of the models are not even obtainable under the current experimental setup, where the temperatures of the supply and discharge cold water to and from the AHU, being the second input and output of the system, are not measured. It is, therefore believed, that the model obtained of the AHU presented in this section offers a compromise solution between complexity, predictive accuracy and practical realisability.

5.5.1 First principles analysis

As in the case of the manufacturing zone submodel, the lumped parameter modelling approach has also been adopted, see (Zajic et al. 2012). The cooling coil, being the main component of the AHU, is considered to behave as a perfectly mixed vessel, therefore the discharge cold water temperature, denoted $T_{wo}(t)$ [$^{\circ}C$], is assumed to be equal to the mean temperature of the whole coil. The energy

balance on the water side of the coil is then given by

$$C \frac{dT_{wo}(t)}{dt} = m_w(t)c_w [T_{wi} - T_{wo}(t)] - UA [T_{wo}(t) - T_{ao}(t)] \quad (5.32)$$

where $C [J/^\circ C]$ denotes the overall thermal capacity (sum of water and metal body of the coil thermal capacities), $m_w(t) [kg/s]$ denotes the water mass-flow rate, $c_w [J/kg^\circ C]$ is the water specific heat capacity, $U [J/m^2^\circ C]$ is the effective heat transfer coefficient, and $A [m^2]$ is the effective coil surface. The supply chilled water temperature, denoted $T_{wi} [^\circ C]$, is assumed to be constant and $T_{ao}(t)$ is the temperature of the outflow air being the system output. Assuming instantaneous heat exchange between the air and cooling coil the energy balance on the air side is

$$0 = UA [T_{wo}(t) - T_{ao}(t)] - m_a c_a [T_{ao}(t) - T_{ai}(t)] \quad (5.33)$$

where $T_{ai}(t)$ is the inflow air temperature being the second system input and constants m_a and c_a are defined in (5.9).

The water mass-flow rate entering the coil is modelled by

$$m_w(t) = M_w \phi(u(t)), \quad (5.34)$$

where M_w denotes the maximal water mass-flow rate for a fully open valve, i.e. $u(t) = 1$, and $\phi(\cdot)$ represents the valve static characteristic (Hammerstein-type nonlinearity). The valve installed on the plant has a linear inherent characteristic in the range of $\langle 0, 30 \rangle$ [%] and an equal percentage inherent characteristic in the range of $\langle 30, 100 \rangle$ [%] of the stem position. It is, therefore, assumed that the Hammerstein nonlinearity can be described by a 5th order polynomial, i.e.

$$v(t) = \phi(u(t)) = \sum_{i=1}^5 p_i u^i(t), \quad (5.35)$$

where $p_{1,\dots,5}$ are constant coefficients to be estimated. It is known that when $u(t) = 1$ then $v(t) = 1$, so that the appropriate scaling is $p_1 = 1 - \sum_{i=2}^5 p_i$, see (3.88). Subsequently, the constraint static polynomial function, defined in (3.89), is

$$v(t) = u(t) + \sum_{i=2}^5 p_i [-u(t) + u^i(t)], \quad \text{for } u(t) \in \langle 0, 1 \rangle \quad (5.36)$$

hence only $p_{2,\dots,5}$ coefficients need to be estimated.

Further simplifying assumptions have been made regarding the heat transfer coefficient U . The heat transfer coefficient on the water side depends, in a non-linear manner, on the water mass-flow rate $m_w(t)$, see (Jonsson & Palsson 1991). While the heat transfer coefficient on the air side predominantly depends, exponentially, on the outflow air temperature $T_{ao}(t)$, see (Underwood 2000). The heat transfer coefficients on the water and air sides have been, however, considered to be constant and equal. Additionally, it is noted that during the normal operation of the HVAC system the air is dehumidified to $T_{drm} = -10$ [$^{\circ}C$] (measured in terms of dew-point temperature), while the temperature of the chilled supply water is $T_{wi} = 4.5$ [$^{\circ}C$]. Therefore, the temperature of the processed air is always above its dew-point temperature, hence no dew condensates on the surface of the cooling coil, i.e. only sensible cooling occurs. In the case where condensation took place this would have to be reflected in the modelling assumptions, see (Wang & Hihara 2003).

Using the differential operator s and the definition of the water mass-flow rate (5.34) the energy balance equation on the water side (5.32) can be conveniently expressed as follows

$$\left[s + \frac{Mc_w}{C}v(t) + \frac{UA}{C} \right] T_{wo}(t) = \frac{Mc_w T_{wi}}{C}v(t) + \frac{UA}{C}T_{ao}(t) \quad (5.37a)$$

$$T_{wo}(t) = \frac{\frac{Mc_w T_{wi}}{C}v(t) + \frac{UA}{C}T_{ao}(t)}{s + \frac{Mc_w}{C}v(t) + \frac{UA}{C}} \quad (5.37b)$$

Subsequently, substituting (5.37b) into the energy balance equation on the air side (5.33) for the unknown discharge water temperature $T_{wo}(t)$ and rewriting the resulting expression in a transfer function form gives

$$\begin{aligned} T_{ao}(t) = & \frac{\beta_{1,0}}{s + \alpha_1}v(t) + \frac{\eta_{2,1}}{s + \alpha_1}v(t)T_{ao}(t) + \frac{\beta_{3,0}s + \beta_{3,1}}{s + \alpha_1}T_{ai}(t) \\ & + \frac{\eta_{4,1}}{s + \alpha_1}v(t)T_{ai}(t) \end{aligned} \quad (5.38)$$

where the parameters are defined as

$$\begin{aligned} \alpha_1 = \frac{m_a c_a U A}{U A C + m_a c_a C}, \quad \beta_{1,0} = \frac{M c_w U A T_{wi}}{U A C + m_a c_a C}, \quad \eta_{2,1} = -\frac{M c_w}{C} \\ \beta_{3,0} = \frac{m_a c_a C}{U A C + m_a c_a C}, \quad \beta_{3,1} = \frac{m_a c_a U A}{U A C + m_a c_a C}, \quad \eta_{4,1} = \frac{m_a c_a M c_w}{U A C + m_a c_a C} \end{aligned} \quad (5.39)$$

and the intermediate input $v(t)$ is defined in (5.35). The product between the input $v(t)$ and output $T_{ao}(t)$ in the second transfer function of (5.38) represents a bilinear-type nonlinearity, which affects the steady-state gain and the time con-

stant such that these depends on the operating point. This nonlinearity arises from the product of the water mass-flow rate $m_w(t)$ and the outflow water temperature $T_{wo}(t)$ in the energy balance equation (5.32). The second nonlinearity, in (5.38), is the product between the two inputs, i.e. $T_{ai}(t)$ and $v(t)$. If the nonlinear model of the AHU was linearised, this nonlinearity would ensure that the resulting steady-state gain between valve position $u(t)$ and the outflow air temperature $T_{ao}(t)$ is negative for the case when $T_{ai}(t) > T_{wi}$, i.e. cooling application, or positive for the case $T_{ai}(t) < T_{wi}$, i.e. heating application.

5.5.2 Preliminary system identification

The parameters of the nonlinear model structure suggested by the first principles analysis (5.38) are estimated based on the measured input-output data. Assuming a pure time transportation delay on the input $u(t_k)$, denoted τ_u [s], and on the second input $T_{ai}(t_k)$, denoted τ_{ai} [s], and assuming white, zero mean, additive measurement noise $e(t_k)$; the overall model to be estimated then constitutes a static input function followed by a nonlinear dynamic submodel, hence

$$v(t_k) = u(t_k) + \sum_{i=2}^5 p_i [-u(t_k) + u^i(t_k)] \quad (5.40a)$$

$$\begin{aligned} T_{ao}(t_k) = & \frac{\beta_{1,0}}{s + \alpha_1} v(t_k - \tau_u) + \frac{\eta_{2,1}}{s + \alpha_1} v(t_k - \tau_u) T_{ao}(t_k) \\ & + \frac{\beta_{3,0}s + \beta_{3,1}}{s + \alpha_1} T_{ai}(t_k - \tau_{ai}) + \frac{\eta_{4,1}}{s + \alpha_1} v(t_k - \tau_u) T_{ai}(t_k - \tau_{ai}) + e(t_k) \end{aligned} \quad (5.40b)$$

Consequently, two parameter sets need to be estimated, one corresponding to the static part and one corresponding to the dynamic part of the model, i.e. $\boldsymbol{\theta}_n = [p_2, \dots, p_5]^T$ and $\boldsymbol{\theta}_{lb} = [\alpha_1, \beta_{1,0}, \eta_{2,1}, \beta_{3,0}, \beta_{3,1}, \eta_{4,1}]^T$, respectively. The overall nonlinear model of the AHU is bilinear in the parameters. By exploiting this property it is possible to solve separately for the unknown parameter vectors $\boldsymbol{\theta}_n$ and $\boldsymbol{\theta}_{lb}$ by the designed HSRIVC and HBSRIVC parameter estimation methods, introduced in Chapter 3.

The dynamic submodel (5.40b) has first order linear dynamics, one bilinear term and one multiplicative nonlinear term, which is a product between the two system inputs. Since, the two system inputs are known, the last nonlinear term can be treated as a new input. Therefore, the overall model of the AHU (5.40) can be viewed as a multi-input single-output Hammerstein-bilinear model, where the individual inputs are $v(t_k - \tau_u)$, $T_{ai}(t_k - \tau_{ai})$ and $v(t_k - \tau_u)T_{ai}(t_k - \tau_{ai})$. Subsequently, in order to estimate the unknown model parameters, including

the input delays, the constrained HSRIVC algorithm 3.4 is chosen. The HSRIVC algorithm has been applied with the following settings: The convergence criterion monitoring the maximum relative change of the parameter estimate, defined in (3.80), is selected to be $\epsilon = 1 \times 10^{-5}$. The prefilter of the HSRIVC algorithm is initialised with the single breakpoint frequency parameter equal to $\lambda = 0.004$. The static input nonlinearity is assumed to be linear $v(t_k) = u(t_k)$, hence setting $\hat{\theta}_n^{j=0} = [0, 0, 0, 0]^T$, where j denotes the iteration index.

Similarly as in the case of the manufacturing zone temperature submodel, the two separate data sets, acquired 19th July and 20th July 2011, are used. The first data set is exclusively used for the parameter estimation and the second data set is used for the model validation only. The measured, noise contaminated, input signal $T_{ai}(t_k)$ is noise prefiltered using zero-phase second order Butterworth filter with a designed cut-off frequency of 5^{-2} [Hz], which has been selected mainly based on visual inspection. The same sampling interval used for the data acquisition is used for the parameter estimation, i.e. $h = 1$ [s]. Considering the system dynamics, it is believed that this sampling interval is sufficiently small and permits for the parameter estimation in the continuous-time domain. Additionally, the baselines are subtracted from the measured input and output signals. The baselines are selected to be the mean value of the first ten samples, i.e. $\bar{T}_{ai} = (1/10) \sum_{k=1}^{10} T_{ai}(t_k) = 23.5054$ [$^{\circ}C$], $\bar{u} = (1/10) \sum_{k=1}^{10} u(t_k) = 0$ and $\bar{T}_{ao} = (1/10) \sum_{k=1}^{10} T_{ao}(t_k) = 25.1438$ [$^{\circ}C$].

The delays τ_u and τ_{ai} on the inputs $u(t_k)$ and $T_{ai}(t_k)$, respectively, are estimated by minimising the *IAE* criterion (5.1). The *IAE* criterion has been computed for all combinations of τ_u and τ_{ai} in a predefined range and the results are shown on the left side of Figure 5.11. The value of the achieved cost V , defined in (3.60), is also displayed. The right side of the Figure 5.11 considers delay estimation of the simplified model derived in a subsequent section. The minimum value of the *IAE* is achieved when $\tau_u = 55$ [s] and $\tau_{ai} = 68$ [s]. The value of the delay τ_{ai} seems to be overestimated, because it is known that the time required for the air to progress through the AHU is around 3 [s]. It is observed, in Figure 5.11, that the influence of τ_{ai} on the value of computed *IAE* is low and relatively constant for a particular choice of τ_u . It is concluded, that the possible overestimation of the delay τ_{ai} is caused by not having a sufficiently exciting input $T_{ai}(t_k)$, which is correlated with the output $T_{ao}(t_k)$ due to the particular experimental setup.

Subsequently, for the time delays $\tau_u = 55$ [s] and $\tau_{ai} = 68$ [s] obtained, the estimated model parameters are given in Table 5.1 with the corresponding esti-

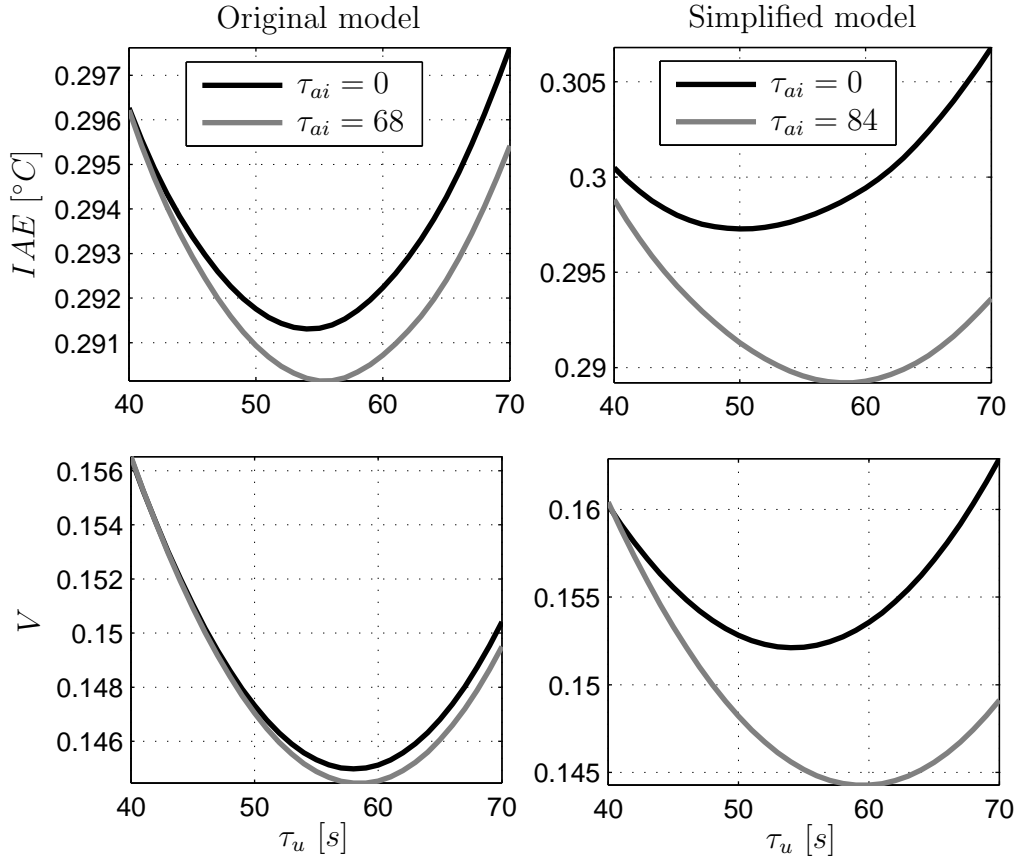


Figure 5.11: Input delay estimation based on original and simplified model: cost V and IAE criterion plotted against delay τ_u for different values of delay τ_{ai} .

mated standard errors provided in the parentheses. Most of the standard errors are relatively small, compared to the value of estimated parameters, indicating good accuracy of the parameter estimates obtained. This is with the exception of the standard errors related to the parameters $\beta_{3,0}$ and $\eta_{4,1}$, which are relatively large indicating poor accuracy of the parameter estimates and possible identifiability issues.

Subsequently, the simulation results with $R_T^2 = 99.2557$ [%] and $IAE = 0.2901$ [$^{\circ}C$] are presented in Figure 5.12 for the estimation data set. The performance criteria have also been evaluated for the validation data set. These are $R_T^2 = 99.0801$ [%] and $IAE = 0.3747$ [$^{\circ}C$], respectively, and the accompanying simulation results are presented in Figure 5.13. The system output of the estimation and validation data sets has been simulated for the inputs with subtracted bases, hence each simulated output starts at a zero value. When plotting the results,

Table 5.1: The estimated parameters of the original model and simplified model with the corresponding estimated standard errors provided in the parentheses.

	Original	Simplified		Original	Simplified
α_1	3.2470×10^{-3} (4.2513×10^{-6})	3.2914×10^{-3} (3.9801×10^{-6})	p_1	0.4515 (-)	0.4169 (-)
$\beta_{1,0}$	-10.489×10^{-2} (1.2890×10^{-4})	-10.762×10^{-2} (1.2894×10^{-4})	p_2	12.785 (0.0545)	12.988 (0.0542)
$\eta_{2,1}$	-4.2453×10^{-3} (7.1550×10^{-6})	-4.3944×10^{-3} (7.2997×10^{-6})	p_3	-47.213 (0.1623)	-47.789 (0.1615)
$\beta_{3,0}$	19.968×10^{-3} (2.2439×10^{-3})	2.1253×10^{-3} (3.6812×10^{-6})	p_4	61.573 (0.1955)	62.275 (0.1948)
$\beta_{3,1}$	2.0842×10^{-3} (4.8168×10^{-6})		p_5	-26.596 (0.0818)	-26.891 (0.0815)
$\eta_{4,1}$	4.0924×10^{-6} (9.7729×10^{-6})				

the subtracted bases have been added, so that the graphical results correspond to the actual values.

Figures 5.12 and 5.13 each comprise three subplots. In each figure, the upper plot shows measured (grey solid line) and simulated (black solid line) outflow air temperature $T_{ao}(t_k)$. The middle plot shows the simulation error $e(t_k)$, defined in (5.2), for the currently estimated model (black solid line) and simplified model (grey solid line), which is estimated in the subsequent section. The lower plot shows inputs $u(t_k)$ (grey solid line) and $T_{ai}(t_k)$ (black solid line). Note that the temperature range of the inflow air is $T_{ai} \in \langle 20.4027, 32.6651 \rangle$ [$^{\circ}C$] for the estimation data set and $T_{ai} \in \langle 20.0044, 31.6228 \rangle$ [$^{\circ}C$] for the validation data set.

The estimated error $e(t_k)$ does not have white noise properties and is also correlated with the first system input $u(t_k)$, as it is clearly visible from Figure 5.12. This indicates that not all of the system dynamics have been captured by the deterministic part of the proposed model (5.40). Nevertheless, the results obtained in terms of the IAE and R_T^2 criterion are satisfactory for the intended model purpose, hence the model is deemed to be valid. Additionally, in the case of the validation data set a large simulation error of $e(t_k) = -3$ [$^{\circ}C$] is observed at time instance 415 [min], see middle part of Figure 5.13. This error has been caused by an unrelated experiment on the AHU, in which the cooling valve of the AHU has been manually modulated in an attempt to measure the valve static characteristic. Because of the scarcity of good quality measurements this data set has had to be used for the validation purposes. Note, tat this simulation

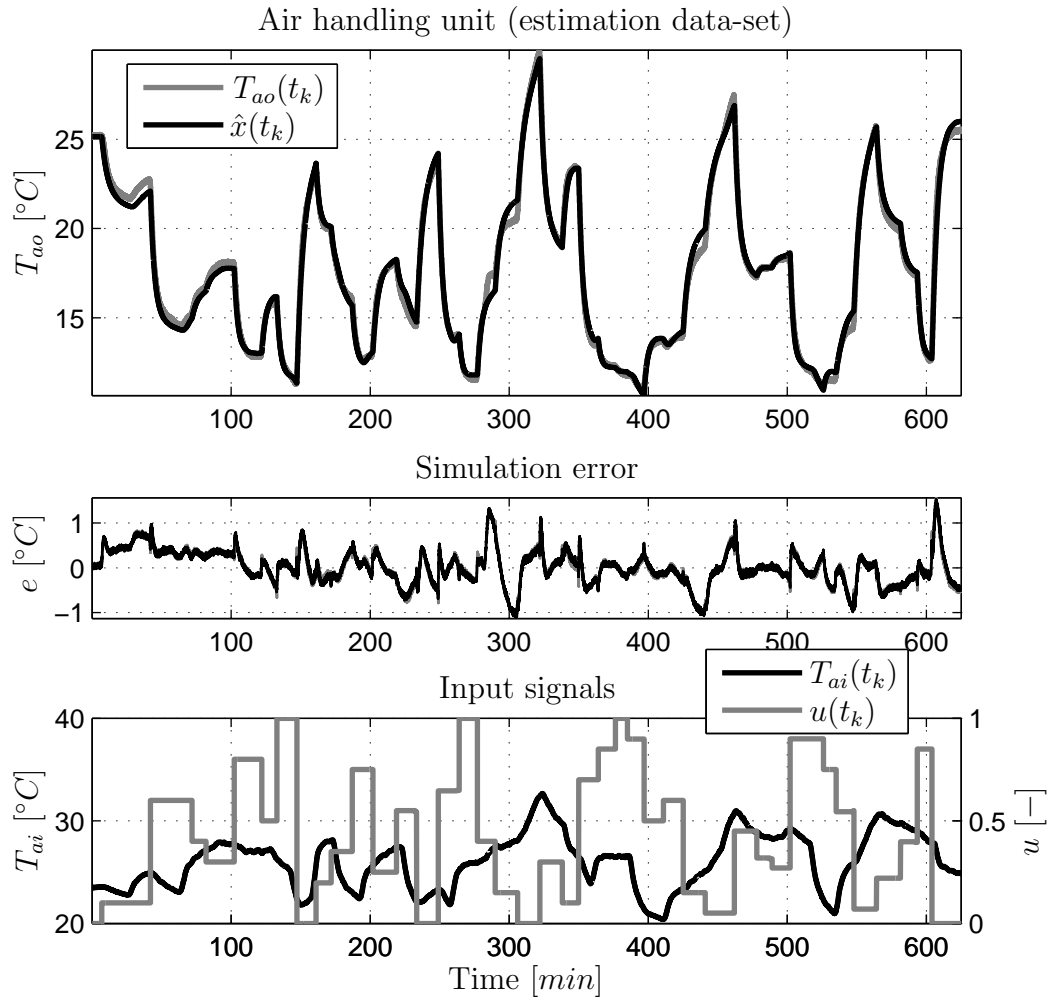


Figure 5.12: The upper plot shows measured (grey solid line) and simulated (black solid line) outflow air temperature. The middle plot shows the simulation error for original model (black solid line) and simplified model (grey solid line). The lower plot shows system inputs, i.e. fractional valve position (grey solid line) and the inflow air temperature (black solid line). Estimation data-set is used.

error is not related to the outlier observed in the measurement of the zone return temperature plotted in Figure 5.9.

The estimated valve characteristic is shown in Figure 5.14. Based on the technical documentation, the cooling valve has a linear inherent characteristic for the range $\langle 0, 30 \rangle$ [%] of stem position and equal percentage inherent characteristic in the range of $\langle 30, 100 \rangle$ [%], which is in agreement with the shape of the estimated characteristic. It can be observed, in Figure 5.14, that in the range of $\langle 87, 100 \rangle$ [%] the estimated characteristic curve is above value of unity. For increasing

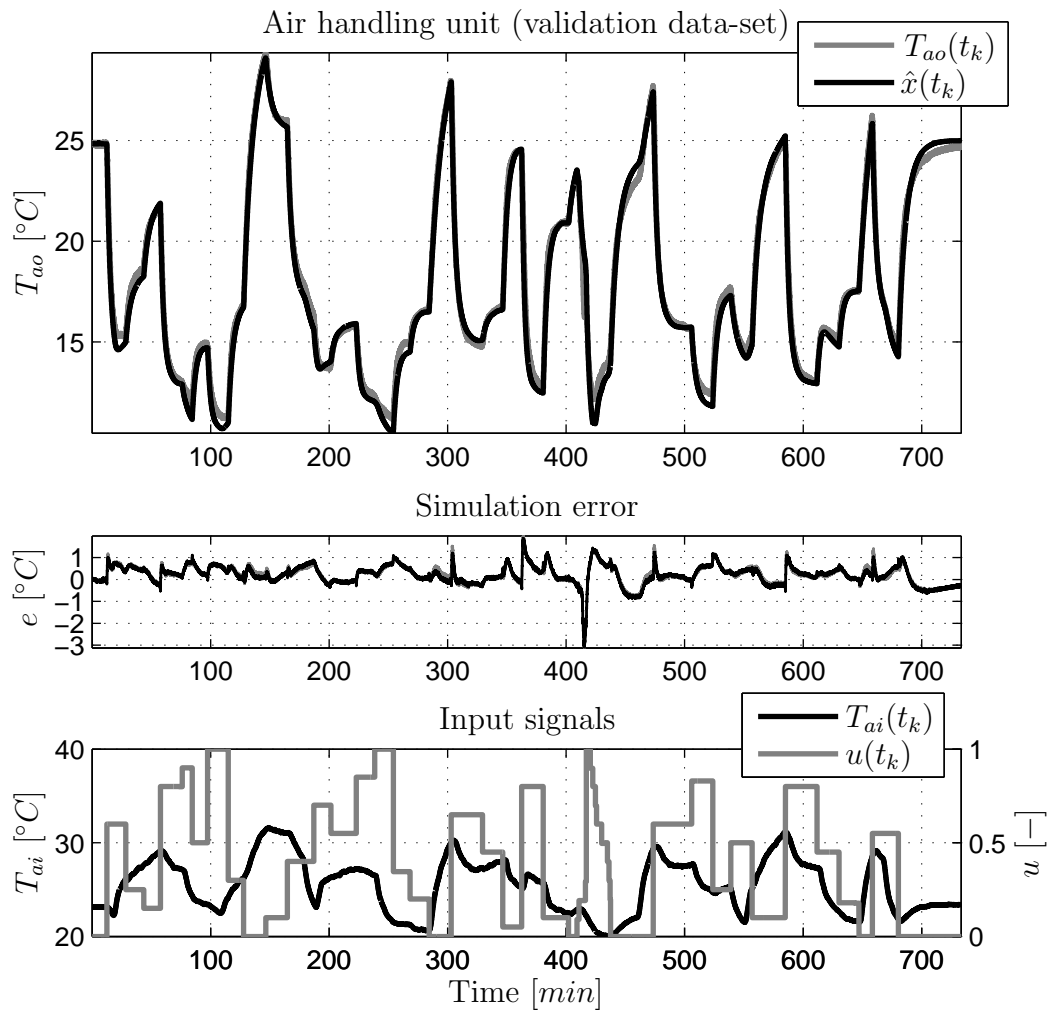


Figure 5.13: The upper plot shows measured (grey solid line) and simulated (black solid line) outflow air temperature. The middle plot shows the simulation error for original model (black solid line) and simplified model (grey solid line). The lower plot shows system inputs, i.e. fractional valve position (grey solid line) and the inflow air temperature (black solid line). Validation data-set is used.

values of $u(t_k)$ the intermediate input $v(t_k)$ rises at first and as the value of input $u(t_k)$ further increases the value of $v(t_k)$ then decreases. In other words, as the cooling valve opens the water mass-flow rate decreases, which is not considered to be physically feasible. It is assumed, that this has been caused by not having sufficiently informative measured input-output data over the whole operation range.

Additionally, it has been possible to obtain one unique measurement of the actual valve characteristic. The measured data points are depicted in Figure 5.14 by

black circles and the actual measurements of the chilled water mass-flow rate are given in Table 5.2. The water mass-flow rate has been measured using an orifice plate flowmeter. Unfortunately, it has not been possible to repeat the experiment and validate the results obtained nor the accuracy of the corresponding measurements. Therefore, the measured characteristic is not necessarily representative and should be treated as such.

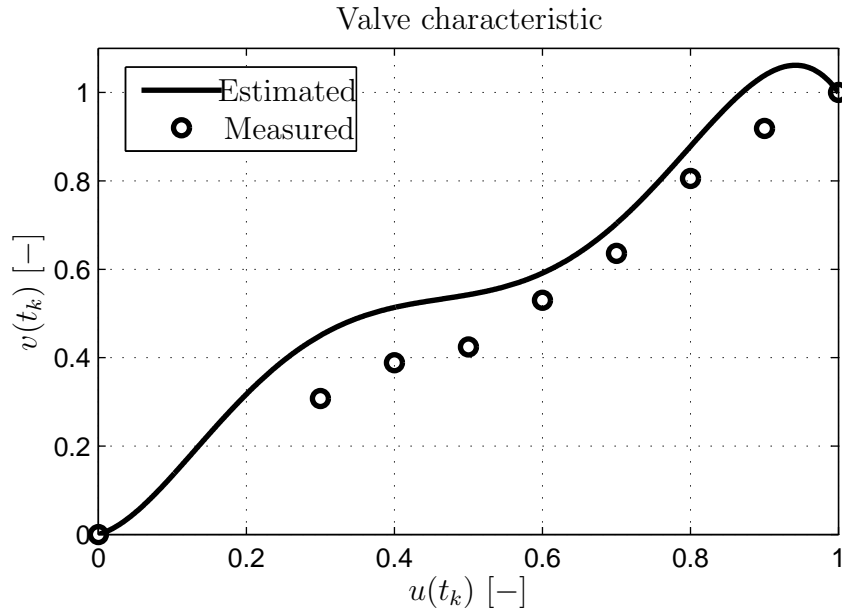


Figure 5.14: Estimated (reconstructed) cooling valve characteristic. For comparison the measured data points are depicted by black circles.

Table 5.2: Measured chilled water mass-flow rate through the cooling valve. The corresponding, normalised, intermediate input is also provided.

$u(t_k)$	$m_w(t_k)$ [l/s]	$v(t_k)$
1	2.83	1
0.9	2.6	0.9187
0.8	2.28	0.8057
0.7	1.8	0.6360
0.6	1.5	0.5300
0.5	1.2	0.4240
0.4	1.1	0.3887
0.3	0.87	0.3074

5.5.3 Final system identification

Not all regression terms suggested by the first principles system analysis are required to predict the outflow air temperature of the AHU with sufficient accuracy.

It has been noted, that the estimated standard errors associated with the parameters $\beta_{3,0}$ and $\eta_{4,1}$, provided in Table 5.1, are relatively large. Therefore, the following simplified model structure is proposed

$$v(t_k) = u(t_k) + \sum_{i=2}^5 p_i [-u(t_k) + u^i(t_k)] \quad (5.41a)$$

$$\begin{aligned} T_{ao}(t_k) &= \frac{\beta_{1,0}}{s + \alpha_1} v(t_k - \tau_u) + \frac{\eta_{2,1}}{s + \alpha_1} v(t_k - \tau_u) T_{ao}(t_k) \\ &+ \frac{\beta_{3,0}}{s + \alpha_1} T_{ai}(t_k - \tau_{ai}) + e(t_k) \end{aligned} \quad (5.41b)$$

Comparing the structure of the simplified model (5.41) with the original nonlinear model (5.40), the last transfer function term of the originally proposed model (5.40) has been discarded together with the parameter $\beta_{3,0}$. Subsequently, the simplified model obtained is a two-input single-output Hammerstein-bilinear type model.

In order to assess the importance of the individual transfer functions in the original model (5.40) and in the newly proposed simplified model (5.41); it is noted that these nonlinear models can be decomposed and simulated separately, respectively, as follows

$$\hat{x}_1(t_k) = \frac{\beta_{1,0}}{s + \alpha_1} v(t_k - \tau_u) \quad (5.42a)$$

$$\hat{x}_2(t_k) = \frac{\eta_{2,1}}{s + \alpha_1} v(t_k - \tau_u) \hat{x}(t_k) \quad (5.42b)$$

$$\hat{x}_3(t_k) = \frac{\beta_{3,0}s + \beta_{3,1}}{s + \alpha_1} T_{ai}(t_k - \tau_{ai}) \quad (5.42c)$$

$$\hat{x}_4(t_k) = \frac{\eta_{4,1}}{s + \alpha_1} v(t_k - \tau_u) T_{ai}(t_k - \tau_{ai}) \quad (5.42d)$$

$$\hat{x}(t_k) = \hat{x}_1(t_k) + \hat{x}_2(t_k) + \hat{x}_3(t_k) + \hat{x}_4(t_k) \quad (5.42e)$$

and

$$\hat{x}_1(t_k) = \frac{\beta_{1,0}}{s + \alpha_1} v(t_k - \tau_u) \quad (5.43a)$$

$$\hat{x}_2(t_k) = \frac{\eta_{2,1}}{s + \alpha_1} v(t_k - \tau_u) \hat{x}(t_k) \quad (5.43b)$$

$$\hat{x}_3(t_k) = \frac{\beta_{3,0}}{s + \alpha_1} T_{ai}(t_k - \tau_{ai}) \quad (5.43c)$$

$$\hat{x}(t_k) = \hat{x}_1(t_k) + \hat{x}_2(t_k) + \hat{x}_3(t_k) \quad (5.43d)$$

where $\hat{x}(t_k)$ denotes the simulated system output $T_{ao}(t_k)$ and $\hat{x}_{1,\dots,4}$ are simulated

outputs of the individual transfer function terms. The average power of the individual simulated outputs is evaluated by the *RMS* measure defined as

$$RMS(\hat{x}_i(t_k)) = \sqrt{\frac{1}{N} \sum_{k=1}^N \hat{x}_i^2(t_k)} \quad (5.44)$$

for $i = 1, \dots, 4$. The results obtained are tabulated in Table 5.3. It is observed, that the *RMS* measure of the signal $\hat{x}_4(t_k)$ is at least one hundred times smaller than the second smallest *RMS* value of the original model. This is caused by the inflow air temperature varying only in a limited range of $T_{ai} \in (20.0044, 31.6228)$ [$^{\circ}C$]. Although, the last nonlinear term of the original model (5.41) has a clear physical interpretation its contribution to the predicted outflow air temperature is, within the considered range of operation, negligible. The *IAE* and R_T^2 model fit measures are also provided in Table 5.3 for estimation and validation data sets. It can be seen, that in terms of these measures the simplified model performs virtually the same as the original model. Therefore, for the subsequent control analysis and design the proposed simplified model (5.41) will be used.

Table 5.3: The *RMS* measure computed for the original and simplified model. The associated *IAE* and R_T^2 model fit measures are evaluated for the estimation and validation data sets, respectively.

	RMS				Estimation		Validation	
	\hat{x}_1	\hat{x}_2	\hat{x}_3	\hat{x}_4	<i>IAE</i>	R_T^2	<i>IAE</i>	R_T^2
Original	17.82	8.105	2.282	0.002	0.2901	99.256	0.3751	99.094
Simplified	17.99	8.271	2.297	-	0.2892	99.258	0.3760	99.067

The estimated parameters of the simplified model are given in Table 5.1, where the applied HSRIVC algorithm had the equivalent settings as for the original model. The delays τ_u and τ_{ai} on inputs $u(t_k)$ and $T_{ai}(t_k)$, respectively, are estimated by minimising the *IAE* criterion (5.1). The minimum value of *IAE* is achieved when $\tau_u = 58$ [s] and $\tau_{ai} = 84$ [s], see the right side of Figure 5.11. Additionally, the value of the achieved cost V , defined in (3.60), is also computed and is shown in Figure 5.11. The simulation results are provided in Figures 5.12 and 5.13 for the estimation and validation data sets, respectively. The simulated system output is not distinguishable in the plot from the simulated output of the original model. Therefore, only the simulation error (grey solid line) is shown in the middle subplot of these figures.

5.5.4 Adjustment of estimated parameters for a new operating point

The dynamic bilinear submodel of the estimated Hammerstein-bilinear model (5.41) representing the AHU has operating point dependent dynamics. Consequently, the estimated model parameters are also operating point dependent. In order to show this dependency, consider the following definition of the measured signals

$$T_{ao,b}(t_k) = T_{ao}(t_k) + \bar{T}_{ao} \quad (5.45a)$$

$$T_{ai,b}(t_k) = T_{ai}(t_k) + \bar{T}_{ai} \quad (5.45b)$$

$$u_b(t_k) = u(t_k) + \bar{u} \quad (5.45c)$$

where the subscript b denotes that the measured signals have baselines, while the signals without the subscript b denote the baseline compensated signals, i.e. these signals start at the zero value. Additionally, because of the static relationship between the intermediate input $v(t_k)$ and the measured input $u(t_k)$, the following holds

$$v_b(t_k) = \phi(u_b(t_k)) = v(t_k) + \bar{v} \quad (5.46)$$

Without loss of generality, time delays τ_u and τ_{ai} are omitted together with the noise term $e(t_k)$ and only the bilinear submodel (5.41b) of the Hammerstein-bilinear model (5.41) is considered in the following discussion. Re-expressing the bilinear submodel using the original, measured, input-output signals (5.45) leads to

$$T_{ao,b}(t_k) = \frac{\beta_{1,0}}{s + \alpha_1} v_b(t_k) + \frac{\eta_{2,1}}{s + \alpha_1} v_b(t_k) T_{ao,b}(t_k) + \frac{\beta_{3,0}}{s + \alpha_1} T_{ai,b}(t_k) + o \quad (5.47)$$

where o [$^{\circ}C$] denotes a static offset term, which can be viewed as an additional constant external input to the system. Subsequently, substituting for the measured signals from (5.45) leads to

$$\begin{aligned} T_{ao}(t_k) + \bar{T}_{ao} &= \frac{\beta_{1,0}}{s + \alpha_1} v(t_k) + \frac{\eta_{2,1}}{s + \alpha_1} v(t_k) T_{ao}(t_k) + \frac{\beta_{3,0}}{s + \alpha_1} T_{ai}(t_k) \\ &+ \frac{\beta_{1,0}}{s + \alpha_1} \bar{v} + \frac{\eta_{2,1}}{s + \alpha_1} \bar{v} \bar{T}_{ao} + \frac{\beta_{3,0}}{s + \alpha_1} \bar{T}_{ai} + o \\ &+ \frac{\eta_{2,1}}{s + \alpha_1} v(t_k) \bar{T}_{ao} + \frac{\eta_{2,1}}{s + \alpha_1} \bar{v} T_{ao}(t_k) \end{aligned} \quad (5.48)$$

It is noted from (5.48), that the base \bar{T}_{ao} must be equal to

$$\bar{T}_{ao} = \frac{\beta_{1,0}}{s + \alpha_1} \bar{v} + \frac{\eta_{2,1}}{s + \alpha_1} \bar{v} \bar{T}_{ao} + \frac{\beta_{3,0}}{s + \alpha_1} \bar{T}_{ai} + o \quad (5.49)$$

and after any transient response and effects due to initial conditions decays, the operator $s \rightarrow 0$, so that (5.49) becomes

$$\bar{T}_{ao} = \frac{\beta_{1,0}}{\alpha_1} \bar{v} + \frac{\eta_{2,1}}{\alpha_1} \bar{v} \bar{T}_{ao} + \frac{\beta_{3,0}}{\alpha_1} \bar{T}_{ai} + o \quad (5.50)$$

Since the equality (5.49) holds, all the static terms in (5.48) are effectively cancelled and only the dynamic part of the model (5.48) is considered, hence

$$\begin{aligned} T_{ao}(t_k) &= \frac{\beta_{1,0}}{s + \alpha_1} v(t_k) + \frac{\eta_{2,1}}{s + \alpha_1} v(t_k) T_{ao}(t_k) + \frac{\beta_{3,0}}{s + \alpha_1} T_{ai}(t_k) \\ &\quad + \frac{\eta_{2,1}}{s + \alpha_1} v(t_k) \bar{T}_{ao} + \frac{\eta_{2,1}}{s + \alpha_1} \bar{v} T_{ao}(t_k) \end{aligned} \quad (5.51)$$

Subsequently, the last two transfer functions of (5.51) can be combined with the whole model as follows

$$\begin{aligned} \left[1 - \frac{\eta_{2,1} \bar{v}}{s + \alpha_1} \right] T_{ao}(t_k) &= \frac{[\beta_{1,0} + \eta_{2,1} \bar{T}_{ao}]}{s + \alpha_1} v(t_k) + \frac{\eta_{2,1}}{s + \alpha_1} v(t_k) T_{ao}(t_k) + \frac{\beta_{3,0}}{s + \alpha_1} T_{ai}(t_k) \\ \frac{s + [\alpha_1 - \eta_{2,1} \bar{v}]}{s + \alpha_1} T_{ao}(t_k) &= \frac{[\beta_{1,0} + \eta_{2,1} \bar{T}_{ao}]}{s + \alpha_1} v(t_k) + \frac{\eta_{2,1}}{s + \alpha_1} v(t_k) T_{ao}(t_k) + \frac{\beta_{3,0}}{s + \alpha_1} T_{ai}(t_k) \\ T_{ao}(t_k) &= \frac{\tilde{\beta}_{1,0}}{s + \tilde{\alpha}_1} v(t_k) + \frac{\eta_{2,1}}{s + \tilde{\alpha}_1} v(t_k) T_{ao}(t_k) \\ &\quad + \frac{\beta_{3,0}}{s + \tilde{\alpha}_1} T_{ai}(t_k) \end{aligned} \quad (5.52)$$

where the operating point dependent parameters $\tilde{\beta}_{1,0}$ and $\tilde{\alpha}_1$ are defined as

$$\tilde{\beta}_{1,0} = \beta_{1,0} + \eta_{2,1} \bar{T}_{ao} \quad (5.53a)$$

$$\tilde{\alpha}_1 = \alpha_1 - \eta_{2,1} \bar{v} \quad (5.53b)$$

During the parameter estimation stage, the baselines are subtracted from the measured input-output signals, so that the offset is effectively eliminated and the parameters of the bilinear submodel (5.52) are estimated. It is then observed, that by estimating the bilinear submodel using the baseline compensated input-output signals, i.e. estimating at zero operating point, the parameters $\tilde{\beta}_{1,0}$ and $\tilde{\alpha}_1$ are in fact estimated instead of the desired $\beta_{1,0}$ and α_1 , respectively. Subsequently, if it is required to simulate or to use the bilinear submodel at the original point

of operation the estimated parameters must be adjusted for this, cf. (5.53), according to

$$\begin{aligned}
 \beta_{1,0} &= \tilde{\beta}_{1,0} - \eta_{2,1} \bar{T}_{ao} \\
 &= -10.762 \times 10^{-2} + 4.3944 \times 10^{-3} \times 25.1438 \\
 &= 2.8716 \times 10^{-3}
 \end{aligned} \tag{5.54a}$$

$$\begin{aligned}
 \alpha_1 &= \tilde{\alpha}_1 + \eta_{2,1} \bar{v} \\
 &= 3.2914 \times 10^{-3} - 4.3944 \times 10^{-3} \times 0 \\
 &= 3.2914 \times 10^{-3}
 \end{aligned} \tag{5.54b}$$

Using the operating point adjusted parameters $\beta_{1,0}$ and α_1 , given in (5.54), the outflow air temperature can be simulated at its original point of operation, using the measured input signals $v_b(t_k)$ and $T_{ai,b}(t_k)$, according to

$$\hat{x}(t_k) = \frac{\beta_{1,0}}{s + \alpha_1} v_b(t_k) + \frac{\eta_{2,1}}{s + \alpha_1} v_b(t_k) \hat{x}(t_k) + \frac{\beta_{3,0}}{s + \alpha_1} T_{ai,b}(t_k) + o \tag{5.55}$$

where $\hat{x}(t_k)$ [$^{\circ}C$] denotes the simulated output corresponding to $T_{ao,b}(t_k)$. Considering the static relation (5.50) the offset term o is defined as

$$o = \bar{T}_{ao} - \frac{\beta_{1,0}}{\alpha_1} \bar{v} - \frac{\eta_{2,1}}{\alpha_1} \bar{v} \bar{T}_{ao} - \frac{\beta_{3,0}}{\alpha_1} \bar{T}_{ai} \tag{5.56}$$

Noting, that for the current application $\bar{u} = 0$ the following holds, $\bar{v} = 0$, so that the offset term can be computed as follows

$$\begin{aligned}
 o &= \bar{T}_{ao} - \frac{\beta_{3,0}}{\alpha_1} \bar{T}_{ai} \\
 &= 25.1438 - \frac{2.1253 \times 10^{-3}}{3.2914 \times 10^{-3}} 23.5054 \\
 &= 9.9662 \text{ [}^{\circ}C\text{]}
 \end{aligned} \tag{5.57}$$

Finally, the adjustment of the bilinear model parameters can be interpreted as follows: By adjusting the bilinear model parameters, as proposed in (5.54), it is possible to obtain the same dynamic bilinear behaviour at any desired point of operation. In other words, the operating point dependent dynamic behaviour of the bilinear model can be reproduced at any desired point of operation. This then holds for any bilinear model considered in this thesis and is a result which is also directly applicable to bilinear models of higher order.

Inferring available information from data-based model

It is noted, that the third transfer function of the first principles model of the AHU (5.38), repeated below

$$\frac{\beta_{3,0}s + \beta_{3,1}}{s + \alpha_1} T_{ai}(t) \quad (5.58)$$

has a unity steady-state gain due to the conservation of energy within the system, i.e.

$$SSG_3 = \frac{\beta_{3,1}}{\alpha_1} = 1 \quad (5.59)$$

In other words, in the case where the cooling valve is fully closed and no heat loss occurs, the outflow air temperature must be equal to the inflow air temperature. However, the estimated steady-state gain of the third transfer function of the simplified model (5.43c) is not unity, but rather

$$\begin{aligned} SSG_3 &= \frac{\hat{\beta}_{3,0}}{\hat{\alpha}_1} \\ &= \frac{2.1253 \times 10^{-3}}{3.2914 \times 10^{-3}} \\ &= 0.6457 \end{aligned} \quad (5.60)$$

where the hat above the parameters denotes that these parameters are estimated. Since, the estimated SSG_3 is less than unity, then a heat gain (or heat loss) is present within the system. The heat gain is in fact manifested by the presence of the offset term o , which has been calculated in (5.57) to be 9.9662 [°C].

Following the same reasoning as for the manufacturing zone temperature sub-model, stated in Subsection 5.4.2, there must exist an effective ambient temperature, denoted T_a [°C], such that, cf. (5.23),

$$o = SSG_4 T_a \quad (5.61)$$

Additionally, due to the conservation of the energy within the system the following must hold, cf. (5.20c), i.e.

$$SSG_3 + SSG_4 = 1 \quad (5.62)$$

Knowing the value of constant offset term from (5.57) and considering the definition of the offset term given in (5.61), the effective ambient temperature is

computed as follows

$$\begin{aligned}
 T_a &= \frac{o}{SSG_4} \\
 &= \frac{\bar{T}_{ao} - SSG_3 \bar{T}_{ai}}{1 - SSG_3} \\
 &= \frac{25.1438 - 0.6457 \times 23.5054}{1 - 0.6457} \\
 &= 28.1296 \text{ [}^\circ\text{C]} \tag{5.63}
 \end{aligned}$$

The estimated ambient temperature of $T_a = 28.1296 \text{ [}^\circ\text{C]}$ is approximately equal to the measured temperature of $30.1 \text{ [}^\circ\text{C]}$ provided in the special observation stated in the Subsection 5.2.2. Therefore, using the estimated model it is possible to calculate the effective ambient temperature, which then indicates a presence of a large heat gain (caused by the electric motor of the main fan).

5.6 Manufacturing zone humidity model

A continuous-time model predicting the humidity levels within the manufacturing zone is identified in a black-box manner. Based on the technical insight gained into the investigated HVAC system, and based on the on-site experiments, the Hammerstein-bilinear model structure is selected as a candidate model. The black-box modelling approach is chosen due to the complex nonlinear nature of the modelled system caused by the combined heat and mass transfer processes and general lack of control oriented first principles (and black-box) models in the literature.

The desiccant rotor of the dehumidification unit is the main active component involved in the dehumidification of the conditioned air. The existing models of the desiccant rotors are reviewed in (Ge et al. 2008), where such models are intended for the design, performance evaluation and manufacturing purposes only. There are two main groups of available models. The first group includes data-based static models, see (Beccali et al. 2003, Jeong & Mumma 2005). The second group of models uses physical laws to model the main static and dynamic characteristics of the desiccant rotors, see (Zheng & Worek 1993, Dai, Wang & Zhang 2001, Zhang, Dai & Wang 2003, Nia, Paassen & Saidi 2006). One of the key parameters determining the efficacy of the DU is the rotational speed of the desiccant rotor. In order to find the optimal value of the rotational speed, the models based on physical laws are commonly used. These models are governed by a set of coupled

nonlinear partial differential equations, which are evaluated for every air flute of the desiccant rotor and continuously solved for new boundary conditions as the rotor moves. Commonly, only the steady-state solution is sought. It should be pointed out, that none of the reviewed models is suitable for the purpose of control tuning and design. The static models do not explain the system dynamics, while the first principles based models are not practical due their complexity and computational demands. Therefore, the relatively simple yet reasonably accurate Hammerstein-bilinear model structure is proposed instead.

The considered system input is the gas valve position $u_g(t_k)$. Unless stated otherwise, the subscript g is omitted and the gas valve position is denoted $u(t_k)$ in this section only. The system output is the detrended return air dew-point temperature T_{dr} , which is defined as the measured return air dew-point temperature minus the estimated trend (load), i.e. $T_{dr} = T_{drm} - T_{dt}$. A gas flow meter has been additionally installed in order to be able to monitor the gas consumption of the HVAC system under investigation. This has allowed the gas valve static characteristic to be measured prior to system identification. The measured gas valve characteristic is subsequently used as a starting point during the system identification exercise. The final estimated static characteristic, being part of the Hammerstein-bilinear model, then includes the combined effects of the static characteristics of all components such as the desiccant rotor and the gas valve.

5.6.1 Trend model

A unique data set has been acquired 7th January 2012. During this day the outdoor humidity had dropped, causing a step-like decrease of the measured dew-point temperature of the fresh air supply (step input), see lower plot of Figure 5.15. Subsequently, this has allowed the linear dynamic model of the resulting trend, measured within the manufacturing zone, to be identified. The gas valve position was at low fire $u_g(t_k) = 24$ [%] and the cooling valve was closed $u_c(t_k) = 0$ [%]. Due to the operation of the DU at low fire a static offset, denoted o [$^{\circ}C$], is introduced into the measurement of the return air dew-point temperature. However, all of the dynamic changes are caused by the fresh air supply only. Therefore, the linear model representing the dynamic influence of the fresh air supply on the measurement of the return air dew-point temperature can be obtained. The measured return air dew-point temperature is then defined as follows

$$T_{drm} = T_{dt} + o \tag{5.64}$$

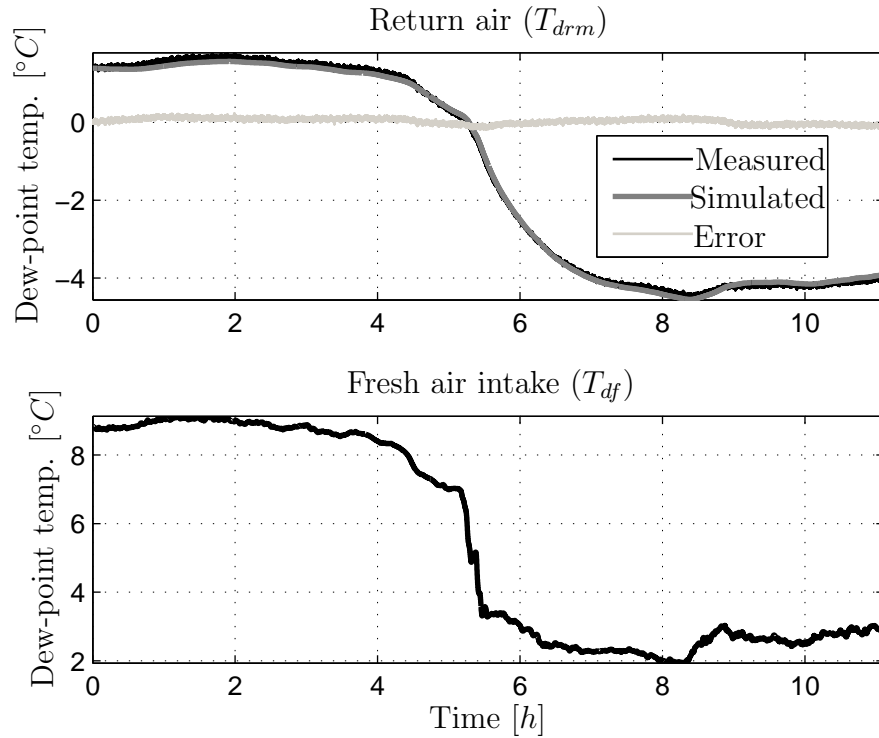


Figure 5.15: The upper plot shows measured (black solid line) and simulated (grey solid line) return air dew-point temperature together with the corresponding simulation error (light grey solid line). The lower plot shows measured fresh air intake dew-point temperature. The sampling time interval is $h = 1$ [s]

The considered system input is the measured fresh air dew-point temperature T_{df} and the system output is the measured return air dew-point temperature T_{drm} . The noisy measured input T_{df} has been prefiltered by a zero-phase second order Butterworth filter designed with a cut-off frequency of 5^{-2} [Hz], which has been selected mainly based on visual inspection. The sampling interval for the continuous-time trend model estimation is selected to be $h = 1$ [s]. Prior to the parameter estimation stage the baselines are subtracted from the measured input and output signals, hence the static offset o is effectively eliminated so that $T_{drm} = T_{dt}$. The baselines are selected to be the mean values of the first ten samples, i.e. $\bar{T}_{df} = (1/10) \sum_{k=1}^{10} T_{df}(t_k) = 8.8331$ [$^{\circ}\text{C}$] and $\bar{T}_{drm} = (1/10) \sum_{k=1}^{10} T_{drm}(t_k) = 1.3929$ [$^{\circ}\text{C}$]. Note that due to the operation of the DU $\bar{T}_{drm} < \bar{T}_{df}$.

In order to determine the model order and presence of any effective time delay the function `rivcid` in the Captain Toolbox for Matlab, (Taylor, Pedregal, Young & Tych 2007), has been applied. This function uses the SRIVC method to estimate the preselected set of CT linear TF models having different model orders

and delays. The selected model is a first order linear model with a corresponding $YIC = -21.2835$, defined in (5.6), which indicates good model fit and parsimonious parameterization. The estimated effective time delay is null. For this selected model order, the SRIVC algorithm, as described in 3.1, has been applied with the following settings: The convergence criterion monitoring the maximum relative change of the parameter estimates, defined in (3.25), is selected to be $\epsilon = 1 \times 10^{-10}$. The prefilter of the SRIVC algorithm is initialised with the single breakpoint frequency parameter equal to $\lambda = 0.001$. The final estimated model takes the form

$$T_{dt}(t_k) = \frac{\beta_0}{s + \alpha_1} T_{df}(t_k) \quad (5.65)$$

where the estimated model parameters are

$$\begin{aligned} \alpha_1 &= 5.2401 \times 10^{-4} (4.4867 \times 10^{-7}) \\ \beta_0 &= 4.6395 \times 10^{-4} (3.7314 \times 10^{-7}) \end{aligned}$$

with the corresponding standard errors provided in the parentheses. The estimated standard errors are relatively small, compared to the value of estimated parameters, indicating good accuracy of the obtained parameter estimates.

The simulation results are presented in Figure 5.15. The upper plot of Figure 5.15 shows the measured (black solid line) and simulated (grey solid line) return air dew-point temperature according to (5.64) together with the corresponding simulation error (light grey solid line). The lower plot shows the measured fresh air supply dew-point temperature. The computed model fit criteria are $R_T^2 = 99.9172$ [%] and $IAE = 0.0724$ [$^{\circ}C$], which indicate a good model fit. The offset term used for the system simulation is computed as

$$\begin{aligned} o &= \bar{T}_{drm} - \frac{\beta_0}{\alpha_1} \bar{T}_{df} \\ &= 8.8331 - \frac{4.6395 \times 10^{-4}}{5.2401 \times 10^{-4}} 1.3929 \\ &= -6.4277 [^{\circ}C] \end{aligned} \quad (5.66)$$

where the negative value of the offset term indicates that part of the moisture within the conditioned air is removed by the DU. The computed steady-state gain is $SSG = 0.8854$, while the system time constant is $T = 31.8058$ [min]. It is expected that the computed steady-state gain is lower than unity, i.e. $SSG < 1$, because of the mass conservation within the system. The estimated time constant indicates slow system dynamics.

5.6.2 Gas valve characteristic

The gas valve characteristic has been measured at seven distinct gas valve fractional positions on 11th August 2010. In order to obtain a single measurement on the characteristic curve the gas valve has been fixed at a constant position for a time interval of 40 [min]. During this time interval the gas consumption has been measured by the installed gas flow meter. Subsequently, the gas volumetric flow, denoted V_g [m^3/h], has been computed as an average value of measured consumed gas per time period of 40 [min]. The results are provided in the first and second columns of Table 5.4. The intermediate input $v(t_k)$, corresponding to the gas valve position $u(t_k)$, is then computed as a normalised value of the measured gas flow, i.e. $v(t_k) = V_g / \max(V_g)$. The values of $v(t_k)$ are provided in the last column of Table 5.4.

Table 5.4: Measured gas volumetric flow for different gas valve positions. Having the gas calorific value, the heating power is also provided.

$u(t_k)$	$V_g(t_k)$ [m^3/h]	$P(t_k)$ [kW]	$v(t_k)$
1	3.2791	35.5238	1
0.8	3.2652	35.3726	0.9957
0.6	3.1892	34.5496	0.9726
0.45	2.7201	29.4672	0.8295
0.35	1.7661	19.1330	0.5386
0.27	0.8211	8.8956	0.2504
0	0	0	0

The individual measured points are depicted in Figure 5.16 by black circles. The measured gas valve characteristic takes the form of an S-shaped power curve. So far, the introduced parameter estimation methods, such as the HSRIVC and HBSRIVC methods, were based on the assumption that a polynomial function is able to model the given static function. The disadvantage of using polynomial functions is the fact that such functions do not level off, saturate, to a constant value, however the given static characteristic does level off. In fact, for the gas valve opening of approximately $u(t_k) = 80$ [%] the maximal gas volumetric flow is achieved. Therefore, in a similar manner to (Taylor, Shaban, Stables & Ako 2007), the following logistic based growth function, cf. (2.58), is assumed

$$v(t_k) = \frac{v_{max}}{1 + p_1 \exp(-p_2 u(t_k))} \quad (5.67)$$

where v_{max} denotes the limiting value (carrying capacity) parameter, while p_1 and p_2 are constant coefficients which are yet to be estimated. The limiting value

parameter is set to unity, i.e. $v_{max} = 1$. This then automatically normalises the steady-state gain of the static function to unity, cf. discussion on the constrained HBSRIVC method provided in Subsection 3.4.2.

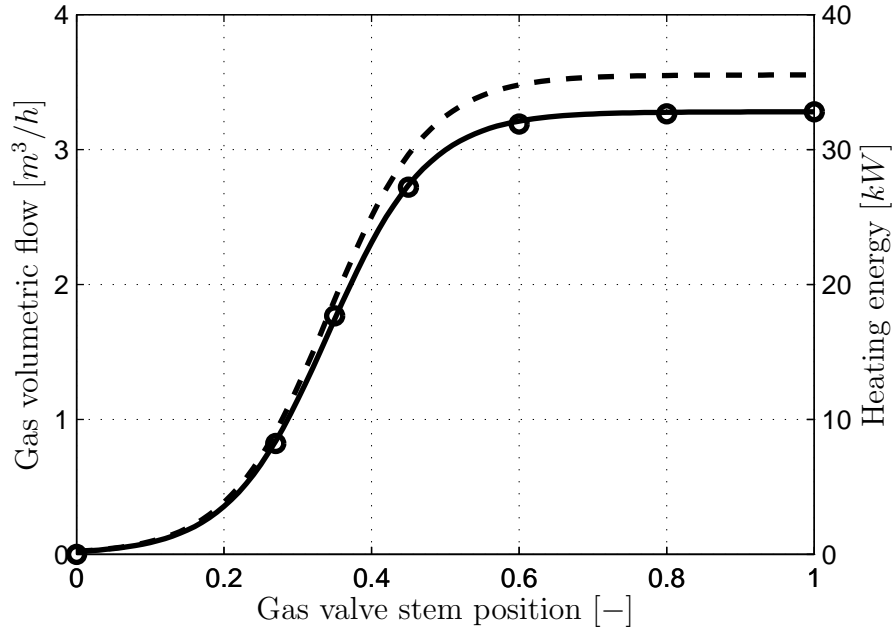


Figure 5.16: Estimated gas valve characteristic (black solid line) and heating power (black dashed line). The measured data points are depicted by circles.

The parameter vector, denoted $\boldsymbol{\theta}_n$, consisting of parameters p_1 and p_2 is defined as

$$\boldsymbol{\theta}_n = \begin{bmatrix} p_1 & p_2 \end{bmatrix}^T \quad (5.68)$$

In order to find the unknown parameter vector $\boldsymbol{\theta}_n$ the scalar cost function, denoted V , is formulated as follows

$$V(\boldsymbol{\theta}_n) = \frac{1}{N} \sum_{k=1}^N \varepsilon(t_k)^2 = \frac{1}{N} \sum_{k=1}^N [v(t_k) - \hat{x}(\boldsymbol{\theta}_n, t_k)]^2 \quad (5.69)$$

where N denotes the total number of samples and $\hat{x}(\boldsymbol{\theta}_n, t_k)$ is the modelled (simulated) static characteristic using the estimated parameter values. The cost function (5.69) is defined as the average sum of squared differences between the measured and the modelled static characteristic. The estimation problem then consists of minimising the cost function (5.69) with respect to the unknown pa-

parameter vector θ_n , i.e.

$$\hat{\theta}_n = \arg \min_{\theta_n} V(\theta_n) \quad (5.70)$$

where the estimated parameter vector is denoted by the hat notation.

Since the static characteristic is parameterized by a function (5.67), which is nonlinear with respect to its parameters, a closed form solution cannot be formulated and a numerical optimisation routine must be employed. The available standard optimisation routine `fminsearch` of Matlab (software version 2010b), which uses the Nelder-Mead simplex method, is applied to solve for the optimisation problem (5.70). The optimisation routine has been initialised with $\theta_n = [1 \ 1]^T$, subsequently the estimated parameter vector is found to be

$$\hat{\theta}_n = \left[\begin{array}{cc} 162.2751 & 14.8972 \end{array} \right]^T \quad (5.71)$$

Note that the standard errors of the parameter estimates are not provided by the Matlab optimisation routine.

Having the estimated parameter values (5.71), the modelled static characteristic is shown in Figure 5.16 as a black solid line. Note, that the gain of the modelled static characteristic has been normalised to unity, i.e. $v_{max} = 1$, so that in order to plot the gas valve characteristic in its original scale the computed value $\hat{v}(\hat{\theta}_n, t_k)$ has been multiplied by the maximal measured gas volumetric flow, denoted $V_{g,max}$ [m^3/h], which is 3.2791 [m^3/h]. Additionally, for the purpose of potential energy consumption analysis the heating power can be computed according to

$$P(t_k) = CV \frac{1000}{3600} V_{g,max} v(t_k) \quad (5.72)$$

Here, $P(t_k)$ [kW] denotes the heating power, CV [MJ/m^3] is the gas calorific value and 1000/3600 is a constant (conversion of units). The gas calorific value was $CV = 39$ [MJ/m^3] on 11th August 2010. The computed heat power characteristic is shown in Figure 5.16 as the black dashed line.

5.6.3 Final system identification

The proposed model structure for the zone humidity model is of the Hammerstein-bilinear form. The input static nonlinearity is parameterized by the logistic growth function used to model the gas valve static characteristic (5.67). Although, the overall input static nonlinearity includes the combined effects of all the nonlinear components and processes within the system, it is assumed that the saturation type gas valve characteristic dominates the shape of the input

nonlinearity. The overall zone humidity model then takes the following form

$$v(t_k) = \frac{1}{1 + p_1 \exp(-p_2 u(t_k))} \quad (5.73a)$$

$$T_{dr}(t_k) = \frac{\beta_0}{s + \alpha_1} v(t_k - \tau_u) + \frac{\eta_1}{s + \alpha_1} v(t_k - \tau_u) T_{dr}(t_k) + e(t_k) \quad (5.73b)$$

$$T_{drm}(t_k) = T_{dr}(t_k) + T_{dt}(t_k) \quad (5.73c)$$

Having measured the dew-point temperature of the fresh supply air the trend T_{dt} is simulated using the identified trend model (5.65). Subsequently, using (5.73c) the dew-point temperature of the return air, being the system output in (5.73b), is computed as

$$T_{dr}(t_k) = T_{drm}(t_k) - T_{dt}(t_k) \quad (5.74)$$

The parameter vectors corresponding to the static and dynamic submodel of the overall Hammerstein-bilinear model (5.73), respectively, are defined as

$$\boldsymbol{\theta}_n = \begin{bmatrix} p_1 & p_2 \end{bmatrix}^T \quad (5.75a)$$

$$\boldsymbol{\theta}_{lb} = \begin{bmatrix} \alpha_1 & \beta_0 & \eta_1 \end{bmatrix}^T \quad (5.75b)$$

The parameter estimation task is then formulated as the following optimisation problem

$$\hat{\boldsymbol{\theta}}_n = \arg \min_{\boldsymbol{\theta}_n} V(\boldsymbol{\theta}_n, \hat{\boldsymbol{\theta}}_{lb}) \quad (5.76)$$

The estimate is denoted using the hat notation and the minimised cost function $V(\boldsymbol{\theta}_n)$ is defined as

$$V(\boldsymbol{\theta}_n, \hat{\boldsymbol{\theta}}_{lb}) = \frac{1}{N} \sum_{k=1}^N \varepsilon(t_k)^2 = \frac{1}{N} \sum_{k=1}^N \left[T_{dr}(t_k) - \hat{x}(\boldsymbol{\theta}_n, \hat{\boldsymbol{\theta}}_{lb}, t_k) \right]^2 \quad (5.77)$$

where $\hat{x}(\boldsymbol{\theta}_n, \hat{\boldsymbol{\theta}}_{lb}, t_k)$ denotes the simulated system output $T_{dr}(t_k)$ based on the sought parameter vector $\boldsymbol{\theta}_n$ and estimated $\hat{\boldsymbol{\theta}}_{lb}$.

In a similar manner to the optimisation task stated in Subsection 5.6.2 regarding the gas valve static characteristic estimation problem, the static input function (5.73a) is nonlinear with respect to its parameters. Therefore, the available standard optimisation routine `fminsearch` of Matlab (software version 2010b) is applied to solve the optimisation problem (5.76). This optimisation routine is of an iterative nature searching for the parameter vector $\boldsymbol{\theta}_n$, where in each iteration the SRIVC parameter estimation method 3.1, configured for bilinear

model parameter estimation, is applied to solve for the parameter vector θ_{lb} . The `fminsearch` optimisation routine is initialised with the found parameters of the gas valve static characteristic stated in (5.71). The SRIVC algorithm has been applied with the following settings: The convergence criterion monitoring the maximum relative change of the parameter estimates, defined in (3.25), is selected to be $\epsilon = 1 \times 10^{-5}$. The prefilter of the SRIVC algorithm is initialised with the single breakpoint frequency parameter, such that $\lambda = 0.001$.

Two separate data sets are used. The first data set, acquired 15th January 2012, is used exclusively for the model parameter estimation. While the second data set, acquired 14th January 2012, is used for the model validation purposes only. The original data were measured with a sampling interval of $h = 1$ [s]. Considering the slow system dynamics the measured data have been subsequently downsampled to $h = 5$ [s] for the purpose of parameter estimation. The baselines are subtracted from the measured input and output signals, where the baselines are computed as the mean values of the first ten signal samples. All the considered baselines are: $\bar{T}_{drm} = (1/10) \sum_{k=1}^{10} T_{drm}(t_k) = -6.4748$ [°C], $\bar{T}_{dr} = (1/10) \sum_{k=1}^{10} T_{dr}(t_k) = -5.3967$ [°C], $\bar{T}_{df} = (1/10) \sum_{k=1}^{10} T_{df}(t_k) = -1.2177$ [°C] and $\bar{u} = (1/10) \sum_{k=1}^{10} u(t_k) = 0.2400$.

The input delay τ_u is estimated by minimising the *IAE* criterion (5.1). The *IAE* criterion has been computed for a predefined range of input delays and the results are shown on the left side of Figure 5.17. The input delay obtained, which minimises the *IAE* criterion, is $\tau_u = 135$ [s]. The value of the cost V achieved, defined in (5.77), is additionally displayed on the right side of Figure 5.17.

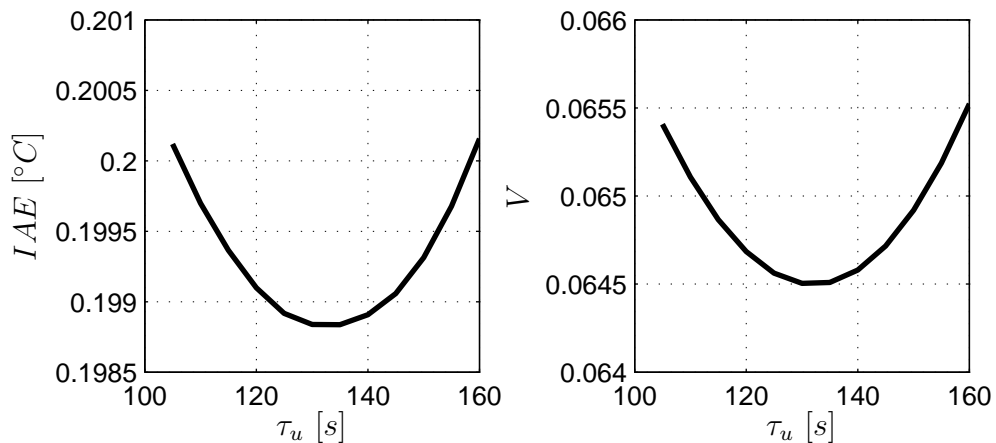


Figure 5.17: Input delay estimation: *IAE* and cost V criterion plotted against delay τ_u on left and right sides, respectively. Sampling time interval is $h = 5$ [s].

The estimated parameters corresponding to the static and dynamic submodel of the Hammerstein-bilinear model (5.73), respectively, are

$$p_1 = 3201.5646 \quad (5.78a)$$

$$p_2 = 20.1539 \quad (5.78b)$$

and

$$\alpha_1 = 6.6758 \times 10^{-4} (1.1141 \times 10^{-6}) \quad (5.79a)$$

$$\beta_0 = -5.0520 \times 10^{-2} (8.3081 \times 10^{-5}) \quad (5.79b)$$

$$\eta_1 = -1.5062 \times 10^{-3} (2.6049 \times 10^{-6}) \quad (5.79c)$$

where the corresponding standard errors are provided in the parentheses. The negative sign of the estimated η_1 parameter indicates a saturation type steady-state characteristic of the dynamic submodel, while the negative sign of the β_0 parameter indicates that the moisture is removed from the conditioned air. Considering the static input function (5.73a) and using the estimated parameters p_1 and p_2 the estimated static input nonlinearity is depicted in Figure 5.18 by a solid black line. For comparison, the gas valve static characteristic, measured and estimated in Subsection 5.6.2, is also shown in Figure 5.18 as a solid grey line. It can be observed, that the static input nonlinearity has a steeper gradient, but saturates approximately at the same valve position.

The simulation results with $R_T^2 = 99.854$ [%] and $IAE = 0.1988$ [$^{\circ}C$] are presented in Figure 5.19 for the estimation data set. The simulation results for the validation data set are presented in Figure 5.20 with the performance criteria $R_T^2 = 99.277$ [%] and $IAE = 0.4242$ [$^{\circ}C$] being achieved. The simulation results obtained show a good model fit despite the relative simplicity of the adopted model. The simulation results presented have been obtained such that the estimated zone humidity model parameters (5.79) have been adjusted for the subtracted baselines of the estimation data set. This procedure is explained in detail subsequently in Subsection 5.6.4.

Figures 5.19 and 5.20 each comprise three subplots. In each figure, the upper plot shows measured (grey solid line) and simulated (black solid line) return air dew-point temperature $T_{dr}(t_k)$. The middle plot shows the simulation error. The lower plot shows the fractional gas valve position (grey solid line) and the simulated trend (black solid line). The measured return air dew-point temperature $T_{drm}(t_k)$ is not shown, however, having the simulated trend, this can be inferred

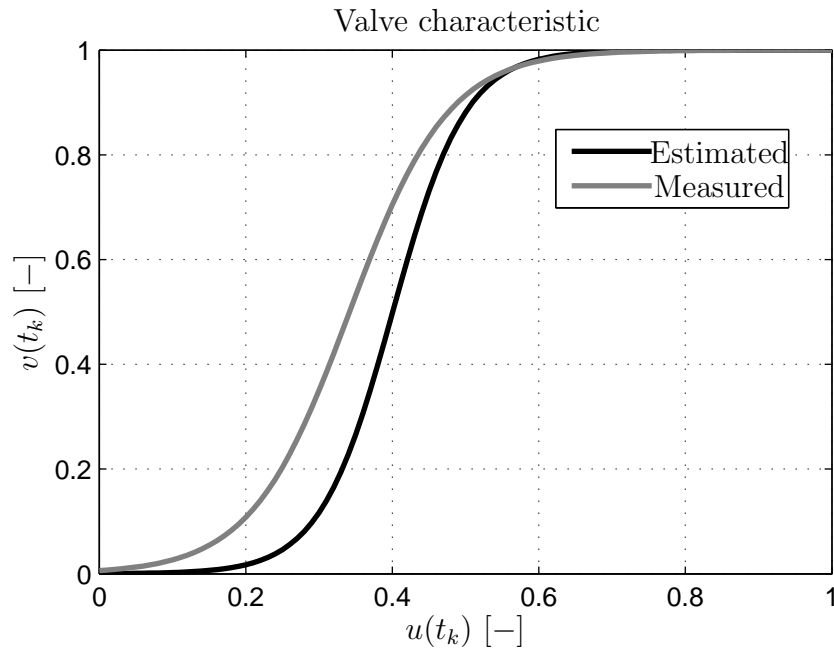


Figure 5.18: Estimated (reconstructed) gas valve characteristic (black solid line). For comparison the valve characteristic based on the measured data is also shown (grey solid line).

using the relation (5.74). Oscillations are observed in the simulation error of both the estimation and validation data sets. Furthermore, the amplitude of the oscillations is observed to be operating point dependent, where for lower air humidity the amplitude increases. This observation is in an agreement with that made in Subsection 5.2.1.

5.6.4 Adjustment of estimated parameters for a new operating point

The adjustment of the estimated parameters for a new operating point has been explained in detail in Subsection 5.5.4. The parameters of the bilinear submodel (5.73b) are known to be operating point dependent. The baselines of the input-output signals were subtracted prior to model parameter estimation, hence the input-output signals start (approximately) at zero values. Therefore, the estimated parameters of the bilinear submodel, provided in (5.79), are valid only at a zero operation point. Subsequently, if the model is required to correspond to the original point of operation, e.g. for simulation purposes, the estimated parameters must be adjusted for this.

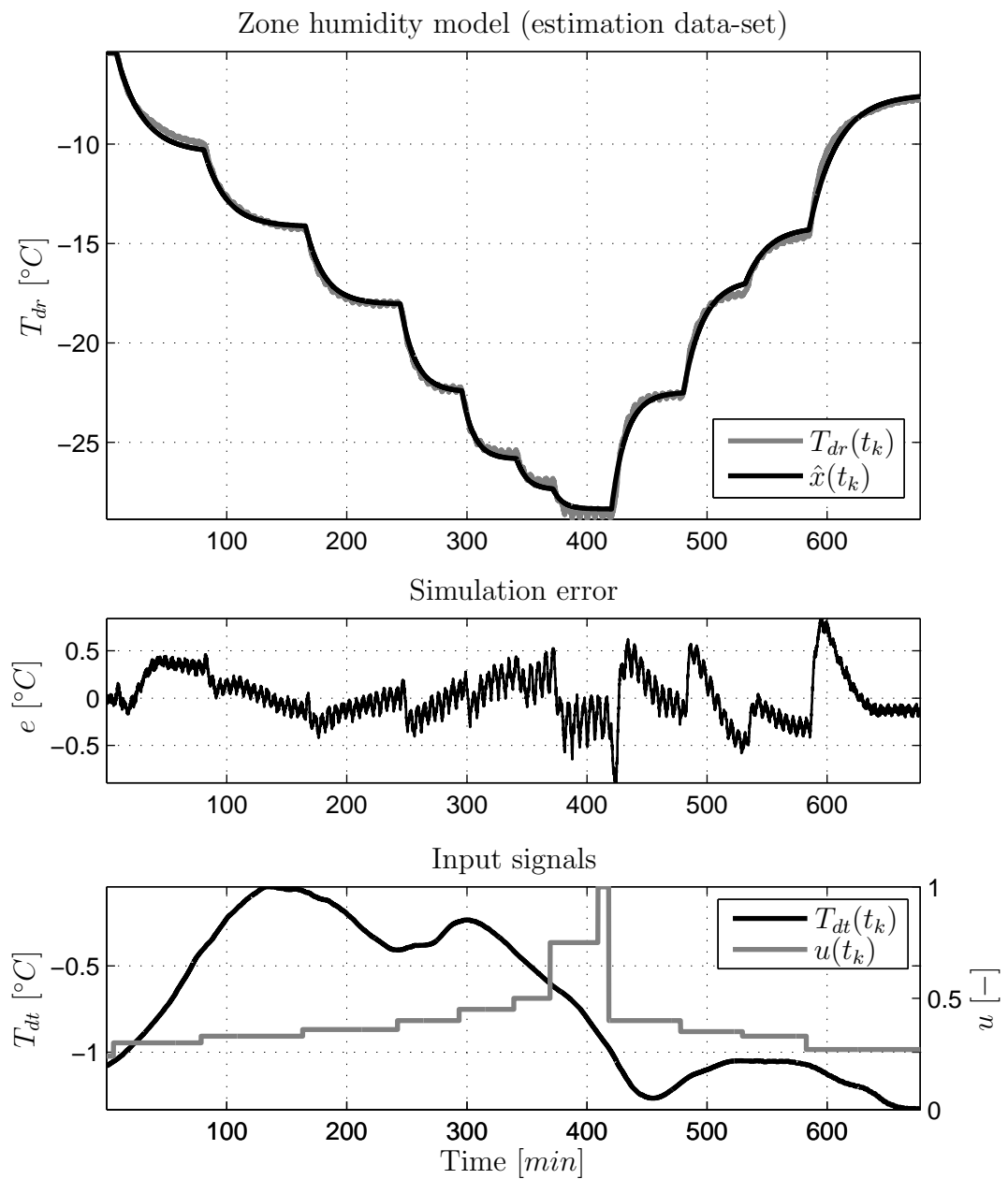


Figure 5.19: The upper plot shows measured (grey solid line) and simulated (black solid line) return air dew-point temperature. The middle plot shows the simulation error. The lower plot shows the fractional gas valve position (grey solid line) and the estimated trend (black solid line). The estimation data-set is used with a sampling time interval $h = 5$ [s].

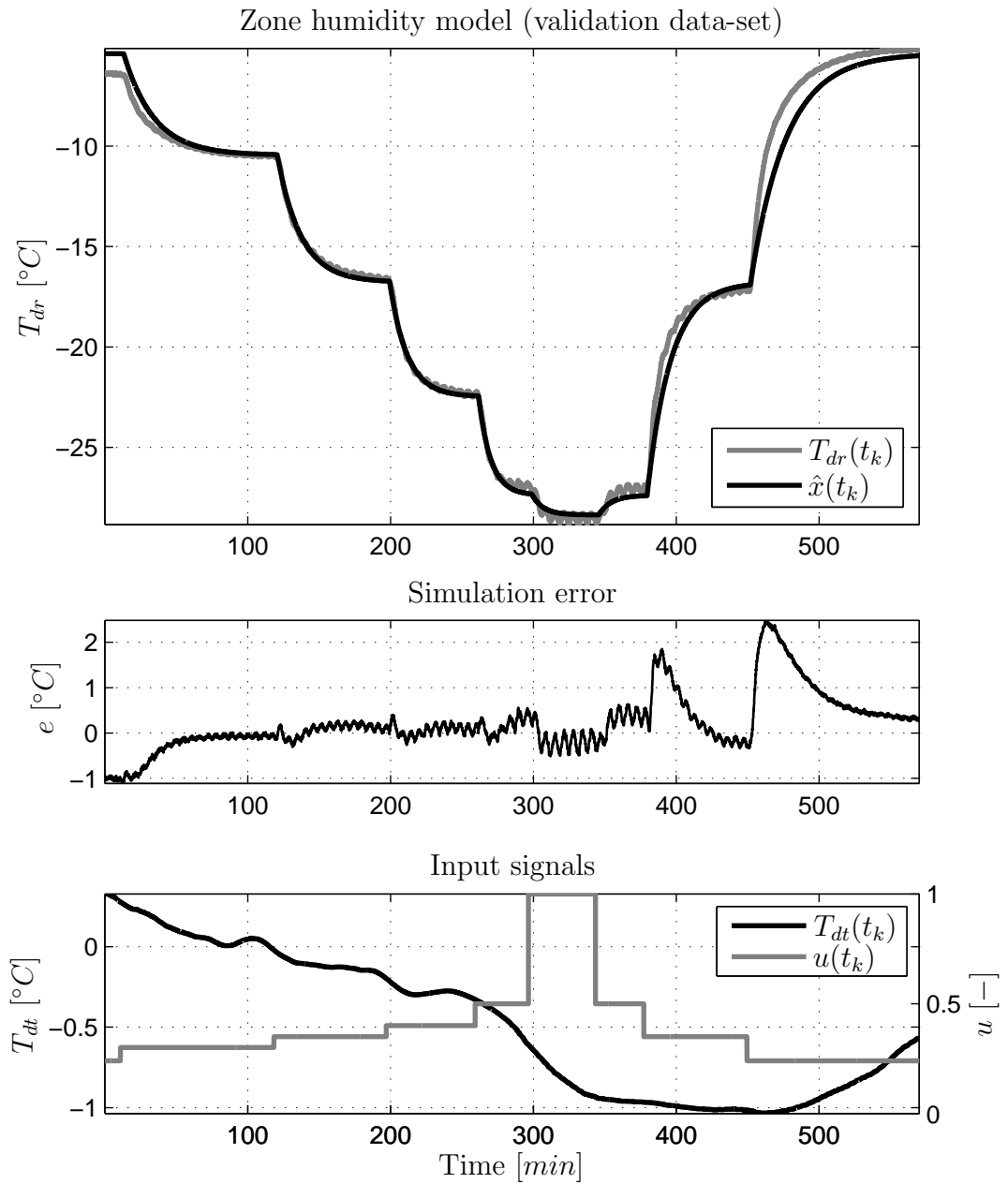


Figure 5.20: The upper plot shows measured (grey solid line) and simulated (black solid line) return air dew-point temperature. The middle plot shows the simulation error. The lower plot shows the fractional gas valve position (grey solid line) and the estimated trend (black solid line). The validation data-set is used with a sampling time interval $h = 5$ [s].

The same notation of measured signals, as used in (5.45), is adopted, hence consider the following definition for the measured signals

$$T_{dr,b}(t_k) = T_{dr}(t_k) + \bar{T}_{dr} \quad (5.80a)$$

$$u_b(t_k) = u(t_k) + \bar{u} \quad (5.80b)$$

$$v_b(t_k) = v(t_k) + \bar{v} \quad (5.80c)$$

the subscript b denotes the measured signals together with their baselines (the letter being denoted by the bar notation). Using the gas valve position baseline $\bar{u} = 0.2400$ as the input to the estimated static input function (5.73a), the corresponding baseline for the intermediate input is $\bar{v} = 0.0379$. Additionally, the parameters α_1 and β_0 estimated in (5.79) are renamed to $\tilde{\alpha}_1$ and $\tilde{\beta}_0$, respectively. The tilde above the parameters then indicates that these were estimated using the baseline compensated input-output signals, i.e. at the baseline compensated operating point.

The estimated parameters $\tilde{\alpha}_1$ and $\tilde{\beta}_0$ are adjusted for the original working point (\bar{v}, \bar{T}_{dr}) as follows, cf. (5.54), i.e.

$$\begin{aligned} \beta_0 &= \tilde{\beta}_0 - \eta_1 \bar{T}_{dr} \\ &= -5.0520 \times 10^{-2} - 1.5062 \times 10^{-3} \times 5.3967 \\ &= -5.8648 \times 10^{-2} \end{aligned} \quad (5.81a)$$

$$\begin{aligned} \alpha_1 &= \tilde{\alpha}_1 + \eta_1 \bar{v} \\ &= 6.6758 \times 10^{-4} - 1.5062 \times 10^{-3} \times 0.03789 \\ &= 6.1051 \times 10^{-4} \end{aligned} \quad (5.81b)$$

Subsequently, using the operating point adjusted parameters β_0 and α_1 , computed in (5.81), the return air dew-point temperature can be simulated at its original point of operation, using the measured input signal $v_b(t_k)$, according to

$$\hat{x}(t_k) = \frac{\beta_0}{s + \alpha_1} v_b(t_k) + \frac{\eta_1}{s + \alpha_1} v_b(t_k) \hat{x}(t_k) + o \quad (5.82)$$

where \hat{x} [$^{\circ}C$] denotes the simulated output corresponding to $T_{dr,b}$. The constant offset o can be interpreted as an external constant input acting on the system

and in a similar manner to (5.56) is computed as

$$\begin{aligned}
 o &= \bar{T}_{dr} - \frac{\beta_0}{\alpha_1} \bar{v} - \frac{\eta_1}{\alpha_1} \bar{v} \bar{T}_{dr} \\
 &= -5.3967 + \frac{5.0520 \times 10^{-2}}{6.6758 \times 10^{-4}} 0.03789 - \frac{1.5062 \times 10^{-3}}{6.6758 \times 10^{-4}} 0.0378 \times 5.3967 \\
 &= -2.2613 \text{ [}^\circ\text{C]} \tag{5.83}
 \end{aligned}$$

Finally, using the operating point adjusted parameters β_0 and α_1 the system time constant and steady-state gain can be calculated. The time constant T , defined in (2.73), varies in the range $T \in \langle 1637.99, 472.441 \rangle$ [s] for the input values $u(t_k) \in \langle 0, 1 \rangle$. The input dependent steady-state gain, according to definition (2.69), varies in the range $S SG \in \langle -96.0643, -27.7077 \rangle$ for the corresponding values of the input signal $u(t_k) \in \langle 0, 1 \rangle$.

5.7 Conclusions

The dynamic control oriented air temperature and humidity models of an environmentally controlled clean room manufacturing zone have been identified. Overall, three separate models have been identified, where different modelling approaches have been adopted to reflect the particular identification scenarios. All models presented have been estimated in the continuous-time domain, because of the subsequent physical interpretability.

The air temperature model of the environmentally controlled manufacturing zone comprises two submodels in a series connection, which are the air handling unit temperature submodel and the zone (room) temperature submodel. The zone temperature submodel has been identified in a black-box manner, where a second order linear model structure has been selected based on the Young's information criterion. Additionally, a lumped parameter first principles modelling approach has also been adopted. The resulting first principles model has the same model structure as that obtained based on the measured data only, which confirms the selected model order. Moreover, relating the identified zone temperature submodel to physical laws has allowed a unique heat load disturbance model to be obtained, which can be used during the control design and tuning procedure.

A grey-box modelling approach has been chosen to identify the air handling unit temperature submodel. Because the scope of the possible data acquisition experimentation has been limited, a first principles analysis has been used to select an initial candidate model structure. Naturally, not all of the model pa-

parameters suggested by such an analysis have been identifiable from the available measurements. Therefore, some parameters have been discarded, which resulted in a simplified, yet accurate and well structured Hammerstein-bilinear model.

The manufacturing zone humidity model has been identified in a black-box manner. The first principles analysis has been considered to be too complex and impractical due to the coupled nonlinear heat and mass transfer processes occurring within the desiccant rotor based dehumidification unit. Based on the engineering insight into the modelled HVAC system, and coupled with the on-site experiments, a Hammerstein-bilinear type model has been selected. A good model fit has been achieved despite the relative simplicity of the proposed model structure. It is believed, that this has been the first time the Hammerstein-bilinear type model has been used to model such a dehumidification process.

The steady-state and dynamic behaviour of the bilinear model is operating point dependent. Therefore, the parameters of the bilinear model are also operation point dependent. It is advantageous to subtract the baselines of the measured system input-output signals prior to any model parameter estimation. However, this also means that the bilinear model parameters have been estimated at a different point of operation than the actual system point of operation. Consequently, the estimated parameters of the bilinear model are valid only for the input signals with the subtracted baselines. A procedure to adjust the estimated parameters for an original (or indeed any) operation point has been suggested. This procedure then allows the bilinear model to be simulated at any given point of operation, while the dynamic behaviour of the bilinear model is retained. It is believed, that this procedure is new within the context of the identification and model parameter estimation of bilinear system models.

Chapter 6

Control analysis and tuning of an industrial HVAC control system

6.1 Introduction

The aim of this chapter is to select a set of control gains for an existing designed and installed commercial HVAC control system¹. This control system makes use of a standard fixed gain proportional-integral, PI, controller. The relative complexity and the nonlinear characteristics of the HVAC system together with the non-stationary operational conditions within which the system has to operate render the selection of control gains to be a non-trivial task in practice (Underwood 1999, Lim, Rasmussen & Swaroop 2009).

The control tuning of two PI feedback control loops is considered. The control system is required to regulate the manufacturing zone air (dry-bulb) temperature and the manufacturing zone air dew-point temperature at constant set-point values (regulatory control setup). It is not possible to interfere with the computer implementation of the commercial control algorithm, which limits the scope of possible experimental work. It is, however, possible to freely change the control gains or to suggest new temperature and humidity control set-points.

The originally implemented PI control gains led to an undesirable dynamical behaviour of the controlled HVAC system. Both, the regulated air dry-bulb and dew-point temperatures have been observed to oscillate around the demanded set-points (control hunting) for certain operation ranges. In return, this causes wear on control actuators and control valves and may also lead to energy inefficient operation of the whole HVAC system (Lim et al. 2009). Furthermore, because of

¹IQ3-type control system designed by Trend Control Systems Ltd, UK. Trend 963 operator software provides graphical displays for the control system.

poor control tuning the chosen control safety margin for the humidity control loop is considered to be over-large, see Subsection 6.1.2. The control safety margin, also known as a back-off region (Rangaiah & Kariwala 2012), is defined as a difference between the control set-point and the product specification limit. In other words, the control set-point is selected such that despite the poor control performance the regulated variable will never exceed the product specification limit, hence assuring product safety. Consequently, more energy is required to maintain such a large safety margin.

The proposed set of control gains should guarantee a stable control throughout the whole considered operation range, while offering good load disturbance rejection. In return, this will allow the humidity control loop set-point to be adjusted for operation close to the product specification limit, where the highest profitability can be obtained. Additionally, stable environmental conditions within the clean manufacturing room may potentially increase the product quality and reduce any potential product defects.

To select the control gains for a single, linear, fixed gain PI controller a first order linear model with input delay, representing the dominant dynamic behaviour of the system, is required (Skogestad 2003, Åström & Hägglund 2006). Since, the HVAC system is nonlinear and its dynamic and steady-state behaviour changes throughout the operation range, the PI controller is tuned at one operating point based on a locally linearised model. To guarantee the closed loop system stability over the whole operating range, the common approach (also adopted in this thesis) is to select a least stable point of operation for the control tuning purposes (Underwood 1990). It is assumed, that the least stable point of operation is that for which the system has the highest process gain. Taking into consideration the cooling applications for which the process gain is negative, then the highest absolute value of the process gain is selected instead. Subsequently, if the system operates at any other operating point than that for which the PI controller has been tuned, then an even more stable closed loop control will be obtained albeit at the expense of a less responsive (slow) control.

The selection of the critical operating point is, however, a non-trivial task in practice and a particularly daunting task to be carried out on the site. Therefore, the nonlinear temperature and humidity models of an environmentally controlled clean room manufacturing zone, which have been identified in the Chapter 5, are adopted for such control analysis. These models are flexible enough to replicate the main dynamic and static nonlinear characteristics of the considered HVAC system over the whole feasible operating range. The result of the control analysis

conducted in Sections 6.2 and 6.3 is the selection of the critical operating points together with the associated linearised models, which are used for the subsequent control tuning of the two considered control loops.

The tuning of the PI controller is, in general, a multi-objective constrained optimisation problem, where a trade-off must be made between (often conflicting) requirements on sensitivity to measurement noise, robustness to process uncertainties, load disturbance attenuation, input usage and set-point response (Åström & Hägglund 2006). To derive the optimal control gains the Skogestad internal model control (SIMC) PI/PID tuning rule has been adopted, see (Skogestad 2003, Skogestad & Grimholt 2012). This rule is model based and is analytically derived based on the desired closed loop response. Here, the requirements on the sensitivity to measurement noise, robustness to process uncertainties and input usage are quantified and condensed to a single criterion, a maximum sensitivity peak, denoted M_s , see (Åström & Hägglund 2006). At the same time, the requirements for the output performance are quantified in terms of integral of absolute error, IAE , of the system output when subject to set-point and load disturbance changes. The SIMC tuning rule then provides PI/PID control gains such that the IAE criterion is minimised (best output performance) subject to a given robustness level M_s , which can be adjusted by a user defined tuning parameter.

6.1.1 Control algorithm

The positional (non-incremental) form of the ideal proportional-integral-derivative (PID) controller, (Åström & Hägglund 2006), is given by

$$u(t) = K_p \left(1 + \frac{1}{T_i s} + T_d s \right) e(t) \quad (6.1)$$

where the control error $e(t)$ is defined as the difference between the demanded set-point $r(t)$ and the system output $y(t)$, i.e. $e(t) = r(t) - y(t)$. The controller parameters are the proportional gain K_p , integral time T_i and derivative time T_d . The control gains T_i and T_d have units of seconds.

The measurement noise prefilter is not implemented on the currently adopted HVAC control system. The measured (sampled) system output is directly used to compute the control error and generate the corresponding control action. This means that the derivative term would then amplify the high-frequency measurement noise causing large variations of the generated control action. Therefore,

due to the absence of noise prefilters, the derivative term of the PID controller is permanently disabled by setting the derivative time to zero, i.e. $T_d = 0$. This, in return, may limit the achievable control performance in terms of set-point following and load disturbance rejection properties. The resulting PI controller can be expressed in a transfer function form as follows

$$C(s) = K_p \left(1 + \frac{1}{T_i s} \right) \quad (6.2)$$

where, in this context, the variable s refers to the Laplace variable, see (Nise 2008). The same notation for the differential operator as for the Laplace variable is adopted, since these are used here in the same manner.

A general block diagram of the feedback control loop is provided in Figure 6.1. Here, $G(s)$ represents the process transfer function and $C(s)$ represents the controller. The input load disturbance, denoted $d(t)$, is considered together with the measurement noise denoted $n(t)$.

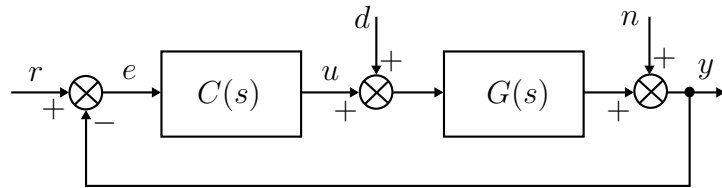


Figure 6.1: Block diagram of feedback control loop.

Digital implementation

To implement the continuous-time PI controller (6.1) in a digital computer environment the integral term must be discretised. From discussion with the supplier of the control system it is known that the Euler backward approximate difference discretisation method has been used, see (Åström & Hägglund 2006). The applied control signal to the system can be expressed as a sum of the control signal due to the proportional action, denoted $u_P(t)$, and the control signal due to the integral action, denoted $u_I(t)$, hence

$$u(t) = u_P(t) + u_I(t) \quad (6.3)$$

Replacing the continuous variables with the corresponding discrete-time variables gives

$$u(k) = u_P(k) + u_I(k) \quad (6.4)$$

where the discrete time index k is adopted. The proportional action of the discretised PI controller is simply computed by

$$u_P(k) = K_p e(k) \quad (6.5)$$

with the control error defined as

$$e(k) = r(k) - y(k) \quad (6.6)$$

From the continuous-time control law (6.1) it can be deduced that the integral term is given by

$$u_I(t) = \frac{K_p}{T_i s} e(t) \quad (6.7)$$

which can be further rearranged to

$$s u_I(t) = \frac{K_p}{T_i} e(t) \quad (6.8)$$

Using Euler backward approximate discretisation method the time derivatives are simply replaced by differences so that

$$\frac{u_I(k) - u_I(k-1)}{h} = \frac{K_p}{T_i} e(k) \quad (6.9)$$

from which it follows that the control action due to the integral term is implemented as

$$u_I(k) = u_I(k-1) + \frac{K_p h}{T_i} e(k) \quad (6.10)$$

The sampling interval h is also known as the rescheduling time of the controller. The rescheduling time of the controller is the interval at which the new control action is calculated and applied. The currently adopted rescheduling time is $h = 3$ [s] in the commercial setup and this value cannot be changed for the purpose of this control analysis.

The investigated HVAC control system also uses an appropriate anti-windup logic to avoid the wind-up effect of the integral term. The details of this logic are not provided since it does not impact the conducted control tuning analysis presented in this chapter. Additionally, control decision logic is used by the temperature control loop to switch between the cooling and heating modes of the air handling unit based on the current heating demand.

6.1.2 Control requirements

Brief overviews of control requirements have already been provided in Section 5.2.4. This section is summarised and further extended here. The product manufacturing requirements are such that the manufacturing zone air temperature must be in the range 21 ± 4 [$^{\circ}\text{C}$] and the air relative humidity must be lower than 20 [%].

Apart from the control system, an independent monitoring system is also installed in ADC UK. The monitoring system uses an independent set of temperature and relative humidity probes to measure the manufacturing zone environmental conditions. In order to assure that the product environmental manufacturing limits are not exceeded tighter limits are in use by the monitoring system. The zone air temperature must be in the range 21 ± 2 [$^{\circ}\text{C}$] and the air relative humidity must be lower than 15 [%] at all times. In the case where these limits are exceeded an alarm is activated. From the control point of view, it is the safety limits of the monitoring system which are of importance and these should not be exceeded.

It is noted that the air relative humidity is directly dependent on the air temperature, while the dew-point temperature is not. Therefore, to reduce the interaction between the temperature and humidity feedback control loops, the air humidity is measured in terms of its dew-point temperature instead of the relative humidity. Subsequently, for the air temperature control range 21 ± 2 [$^{\circ}\text{C}$] the corresponding air humidity (upper) limit in terms of dew-point temperature is -6.6 ± 1.6 [$^{\circ}\text{C}$], see equation (B.12).

The temperature feedback control loop is considered first. The air temperature set-point is set to 21.5 [$^{\circ}\text{C}$] with the dead band ± 0.5 [$^{\circ}\text{C}$]. Since only the cooling mode of the AHU is assumed, then the targeted temperature set-point, denoted $r_T(t)$ [$^{\circ}\text{C}$], is thus $r_T(t) = 22$ [$^{\circ}\text{C}$]. The regulated zone temperature $T_{ar}(t)$, being the system output, can therefore deviate from its set-point value maximally by 1 [$^{\circ}\text{C}$], i.e. the upper temperature limit of 23 minus the set-point value 22 . The range of the manipulated variable (control input) is $u_c(t) = \langle 0, 100 \rangle$ [%], where 0 corresponds to closed and 100 to a fully open cooling valve.

The control set-point for the humidity control loop, denoted $r_H(t)$ [%], is currently set to -10 [%]. Assuming that the zone air temperature is, $r_T(t) = 22$ [$^{\circ}\text{C}$], the humidity set-point value can be converted to relative humidity units using the expression (B.11), see Appendix B, and the value obtained is 10.8 [%], which is below the specification limit of 15 [%]. The control input range is $u_g(t) = \langle 24, 100 \rangle$ [%], where the lower limit of 24 [%] corresponds to the low

fire state and is a safety feature of the dehumidification unit. In the worst case scenario, when the zone air temperature is at its lowest allowed specification limit of 19 [°C] the corresponding dew-point temperature safety limit is only −8.2 [°C], i.e. −6.6 − 1.6 = −8.2. Consequently, this means that the system output $T_{drm}(t)$ can deviate maximally by 1.8 [°C] from its set-point value before this safety limit is reached. While, if the zone air temperature is at its upper specification limit of 23 [°C] the corresponding dew-point temperature safety limit is then −5 [°C], which allows the system output to deviate by 5 [°C] from its set-point value. Clearly, the control tuning of the humidity control loop should account for the worst case scenario, i.e. the allowed deviation of the system output from its set-point is 1.8 [°C].

6.2 Control analysis: Manufacturing zone temperature model

The manufacturing zone temperature model comprises two submodels in a cascade connection, which are the air handling unit temperature submodel identified in Section 5.5 and the zone (room) temperature submodel identified in Section 5.4, respectively. The overall manufacturing zone temperature model is summarised and stated as follows

$$v(t) = \phi(u_c(t)) = \sum_{i=1}^5 p_i u_c^i(t) \quad (6.11a)$$

$$T_{ao}(t) = \frac{\beta_{1,0}}{s + \alpha_1} v(t - \tau_u) + \frac{\eta_{2,1}}{s + \alpha_1} v(t - \tau_u) T_{ao}(t) + \frac{\beta_{3,0}}{s + \alpha_1} T_{ai}(t - \tau_{ai}) + o_1 \quad (6.11b)$$

$$T_{ar}(t) = \frac{\beta_0^r s + \beta_1^r}{s^2 + \alpha_1^r s + \alpha_2^r} T_{as}(t) + T_q(t) + o_2 \quad (6.11c)$$

where the outflow air temperature of the air handling unit (6.11b) acts as an input to the zone temperature submodel (6.11c), i.e. $T_{as}(t) = T_{ao}(t)$. Note, that the use of the continuous-time index t is preferred instead of using the index t_k since all the variables considered are simulated and not sampled (measured). The parameters of the manufacturing zone temperature model are provided in Table 6.1.

The static input nonlinearity (6.11a), scaling the input $u_c(t)$, was originally identified as a normalised 5th order polynomial function (5.41a). For the purpose

Table 6.1: Manufacturing zone temperature model parameters.

Parameter	Value	Parameter	Value	Parameter	Value
p_1	0.4169	$\eta_{2,1}$	-4.3944×10^{-3}	o_1	9.9662
p_2	12.988	$\beta_{3,0}$	2.1253×10^{-3}	o_2	6.1707
p_3	-47.789	α_1^r	53.3769×10^{-4}	τ_u	58
p_4	62.275	α_2^r	15.8771×10^{-7}	τ_{ai}	84
p_5	-26.891	β_0^r	23.2968×10^{-4}	m_a	2.4082
α_1	3.2914×10^{-3}	β_1^r	10.3538×10^{-7}	c_a	1005
$\beta_{1,0}$	2.8716×10^{-3}				

of simulation an equivalent polynomial function, as provided in (6.11a), is a preferred option and has been considered instead. For consistency, the constrained parameter p_1 is calculated such that $p_1 = 1 - \sum_{i=2}^5 p_i$, see (3.88). It should be noted, that the control input $u_c(t)$ is normalised in the range $\langle 0, 1 \rangle$ for the purpose of simulation, while the implemented control system assumes the range $\langle 0, 100 \rangle$ [%].

The bilinear submodel (6.11b) of the air handling unit model was originally defined in (5.55), where the simulated outflow air temperature has been denoted $\hat{x}(t)$ while the notation $T_{ao}(t)$ is used in (6.11b). The parameters α_1 and $\beta_{1,0}$ are adjusted for the operating point according to (5.54). The input-output signals $u_c(t)$, $T_{ai}(t)$ and $T_{ao}(t)$ were originally denoted with the subscript b in (5.55), where this subscript refers to signals that have their original signal baselines unchanged. The subscript b is omitted in (6.11b) for ease of notation. The static offset term o_1 in (6.11b) was originally defined and calculated in (5.57), where the notation o , with no subscript, was adopted.

The zone temperature submodel (6.11c) has been identified in (5.7). In the model (6.11c), as compared to (5.7), the superscript r on the model parameters is used in order to distinguish these from the parameters of the air handling unit bilinear model (6.11b). The presence of the offset term o_2 and temperature $T_q(t)$ (due to heat gain $q(t)$) can be deduced from equation (5.15). The offset term o_2 can be calculated according to expression (5.24), where the offset is denoted by o without any subscript. Using the heat load disturbance model (5.19) the temperature $T_q(t)$ is given by

$$T_q(t) = \frac{\beta_0^r s + \beta_1^r}{s^2 + \alpha_1^r s + \alpha_2^r} \frac{1}{m_a c_a} q(t) \quad (6.12)$$

where the parameters m_a and c_a are also provided in Table 6.1.

For the control analysis purposes the assumed feasible range of the inflow air

temperature is $T_{ai}(t) = \langle 20, 35 \rangle$ [$^{\circ}C$], where 20 [$^{\circ}C$] and 35 [$^{\circ}C$] are the lowest and the highest observed inflow air temperatures, respectively. However, when the parameters of the manufacturing zone temperature model have been estimated the measured lowest and highest inflow air temperatures were 20.4 [$^{\circ}C$] and 32.7 [$^{\circ}C$] (of the estimation data set), respectively. Since the model structure stems from the first principles considerations, it is assumed that the model is valid for a wider range of $T_{ai}(t)$ temperatures than those which were part of the estimation data set. Additionally, the assumed feasible range of the heat gain is $q(t) = \langle 0, 15 \rangle$ [kW]. Considering the number of personnel, power of the machinery and the type of manufacturing process within the air conditioned zone, a higher heat gain than 15 [kW] is not expected.

Both, the inflow air temperature and the heat gain act as load disturbances creating a cooling demand. The inflow air temperature to the air handling unit is mainly determined by the operation of the dehumidification unit and the heat gain is mainly caused by the personnel and machinery producing heat within the manufacturing zone.

6.2.1 Steady-state characteristic

The manufacturing zone temperature model (6.11) with (6.12) has three effective inputs: the manipulated variable $u_c(t)$, and the inflow air temperature $T_{ai}(t)$ together with the heat load $q(t)$ constantly changing the demand for cooling. As the inputs $T_{ai}(t)$ and $q(t)$ are freely changing, the controller computes the new value of the cooling valve position so that the set-point demanded value is achieved.

Assume a ‘perfect’ control in which the system output $T_{ar}(t)$ always tracks the set-point $r_T(t)$ despite the influence of disturbances acting on the system. Under the assumption of such a perfect control, it can then be deduced that only certain combinations of the three system inputs can actually occur. To highlight this idea consider the following example. The inflow air temperature is at its low level and no heat is produced within the zone, i.e. $T_{ai}(t) = 20$ [$^{\circ}C$] and $q(t) = 0$ [kW]. In order to meet the demand set-point value, it is then expected that the cooling valve will be closed rather than fully opened as there is only a small amount of heat to be compensated.

The dynamic behaviour of the manufacturing zone temperature model (6.11) is operating point dependent due the presence of the bilinear submodel (6.11b). Since, only certain combinations of the three considered inputs can occur, then

only certain corresponding dynamic modes of the system will be activated. Therefore, the steady-state characteristic of the manufacturing zone temperature model (6.11) is derived in this section with the view of determining the feasible ranges of operation for the three input signals.

The steady-state characteristic of the manufacturing zone temperature model (6.11) is found, with reference to the load disturbance model (6.12), by setting the value of the differential operator to zero, cf. (2.68), so that

$$T_{ao} = \frac{\beta_{1,0}}{\alpha_1} \phi(u_c) + \frac{\eta_{2,1}}{\alpha_1} \phi(u_c) T_{ao} + \frac{\beta_{3,0}}{\alpha_1} T_{ai} + o_1 \quad (6.13a)$$

$$T_{ar} = \frac{\beta_1^r}{\alpha_2^r} \left(T_{as} + \frac{1}{m_a c_a} q \right) + o_2 \quad (6.13b)$$

where $T_{as} = T_{ao}$. To distinguish the steady-state variables from their continuous counterparts the index t has been omitted. Note, that in the steady-state characteristic (2.68) the subscript ss has been adopted to denote the steady-state variables, however for clarity of the text this notation is omitted here.

The air handling unit submodel (6.13a) is rearranged in terms of its output T_{ao} as follows

$$T_{ao} = \frac{\frac{\beta_{1,0}}{\alpha_1} \phi(u_c) + \frac{\beta_{3,0}}{\alpha_1} T_{ai} + o_1}{1 - \frac{\eta_{2,1}}{\alpha_1} \phi(u_c)} \quad (6.14)$$

and by combining the two submodels given in (6.13b) and (6.14) the steady-state characteristic of the manufacturing zone temperature model is found, hence

$$T_{ar} = \frac{\beta_1^r}{\alpha_2^r} \left(\frac{\frac{\beta_{1,0}}{\alpha_1} \phi(u_c) + \frac{\beta_{3,0}}{\alpha_1} T_{ai} + o_1}{1 - \frac{\eta_{2,1}}{\alpha_1} \phi(u_c)} + \frac{1}{m_a c_a} q \right) + o_2 \quad (6.15)$$

The steady-state characteristic (6.15) is plotted (grey surface) in Figure 6.2 for the input ranges $u_c = \langle 0, 1 \rangle$, $T_{ai} = \langle 20, 35 \rangle$ [$^{\circ}C$] and the heat gain value $q = 0$ [kW]. The solid black and grey curves in Figure 6.2 are not considered at this stage.

To find the feasible combinations of inputs u_c , T_{ai} for a given heat gain the air handling unit submodel (6.13a) is rearranged with respect to the input T_{ai} , hence

$$\begin{aligned} T_{ai} &= \frac{\alpha_1}{\beta_{3,0}} \left(T_{ao} - \frac{\beta_{1,0}}{\alpha_1} \phi(u_c) - \frac{\eta_{2,1}}{\alpha_1} \phi(u_c) T_{ao} - o_1 \right) \\ &= \frac{\alpha_1}{\beta_{3,0}} \left[\left(1 - \frac{\eta_{2,1}}{\alpha_1} \phi(u_c) \right) T_{ao} - \frac{\beta_{1,0}}{\alpha_1} \phi(u_c) - o_1 \right] \end{aligned} \quad (6.16)$$

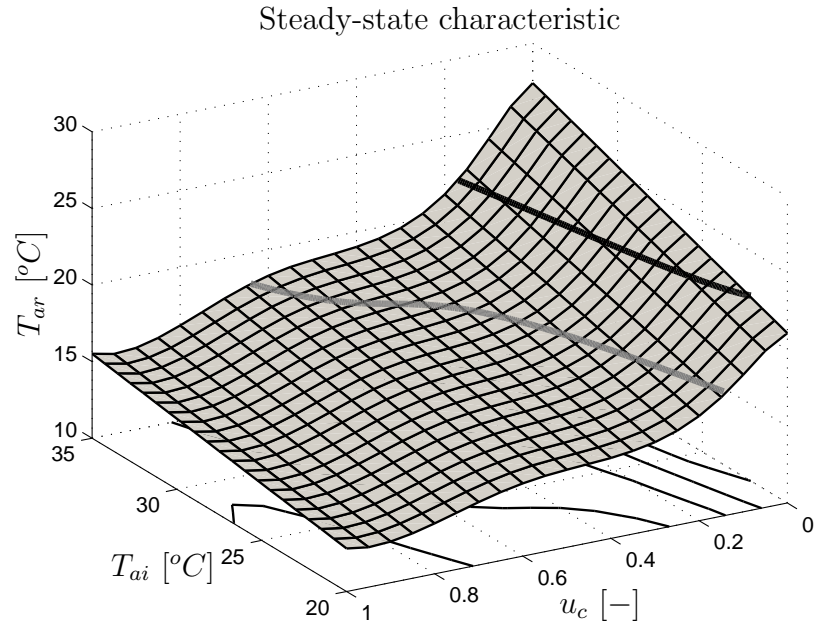


Figure 6.2: Manufacturing zone temperature model steady-state characteristic shown for heat gain value $q = 0$ [kW]. The solid black and grey isocline curves of constant T_{ar} refer to feasible combinations of inputs u_c and T_{ai} for heat gains $q = 0$ and $q = 15$ [kW], respectively, such that the set-point $r_T = 22$ [°C] is achieved.

The zone temperature submodel (6.13b) is then rearranged with respect to its input T_{as} as follows

$$T_{as} = \frac{\alpha_2^r}{\beta_1^r} \left(T_{ar} - \frac{\beta_1^r}{\alpha_2^r} \frac{1}{m_a c_a} q - o_2 \right) \quad (6.17)$$

and in steady-state operation the system output is equal to the set-point, i.e. $T_{ar} = r_T$, so that (6.17) becomes

$$T_{as} = \frac{\alpha_2^r}{\beta_1^r} \left(r_T - \frac{\beta_1^r}{\alpha_2^r} \frac{1}{m_a c_a} q - o_2 \right) \quad (6.18)$$

Since the outflow air temperature of the air handling unit is equal to the supply air temperature to the manufacturing zone, the relation (6.18) is substituted for the temperature T_{ao} in (6.16), giving the steady-state relation between the considered

model inputs

$$T_{ai} = \frac{\alpha_1}{\beta_{3,0}} \left[\frac{\alpha_2^r}{\beta_1^r} \left(1 - \frac{\eta_{2,1}}{\alpha_1} \phi(u_c) \right) \left(r_T - \frac{\beta_1^r}{\alpha_2^r} \frac{1}{m_a c_a} q - o_2 \right) - \frac{\beta_{1,0}}{\alpha_1} \phi(u_c) - o_1 \right] \quad (6.19)$$

The upper left plot of Figure 6.3 shows the steady-state relation (obtained using (6.15)) between the system output T_{ar} and input u_c for constant inflow air temperatures $T_{ai} = 20$ [$^{\circ}C$] (grey solid line) and $T_{ai} = 35$ [$^{\circ}C$] (black solid line) and heat gain $q = 0$ [kW]. The corresponding lower left plot of Figure 6.3 shows the steady-state relation (obtained using (6.19)) between inputs T_{ai} and u_c for set-point value $r_T = 22$ [$^{\circ}C$] and heat gain $q = 0$ [kW]. The solid black line of the lower left plot then highlights the region for which $T_{ai} = \langle 20, 35 \rangle$. The right side of Figure 6.3 then mirrors the static characteristic curves which are on the left side, but for a heat gain value $q = 15$ [kW]. The highlighted (black solid line) static curves of the lower left and right plots show the feasible combinations of the inputs T_{ai} and u_c for a heat gain value of 0 and 15 [kW], respectively. These are also shown in the Figure 6.2 as the solid black ($q = 0$ [kW]) and the solid grey ($q = 15$ [kW]) isocline curves.

It can be observed from Figure 6.3, that for the inflow air temperature range $T_{ai} = \langle 22.16, 35 \rangle$ [$^{\circ}C$] and the heat gain value $q = 0$ [kW], the corresponding cooling valve position range is $u_c = \langle 0, 17.19 \rangle$ [%]. In other words, the cooling valve will not open more than 17.19 [%] if the gain within the manufacturing zone is $q = 0$ [kW] and the demanded set-point value is $r_T = 22$ [$^{\circ}C$]. Note, that under zero heat gain load the cooling valve is already closed when $T_{ai} = 22.16$ [$^{\circ}C$] so that in the temperature range $T_{ai} = \langle 20, 22.16 \rangle$ [$^{\circ}C$] the valve is closed (negative values of valve opening are infeasible). Similarly, for the heat gain $q = 15$ [kW] the operating range of the cooling valve position is constrained to $u_c = \langle 14.12, 64.29 \rangle$ [%] for the considered inflow air temperature range $T_{ai} = \langle 20, 35 \rangle$ [$^{\circ}C$].

6.2.2 Process gain and time constants

The notion of the process gain and time constant has been introduced in Section 2.6, where the selected static and dynamic properties of the Hammerstein-bilinear models have been examined. The manufacturing zone temperature model (6.11) process gain, denoted K_T , can be computed as a product of the process gains of the air handling unit submodel, denoted K_{AHU} , and process gain of the zone

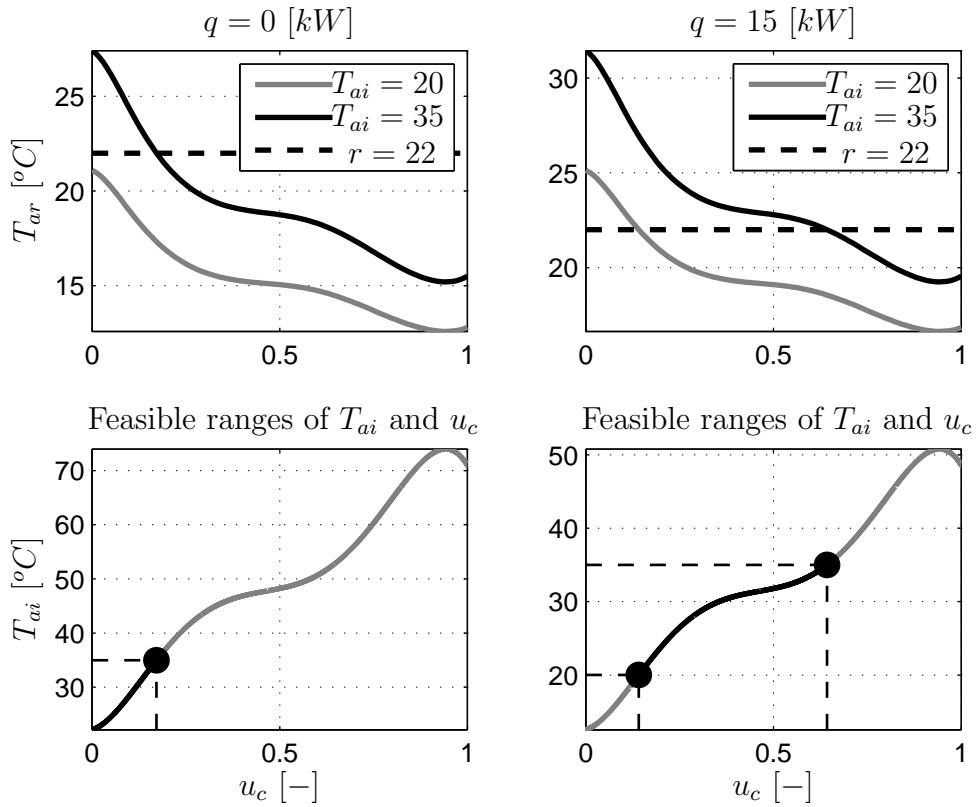


Figure 6.3: The upper plots show the steady-state characteristics for a constant temperature T_{ai} and heat gain values 0 and 15 [kW]. While, the corresponding lower plots show the steady-state characteristic curves for constant set-point value $r_T = 22$ [°C], where $r_T = T_{ar}$.

temperature submodel, denoted K_R , so that

$$K_T = K_{AHU}K_R \quad (6.20)$$

The relations for process gains K_{AHU} and K_R are derived individually in the following two subsections together with the corresponding process time constants. The time constant of the air handling unit submodel is denoted T_{AHU} [s] and the time constant of the zone temperature submodel is denoted T_R [s]. Subsequently, the overall process gain K_T is evaluated with respect to the feasible set of system inputs found in the previous Section 6.2.1.

Air handling unit

The process gain is defined as the sensitivity of the system output to changes in the manipulated variable (cooling valve position). Therefore, taking the deriva-

tive of the steady-state characteristic (6.15) with respect to the control input u_c leads to

$$K_{AHU} = \frac{\eta_{2,1} \frac{\beta_{1,0}}{\alpha_1} \phi(u_c) + \frac{\beta_{3,0}}{\alpha_1} T_{ai} + o_1}{\alpha_1 \left(1 - \frac{\eta_{2,1}}{\alpha_1} \phi(u_c)\right)^2} \psi(u_c) + \frac{\beta_{1,0}}{\alpha_1} \frac{1}{1 - \frac{\eta_{2,1}}{\alpha_1} \phi(u_c)} \psi(u_c) \quad (6.21)$$

where $\psi(u_c)$ is the derivative of the function $\phi(u_c)$ with respect to the variable u_c derived in (2.71) and repeated below

$$\psi(u_c) = \frac{d\phi(u_c)}{du_c} = \sum_{i=1}^5 ip_i u_c^{i-1} \quad (6.22)$$

It is noted, in equation (6.21), that the process gain K_{AHU} depends on the value of the inputs u_c and T_{ai} as well as on the value of the offset term o_1 .

The corresponding time constant is computed according to (2.73), hence

$$T_{AHU} = \frac{1}{\alpha_1 - \eta_{2,1} \phi(u_c)} \quad (6.23)$$

where, it is noted, that the time constant is also a control input dependent variable.

Zone temperature submodel

The zone temperature submodel (6.11c) has two real poles with corresponding time constants $T_1 = 199.144$ [s] (fast dynamic model) and $T_2 = 3162.73$ [s] (slow dynamic mode), which were calculated in Subsection 5.4.1. The response of the zone temperature submodel is dominated by the slow mode over a long time horizon (approximately $5 \times T_2$ and more). From the control perspective the slow mode is of no interest, see (Underwood 1999). The slow mode is approximately sixteen times slower than the fast mode and will appear as a ‘drift’ in the measured system output, which will be inherently compensated for by the integral action of the PI controller.

To place emphasis on the fast mode only, the zone temperature submodel is reduced to a first order linear model via a system identification, data-based, model order reduction approach. Such an approach has been applied in a similar manner to a model order reduction problem of a high-order, nonlinear, glasshouse simulation model in (Lees, Young, Chotai & Tych 1995). The input $T_{as}(t)$ to the zone temperature submodel is perturbed with a step input function, where the input-output data set obtained is used for subsequent parameter estimation of a

reduced order model. Since, the targeted reduced order model is of first order, the use of a single step input function is deemed to be sufficiently exciting.

The crucial aspect of such a model order reduction analysis is the selection of the simulation time, or equivalently, the length of the step input response. The selection of the simulation time impacts the type of dynamic modes which are captured by the reduced order model. After the step input is applied, sufficient time should be allowed for the fast mode to fully exhibit itself. However, as the simulation time increases the slow mode starts to dominate the step response and the identified reduced order model captures the slow (dominant) mode as well. It is assumed, that the simulation time $N = 5 \times T_1 \approx 955$ [s] is sufficiently long enough for the fast mode to fully exhibit itself, while being short enough so that the slow mode will not dominate the transient response. The simulation time of five times the time constant of interest has been selected, because it is the time it takes for a step response to reach 99.33 [%] of its final value, see (Nise 2008).

The considered model orders are $n = 1$ and $m = 0$. No time delay is present since, using the partial fraction expansion, the zone temperature submodel which has no input time delay can be decomposed and simulated as a sum of two first order processes. The SRIVC parameter estimation method, provided in Algorithm 3.1, has been applied to the simulated input-output data set with the following settings: The convergence criterion for monitoring the maximum relative change of the parameter estimates, defined in (3.25), is selected to be $\epsilon = 1 \times 10^{-10}$. The prefilter of the SRIVC algorithm is initialised with the single breakpoint frequency parameter equal to $\lambda = 0.01$. The final estimated model takes the form

$$T_{ar}(t) = \frac{\bar{\beta}_0^r}{s + \bar{\alpha}_1^r} T_{as}(t) \quad (6.24)$$

where the estimated model parameters of the reduced order model, denoted with a bar notation, are found to be

$$\bar{\alpha}_1^r = 44.5808 \times 10^{-4} \quad (6.25a)$$

$$\bar{\beta}_0^r = 22.3571 \times 10^{-4} \quad (6.25b)$$

The process gain and time constant of the reduced order model representing the zone manufacturing submodel are, respectively,

$$K_R = 0.5015 \quad (6.26a)$$

$$T_R = 224.3117 \text{ [s]} \quad (6.26b)$$

It is noted, that the time constant T_R is close to T_1 , however, it also partially accounts for the slow time constant T_2 which influences the initial transient step response of the system². The model order reduction simulation results are presented in the left-hand side plot of Figure 6.4. In this plot, the output of the full order model (grey solid line) is plotted together with the simulated output of the reduced order model (black solid line). The achieved model fit criteria are $R_7^2 = 99.9476$ [%], $IAE = 0.00258$ [$^{\circ}C$] and $YIC = -21.0381$, all indicating good model fit.

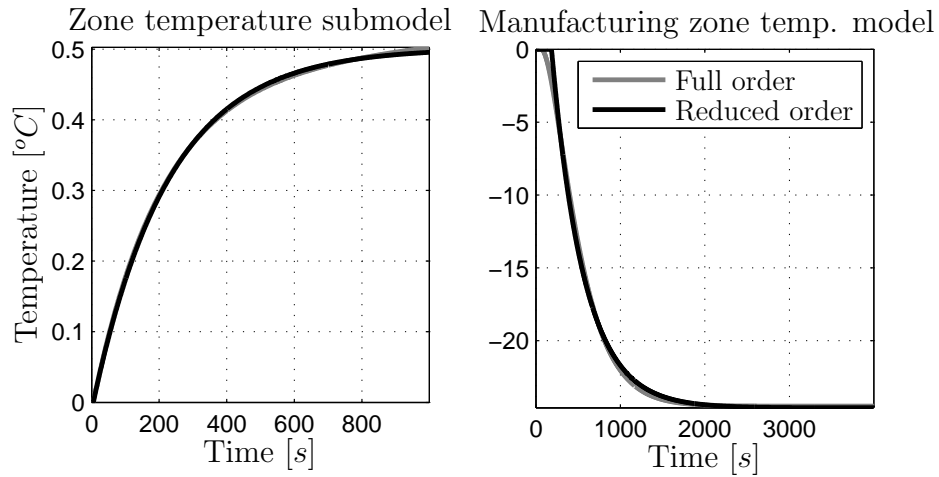


Figure 6.4: Model order reduction simulation results for the zone temperature submodel (left-hand side) and the overall manufacturing zone model (right-hand side). The output of the full order model (grey solid line) is plotted together with the simulated output of the reduced order model (black solid line). In both cases the step input is considered.

Process gain and time constant analysis

The process gain of the manufacturing zone temperature model, defined in (6.20), comprising the process gains K_{AHU} , provided in (6.21), and K_R , provided in (6.26a), is shown in Figure 6.5 for input ranges $u_c = \langle 0, 1 \rangle$ and $T_{ai} = \langle 20, 35 \rangle$ [$^{\circ}C$]. Having found the feasible combinations of the inputs u_c , T_{ai} and q based on the steady-state characteristic curves obtained in Subsection 6.2.1, it is then possible to find the corresponding feasible sets of process gains. Subsequently,

²Note, that again similar to Chapter 5, the numerical results are quoted to 4 decimal places accuracy even though in some cases this might lead to 7 or 8 significant figures. It is recognised from engineering viewpoint that such accuracy cannot be achieved. However in the final control implementation these values are reduced to 3 significant figures.

in Figure 6.5 the solid black and grey curves show the feasible sets of process gains for the heat gain values $q = 0$ and $q = 15$ [kW], respectively, such that the set-point $r_T = 22$ [°C] is achieved. It can be observed that the process gain surface has a wave-like shape declining in a direction of decreasing cooling valve fractional position (manipulated variable) and inclining towards the increasing values of the inflow air temperature.

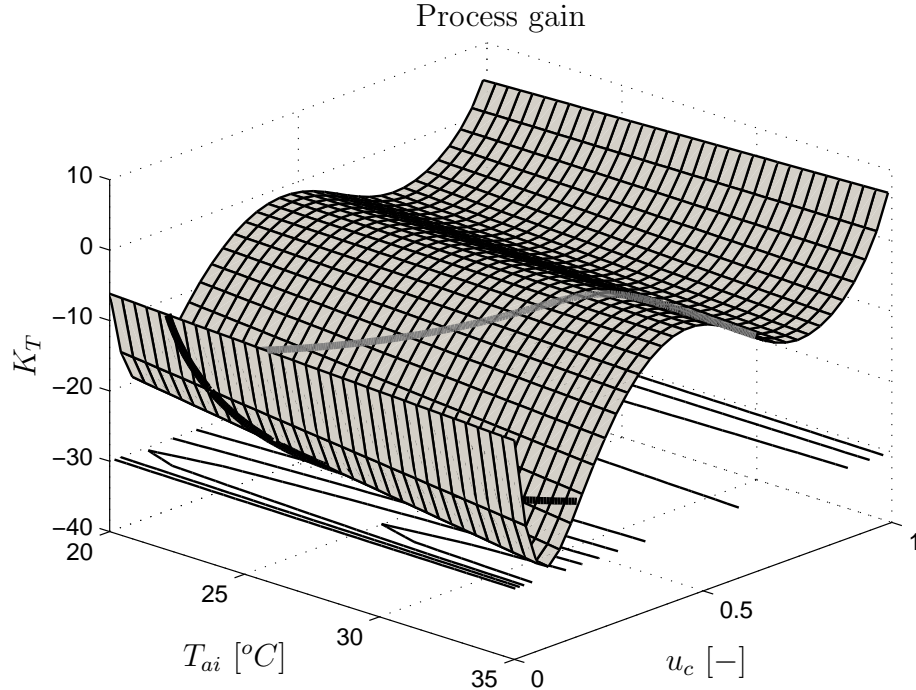


Figure 6.5: Manufacturing zone temperature model process gain. The solid black and grey curves show feasible sets of process gains for heat gains $q = 0$ and $q = 15$ [kW], respectively, such that the set-point $r_T = 22$ [°C] is achieved.

The feasible sets of process gains for heat gain $q = 0$ [kW] (black solid line) and $q = 15$ [kW] (dark grey solid line) are shown in more detail in the right-hand side plot of Figure 6.6. From the control point of view the most critical process gain is the one with the highest absolute value. In the considered cooling application, therefore, the most critical gain is $K_T = -24.4959$ (depicted as a black dot) occurring at $u_c = 10.3$ [%], $T_{ai} = 28.7611$ [°C] and $q = 0$ [kW]. While the least critical gain has value -1.7539 (grey dot) occurring at $u_c = 46.3$ [%], $T_{ai} = 31.4249$ [°C] and $q = 15$ [kW]. For comparison, the isoclines of constant inflow air temperatures are shown for temperatures 20 [°C] (light grey solid line) and 35 [°C] (light grey dashed line). It can be observed, that the absolute lowest

value (the most critical) process gain of -28.6522 would occur at $u_c = 8.3$ [%] for $T_{ai} = 35$ [$^{\circ}\text{C}$]. However, from the conducted steady-state analysis of feasible combinations of system inputs such a process gain could not occur, therefore, is not considered.

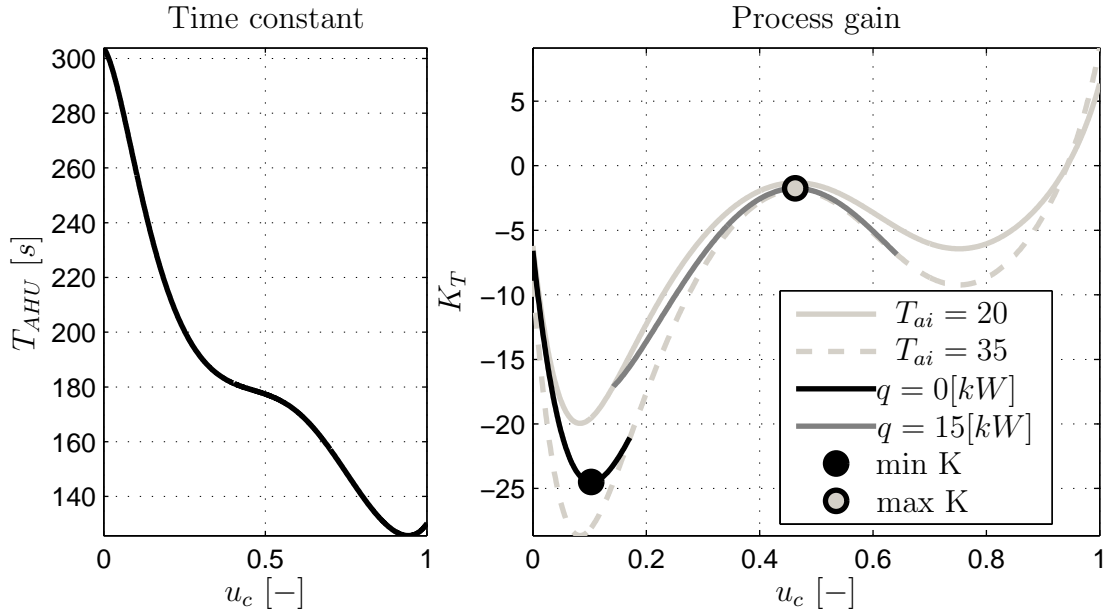


Figure 6.6: The left-hand side plot shows the time constant of the air handling unit submodel as a function of control input. The right-hand side plot shows the feasible sets of process gains for heat gain $q = 0$ [kW] (black solid line) and $q = 15$ [kW] (dark grey solid line). The minimal process gain is highlighted by a black dot, while the maximal process gain by a grey dot. The isoclines of constant input T_{ai} are shown for temperatures 20 [$^{\circ}\text{C}$] (light grey solid line) and 35 [$^{\circ}\text{C}$] (light grey dashed line).

The left-hand side plot of Figure 6.6 shows the time constant of the air handling unit submodel as a function of the control input. For the selected critical gain $K_T = -24.4959$, which occurs for the input value $u_c = 10.3$ [%], the corresponding time constant of the air handling unit submodel is $T_{AHU} = 257.3625$ [s], which has been calculated using the relation (6.23).

6.2.3 Model order reduction

The critical operating point obtained, where the system has the highest absolute value of the overall process gain, i.e. $K_T = -24.4959$, occurs for the following input values $u_c = 10.3$ [%], $T_{ai} = 28.7611$ [$^{\circ}\text{C}$] and $q = 0$ [kW]. At this operating point the process time constant of the air handling unit submodel is $T_{AHU} =$

257.3625 [s]. The relevant time constant for control of the zone temperature submodel, which is in a series connection with the air handling unit submodel, has been found to be $T_R = 224.3117$ [s]. Additionally, the time delay $\tau_u = 58$ [s] is present on the control input $u_c(t)$. The resultant second order (linearised) transfer function model with time delay, denoted $G_T(s)$, is given by

$$\begin{aligned} G_T(s) &= \frac{T_{ar}(s)}{U(s)} = \frac{K_T}{(T_{AHU}s + 1)(T_Rs + 1)} \exp(-\tau_u s) \\ &= \frac{-24.4959}{(257.3625s + 1)(224.3117s + 1)} \exp(-58s) \end{aligned} \quad (6.27)$$

where $T_{ar}(s)$ and $U(s)$ denote the Laplace transforms of the continuous signals $T_{ar}(t)$ and $u_c(t)$, respectively. Applying the second time shift theorem the delayed input signal $u_c(t - \tau_u)$ is transformed to $\exp(-s\tau_u)U(s)$, (Nise 2008). The notion of the transfer function in the s-domain is preferred, because this facilitates the use of block diagram algebra, (Nise 2008), which is used in the forthcoming Section 6.4.

The two time constants of the derived linear manufacturing zone temperature model (6.27) have the same order of magnitude and the faster time constant is larger than the time delay, i.e. $T_R > \tau_u$. Skogestad (2003) refers to such a model as being a dominant second order model and recommends the use of the PID controller. The derivative action term of a PID controller then would help to speed up the closed-loop transient response allowing for tight control tuning (Åström & Hägglund 2006). However, the derivative action term is switched off, cf. Subsection 6.1.1, so that only a PI controller can be applied in the current application. Therefore, to obtain the control gains of the PI controller, the second order model (6.27) must be reduced to a first order plus delay model.

A system identification based model order reduction approach has been adopted, in a similar manner to (Lees et al. 1995). The step input response of the second order model (6.27) is shown (grey solid line) in the right-hand side plot of Figure 6.4. Subsequently, the simulated input-output data set obtained is used to estimate the parameters of the reduced order model. The SRIVC parameter estimation method, as stated in Algorithm 3.1, has been applied with the following settings: The convergence criterion (3.25) is $\epsilon = 1 \times 10^{-10}$ and the prefilter of the SRIVC algorithm is initialised with the single breakpoint frequency parameter equal to $\lambda = 0.01$. The model orders are known, i.e. $n = 1$ and $m = 0$, while to select the value of the input delay the YIC (5.6) has been adopted. The final

estimated model takes the form

$$\begin{aligned}
 G_T(s) &= \frac{K_T}{T_T s + 1} \exp(-\tau_T s) \\
 &= \frac{-24.6129}{381.6204s + 1} \exp(-180s)
 \end{aligned} \tag{6.28}$$

where T_T [s] denotes the process time constant of the reduced order linearised manufacturing zone temperature model and τ_T [s] denotes the input delay.

The simulated step response of the reduced order model (6.28) is shown (black solid line) on the right-hand side of Figure 6.4. The coefficient of determination achieved, $R_T^2 = 99.7426$ [%], is close to 100 [%] and the calculated integral of absolute error criterion $IAE = 0.2037$ [$^{\circ}C$] is low, meaning that the reduced order model explains the simulated data well. The obtained Young's criterion is $YIC = -18.8744$, where a large negative value indicates a well defined model structure (including the input delay).

It should be emphasised, that instead of reducing the second order linearised model (6.27) the original Hammerstein-bilinear manufacturing zone temperature model (6.11), with reduced zone temperature submodel (6.24), could have been used for the linearisation purposes directly. The linearised model obtained would then be equivalent to that obtained in (6.28).

Based on the conducted control analysis the critical operating point is known. Therefore, the simulated input-output perturbation data set can be obtained using the manufacturing zone temperature model, which has been excited around this critical operating point. During such simulation, the inputs T_{ai} and q are held constant at their respective critical values, while the control input is perturbed. The perturbation signal should be small in magnitude so that the output of the nonlinear system is not driven far away from the critical operating point, e.g. a step response from $u_c = 10.3$ to $u_c = 10.4$ would be a suitable perturbation signal. Subsequently, the first order linearised model can be estimated using the SRIVC algorithm.

6.3 Control analysis: Manufacturing zone humidity model

The manufacturing zone humidity model has been identified in Section 5.6. The model comprises a static input nonlinearity followed by the bilinear dynamic submodel and the measured output is additionally influenced by the humidity

trend caused by the fresh air supply. The manufacturing zone humidity model is summarised and stated as follows

$$v(t) = \phi(u_g(t)) = \frac{1}{1 + p_1 \exp(-p_2 u_g(t))} \quad (6.29a)$$

$$T_{dr}(t) = \frac{\beta_0}{s + \alpha_1} v(t - \tau_u) + \frac{\eta_1}{s + \alpha_1} v(t - \tau_u) T_{dr}(t) + o \quad (6.29b)$$

$$T_{dt}(t) = \frac{\beta_0^r}{s + \alpha_1^r} T_{df}(t) \quad (6.29c)$$

$$T_{drm}(t) = T_{dr}(t) + T_{dt}(t) \quad (6.29d)$$

with the parameters provided in Table 6.2.

The static input nonlinear function (6.29a), scaling the fractional gas valve position, was originally defined in (5.73a) with the model parameters estimated in (5.78). Note, that the control input $u_g(t)$ is normalised in the range $\langle 0, 1 \rangle$ for simulation purposes, while the implemented control system assumes a range $\langle 0, 100 \rangle$ [%]. Subsequently, the bilinear dynamic submodel (6.29b) is as originally defined in (5.82). The parameters of this model have been estimated in (5.79), where the parameters α_1 and β_0 are adjusted for the operating point according to (5.81). The static offset term o has been defined and calculated in (5.83). Lastly, the humidity trend model (6.29c) has been identified in (5.65), where the model parameters are also provided. Note, that the new notation of the trend model parameters has been adopted (superscript r has been added) as compared to the original notation used in model (5.65). This has been made in order to distinguish the humidity trend model parameters from the parameters of the bilinear submodel (6.29b).

To find the process gain of the manufacturing zone humidity model (6.29) the steady-state characteristic needs to be found first. The models (6.29b) and (6.29c) are substituted for outputs $T_{dr}(t)$ and $T_{dt}(t)$ in (6.29d), respectively, and setting the value of the differential operator to zero gives the desired steady-state

Table 6.2: Manufacturing zone humidity model parameters.

Parameter	Value	Parameter	Value
p_1	3201.5646	α_1^r	5.2401×10^{-4}
p_2	20.1539	β_0^r	4.6395×10^{-4}
α_1	6.1051×10^{-4}	o	-2.2613
β_0	-5.8648×10^{-2}	τ_u	135
η_1	-1.5062×10^{-3}		

characteristic, cf. (6.15), hence

$$T_{drm} = \frac{\frac{\beta_0}{\alpha_1}\phi(u_g) + o}{1 - \frac{\eta_1}{\alpha_1}\phi(u_g)} + \frac{\beta_0^r}{\alpha_1^r}T_{df} \quad (6.30)$$

where to distinguish the steady-state variables from their continuous counterparts the index t has been omitted. Subsequently, by taking the derivative of the steady-state characteristic (6.30) with respect to the control input u_g leads to the expression for the process gain, so that

$$K_H = \frac{\eta_1 \frac{\beta_{1,0}}{\alpha_1}\phi(u_g) + o}{\alpha_1 \left(1 - \frac{\eta_1}{\alpha_1}\phi(u_g)\right)^2} \psi(u_g) + \frac{\beta_0}{\alpha_1} \frac{1}{1 - \frac{\eta_1}{\alpha_1}\phi(u_g)} \psi(u_g) \quad (6.31)$$

where K_H denotes the process gain of the manufacturing zone humidity model and $\psi(u_g)$ denotes the derivative of the function $\phi(u_g)$ with respect to the variable u_g . The function $\psi(u_g)$ is then given by

$$\psi(u_g) = \frac{d\phi(u_g)}{du_g} = \frac{p_1 p_2}{\exp(p_2 u_g) \left[1 + \frac{p_1}{\exp(p_2 u_g)}\right]^2} \quad (6.32)$$

It is noted, in equation (6.31), that the value of the process gain K_H is a system input dependent quantity, as expected. However, it is also noted, that the value of the process gain K_H is independent of the second input T_{df} . The associated process time constant of the manufacturing zone humidity model is then defined as follows, cf. (2.73), i.e.

$$T_H = \frac{1}{\alpha_1 - \eta_1 \phi(u_g)} \quad (6.33)$$

where T_H [s] denotes the process time constant.

The process gain K_H is plotted in Figure 6.7 as a function of the input u_g in the range $\langle 0.24, 1 \rangle$. It is observed, that the value of the critical gain is $K_H = -131.4970$, which occurs at $u_g = 33.9$ [%]. The associated process time constant is then $T_H = 1054.0164$ [s] as can be observed in the left-hand side plot of Figure 6.7. Subsequently, the linear first order with time delay transfer function model representing the dynamic behaviour of the Hammerstein-bilinear manufacturing zone humidity model (6.29) at critical operating point, for which $u_g = 33.9$ [%],

is given by

$$\begin{aligned} G_H(s) &= \frac{K_H}{T_H s + 1} \exp(-\tau_H s) \\ &= \frac{-131.4970}{1054.0164s + 1} \exp(-135s) \end{aligned} \quad (6.34)$$

where the value of the input time delay τ_u remains unchanged and is renamed to τ_H for consistency of notation.

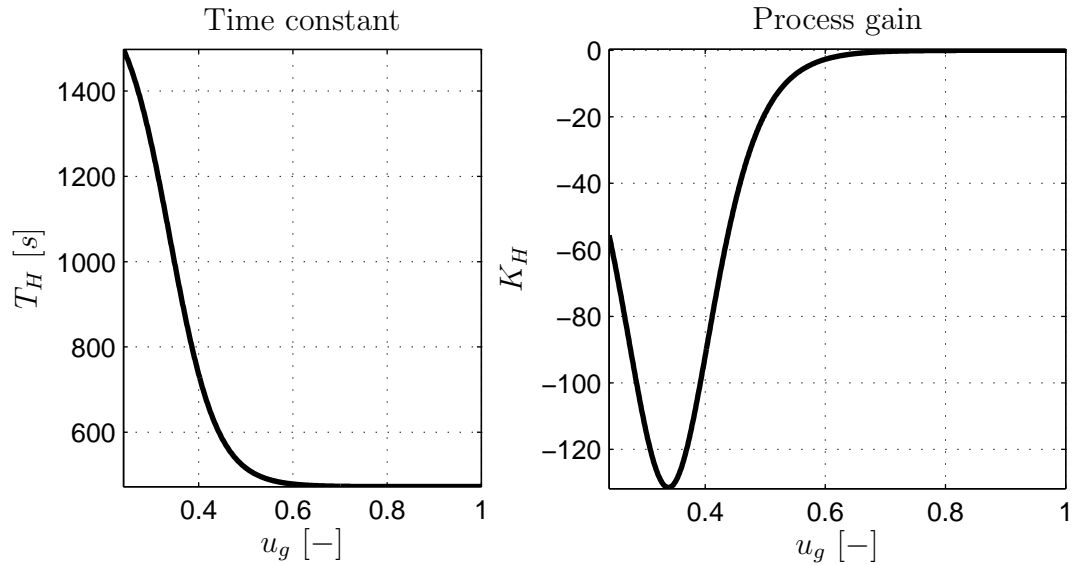


Figure 6.7: Manufacturing zone humidity model. The left-hand side plot shows the process time constant T_H as a function of control input u_g . The right-hand side plot shows the process gain K_H as a function of control input.

6.4 Control tuning

The implemented control system in Abbott Diabetes Care assumes the input signals to be in the range $u = \langle 0, 100 \rangle$ [%], while the derived linearised manufacturing zone temperature and humidity models assume the input signal to be normalised in the range $u = \langle 0, 1 \rangle$. Therefore, the process gains of these two models must be divided by 100 so that the models can be used for the purpose of control tuning. Additionally, the digital implementation of the PI controller introduces half of the effective rescheduling time delay in the control loop. Skogestad (2003) recommends in such circumstances to add half of the rescheduling time to the modelled time delay.

Dividing the process gain of the linearised manufacturing zone temperature model (6.28) by 100 and adding half of the rescheduling time to the modelled time delay, i.e. $\tau_T + h/2$, the linearised temperature model considered for subsequent control tuning is

$$G_T(s) = \frac{-0.2461}{381.6204s + 1} \exp(-181.5s) \quad (6.35)$$

with $K_T = -0.2461$, $T_T = 381.6204$ [s] and $\tau_T = 181.5$ [s]. The linearised manufacturing zone humidity model (6.34) then becomes

$$G_H(s) = \frac{-1.3150}{1054.0164s + 1} \exp(-136.5s) \quad (6.36)$$

with $K_H = -1.3150$, $T_H = 1054.0164$ [s] and $\tau_H = 136.5$ [s].

The adopted SIMC tuning rule for the PI controller, proposed in (Skogestad 2003, Skogestad & Grimholt 2012), is stated as follows

$$K_p = \frac{1}{K} \frac{T}{T_c + \tau} \quad (6.37)$$

$$T_i = \min\{T, 4(T_c + \tau)\} \quad (6.38)$$

where K denotes the process gain, T [s] denotes the process time constant, τ denotes the time delay and T_c is the tuning parameter. The tuning parameter T_c is the desired process time constant of the closed-loop system.

The robustness measure considered by the SIMC tuning rule is the maximum sensitivity peak M_s , see Remark 6.1 for the definition. Åström & Hägglund (2006) state that ‘reasonable’ values for the maximum sensitivity are in the interval $M_s = \langle 1.25, 2 \rangle$. The larger values of M_s correspond to active, less robust, control setting, while the lower values correspond to stable and slow closed-loop response. Therefore, by adjusting the M_s stability criterion the trade-off between the control stability and performance is made. To obtain ‘tight control’ performance subject to good robustness (smooth control), it is recommended in (Skogestad 2003) to select T_c to be the time delay, i.e. $T_c = \tau$. Consequently, if $T_c = \tau$ then the guaranteed minimal robustness by the SIMC tuning rule is $M_s = 1.59$.

Remark 6.1 The maximum sensitivity peak, denoted M_s , is the worst case amplification of the load disturbances and is also a robustness measure when considering the influence of process uncertainties on the closed-loop performance (Åström & Hägglund 2006).

Consider the block diagram representation of the control system given in Figure 6.1 and let the Laplace transforms of the load disturbance signal, the mea-

surement noise signal and the system output to be denoted by $D(s)$, $N(s)$ and $Y(s)$, respectively. The closed-loop system response, denoted $Y_{cl}(s)$, of the system to signals $D(s)$ and $N(s)$ is

$$Y_{cl}(s) = \frac{G(s)}{1 + C(s)G(s)}D(s) + \frac{1}{1 + C(s)G(s)}N(s) \quad (6.39)$$

and the open-loop system response, denoted $Y_{ol}(s)$, is expressed as

$$Y_{ol}(s) = G(s)D(s) + N(s) \quad (6.40)$$

Defining the sensitivity transfer function, denoted $S(s)$, to be

$$S(s) = \frac{1}{1 + C(s)G(s)} \quad (6.41)$$

then the following relation between the system closed-loop and open-loop responses holds

$$\frac{Y_{cl}(s)}{Y_{ol}(s)} = S(s) \quad (6.42)$$

The relation (6.42) shows the effect of feedback on the attenuation of load disturbance $D(s)$ and noise $N(s)$ signals under closed-loop control. The worst case amplification of the load disturbances is the maximum sensitivity, thus M_s is defined as

$$M_s = \max_{\omega} |S(j\omega)| \quad (6.43)$$

where $S(j\omega)$ denotes the frequency response function of $S(s)$ and ω [rad/s] is the frequency. ■

The SIMC tuning rule (6.37) has been applied to the linearised manufacturing zone temperature and humidity models, stated in (6.35) and in (6.36), respectively. The PI controller gains obtained are given in Table 6.3 together with the originally implemented control gains (by Trend Control Systems Ltd). The integral time constant T_i is provided in minutes, rather than seconds, since the control system accepts only minutes as units of time.

It can be seen in Table 6.3, that the originally implemented control gains are the same for both the temperature and humidity control loops. Comparing the original and newly proposed proportional gains, it can be noted that the original proportional gains are very high (absolute value) compared to the newly proposed gains. Additionally, the integral time constants of the original controller are low compared to the newly proposed constants. This indicates, that the original

Table 6.3: The originally implemented and newly proposed PI control gains for the temperature and humidity control loops.

Temperature control loop	
Originally implemented	Newly proposed
$K_p = -30$ $T_i = 5$ [min]	$K_p = -4.27$ $T_i = 6.36$ [min]
Humidity control loop	
Originally implemented	Newly proposed
$K_p = -30$ $T_i = 5$ [min]	$K_p = -2.94$ $T_i = 17.6$ [min]

control tuning has been rather aggressive, which eventually leads to the observed oscillations in the controlled process variables.

6.4.1 Closed-loop system stability

The newly proposed control gains, given in Table 6.3, are used to calculate the maximum sensitivity values for the temperature and humidity control loops at the point of tuning. The maximum sensitivity is calculated according to definition (6.43), where the sensitivity function $S(s)$, defined in (6.41), is required. The sensitivity function for the temperature control loop is given by

$$S_T(s) = \frac{1}{1 + C(s)G_T(s)} \quad (6.44)$$

where $C(s)$ is the transfer function of the PI controller defined in (6.2) and $G_T(s)$ is the transfer function of the linearised manufacturing zone temperature model given in (6.35). The sensitivity function for the humidity control loop is defined as follows

$$S_H(s) = \frac{1}{1 + C(s)G_H(s)} \quad (6.45)$$

where $G_H(s)$ is the linearised manufacturing zone humidity model provided in (6.36). Subsequently, the Matlab (software version 2011b) function `bode` has been applied to find the maximum sensitivity values of $S_T(s)$ and $S_H(s)$. It has been found that the maximum sensitivity is the same for both control loops with the corresponding value $M_s = 1.5905$, which is in agreement with the expected values.

Once the PI controller for the temperature and humidity control loop has been designed at the selected operating point, it is desirable to examine the close-loop system stability over the whole operational range of the HVAC system. Therefore,

a bank of linearised models spanning the considered feasible operational ranges of the nonlinear manufacturing zone humidity and temperature models have been obtained. The linearised models have been obtained in the same manner as the single linearised models at the assumed least stable point of operation. The feasible operational range for the temperature model is $u_c = \langle 0, 17.19 \rangle$ [%], $T_{ai} = \langle 22.16, 35 \rangle$ [°C] and $q = 0$ [kW], see the steady-state characteristic analysis in Subsection 6.2.1. The considered operational range for the humidity model is $u_g = \langle 24, 100 \rangle$ [%]. Subsequently, having obtained a bank of linearised models the M_s robustness measure has been evaluated using the derived PI controllers for both the temperature and humidity control loops.

Figure 6.8 shows the maximum sensitivity as a function of the control input for the temperature control loop (left-hand side subplot) and the humidity control loop (right-hand side subplot). The grey solid lines highlight the point of operation for which the PI controllers have been tuned, where the achieved robustness is $M_s = 1.5905$ and the valve positions are $u_c = 10.3$ [%] and $u_g = 33.9$ [%]. Considering the temperature control loop the highest maximum sensitivity, which is also the least stable point of operation, is $M_s = 1.5910$ obtained at $u_c = 10.4$ [%]. The highest maximum sensitivity for the humidity control loop is $M_s = 1.6499$ occurring at $u_g = 36.6$ [%].

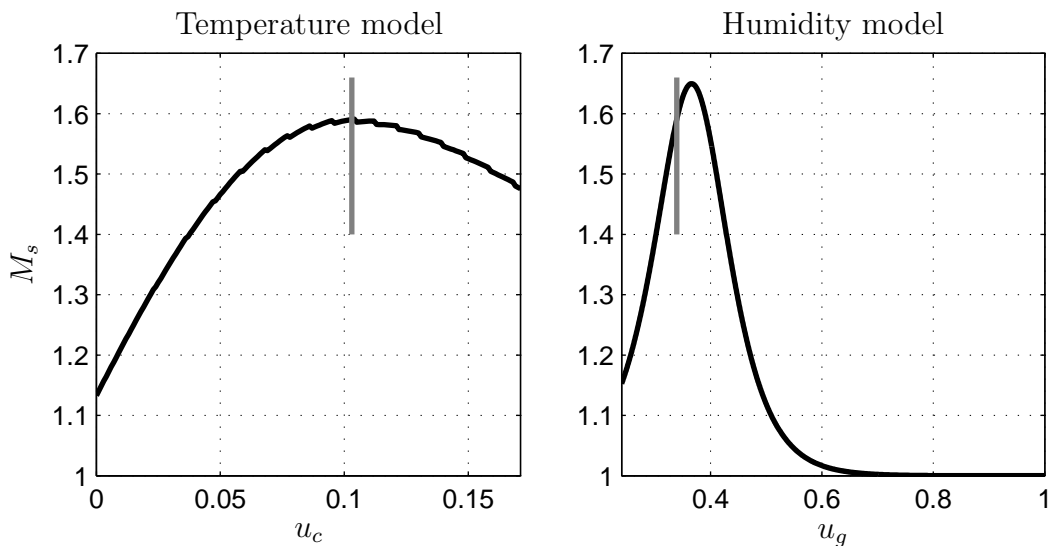


Figure 6.8: The maximum sensitivity peak value as a function of the control input (black solid line) plotted for the manufacturing zone temperature model (left-hand side plot) and manufacturing zone humidity model (right-hand side plot), respectively. The grey solid line highlights the point of operation for which the PI controller has been tuned.

It has been assumed, that the least stable point of operation is that for which the system has the highest (absolute value of) process gain. However, such a simplifying assumption does not take into account the influence of the varying (input dependent) process time constant on the closed-loop system stability. Figure 6.8 shows that if the maximum sensitivity is used as a measure of the closed-loop stability, then the least stable operating points occur at $u_c = 10.4$ [%] and $u_g = 36.6$ [%] for the temperature and humidity control loops rather than $u_c = 10.3$ [%] and $u_g = 33.9$ [%], respectively. The highest recommended maximum sensitivity is $M_s = 2$, see (Åström & Hägglund 2006), while the highest observed maximum sensitivity is $M_s = 1.6499$ for the humidity control loop. Therefore, the designed PI control gains, given in Table 6.3, are considered to be valid.

6.5 Implementation results

Figure 6.9 shows the measured control inputs and system outputs for the temperature and humidity control loops, respectively. The original control gains have been in use, see Table 6.3, and the data set has been acquired 29th April 2012. It is observed, that both control inputs, i.e. the cooling valve position $u_c(t_k)$ and the gas valve position $u_g(t_k)$, are highly varying. Consequently, the measured return air temperature T_{ar} and measured return air dew-point temperature T_{drm} oscillate around their respective set-point values (dashed grey line). It can be concluded that the original control implementation is overactive and not appropriate for the current application.

Figure 6.10 shows the implementation results for the newly proposed control gains. The measurements have been acquired 13st July 2012. The implementation results for the temperature control loop are considered first. It is observed, that accurate and stable control performance has been achieved. Furthermore, it is noted that a small, in magnitude, chattering of the control input is present. It should be emphasised, however, that it is the command signal, i.e. the computed output of the controller, which has been plotted and not the cooling valve position (movement) itself. After detailed examination of the shape of the control input signal, it can be seen that the shape of the oscillations is not of a sinusoidal character, as it would be in the case of tight (aggressive) control tuning, but resembles rather a sawtooth wave signal. This triangular shape indicates, that the oscillations are not caused by inappropriate tuning, but may be attributed to the so called valve stiction effect (Shinskey 1996). The valve stiction is caused by friction forces inside the valve, which prevent the valve from moving until

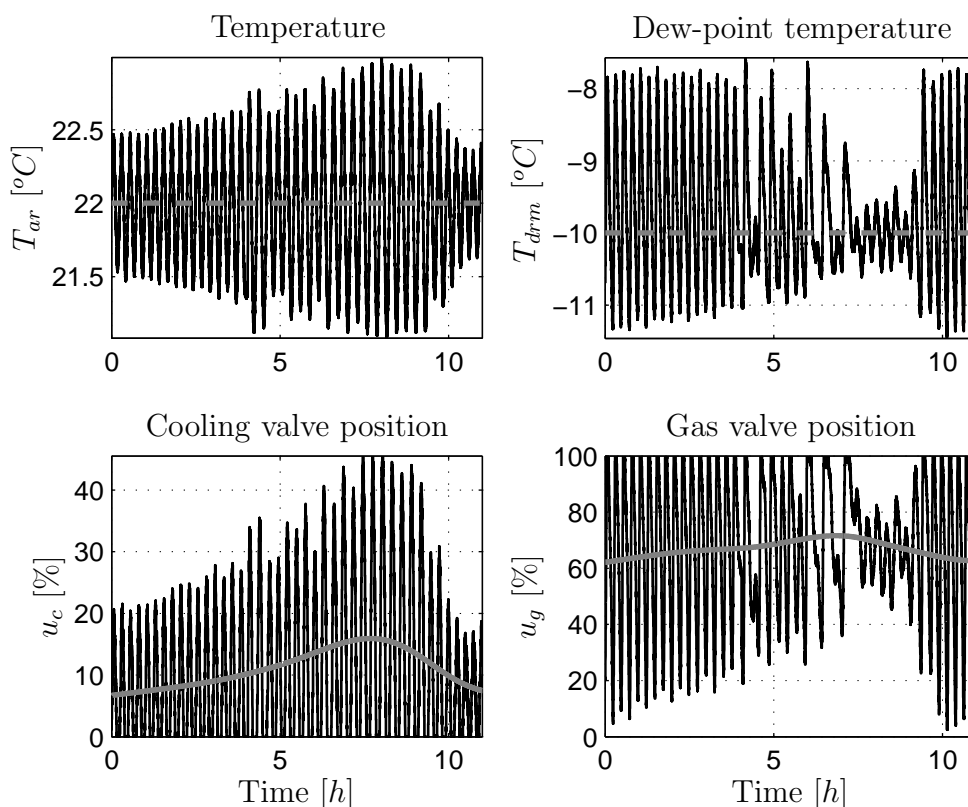


Figure 6.9: Measured input-output data for the original control tuning. The two left-hand side subplots relates to the temperature control loop, while the two right-hand side subplots relates to the humidity control loop. The dashed grey lines show the respective control set-points. The solid grey lines show the estimated trends for the valve movements.

the new demanded valve stem position is greater than a certain threshold value. Therefore, the technical limits of the HVAC system have been reached and further control improvements are not considered to be feasible.

The implementation results for the humidity control loop are shown in the two right-hand side subplots of Figure 6.10. It is observed that a smooth and stable control performance has been achieved together with good set-point tracking. Subsequently, Figure 6.11 shows in more detail the first 30 minutes of the measured input-output data. It can be observed, that the oscillatory pattern is present in the measurement of the return dew-point temperature. This is the same oscillatory pattern, which has been described in detail in Section 5.2.1. More importantly, it can be observed that the control input (gas valve command signal) also oscillates accordingly, i.e. the PI controller reacts to the measured

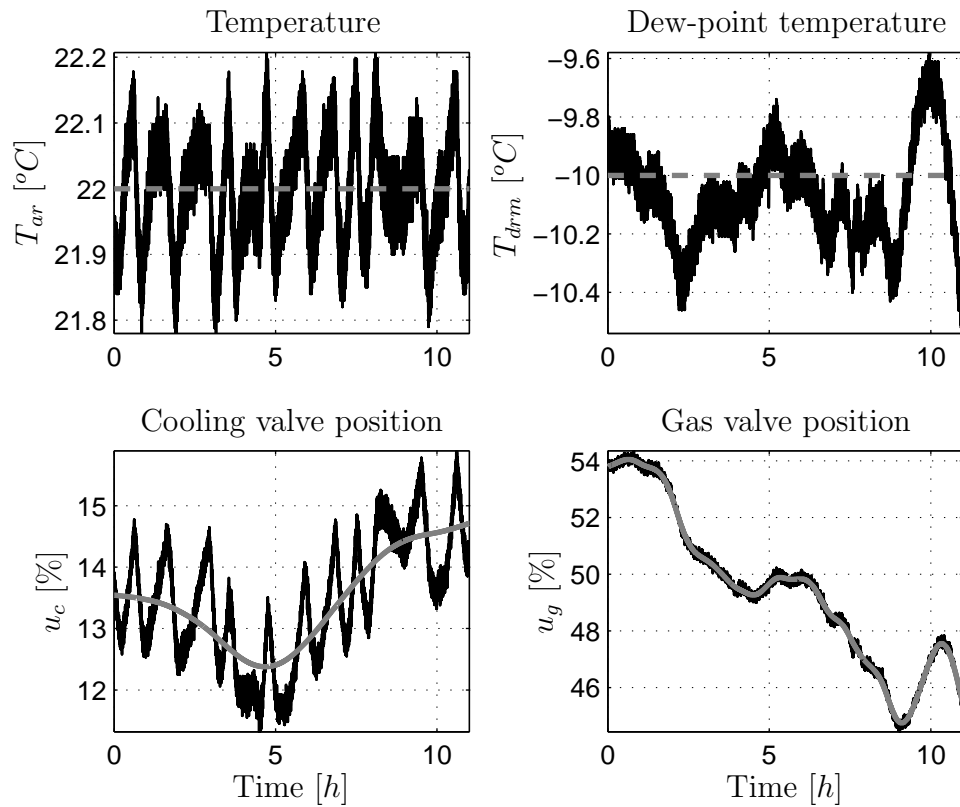


Figure 6.10: Implementation results for the proposed control tuning. The two left-hand side subplots relates to the temperature control loop, while the two right-hand side subplots relates to the humidity control loop. The dashed grey lines show the respective control set-points. The solid grey lines show the estimated trends for the valve movements.

oscillations. Consequently, it is assumed that the observed ‘oscillatory pattern’ may have potentially induced the sustained oscillatory behaviour of the closed-loop system having the original control gains, as observed in Figure 6.9.

6.5.1 Evaluation of implementation results

There are two main control interests, which can be extracted from the acquired measurements. It is desirable to know how accurately the controller is able to regulate the process variable (air temperature or air humidity) around the control set-point. The second control interest is how smooth and non-oscillatory the control action is.

The ability of the controller to track the demanded set-point is evaluated by calculating a mean value of the two regulated process variables together with

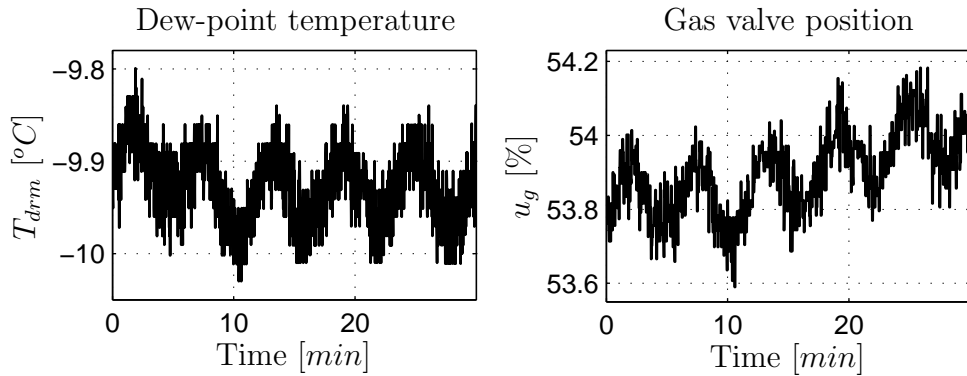


Figure 6.11: Implementation results for the proposed control tuning, zoomed in for the first 30 minutes of measured input-output data for the humidity control loop.

the associated standard deviations. The mean value of the measured return air temperature, denoted \bar{T}_{ar} [$^{\circ}C$], and the mean value of the measured return air dew-point temperature, denoted \bar{T}_{drm} [$^{\circ}C$], should be as close as possible to the demanded set-points. The associated standard deviations, denoted $SD_{\bar{T}_{ar}}$ [$^{\circ}C$] and $SD_{\bar{T}_{drm}}$ [$^{\circ}C$], respectively, should be sufficiently small. The standard deviations are calculated based on the definition given in equation (3.120).

The smoothness of the control signal is assessed by calculating the standard deviations of the cooling valve and gas valve de-trended control inputs, denoted SD_{u_c} [%] and SD_{u_g} [%], respectively. The standard deviation should be as small as possible. In other words, it is undesirable to have highly fluctuating (high SD value) control signals because of the excessive wear and tear of the control valves and potential non-optimal energy utilisation of the HVAC system. The control signals contain trends, displayed by grey solid lines in Figures 6.9 and 6.11, which are caused by controller compensating for external disturbances, e.g. outdoor temperature changes. It is assumed, that the input signal trends are of a slow character, while the fast oscillations and signal chattering is due to the control setting. It is the fast component of the measured control input signals, which is of interest when evaluating the control performance. Therefore, estimated trends are firstly subtracted from the corresponding measured control input signals and the standard deviations are calculated based on the de-trended signals.

To extract the trend of the input signals the integrated random walk smoothing and decimation function `irwsm` implemented in Captain Toolbox for Matlab, (Taylor, Pedregal, Young & Tych 2007), has been applied. This function uses a fixed interval smoothing algorithm based on the family of state-space random walk models, see (Young 2011) and references there in. The `irwsm` function has been

applied with the following settings: the integrated random walk model has been selected as the basis for the trend estimation and the noise variance ratio (NVR) hyper-parameter is selected based on visual inspection to be $NVR = 1 \times 10^{-14}$ for all the measured data except the $u_g(t_k)$ generated based on the newly proposed control gains. The NVR parameter used for the trend computation of the gas valve position input signal generated based on the newly proposed control gains is $NVR = 1 \times 10^{-11}$.

The final results are given in Table 6.4. It is clearly evident, that the implementation of the newly proposed control gains led to the overall improvement of the control performance. The calculated mean value of the measured return air temperature and dew-point temperature are closer to the demanded set-point and the associated standard deviations are significantly reduced, i.e. better tracking performance has been achieved. At the same time the actuation of the cooling valve and gas valve have been found to be significantly reduced.

Table 6.4: The control tuning results. The mean values and the associated standard deviations of the system outputs are shown together with the standard deviations of the control input signals.

Temperature control loop

Original tuning	Proposed tuning
$\bar{T}_{ar} = 21.9666 [^{\circ}C]$	$\bar{T}_{ar} = 21.9936 [^{\circ}C]$
$SD_{\bar{T}_{ar}} = 0.4490 [^{\circ}C]$	$SD_{\bar{T}_{ar}} = 0.0761 [^{\circ}C]$
$SD_{u_c} = 11.8634 [\%]$	$SD_{u_c} = 0.6044 [\%]$

Humidity control loop

Original tuning	Proposed tuning
$\bar{T}_{drm} = -9.7348 [^{\circ}C]$	$\bar{T}_{drm} = -10.0701 [^{\circ}C]$
$SD_{\bar{T}_{drm}} = 0.9326 [^{\circ}C]$	$SD_{\bar{T}_{drm}} = 0.1630 [^{\circ}C]$
$SD_{u_g} = 25.6863 [\%]$	$SD_{u_g} = 0.1204 [\%]$

To further highlight the increased accuracy in the control of the process variables, Figure 6.12 shows the absolute value of the control error as a percentage of time. The control error is defined as the difference between the control set-point and the measured process variable and is defined in equation (6.6). Considering the temperature control loop first, it can be observed in Figure 6.12, that the absolute value of the control error never exceeded value of $0.22 \text{ }^{\circ}C$ as compared to the original value of $0.98 \text{ }^{\circ}C$. Similarly, considering the humidity control loop, the absolute value of the control error never exceeded value of $0.53 \text{ }^{\circ}C$ as compared to the original value of $2.4 \text{ }^{\circ}C$. This translates to a factor of four times in terms

of an increase in the control accuracy of the air temperature and almost a factor of five times increase in the control accuracy of the air dew-point temperature.

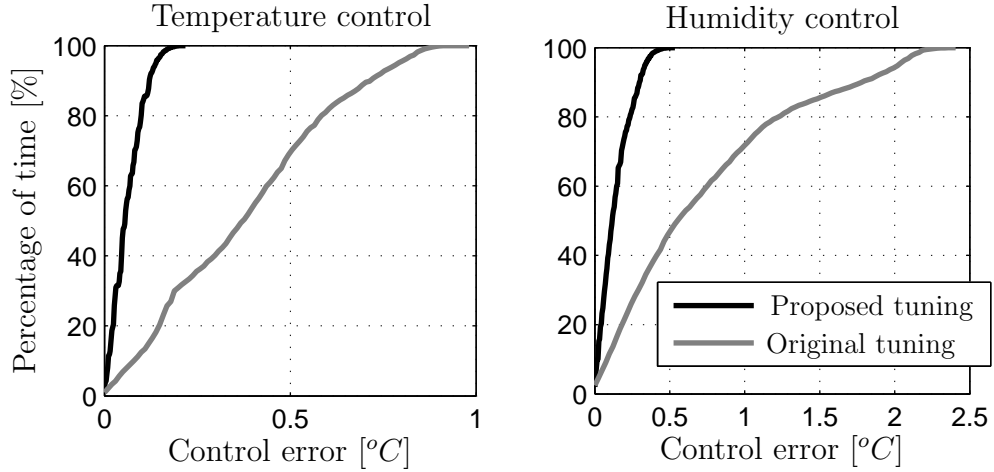


Figure 6.12: Absolute value of control error shown as a percentage of time.

6.6 Gas consumption analysis

A stable and tight control performance has been achieved by tuning the temperature and humidity feedback control loops. In return, this allows for operation close to the product specification limits, where the highest profitability can be obtained. The steady-state characteristic between the control humidity set-point and gas consumption of the dehumidification unit is obtained and analysed. In this regard, it is possible to evaluate the economical benefits of adjustment of the control set-point closer to the product specification limit. Moreover, such an energy characteristic may be used to assist in the decision of choosing an appropriate safety margin, i.e. the distance between the set-point and the product specification limit, where there is a trade-off between manufactured product safety and the economical benefits.

Under closed-loop operation in steady-state, the system output matches the demanded set-point. Therefore, considering the steady-state characteristic of the manufacturing zone humidity model derived in (6.30), and replacing the system output with the set-point, i.e. $T_{drm} = r_H$, the characteristic relating the control

input and humidity set-point is given by

$$\phi(u_g) = \frac{1}{1 + p_1 \exp(-p_2 u_g)} \quad (6.46a)$$

$$r_H = \frac{\frac{\beta_0}{\alpha_1} \phi(u_g) + o}{1 - \frac{\eta}{\alpha_1} \phi(u_g)} + \frac{\beta_0^r}{\alpha_1^r} T_{df} \quad (6.46b)$$

where the static input function has been originally defined in (6.29a) and the model parameters are provided in Table 6.2.

The static characteristic (6.46) shows the steady-state relationship between the gas valve position u_g and the set-point value r_H . Subsequently, the relationship between the gas valve position and the actual gas consumption of the dehumidification unit is, cf. (5.67), hence

$$V_g = \frac{V_{g,max}}{1 + p_1^r \exp(-p_2^r u_g)} \quad (6.47)$$

where V_g [m^3/h] denotes the gas volumetric flow and $V_{g,max}$ [m^3/h] denotes the maximal gas volumetric flow measured for a fully opened gas valve. The maximal gas volumetric flow is equal to $V_{g,max} = 3.2791$ [m^3/h], see Table 5.4. The parameters p_1^r and p_2^r are estimated in (5.71), where these parameters are denoted p_1 and p_2 , respectively. The superscript r has been added to highlight that these parameters differ in value from parameters p_1 and p_2 used in (6.46).

For the considered gas consumption analysis the value of the dew-point temperature of the fresh air supply T_{df} is required. Since such temperature will vary based on the day to day weather conditions it would be advantageous to know the average annual T_{df} temperature, which would then reflect an average annual gas consumption of the dehumidification unit. Unfortunately, the readings of this temperature are not recorded as standard practice, hence the average annual value is not available. However, the average annual dew-point temperature of the outdoor air is available and is used here instead. The average annual dew-point temperature of the outdoor air for years 2010, 2011 and 2012 is 7.3 [$^{\circ}C$], 6.8 [$^{\circ}C$] and 4.3 [$^{\circ}C$], respectively. These dew-point temperatures were recorded by a weather station with designation number IOXFORDS29³ in Minster Lovell, Witney, UK, which is located 2.5 [km] away from the Abbott Diabetes Care site.

The difference between the average annual dew-point temperature of the outdoor air and the temperature of the fresh air supply is that the average annual dew-point temperature of the fresh air supply will be lower. If the dew-point

³The data were retrieved from www.wunderground.com.

temperature of the outdoor air, entering the fresh air plant, is higher than 10 °C, then part of the air moisture will condense on the cooling coil of the fresh air plant. Therefore, the average annual gas consumption deduced based on the conducted gas consumption analysis will be somewhat inflated.

For the gas valve position in the range $u_g = \langle 0.24, 1 \rangle$ the corresponding set-point values and gas volumetric flows are calculated using (6.46) and (6.47), respectively. Subsequently, the results are shown in Figure 6.13, where the humidity set-point is expressed in terms of a dew-point temperature scale (the left-hand side plot) and in terms of a relative humidity scale (the right-hand side plot) assuming $r_T = 22$ [°C]. Two static characteristic curves for the average annual fresh air supply air dew-point temperatures $T_{df} = 7.3$ [°C] (black solid line) and $T_{df} = 4.3$ [°C] (dark grey solid line) are shown. The humidity set-point is $r_H = -10$ [°C] (black dashed line), which is plotted on the left-hand side plot. The equivalent set-point value in terms of the relative humidity scale is an air temperature dependent quantity. In the case when the air handling unit is in cooling mode the zone temperature set-point is $r_T = 22$ [°C], while for the heating mode the zone temperature set-point is $r_T = 21$ [°C], see Subsection 6.1.2. Consequently, with reference to Subsection 6.1.2, the corresponding zone relative humidity set-point values are $r_H = 10.8$ [%] at $r_T = 22$ [°C] (light grey dashed line) and $r_H = 11.5$ [%] at $r_T = 21$ [°C] (dark grey dashed line), see left-hand side of Figure 6.13.

6.6.1 Observations

Figure 6.13 shows that the gas consumption characteristic has an approximately constant negative slope in the region of the control safety margin, i.e. the distance between the set-point and the product specification limit. The gas consumption characteristic decreases at a rate of approximately 0.1 [m³/h] of gas volumetric flow per 1 [°C] of the set-point value (dew-point temperature scale). Therefore, if the set-point is to be increased, i.e. the control safety margin is reduced, then the gas consumption of the dehumidification unit could be reduced by approximately 0.1 [m³/h] per 1 [°C] of the set-point adjustment.

Considering the left-hand side plot of Figure 6.13, it is noted, that the characteristic curve moves horizontally towards the decreasing values of r_H for decreasing values of T_{df} , while its shape is preserved. Although the ‘exact’ value of T_{df} is unknown and changes on day to day bases, its value has only a small influence on the slope of the characteristic curve for a given set-point value (in the control

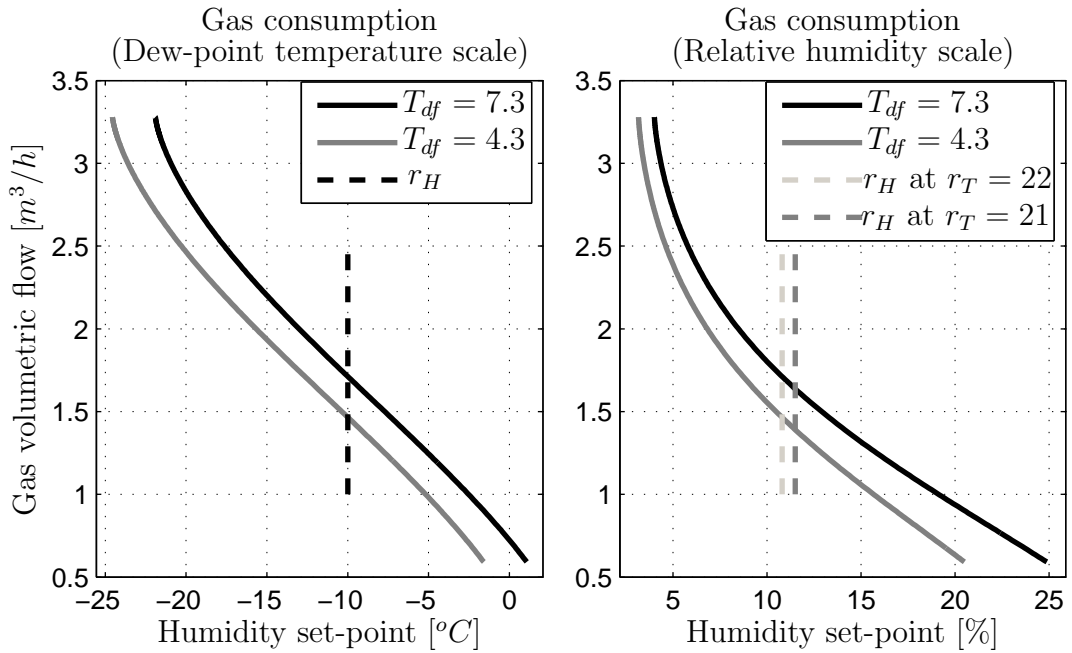


Figure 6.13: Gas consumption of the dehumidification unit as a function of the manufacturing zone humidity set-point.

safety margin region). In other words, the potential for gas savings by set-point adjustment is approximately preserved, despite the variations of the actual value of T_{df} .

Furthermore, it should be emphasised, that increasing the humidity set-point decreases the amount of heat generated by the dehumidification unit. Consequently, the air handling unit must remove less heat from the conditioned air so that the demanded zone temperature set-point is achieved. Therefore, less chilled water is required by the air handling unit, which additionally generates electricity savings on the side of the water chillers, see (Zajic, Larkowski, Hill & Burnham 2011) for a more detailed discussion.

6.7 Conclusions

The control analysis and tuning of an industrial HVAC control system has been investigated. The Hammerstein-bilinear air temperature and humidity models of an environmentally controlled clean room manufacturing zone identified in Chapter 5, have been used for the purpose of control analysis. The main results of the control analysis has been the selection of feasible operation ranges of the HVAC system and the subsequent selection of critical operating points for which the

control system has been tuned. It should be emphasized, that the uncertainties of the model parameter estimates could have been potentially taken into consideration during the control analysis and design stage providing enhanced insights into the closed-loop control performance.

The control analysis has revealed that only certain combinations of system outputs and inputs are feasible if the control system regulates the system outputs (air temperature and humidity) at the demanded set-points. Therefore, not all dynamic modes of the nonlinear HVAC system are active, which greatly limits the operating space for which the control system should be tuned. Therefore, the knowledge of the system nonlinearities is beneficial and, in return, reinforces the advantage of possessing a well structured nonlinear models prior to control tuning and design.

The obtained PI control gains have been implemented and tested on the HVAC system located in Abbott Diabetes Care, UK. The implementation of the newly proposed control gains has led to an overall improvement of the control performance. The originally observed oscillatory behaviour of the closed-loop control system has been eliminated and accurate set-point tracking has been achieved despite the influence of the load disturbances on the system.

The last contribution of this chapter highlights the potential for energy (gas) savings via the adjustment of the humidity control set-point. It is argued, that the improved control performance allows for the operation closer to the air humidity product specification limit, where the highest profitability can be obtained. The steady-state characteristic between the control humidity set-point and gas consumption of the dehumidification unit has been obtained. In this regard, it is possible to evaluate the economical benefits of adjustment of the control set-point closer to the product specification limit, where there is a trade-off between manufactured product safety and the potential for significant economical benefits.

Chapter 7

Conclusions & future research directions

7.1 Conclusions

Motivated by the physical phenomena occurring in a general HVAC system a Hammerstein-bilinear model structure has been introduced, which offers improved modelling capabilities yet retains a close link to well understood linear models. The well established simplified refined instrumental variable method for linear transfer function model parameter estimation has been extended to encompass a Hammerstein-bilinear model class both in the continuous-time and discrete-time domains. An emphasis has been placed on the applicability of the algorithms to real problems and the ability of the algorithms to work under real system identification scenarios. The resulting parameter estimation algorithms are in themselves innovative in the system identification area and complement a variety of existing algorithms. Furthermore, due to the flexibility of the introduced Hammerstein-bilinear model structure it is possible to adequately model physical phenomena occurring in a wide range of real systems, which increases the applicability of the presented research. This, in return, forms the basis for the concept of a so-called Hammerstein-bilinear approach to modelling and control of real-world systems.

The Hammerstein-bilinear model class comprises Hammerstein and bilinear model structures as special cases, which, within the latter, linear models coexist as a special subclass. It has been shown, that the Hammerstein-bilinear model structure then combines the advantages of its constituent parts and can exhibit both, input dependent dynamic behaviour and increased flexibility of the steady-

state characteristics including the input multiplicity. Furthermore, since the input to the bilinear submodel is scaled by the static nonlinear function, the input dependent dynamics of the bilinear submodel also depend on the form of the static nonlinear function. However, it is this input dependent, hence static nonlinear function dependent, dynamic and steady-state behaviour of the Hammerstein-bilinear model, which creates a challenging system identification problem with potential benefits for real-world applications.

The most significant algorithmic outcome of this thesis has been the proposed extensions of the simplified refined instrumental variable parameter estimation method to handle the Hammerstein-bilinear model class. The simplified refined instrumental variable parameter estimation method is a unified time domain approach and the designed extensions have inherited this property. Therefore, the designed algorithms have been presented both in the continuous-time and discrete-time domains. There are several advantages of using continuous-time models for identification over the discrete-time counterparts. The single, most exploited, advantage in this thesis has been the preservation of the *a priori* physical knowledge incorporated in the continuous-time model structures, which has provided a physically meaningful insight into the modelled (analysed) system. However, it is emphasised that the presented estimation methods, both in the continuous-time and discrete-time domains, have been designed to complement one another and should be chosen based on the intended purpose of the estimated models. Additionally, the discrete-time parameter estimation methods require less *a priori* knowledge during the initialisation stage, therefore these methods can be used to appropriately initialise the continuous-time based methods should this be necessary.

The research has mainly focused on the estimation methods in the continuous-time domain due to the aforementioned physical interpretability of the continuous-time models and the fact that there is a paucity of research in the literature in the area of estimation of bilinear and Hammerstein-bilinear model structures in the continuous-time domain. The simplified refined instrumental variable method for the estimation of continuous-time transfer function models, abbreviated SRIVC, has been extended to the bilinear case, where the corresponding algorithm has been abbreviated BSRIVC. The proposed BSRIVC algorithm is capable of estimation of higher order time-invariant single-input single-output bilinear models directly from the sampled input-output data. For the purpose of parameter estimation the bilinear model has been interpreted in time-step quasi-linear transfer function form, where the denominator parameters are system input dependent

quantities. The SRIVC algorithm uses a state variable filter approach to generate the filtered time derivatives of sampled input-output signals, where a linear optimal prefilter is selected as the auto-regressive part of the estimated transfer function model. Since the BSRIVC algorithm is based on the time-step quasi-linear transfer function interpretation of the estimated bilinear model, the parameters of the optimal prefilter are also system input dependent, i.e. the prefilter is adaptive and no longer linear. Subsequently, to solve for the unknown parameter estimates an iterative, bootstrapping, solution has been employed, where the parameters of the optimal prefilter are updated in an iterative manner based on the latest estimate of the transfer function model parameters.

Exploiting the iterative nature of the BSRIVC algorithm, and postulating that the static input function is parameterized by a linear-in-parameters polynomial function of finite order, the Hammerstein-bilinear SRIVC (HBSRIVC) algorithm has been designed for the estimation of Hammerstein-bilinear models. This general estimation algorithm then includes the BSRIVC and SRIVC algorithms as special cases in a similar manner to the Hammerstein-bilinear model structure including Hammerstein and bilinear model structures as special cases. Furthermore, the HBSRIVC algorithm is applicable to Hammerstein models as well. The proposed parameter estimation methods differ from the existing, reviewed methods, in their simplicity of implementation, usage and the noise scenarios under which consistent parameter estimates are obtained.

A further significant contribution presented in this thesis is the observation that if the parameters of the considered continuous-time single-input single-output bilinear model are constrained in a predefined way, then the original bilinear model can be interpreted for the purpose of parameter estimation as a two-input single-output linear (in structure) transfer function model. In return, this facilitates the use of well established linear parameter estimation methods. Based on this observation, the SRIVC algorithm has been configured for such an identification scenario and, in a similar manner to the HBSRIVC algorithm, the iterative HSRIVC algorithm has been proposed for the estimation of Hammerstein(-bilinear) models. Since the bilinear model parameters are restricted, the applicability of this approach is also system identification case scenario specific. However, it has been demonstrated on a simple example of a first principles model of a heat exchanger, that the constrained bilinear model structure may naturally occur in the case of HVAC system applications. The developed approach provides a conceptual stepping stone towards the more general less restricted extensions.

The SRIVC and HSRIVC parameter estimation methods configured for the bilinear and Hammerstein-bilinear model estimation can be viewed as being complementary to the BSRIVC and HBSRIVC algorithms, respectively, and can be used during the initialisation stages of these. The main difference comprises the use of linear prefilters instead of adaptive, input dependent, prefilters. This creates a set of linear parameter estimation methods, which are straightforward to initialise, and the implementation complexity is reduced.

It is advantageous to subtract the baselines (initial values) of the measured system input-output signals prior to model parameter estimation. This, of course, does not impose any problems when a linear model is being estimated. However, the steady-state and dynamic behaviour of the bilinear model is operating point dependent. Therefore, the estimated parameters of the continuous-time (or discrete-time) bilinear model are also operating point dependent quantities. Consequently, the estimated parameters of the bilinear model are valid only for the input-output signals with the subtracted baselines.

By exploiting the mathematical structure of the bilinear models a procedure to adjust the estimated parameters for a prescribed (or any) operating point has been suggested. This procedure then allows the steady-state and dynamic characteristics of the bilinear model to be corrected for any given operating point, while the estimated model parameters are obtained for the baseline operating point, thus retaining the input dependency of the model. To the best knowledge of the author, it is believed that such a procedure has not to date been considered within the context of the bilinear model parameter estimation problem. Note, that the estimated parameters of the static input nonlinearity are not influenced by the operating point of the system, hence these do not need to be adjusted (modified).

7.1.1 Heating ventilation and air conditioning system application

The use of the designed parameter estimation methods has been demonstrated on the modelling and control implementation challenge of the industrial HVAC system located at Abbott Diabetes Care, UK. Moreover, it has been this intended application to HVAC systems, which has motivated the development of the presented identification methods and approaches in the first place. The research aim has been to develop dynamic control system design oriented air temperature and humidity models of an environmentally controlled clean room manufacturing

zone. These are considered to be suitable for subsequent control analysis and tuning of the associated commercial HVAC control system. In return, the well tuned control system permits an energy efficient operation of the HVAC system leading to an overall reduction in energy consumption.

The identified models are innovative in themselves and are contributions to the field of HVAC systems modelling. Overall, three separate control oriented models have been identified in the continuous-time domain, namely, a linear zone (room) temperature model, a Hammerstein-bilinear temperature model of an industrial air handling unit and a Hammerstein-bilinear manufacturing zone humidity model. The continuous-time domain has been selected mainly because of the physical meaningful insight gained into the behaviour of the modelled system and suitability of the continuous-time models for the conducted control analysis and tuning of the corresponding commercial HVAC control system.

To the best knowledge of the author a significant contribution to the field of HVAC system modelling has been the single development of the Hammerstein-bilinear manufacturing zone humidity model, which relates the manipulated variable (control input) to the regulated manufacturing zone air humidity. The single active component of the HVAC system, which removes the moisture from the conditioned air, is the desiccant rotor based dehumidification unit. The reviewed models of the desiccant rotors are predominantly intended for the design and performance evaluation of the dehumidification units, i.e. models for design purposes. The reviewed models of the desiccant rotors, however, have not been found to be suitable for the purpose of control; these models are either static and do not encompass the system dominant dynamic behaviour or the models are too complex, being based on physical laws and computationally demanding.

In the context of models for control analysis and tuning, it is considered that the zone humidity model has not been modelled using a Hammerstein-bilinear approach before, and furthermore the advantages of such an approach have been realised for the first time. Whilst the suboptimal control performance on such plants is tolerable, the increased energy consumption is becoming increasingly an issue nowadays with concern for high energy costs and the effect on the natural environment. Therefore, it can only be assumed, that the general paucity of control oriented models within the literature has been caused, to some extent, by a lack of demand in the past, where the energy consumption issue has not been the main consideration. The HVAC commercial control system has been re-tuned using the models developed for the HVAC system and components, whereby improved control has been achieved via a greater insight into factors

such as nonlinear input dependent process gains and time constants.

The greater insights afforded by knowledge of the system nonlinearities when adopting a nonlinear model based approach are immense, and the corresponding well structured mathematical models, e.g. the Hammerstein-bilinear modelling and control approach applied to the HVAC system, provides a transparent, well grounded engineering framework. Such a framework allows not only effective control but also, and probably more importantly, a well structured approach for nonlinear systems modelling, analysis and design.

7.2 Proposals for future work

The potential research topics of interest, which either directly stem from or are motivated by the conducted research into the Hammerstein-bilinear modelling and control approach, are summarised below:

- A development of recursive realisations of some of the proposed parameter estimation methods, both in continuous-time and discrete-time domains, would be an area of an immediate research interest. The recursive implementations of the proposed estimation methods could be used off-line, where such recursive estimation/analysis would provide further insight into the modelled system. Furthermore, the recursive realisations for an on-line implementation are also worth considering.
- Extensions of the designed parameter estimation methods for bilinear and Hammerstein-bilinear model structures to handle an auto-regressive with moving-average (ARMA) process noise model. This would broaden the noise scenarios under which an unbiased and statistically efficient parameter estimates are obtained. Therefore, the proposed further extensions would be based on the refined instrumental variable methods, summarised in (Young 2011), instead of the currently utilised simplified refined instrumental variable methods.
- Investigate further extensions of the simplified refined instrumental variable method to encompass a bilinear-Wiener and Hammerstein-bilinear-Wiener nonlinear model structures. It is assumed, that such extensions would even further increase the applicability of the presented research for a wider class of real-world problems, while retaining a well structured mathematical framework for nonlinear control system design.

- Another research area of interest might be that of model based robust control design, where such methods may incorporate the knowledge about the system nonlinearities as parameter uncertainties of a linear model structure upon which the control law is derived. Olalla, Queinnec, Leyva & Aroudi (2011) considered a robust control design based on a bilinear system model. It is proposed to further extended and build on such an approach to accommodate for the Hammerstein-bilinear model structure.
- An Investigation of convergence properties of the proposed parameter estimation methods via numerical studies would be of interest. Such a convergence analysis should be conducted alongside the selection of persistently exciting input signals for bilinear and Hammerstein-bilinear models. Barker et al. (2004) propose an optimisation procedure for the design of optimal multi-level input signals for Hammerstein model estimation. It is believed that such an approach could be potentially extended for the Hammerstein-bilinear case, where the input dependent dynamic behaviour of the bilinear submodel should be considered.
- It has been assumed, that by design, the influence of the cooling and heating coils of the HVAC air handling unit on the temperature of passing air is equivalent, however having opposite effects. Therefore, it has been anticipated that the identified manufacturing zone temperature model (including the effect of the cooling coil only) can be utilised for the purpose of model based tuning of both the PI controller for the cooling mode and the PI controller for the heating mode. The experimental study presented in Chapter 6, has so far only considered the cooling mode, therefore additional experimental work needs to be carried out to validate the proposed control approach for the heating mode.

References

- Åström, K. J. & Hägglund, T. (2006), *Advanced PID control*, ISA.
- Baheti, R., Mohler, R. & Spang, H. (1980), ‘Second-order correlation method for bilinear system identification’, *IEEE Trans. on Automatic Control* **25**, 1141–1146.
- Bai, E. W. (1998), ‘An optimal two-stage identification algorithm for Hammerstein-Wiener nonlinear systems’, *Automatica* **34**, 333–338.
- Bai, E. W. & Li, K. (2010), ‘Convergence of the iterative algorithm for a general Hammerstein system identification’, *Automatica* **46**, 1891–1896.
- Barker, H. A., Tan, A. H. & Godfrey, K. R. (2004), ‘Optimal levels of perturbation signals for nonlinear system identification’, *IEEE Trans. on Automatic Control* **49**, 1404–1407.
- Beccali, M., Butera, F., Guanella, R. & Adhikari, R. S. (2003), ‘Simplified models for the performance evaluation of desiccant wheel dehumidification’, *Int. J. of Energy Res.* **27**, 17–29.
- Belikov, J., Kotta, P. & Kotta, U. (2010), Realizability of bilinear input/output difference equations: Corrections and extensions, in ‘Proc. of UKACC Int. Conf. on Control 2010’, Coventry University, UK, pp. 138–143.
- Berhe, S. D. & Unbehauen, H. (1998), ‘Bilinear continuous-time systems identification via Hartley based modulating functions’, *Automatica* **34**(4), 499–503.
- Beven, K., Leedal, D., Smith, P. & Young, P. C. (2012), *System Identification, Environmental Modelling, and Control System Design*, Springer, chapter Identification and Representation of State Dependent Non-linearities in Flood Forecasting Using the DBM Methodology, pp. 359–385.
- Brehe, S. D. & Unbehauen, H. (1998), ‘Bilinear continuous-time systems identification via Hartley based modulating functions’, *Automatica* **34**(4), 499–503.

-
- Bruni, C., DiPillo, G. & Koch, G. (1974), 'Bilinear systems: An appealing class of 'nearly linear' systems in theory and applications', *IEEE Trans. on Automatic Control* **19**(4), 334–348.
- Buck, A. L. (1981), 'New equations for computing vapor pressure and enhancement factor', *J. of Applied Meteorology* **20**, 1527–1532.
- Burnham, K. J. (1991), Self-tuning Control for Bilinear Systems, PhD thesis, Coventry Polytechnic, UK.
- Burnham, K. J., Zajic, I. & Larkowski, T. (2011), Review of developments in bilinear systems modelling and control for efficient energy utilization on industrial plant, in 'Proc. of 24th Int. Conf. on Efficiency, Cost, Optimization, Simulation and Environmental Impact of Energy Systems', Novi Sad, Serbia, pp. 1856–1870.
- Çengel, Y. A. & Boles, M. A. (1994), *Thermodynamics: An engineering approach*, McGraw-Hill.
- Chang, F. H. I. & Luus, R. (1971), 'A noniterative method for identification using Hammerstein model', *IEEE Trans. on Automatic Control* **16**, 464–468.
- Coca, D. & Billings, S. A. (1999), 'A direct approach to identification of nonlinear differential models from discrete data', *Mech. Sys. and Signal Processing* **13**(5), 739–755.
- Dai, Y. J., Wang, R. Z. & Zhang, H. F. (2001), 'Parameter analysis to improve rotary desiccant dehumidification using a mathematical model', *Int. J. of Thermal Science* **40**, 400–408.
- Danne, T. (2008), Modeling and control optimisation of a heating ventilation and air conditioning system, Master's thesis, Coventry University, UK.
- Disdell, K. J. (1995), Bilinear Self-tuning Control for Multivariable High Temperature Furnace Applications, PhD thesis, Coventry University, UK.
- Dunoyer, A. (1996), Bilinear self-tuning control and bilinearisation with application to non-linear industrial systems, PhD thesis, Coventry University, UK.
- Dunoyer, A., Balmer, L., Burnham, K. J. & James, D. J. G. (1997), 'On the discretization of single-input single-output bilinear systems', *Int. J. of Control* **68**(2), 361–372.
-

-
- Ekman, M. (2005), Modeling and Control of Bilinear Systems: Applications to the Activated Sludge Process, PhD thesis, Uppsala University, Sweden. <http://uu.diva-portal.org/smash/get/diva2:166996/FULLTEXT01>.
- Ekman, M. (2008), 'Bilinear black-box identification and MPC of the activated sludge process', *J. of Process Control* **18**, 643–653.
- Eskinat, E., Johnson, S. H. & Luyben, W. L. (1991), 'Use of Hammerstein models in identification of nonlinear systems', *AIChE J.* **37**(2), 255–268.
- Gallman, P. G. (1976), 'A comparison of two hammerstein model identification algorithms', *IEEE Trans. on Automatic Control* **21**, 124–126.
- Garnier, H. & Wang, L., eds (2008), *Identification of continuous-time models from sampled data*, Springer.
- Garnier, H. & Young, P. (2012), What does continuous-time model identification have to offer?, in 'Proc. of 16th IFAC Symp. on System Identification'.
- Ge, T. S., Li, Y., Wang, R. Z. & Dai, Y. J. (2008), 'A review of the mathematical models for predicting rotary desiccant wheel', *Renewable & sustainable energy reviews* **12**, 1485–1528.
- Ghiaus, C., Chicinas, A. & Inard, C. (2007), 'Grey-box identification of air-handling unit element', *Control Eng. Practice* **15**, 421–433.
- Goodhart, S. G. (1991), Self-tuning Control of Industrial Systems, PhD thesis, Coventry Polytechnic, UK.
- Hsia, T. C. (1968), Least square method for nonlinear discrete system identification, in 'Asilomar Conf. Circuits and Systems', pp. 423–426.
- Hsia, T. C. (1976), A multi-stage least squares method for identifying Hammerstein model nonlinear systems, in 'IEEE Conf. on Decision and Control', Vol. 15, pp. 934–938.
- Huang, G. (2011), 'Model predictive control of VAV zone thermal systems concerning bi-linearity and gain nonlinearity', *Control Eng. Practice* **19**, 700–710.
- Ifeachor, E. C. & Jervis, B. W. (1993), *Digital signal processing: a practical approach*, Addison-Wesley.

-
- Jakeman, A. J. & Young, P. C. (1979), 'Refined instrumental variable methods of time-series analysis: Part II, multivariable systems', *Int. J. of Control* **29**, 621–644.
- Janczak, A. (2005), *Identification of nonlinear systems using neural networks and polynomial models*, Springer-Verlag.
- Jeong, J. W. & Mumma, S. A. (2005), 'Practical thermal performance correlation for molecular sieve and silica gel loaded enthalpy wheels', *Applied thermal engineering* **25**, 719–740.
- Jonsson, G. & Palsson, O. P. (1991), 'Use of empirical relations in parameters of heat-exchanger models', *Ind. Eng. Chem. Res.* **30**(6), 1193–1199.
- Jonsson, G. R., Lalot, S., Palsson, O. P. & Desmet, B. (2007), 'Use of extended Kalman filtering in detecting fouling in heat exchangers', *Int J. of Heat and Mass Transfer* **50**, 2643–2655.
- Karanam, V. R., Frick, P. A. & Mohler, R. R. (1978), 'Bilinear system identification by Walsh functions', *IEEE Trans. on Automatic Control* **23**, 709–713.
- Kohr, R. H. (1963), 'A method for determination of a differential equation model for simple nonlinear systems', *IEEE Trans. on Electron. Comput.* **12**, 394–400.
- Kotta, U., Nomn, S. & Zinober, A. S. I. (2003), On state space realizability of bilinear systems described by higher order difference equations, in 'Proc. of 42nd IEEE Conf. on Decision and Control', Hawaii, USA, pp. 5685–5690.
- Larkowski, T. (2009), Extended algorithms for the errors-in-variables identification, PhD thesis, Coventry University, UK.
- Larkowski, T. & Burnham, K. J. (2011), Bilinear approach to modelling of continuous stirred tank reactor process, in 'Proc. of ACD Workshop', Budapest, Hungary.
- Laurian, V., Gilson, M., Garnier, H. & Young, P. C. (2008), Refined instrumental variable methods for identification of Hammerstein continuous-time Box-Jenkins models, in 'Proc. of 47th IEEE Conf. on Decision and Control', Cancun, Mexico.

- Le, F., Markovsky, I., Freeman, C. & Rogers, E. (2010), 'Identification of electrically stimulated muscle models of stroke patients', *Control Eng. Practice* **18**, 396–407.
- Le, F., Markovsky, I., Freeman, C. & Rogers, E. (2011), Recursive identification of Hammerstein systems, in 'Proc. of 18th IFAC World Congress', Milan, Italy.
- Lees, M. J., Young, P. C., Chotai, A. & Tych, W. (1995), 'A non-minimal state variable feedback approach to multivariable control of glasshouse climate', *Trans. Inst. Measurement and Control* **17**, 200–211.
- Levenmore, G. (2000), *Building control systems - CIBSE guide H*, Butterworth-Heinemann, Oxford.
- Lim, D., Rasmussen, B. P. & Swaroop, D. (2009), 'Selecting PID control gains for nonlinear HVAC&R systems', *HVAC&R Research* **15**(6), 991–1019.
- Liu, X., Wang, J. & Zheng, W. X. (2011), 'Convergence analysis of refined instrumental variable method for continuous-time system identification', *IET Control Theory and Applications* **5**(7), 868–877.
- Liu, Y. & Bai, E. W. (2007), 'Iterative identification of Hammerstein systems', *Automatica* **43**, 346–354.
- Ljung, L. (1999), *System Identification - Theory for the user*, PTR Prentice Hall Information and System Sciences Series, 2nd edn, Prentice Hall, New Jersey.
- Martineau, S. (2004), Nonlinear Model-based Control System Design with Application to Industrial Furnaces, PhD thesis, Coventry University, UK.
- Martineau, S., Burnham, K. J., Haas, O. C. L., Andrews, G. & Heeley, A. (2003), 'Four-term bilinear PID controller applied to an industrial furnace', *Control Eng. Practice* **12**, 457–464.
- Minihan, J. A. (2001), Design of Bilinear Controllers for Industrial Plant, PhD thesis, Coventry University, UK.
- Mohler, R. R. (1973), *Bilinear control processes: with applications to engineering, ecology and medicine*, Vol. 106 of *Mathematics In Science and Engineering*, Academic Press, UK.

-
- Mohler, R. R. & Kolodziej, W. J. (1980), ‘An overview of bilinear system theory and applications’, *IEEE Trans. on Systems, Man, and Cybernetics* **10**(10), 683–688.
- Narendra, K. S. & Gallman, P. (1966), ‘An iterative method for the identification of nonlinear systems using a Hammerstein model’, *IEEE Trans. on Automatic Control* **11**, 546–550.
- Ni, B., Garnier, H. & Gilson, M. (2012), A refined instrumental variable method for Hammerstein-Wiener continuous-time model identification, in ‘Proc. of 16th IFAC Symp. on System Identification’.
- Nia, F. E., Paassen, D. V. & Saidi, M. H. (2006), ‘Modeling and simulation of desiccant wheel for air conditioning’, *Energy and buildings* **38**, 1230–1239.
- Nise, N. S. (2008), *Control systems engineering*, John Wiley and Sons.
- Olalla, C., Queinnec, I., Leyva, R. & Aroudi, A. E. (2011), ‘Robust optimal control of bilinear DC-DC converters’, *Control Eng. Practice* **19**, 688–699.
- Pearson, R. K. (1999), *Discrete-Time Dynamic Models*, Oxford University Press, New York.
- Pearson, R. K. (2003), ‘Selecting nonlinear model structures for computer control’, *J. of Process Control* **13**, 1–26.
- Pearson, R. K. & Kotta, U. (2004), ‘Nonlinear discrete-time models: state-space vs. I/O representation’, *J. of Process Control* **14**, 533–538.
- Price, L., Young, P., Berckmans, D., Janssens, K. & Taylor, J. (1999), ‘Data-based mechanistic modelling (DBM) and control of mass and energy transfer in agricultural buildings’, *Annual reviews in Control* **23**, 71–82.
- Rangaiah, G. P. & Kariwala, V., eds (2012), *Plantwide control: Recent developments and applications*, John Wiley and Sons.
- Rao, G. P. & Unbehauen, H. (2006), Identification of continuous-time systems, in ‘IEE Proc. of Control Theory Appl.’, Vol. 153, pp. 185–220.
- Shinskey, F. G. (1996), *Process control systems: Application, design and tuning*, McGraw-Hill.
- Singhal, A. & Salsbury, T. I. (2007), ‘Characterization and cancellation of static nonlinearity in HVAC systems’, *ASHRAE Trans.* **113**, 391–399.

-
- Skogestad, S. (2003), ‘Simple analytic rules for model reduction and PID controller tuning’, *J. of Process Control* **13**, 291–309.
- Skogestad, S. & Grimholt, C. (2012), The SIMC method for smooth PID controller tuning, *in* ‘PID control in the third Millennium: Lessons learned and new approaches’, Springer-Verlag, London.
- Stoica, P. & Söderström, T. (1982), ‘Instrumental-variable methods for identification of Hammerstein systems’, *Int. J. of Control* **35**, 459–476.
- Taylor, C. J., Pedregal, D. J., Young, P. C. & Tych, W. (2007), ‘Environmental time series analysis and forecasting with the Captain Toolbox’, *Environmental modelling and software* **22**, 797–814. www.es.lancs.ac.uk/cres/captain.
- Taylor, C. J., Shaban, E. M., Stables, M. A. & Ako, S. (2007), ‘Proportional-integral-plus control applications of state-dependent parameter models’, *J. of Systems and Control Engineering* **221**(7), 1019–1032.
- Thomson, M., Schooling, S. P. & Soufian, M. (1996), ‘The practical application of a nonlinear identification methodology’, *Control Eng. Practice* **4**(3), 295–306.
- Tsang, K. M. & Billings, S. A. (1994), ‘Identification of continuous time nonlinear systems using delayed state variable filters’, *Int. J. of Control* **60**(2), 159–180.
- Underwood, C. P. (1999), *HVAC control systems: Modelling, analysis and design*, E.&F.N. Spon, London.
- Underwood, C. P. (2000), ‘Robust control of HVAC plant I: modelling’, *Building services engineering research and technology* **21**, 53–61.
- Underwood, C. P. & Yik, F. W. H. (2004), *Modelling methods for energy in buildings*, Blackwell Publishing.
- Underwood, D. (1990), Modeling and nonlinear control of a hot-water-to-air heat exchanger, Technical Report TM E-91-01, USACERL.
- Underwood, D. M. & Crawford, R. R. (1991), ‘Dynamic nonlinear modeling of a hot-water-to-air exchanger for control applications’, *AHRAE Ttrans. Research* **97**, 149–155.

-
- Verdult, V. (2002), Nonlinear System Identification: A State-Space Approach, PhD thesis, University of Twente, Netherlands. <http://doc.utwente.nl/38684/1/t0000018.pdf>.
- Wang, J. & Hihara, E. (2003), ‘Predictions of air coil performance under partially wet and totally wet cooling conditions using equivalent dry-bulb temperature method’, *Int. J. of Refrigeration* **26**, 293–301.
- Young, P. (1981), ‘Parameter estimation for continuous-time models – a survey’, *Automatica* **17**(1), 23–39.
- Young, P. C. (1976), ‘Some observations on instrumental variable methods of time-series analysis’, *Int. J. of Control* **23**, 593–612.
- Young, P. C. (2011), *Recursive Estimation and Time-Series Analysis: An Introduction for the Student and Practitioner*, 2nd edn, Springer-Verlag.
- Young, P. C., Foster, M. & Lees, M. J. (1993), A direct approach to the identification and estimation of continuous-time systems from discrete-time data based on fixed interval smoothing, in ‘Proc. of 12th IFAC World Congress’, Pergamon, Oxford, pp. 27–30.
- Young, P. C., Garnier, H. & Gilson, M. (2008), *Identification of continuous-time models from sampled data*, Springer-Verlag, chapter Refined instrumental variable identification of continuous-time hybrid Box-Jenkins models, pp. 91–137.
- Young, P. C. & Jakeman, A. J. (1979), ‘Refined instrumental variable methods of time-series analysis: Part I, SISO systems’, *Int. J. of Control* **29**, 1–30.
- Young, P. C. & Jakeman, A. J. (1980), ‘Refined instrumental variable methods of time-series analysis: Part III, extensions’, *Int. J. of Control* **31**, 741–764.
- Youssef, A., Yen, H. H., Özcan, S. E. & Berckmans, D. (2011), ‘Data-based mechanistic modelling of indoor temperature distributions based on energy input’, *Energy and buildings* **43**, 2965–2972.
- Zajic, I., Larkowski, T., Hill, D. & Burnham, K. J. (2011), Energy consumption analysis of HVAC system with respect to zone temperature and humidity set-point, in ‘Proc. of 18th IFAC World Congress’, Milano, Italy, pp. 4576–4581.

- Zajic, I., Larkowski, T., Hill, D. & Burnham, K. J. (2012), Temperature model of an industrial air handling unit and manufacturing zone, *in* 'Proc. of 16th IFAC Symp. on System Identification', Brussels, Belgium, pp. 656–661.
- Zhang, X. J., Dai, Y. J. & Wang, R. Z. (2003), 'A simulation study of heat and mass transfer in a honeycomb rotary desiccant dehumidifier', *Applied thermal engineering* **23**, 989–1003.
- Zheng, W. & Worek, W. M. (1993), 'Numerical simulation of combined heat and mass transfer processes in a rotary dehumidifier', *Numerical heat transfer* **23**, 211–232.
- Ziemian, S. J. (2002), Bilinear Proportional-Integral-Plus Control, PhD thesis, Coventry University, UK.

Appendices

Appendix A

Models of HVAC system components

A.1 Control valve ideal model

This section freely continues the description of the control valve started in Section 2.5 in which the terms valve inherent characteristic, valve installed characteristic, linear and equal percentage inherent characteristics were introduced.

The ideal linear valve inherent characteristic can be modelled as follows, see (Underwood 1999), i.e.

$$\gamma(u(t)) = f + u(t)(1 - f) \quad (\text{A.1})$$

and the equal percentage inherent valve characteristic as

$$\gamma(u(t)) = f^{(1-u(t))} \quad (\text{A.2})$$

Here $u(t)$ denotes the valve stem fractional position in a range of $\langle 0, 1 \rangle$, where 0 corresponds to a fully closed and 1 to a fully open valve. The valve *let-by* is denoted as f ; even for fully closed valve, i.e. $u(t) = 0$, there could still be a minimum flow of water through the valve, which in practice is maximally around 1% of maximal mass flow rate.

When the valve is installed within the HVAC system and the pipe-work the valve inherent characteristic is influenced by the entire system itself, then we speak about installed valve characteristic, which is derived and provided in

(Underwood 1999), i.e

$$\phi(u(t)) = \frac{\gamma(u(t))}{\sqrt{\gamma^2(u(t))(1 - N_v) + N_v}} \quad (\text{A.3})$$

The valve authority, which is the link between heating system and valve, is defined as

$$N_v = \frac{\Delta p_v}{\Delta p_s} \quad (\text{A.4})$$

where Δp_v is the differential pressure over the fully opened valve at designed conditions and Δp_s denotes the differential pressure over the closed valve. The Δp_s is in fact the maximal locally available water pressure in the HVAC system and N_v is defined in the interval of $N_v = \langle 0, 1 \rangle$. In practice, for commissioned HVAC system, the valve authorities are expected to be in the range $N_v \in \langle 0.2, 0.5 \rangle$. Note that the valve authority of $N_v = 1$ corresponds to the ideal/designed case. This can be achieved if the valve would be small enough compared to the pipe work, i.e. $\Delta p_v \approx \Delta p_s$.

The water mass flow rate through the valve is then

$$\dot{m}(t) = M_w \phi(u(t)) \quad (\text{A.5})$$

where M_w denotes the maximal water mass-flow rate for a fully open valve, i.e. $u(t) = 1$.

The valve stem is modulated by either electric or hydraulic actuator in practice. Unless the actuator dynamics is fast enough compared to the system dynamics or it is assumed that the actuator dynamics can be lumped together with the system dynamics, then the separate dynamic model should be also considered and included in the system identification exercise. The valve actuator dynamics is commonly represented as a first order dynamic system, subsequently the supply water mass flow rate is computed as, (Underwood 1999), i.e.

$$\tau_{valve} \frac{d\dot{m}(t)}{dt} = M_w \phi(u(t)) - \dot{m}(t) \quad (\text{A.6})$$

where τ_{valve} is the valve actuator time constant. The basic model (A.6), however, does not consider the different amount of time it takes to move the valve stem for different distances. Therefore rate limiter should also be considered, so that $d\dot{m}(t)/dt \leq \text{limit}$.



Appendix B

Essential background to Psychrometrics

Psychrometrics is a field of engineering studying gas mixtures in general. The gas mixture of dry air and water vapor is of the main interest in air conditioning applications, because of its impact on the human comfort and the indoor environment. The term atmospheric air, or ‘air’ for short, refers to a mixture of dry air and water vapor. The dry air itself is a mixture of oxygen (approximately 78 [%]), nitrogen (approximately 21 [%]) and other gases. A simplifying assumption is made regarding the two air component properties. It is assumed, that the dry air and the water vapor behave as ideal gases (Çengel & Boles 1994), that is the two substances behave as they are alone and obey the ideal equation of state

$$pV = mRT \quad (\text{B.1})$$

where p [Pa] denotes the gas pressure, V [m^3] denotes the gas volume, m [kg] is the gas mass, T [K] denotes the temperature and R [$J/(kgK)$] is the gas constant. The gas constant of dry air is $R_a = 287$ [$J/(kgK)$] and the gas constant of water vapor is $R_v = 461.5$ [$J/(kgK)$], where the subscripts a and v refers to dry air and water vapor, respectively. Under this assumption, the air pressure is a sum of the partial pressure of dry air, denoted p_a , and of the partial pressure of water vapor, denoted p_v , so that

$$p = p_a + p_v \quad (\text{B.2})$$

In air conditioning applications the air temperature and humidity are important measures, which are being controlled. The two subsequent sections clarify the following terminology and state essential mathematical relations between these: dry-bulb temperature, dew-point temperature, frost-point temperature and rela-

tive humidity. The other measures quantifying the air humidity, such as absolute and specific humidities, are not used in this thesis, hence are not introduced.

B.1 Dry-bulb temperature

The temperature of air measured by thermometer, which is shielded and freely exposed to the air, is called the dry-bulb temperature. In other words, this is the standard temperature measured by thermometer and often refers to the ambient temperature. The temperature is measured in units of Kelvin, denoted $[K]$, which is also the basic SI (International system of units) unit. Other commonly adopted temperature scale is the Celsius scale, having degree Celsius $[^{\circ}C]$ as unit of measurement. The conversion between Kelvin and Celsius scale is

$$[K] = [^{\circ}C] + 273.15 \quad (\text{B.3})$$

In psychrometrics and thermodynamics, the attention must be given to the actual temperature units used as some constants and relations are provided either in $[K]$ or $[^{\circ}C]$ but not necessarily in both.

B.2 Specific and relative humidity

The specific humidity, denoted X , is defined as a ratio of water vapor mass, denoted m_v , to the mass of dry air, denoted m_a , in a given control volume of air, hence

$$X = \frac{m_v}{m_a} \quad (\text{B.4})$$

where the units of X are $[kg \text{ (water vapor)}/kg \text{ (dry air)}]$ or $[g \text{ (water vapor)}/kg \text{ (dry air)}]$. Substituting from (B.1) for m_v and m_a in (B.4) gives the following alternative expression for specific humidity

$$X = \frac{p_v \frac{V}{R_v T}}{p_a \frac{V}{R_a T}} = 0.622 \frac{p_v}{p_a} \quad (\text{B.5})$$

Considering the (B.2), the above expression (B.5) can be also written as

$$X = 0.622 \frac{p_v}{p - p_v} \quad (\text{B.6})$$

where p is a total atmospheric pressure.

The relative humidity, denoted RH , defines the human comfort. Therefore, it is the relative humidity which is commonly measured and controlled. Additionally, the relative humidity also determines how much moisture a water absorbent material can absorb from moist air, which might be critical information when such material is being manufactured. The relative humidity is defined as a ratio between the mass of water vapor m_v to the maximum mass of water vapor, denoted m_g , which could be held at specific control volume at the same conditions (temperature and pressure), so that (Çengel & Boles 1994)

$$RH = \frac{m_v}{m_g} \quad (\text{B.7})$$

Substituting from (B.1) for m_v and m_g in (B.7) gives the following alternative expression for relative humidity

$$RH = \frac{p_v \frac{V}{R_v T}}{p_g \frac{V}{R_v T}} = \frac{p_v}{p_g} \quad (\text{B.8})$$

where p_g [Pa] denotes the saturated water vapor pressure. The relative humidity can be then also defined as the ratio of partial pressure of water vapor to the saturated partial pressure of this water vapor at the same temperature. The ratio (B.7) ranges between zero and one, where zero means no moisture is contained in the air and one states that the air is saturated with the water. Commonly, the ratio (B.8) is multiplied by 100, so that the relative humidity is provided in percentage [%].

The saturated water pressure is a function of the dry-bulb temperature only. This relation can be expressed by empirical Magnus formula (Buck 1981)

$$p_g = a \exp\left(\frac{bT}{c + T}\right) \quad (\text{B.9})$$

where a , b and c are constant parameters, which are directly taken from (Buck 1981) and are provided in Table B.1. This implies that the relative humidity changes with temperature even when the actual mass of the water vapor does not. Therefore, the relative humidity is not often being controlled directly by an air conditioning system, but rather indirectly via the dew-point and frost-point temperature measurements.

Table B.1: The constant parameters of Magnus formula. For $T_d > 0$ [°C] the relative error is < 0.05 [%] over the range $0 \leq T \leq 50$ [°C]. For $T_d \leq 0$ [°C] the relative error is < 0.02 [%] over the range $-50 \leq T \leq 0$ [°C].

Parameter	$T_d \leq 0$ [°C]	$T_d > 0$ [°C]
a	6.1115	6.1121
b	17.966	17.368
c	247.15	238.88

B.3 Dew-point and frost-point temperatures

The dew-point temperature is a measure of the air humidity and directly relates to the so called specific humidity. The dew-point temperature, denoted T_d [K], is defined in (Çengel & Boles 1994) as “the temperature at which condensation begins if the air is cooled at constant pressure”. The condensed water is called the dew. In the case the dew-point temperature is negative, hence the air ambient temperature T must drop below freezing point, the frost is formed instead of the dew. In such case the dew-point temperature is called the frost-point temperature, i.e. for negative values of T_d . However, to simplify the terminology the frost-point temperature is also called the dew-point temperature and based on the actual value of T_d one can recognize whether the dew or frost would form.

Since the dew-point temperature directly relates to the water content of the air, it is possible to calculate the partial pressure of water vapor within the air. If the ambient temperature T of the air decreases, the amount of water the air can hold also decreases (hence the saturated water pressure decreases cf. (B.9)), so that the relative humidity of the air increases. The moment the ambient temperature and the dew-point temperatures are equal the relative humidity is 100 [%]. At this point the partial pressure of water and the saturated partial pressure of water are equal, i.e. $p_v = p_g$ and $T = T_d$. Therefore, having measured the dew-point temperature, it is possible to calculate the partial pressure of water vapor within the air by substituting T_d for T in (B.9), i.e.

$$p_v = a \exp\left(\frac{bT_d}{c + T_d}\right) \tag{B.10}$$

where the constant coefficients are provided in Table B.1 and are the same as for expression (B.9). Considering the definition of the specific humidity (B.6), it can be noted that the dew-point temperature directly relates to the specific humidity via partial pressure of water vapor (B.10).

B.4 Conversion between relative humidity and dew-point temperature

It is often convenient to be able to convert between the relative humidity and the dew-point temperature in both directions. Considering the definition of relative humidity in (B.8) and substituting for partial and saturated partial water pressures from (B.10) and (B.9), respectively, yields

$$RH(T, T_d) = \frac{\exp\left(\frac{bT_d}{c+T_d}\right)}{\exp\left(\frac{bT}{c+T}\right)} \quad (\text{B.11})$$

Equation (B.11) can be rearranged and expressed in terms of the dew-point temperature, hence

$$T_d(T, RH) = \frac{c \left[\ln\left(\frac{RH}{100}\right) + \frac{bT}{c+T} \right]}{b - \ln\left(\frac{RH}{100}\right) - \frac{bT}{c+T}} \quad (\text{B.12})$$

In practical HVAC system applications the installed sensors are commonly measuring the relative humidity. This measurement is then converted to dew-point temperature scale, which is then actually utilised for the control purposes. In this manner, the humidity control loop is decoupled from the ambient temperature control loop.